Long-term effects of thermal variation on the performance of Balanced Twisted Pair Cabling

By

Sile Florence Akinnuoye

A thesis submitted in partial fulfilment of the requirements of
De Montfort University for the Degree of Doctor of Philosophy

School of Engineering and Sustainable Development
Faculty of Computing, Engineering & Media (CEM)
Institute of Engineering Sciences
Centre for Electronic and Communications Engineering
De Montfort University
United Kingdom

29th of October 2019

This thesis is dedicated to:
my parents (Cecilia and Robert Akinnuoye),
my siblings (Mercy, Christianah, Augustine, Franklin and Emmanuel)
and
Dr Jörg-Hein (Jo) Walling.

Acknowledgements

I acknowledge the ALMIGHTY GOD, the author and the finisher of my faith for strengthening me throughout the research period. My sincere gratitude goes to my supervisor, Prof. Alistair Duffy, for his timely guidance and numerous helpful suggestions throughout the research period. I would like to thank De Montfort University for the scholarship offered to me to study for a PhD, and I appreciate the support of the entire staff of DMU on my research.

My profound gratitude goes to Dr Hugh Sasse for his numerous suggestions towards the completion of the PhD. I would like to appreciate the encouragement of Prof Ayodele Ajayi, Prof Boniface Kayode Alese, Prof Biyi Daramola, Dr Boluwaji Akinnuwesi and the endurance of my son (Daniel Olaofe) throughout the research period.

Finally, to the cabling industry leaders: David Kiddoo, John T. Barteld, Pat Hudak, Michelle Melsop, Paul Kish, Dave Hess, Paul Cave, Amanda Shehab, Andy Lewis, Steve Prescott and James Withey. Thank you all for your support during my PhD research work. (***"The improbable we do right away, the impossible takes a little longer")***.

Abstract

Remote powering over the Ethernet (including PoE, PoE+ and PoE++) is currently trending as a cost-effective option to power networked devices using balanced twisted pair cabling. As technology advances and Ethernet penetration grows, more devices are deployed, thereby increasing the cabling density to support these devices. Power delivery through Ethernet cables has numerous benefits, including cost and space saving. However, concurrent high-power transmission and installation conditions could induce local heating, and thus, thermal variation may occur in the cable bundles, and these can be exacerbated by the installation conditions, and sometimes by extreme weather conditions. Over a long time, all these could modify the cable properties, thus affecting the performance of the cabling system and thereby impacting the Ethernet signal integrity. Although Joule heating of the cable bundle is primarily assumed to be concomitants of current transmission through the cable, several fundamental questions around these processes are not yet fully answered. They include: Do cable heating and thermal variations influence the designed transmission parameters of the cable? If yes, how can the cause(s) and effects be accurately measured and reliably validated? In answering some of these questions, a series of experiments were developed and adopted to (1) assess cable bundle heating (2) assess the performance of Balanced Twisted Pair cables subject to repeated thermal variation, both within the specified operating range and beyond to account for the situations where high temperature and localised heating might stress the cables beyond the designed or expected levels (3) assess the performance of Ethernet cable dielectrics to understand some of the root causes of Ethernet cable performance degradation.

The outcome of the research showed that high power (100 watts) deployment over bundled and insulated unshielded Ethernet cables triggered an extremely high-temperature increase (~ 140^0C) that resulted in mechanical failure of the cables' dielectrics and a short circuit between the copper conductors of the cables. Larger cable conductor size, screening of the twisted pair along with Fluoropolymers as the conductor insulation helped the shielded cables not to reach a point of failure when tested in the insulated environments and at high power levels even though there was a temperature rise on the cables.

Moreover, repeated resistive and non- resistive heating have adverse effects on the electrical properties and transmission parameters of Balanced Twisted Pair cables, most notably in the first few cycles. The impact was more pronounced during the cooling phase than the heating phase. Also, the thermal impact was more accentuated in insulated operating condition than in ventilated operating condition. The electrical length of the cable measured by the tester decreased by 0.7 m

due to the effect of repeated non-resistive heating in an insulated environment and at a high temperature of ~120^{0}C but decreased by 0.4 m with ~70^{0}C in a similar insulated environment.

Phase drifts in Balanced Twisted Pair cables were observed to be dependent on the combined effects of mechanical dimension, dielectric constant and frequency. Thermal variation caused a phase change in the Return Loss (RL) signal from 63^0 to 90^0, from 90^0 to 135^0 and from 135^0 to 315^0 respectively. The RL performance of Category 6 U/UTP CoMmunications Plenum rated (CMP) cable failed at 20^{0}C and recovered at 23^{0}C initially, but after the electrical length of the cable had decreased, subsequent failure and recovery temperatures accelerated towards higher temperature (40^{0}C). Similarly, the transition temperatures of the bandwidth of the cavity loaded with the Fluorinated Ethylene Propylene (FEP) from the Category 6 U/UTP CMP cable accelerated during the prolonged thermal cycling. The maximum reduction in the RL value of Category 6A F/UTP cable due to the 40 thermal cycles conducted was observed to be 5 % per degree, whereas the maximum Insertion Loss (IL) increase was 5.8 % per degree. Moreover, for the 24 thermal cycles conducted on Category 6 U/UTP CMP cable, an increase in IL of ~8.3 % per degree was observed while RL decreased by ~6.8 % per degree. Using the Features Selective Validation technique, the comparison between the baseline performance and long-term performance of Category 6A F/UTP permanent link (PL) showed a fair agreement, which implies degradation in the performance of the cable. Furthermore, results showed that impedance varied significantly along the length of the cable due to localised heating of the cable. The impedance along the unheated sides of the cable reverted at every $\frac{\lambda}{2}$ (0.4 m) and $\frac{\lambda}{4}$ (0.2 m) but the impedance profile of the heated middle portion of the cable varied significantly. The results of the Scanning Electron Microscope revealed the deformation in the conductor insulation of a twisted pair sample. Furthermore, the adhesion of the twisted pair conductor insulation to its copper conductor was also observed to be affected near the end of the twisted pair sample. Connector impedance mismatch was observed to be severe on the split pair pins (pair 3,6) than other pairs in the cable. The connector impedance mismatch also dominated the Near End Crosstalk (NEXT) loss at frequencies around 35 MHz. The repeated heating of the cable to a higher temperature of 120^{0}C caused the loss of the PL at room temperature and a DC contact resistance issue which of course resulted in poor intra-pair resistance unbalance between the split pair. The Transverse Conversion Loss (TCL) and Equal Level Transverse Conversion Transfer Loss (ELTCTL) of Category 6 U/UTP CMP PL revealed some imbalances in the structure of the twisted pairs. Also, the equivalent differential mode noise voltages for the TCL values of the cable revealed a voltage spike following the decrease in the electrical length of the cable. More also, Crosstalk performance between the longest and shortest pair in the Category 6A

F/UTP cable was also observed to be better due to the heating of the cable in comparison to the crosstalk loss measured due to the cooling of the cable. Crosstalk performance of the portion insulated cables was initially worse during the first few heating and cooling cycles but improved afterwards. In addition, crosstalk, which was not initially present at the reference plane of the permanent link, was observed to increase rapidly from the point where the electrical length decreased.

The increase in temperature to ~65^0C caused an accentuated frequency shift in the resonance of the FEP, which is the probable cause of the immediate performance degradation of the Category 6 U/UTP CMP cable. The dielectric constant of the extracted FEP rod sample from Category 6 U/UTP CMP cable increased as a consequence of prolonged thermal cycling, particularly during the cooling phase, which also suggests the root cause of the poor RL performance observed during the cooling phase. The increased loss tangent of the FEP during thermal cycling also indicates that IL performance degradation of the Ethernet cables will increase during the heating and cooling process in Ethernet cables. Also, on a long-term, IL performance will drift due to thermal cycling. Furthermore, various signal phase transitions were recorded during the heating and cooling of the cable and its dielectric due to the different behaviour of the molecular transitions. As a result, an echo of RL was measured during the transition between the intermittent and prolonged thermal cycling of the cable, of which can be correlated to the spurious resonance, observed in the resonance of the FEP sample during the transition period. Thus, it could be inferred that immediate and long-term effects of thermal variation influence the designed electrical properties and transmission parameters of Balanced Twisted Pair cables. Also, an immediate and long-term effect of thermal variation on the conductor insulation of the cable has a direct effect on the performance of Balanced Twisted Pair Cables.

Contents

List of figures

List of tables

List of abbreviations

1	ACR	Attenuation to Crosstalk Ratio
2	AP	Access Points
3	AWG	American Wire Gauge
4	BTP	Balanced Twisted Pair
5	Cat	Category
6	CB	Cable Bundle
7	CBs	Cable Bundles
8	CCA	Copper Clad Aluminium
9	CDNEXT	Common Mode Near End Crosstalk
10	CMP	CoMmunications Plenum
11	CMP	Cavity Perturbation Method
12	CMR	CoMmunications Riser
13	CST	Computer Simulation Technology
14	DC	Direct current
15	DM	Differential Mode
16	DSSS	Direct Sequence Spread Spectrum
17	ELTCTL	Equal Level Transverse Conversion Transfer Loss
18	EMC	Electromagnetic Compatibility
19	EMI	Electromagnetic Interference
20	F/UTP	Foiled/Unshielded Twisted Pair
21	FEP	Fluorinated Ethylene Propylene
22	FEXT	Far End Crosstalk
23	FHSS	Frequency-Hopping Spread Spectrum
24	FSV	Feature Selective Validation
25	Gbs	Gigabit per seconds
26	GDM	Global Difference Measure
27	HD	High definition
28	HDPE	High-Density Polyethylene
29	HDTDR	High Definition Time Domain Reflectometry
30	HDTDX	High Definition Time Domain Crosstalk
31	HPD	High Power Device
33	IEEE	Institute of Electrical and Electronics Engineers
34	ILD	Insertion Loss Deviation
35	IoT	Internet of Things
35	IP	Internet Protocol
36	ISO	International Organization for Standardization
37	LoWPAN	Low Personal Area Network
38	LPD	Low Power Device
39	LSOH	Low Smoke Zero Halogen
40	Mbps	Megabit per seconds
41	MU-MIMO	Multi-User, Multiple-Input, Multiple-Output
42	NEXT	Near End Crosstalk
43	ns	nanosecond
44	NVP	Nominal Velocity of Propagation

45	OFDM	Orthogonal Frequency-Division Multiplexing
46	OFDMA	Orthogonal Frequency-Division Multiplexing Access
47	PD	Powered Device
48	PHY	Physical Layer
49	PiMF	Pairs in Metal Foil
50	PL	Permanent Link
51	PoE	Power over Ethernet
52	PoE+	Power over Ethernet Plus
53	PoE++	Power over Ethernet Plus Plus
54	PoF	Power over Fibre
55	PP	Polypropylene
56	PSACR	Power Sum Attenuation to Crosstalk Ratio
57	PSE	Power Sourcing Equipment
58	PSNEXT	Power Sum Near End Crosstalk
59	PTZ	Pan/Tilt/Zoom
60	PVC	Polyvinyl Chloride
61	RRCs	Rectangular Resonant Cavities
62	S/FTP	Shielded/Foiled Twisted Pair
63	SCPI	Standard Commands for Programmable Instruments
64	SELV	Safe Extra Low Voltage
65	SEM	Scanning Electron Microscope
66	TCL	Transverse Conversion Loss
67	TDR	Time Domain Reflectometry
68	TIA	Telecommunications Infrastructure Standard
69	U/UTP	Unshielded/Unfoiled Twisted Pair
70	UPoE	Universal Power over Ethernet
71	VF	Velocity Factor
72	VNA	Vector Network Analyser
73	VoIP	Voice over IP Phones
74	WAP	Wireless Access Points
75	WiGig	Gigabit Wi-Fi

List of symbols

Area of each copper conductor (mm^2)	A
Common mode impedance	Z_{cm}
Copper diameter over its insulation (mm)	A_τ
Diameter of each copper conductor (mm)	d
Dielectric loss	ε"
Dielectric thickness (mm)	τ
Electrical conductivity of copper	σ_c
Electrical conductivity of the dielectric	σ_d
Energised current	i_c
External inductance	L_{ext}
Internal inductance	L_{in}
frequency	f
Permeability of copper conductors ($\frac{H}{m}$)	μ
Permeability of free space ($\frac{H}{m}$)	μ_o
Permittivity of free space	ε_o
pi	π
propagation constant	γ
Radius of the aperture	A_r
Relative permeability of copper conductors	μ_r
Relative permittivity of the conductor insulating material or dielectric constant	ε_r
Seconds	sec
Separation distance between the centres of the two insulated copper conductors (mm)	S_d
Skin depth of copper conductor (m)	δ
Speed of light in a vacuum	c
Surface resistance	R_s

CHAPTER 1 - EVOLUTION OF ETHERNET

Ethernet, as the most ubiquitous type of computer network, is widely used to describe the family of computer networking technologies commonly used in Local Area Networks (LAN), Metropolitan Area Networks (MAN) and Wide Area Networks (WAN). Ethernet was introduced in 1980 and first standardised in 1983 as IEEE 802.3. From the initial form of the Local Area Network (LAN), which was wired LAN, and the interconnection of two or more computers, Ethernet has continued to evolve. In 1997, wireless LAN evolved to link two or more devices in the LAN using radio frequency technology [1]. For instance, Wireless Access Points (WAPs) enable the connectivity of devices such as desktop computers and wireless IP phones to the LAN. Moreover, because of the bandwidth limitation of the cable connecting a computer to a switch port, fast Ethernet evolved. From 1990, the speed of the Ethernet protocol (Table 1.1) has increased over time from 10 Mbps (Ethernet) to 100 Mbps (Fast Ethernet) and then to 1 Gbps (Gigabit Ethernet). Also, due to the growth of multimedia and powerful servers, Multi-Gigabit Ethernet (10 Gbps) evolved. The Multi-Gigabit Ethernet Technology (10 Gbps) has been readily available since 2006 but rarely deployed in the LAN because the Gigabit Ethernet (1 Gbps) was enough to support the need for most desktop users. Additionally, a single run of the LAN cable (Ethernet cable) was adequate to support the transmission bandwidth requirement of the WAPs to operate efficiently [2]. The 10 Gbps Ethernet Technology was designed to be used in data centres and exchanges for the connection of high-end routers, switches, and servers, as well as in high bandwidth trunks between offices. From 1999, the speed of wireless LAN technology (Table 1.2) evolved quickly from 11 Mbps to 1.3 Gbps, outpacing the transmission bandwidth of already deployed LAN cables. According to [3, 4], the new proposed wireless LAN speed: 10 Gbps (P802.11ax) and 100 Gbps (P802.11ay) are expected to be standardised in the very near future. The benefits of the upcoming Gigabit Wi-Fi (WiGig) include streaming of movies and TV shows in Ultra High-Definition (4K); quick download of large files, online gaming without network latency and seamless use of multiple smart devices with maximum Wi-Fi coverage.

Table 1.1: Evolution of Ethernet standards

	Standards	Transmission Speed	LAN Type	Year of ratification
Ethernet I version 1	Ethernet I	10 Mbps	Classic Ethernet	1980
10 Base5	IEEE 802.3	10 Mbps	Classic Ethernet	1983
	Ethernet over twisted pair wiring (100 m)			
10 Base-T	IEEE 802.3i	10 Mbps	Switched Ethernet	1990
100 Base-TX	IEEE 802.3u	100 Mbps	Fast Ethernet	1995
100 Base-T2	IEEE 802.3y	100 Mbps	Fast Ethernet	1998
1000 Base-T	IEEE 802.3ab	1000 Mbps	Gigabit Ethernet	1999
2.5 GBase-T	IEEE 802.3bz	2.5 Gbps	Multi-Gigabit Ethernet	2016
5 GBase-T	IEEE 802.3b	5 Gbps	Multi-Gigabit Ethernet	2016
10 GBase-T	IEEE 802.3an	10 Gbps	Multi-Gigabit Ethernet	2006
	Ethernet over twisted pair wiring (30m)			
25 GBase-T	IEEE 802.3bq	25 Gbps	Multi-Gigabit Ethernet	2016
40 GBASE-T	IEEE 802.3bq	40 Gbps	Multi-Gigabit Ethernet	2016
	Ethernet over single twisted pair (variable length in m)			
10Base-T1	IEEE 802.3cg	10 Mbps	Single Twisted Pair Ethernet	Expected
100Base-T1	IEEE 802.3bw	100 Mbps	Single Pair Automotive Ethernet	2015
1000Base-T1	IEEE 802.3bp	1000 Mbps	Single Twisted Gigabit Ethernet	2016
2.5GBase-T1	IEEE 802.3ch	2.5Gbs	Multi-Gig Automotive Ethernet	Expected
5GBase-T1	IEEE 802.3ch	5Gbs	Multi-Gig Automotive Ethernet	Expected
10GBase-T1	IEEE 802.3ch	10Gbs	Multi-Gig Automotive Ethernet	Expected

Table 1.2: Evolution of wireless standards

Wireless Standards	Modulation Schemes	Frequency	Max. data rate	Year of ratification
IEEE 802.11	FHSS or DSSS	2.4GHz	1.2 Mbps	1997
IEEE 802.11a	OFDM waveform	5.8GHz	11 Mbps	1999
IEEE 802.11b	DSSS	2.4GHz	11 Mbps	1999
IEEE 802.11g	OFDM	2.4GHz	54 Mbps	2003
IEEE 802.11n	OFDM -MIMO	2.4 & 5GHz	450 Mbps	2009
IEEE 802.11ac Wave1	BEAMFORMING	5GHz	1.3 Gbs	2013
P802.11ac Wave2	MU - MIMO	5GHz	3.5 & 6.9 Gbps	2016
IEEE 802.11ad	OFDM -SC	60GHz	6.93 Gbps	2012
P802.11ax	MIMO MU-MIMO OFDMA	2.4 & 5GHz	10 Gbps	Expected
P802.11ay	OFDM-SC	60GHz	20 Gbps	Expected

1.1 Technological advancement in Ethernet applications

The growth in the use of Ethernet technology has also been accompanied by a rapid expansion in remote powering of devices, and thus the advancement of the Power over Ethernet Technology (PoE, PoE+ and PoE++). PoE Technology allows electrical power to be transferred concurrently with data on the same Ethernet cable. Depending on the application requirements, different power levels are transmitted through the cable to the end devices. Under the first generation of PoE (IEEE 802.3af - PoE) [5], the Power Sourcing Equipment (PSE) is capable of transferring up to 15.4 W on two pairs of the minimum specification cabling, Category 5e U/UTP to the powered device (PD). Due to the losses of the line, the 15.4 W transferred from the PSE through a 100-meter length of Category 5e U/UTP cable is reduced to 12.95 W at the PD. Also, the second generation of PoE (IEEE 802.3at - PoE+) [6] is an improved version, which is capable of transferring 30 W from the PSE and delivering about 25.5 W through the two pairs of the minimum specification cabling, to the PD. The benefits of remote powering over Ethernet cables include: (1) flexibility of device placement; for instance, PoE supports WAPs deployment in the ceiling space and dense environments such as stadiums, airports and shopping malls, where the installation of the electrical power outlets would increase costs. (2) It delivers Safe Extra Low Voltage (SELV), which is limited to a peak of 57 DC volts and provided by a power supply, which is isolated from the direct connection to the AC power grid. (3) It allows real-time information sharing between IP-enabled devices. Moreover, the rapidly evolving Internet of Things (IoT) technology, which requires remote powering standards, is further expanding in home networking solutions and large building infrastructure management. Hence, there are now increasing applications of PoE in Building Automation Systems, which include, for example, light control systems, security systems, Heating, Ventilating, and Air Conditioning (HVAC) systems, and energy-monitoring systems. The capability to monitor and collect data from all the devices in the building for analysis with a centralised system enables operational optimisation. PoE enhances network connectivity for applications in control systems for LED Lighting systems (figure 1.1) that form part of digital ceiling Technology.

Figure 1.1: GENISYS PoE LED lighting system [0]

The ability for power, data, and user control to be provided to a light fixture installed in the ceiling space with the use of a single cable, and the functionality for the lights to switch off immediately when they are no longer needed is operationally efficient. Furthermore, the ability of the light to dynamically change colours in a commercial building provides added value beyond illumination, thus enhancing the users' experience. The new PoE application areas have also promoted innovation, particularly in meeting the needs of some of the power-hungry devices. Such devices available today include Digital signage, thin clients, information kiosks, High Definition TVs, thermal cameras with Pan/tilt/zoom features, laptop computers, Nurse call systems, and so on. Moreover, in response to the evolving low-powered and high-powered PoE devices, the IEEE 802.3bt redefined PoE power levels in September 2018 [7]. Table 1.3 shows the PoE landscape today.

Table 1.3: PoE landscape today and beyond

Standards	**Year of ratification**	**PoE Types**	**Energised pairs**	**Power Class**	**Output power at PSE (Watts)**	**Input power at PD (Watts)**
IEEE 802.3af	2003	1	2	0	15.4	12.95
		1		1	4	3.84
		1		2	7	6.49
		1		3	15.4	12.95
IEEE 802.3at	2009	2	2	4	30	25.5
IEEE 802.3bt	2018	3	4	5	45	40
		3		6	60	51
		4		7	75	62
		4		8	100	71

The IEEE 802.3af was redefined as Type 1, which is one of the four power classes from 3.84 watts to 12.95 watts at the PD (table 1.3). The IEEE 802.3at supports Type 1 classes and Type 2 class, which sources (take up) 30 W from the PSE but delivers 25.5 watts at the PD. In addition, the IEEE 802.3bt was defined as Type 3 and Type 4, which comprise of four more power classes. The type 3 and 4 power levels ranging from 45 watts at the PSE and 40 watts at the PD to 100 watts at the PSE and 71 watts at the PD. More also, according to [8], the Single Pair Ethernet (SPE – IEEE P802.3cg and P802.3ch) standards would enable a new class of low- power Ethernet devices that will facilitate networking and powering the billions of endpoint sensors forecasted to be present by the year 2022 [8]. The objective of the IEEE P802.3cg is to support 10-Mbit/s operation in automotive (10Base-T1S) and industrial (10Base-T1L) environments over single balanced twisted-pair cabling. The Multigigabit (IEEE P802.3ch - 2.5, 5, 10 Gbit/s) Automotive

Ethernet PHY task force is also working towards the standardisation of Power over Dataline (PoDL) operations over a variable length of shielded Single Pair Ethernet (SPE) cable with variable in-line connectors.

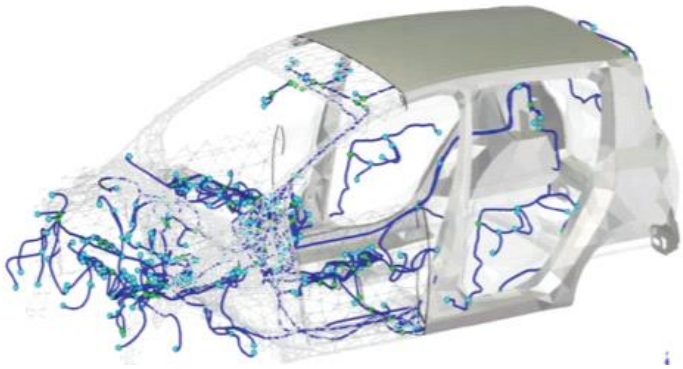

Figure 1.2: Example of an automotive cabling system [9]

1.2 Challenges of remote powering over Ethernet cables

Balanced twisted pair cables were not designed to transmit electrical power with data or alongside data initially, but due to cost and the limitation of the optical fibre, the adoption of balanced twisted pair cables in remote powering applications has been gaining momentum. Additionally, energy conservation and usage are important to the implementation of IoT. However, there are concerns about the quality of the signal passing through the cables when the cables are deployed in different environments as well as when it is operating under thermal varying conditions, at high power levels and high frequencies. The next section highlights some of the challenges being faced, with remote powering over the conventional balanced twisted pair cabling.

1.2.1 Concerns on the effects of high-power deployment and cable bundling

There is a growing demand for high power standardisation for the emerging power-hungry devices in order to take advantage of the potentials of PoE technology. In addition, wireless connections are also becoming the primary mode of connection utilised by the internet users [10], which implies an increase in user density and the concomitant need for high-power Access points to improve wireless coverage and increase the capacity of the wireless network. Moreover, additional high bandwidth, Ethernet cables will be required to support the WAPs in terms of power delivery as well as high data transmission on the network. The increase in cable density for the trunk serving the WAPs means that some cable bundles (CBs) are likely to be thick. Similarly, the

high-power access points will require high power to be delivered, which in turn requires that high electrical current will be transferred through the cables. The increased power transmission through the cable bundle may translate to increased local heating within the cable through Joule heating. The consequential increase in the cable temperature and the attendant fluctuation may impact the mechanical and electrical characteristics of the Ethernet cabling and connectivity [11].

Furthermore, the installed base of PoE is predominantly configured with lower categories of the balanced twisted pair cabling, due to cost, weight and compactness. These lower categories of cable are unshielded twisted pair category 5e and 6 U/UTP cabling which have limited bandwidth and power capabilities. Also, the cables have smaller conductor sizes, so their DC loop resistance per unit length is higher than that of the higher categories of cable. Because of the high current transmission in the cables, the conductors heat up and dissipate the heat through the insulator into the environment. For single cables and smaller CBs installed in the ventilated operating environments and operating within the specified limits of the IEEE 802.3at, the thermal impact is usually minimal, although the performance of some cables decreases within the immediate powering of the cables [11 – 13]. However, the thermal impact is more pronounced with larger CBs installed in pathway systems and improperly ventilated spaces. With large CBs, the cables experience the proximity of heat sources, which result in high operating temperatures. Similarly, when the ambient operating temperature is too high, the natural cooling process may not eradicate the concerns of excessive heating. Additionally, the sustained temperature rise within the CB can cause material ageing, and that will have an impact on the integrity of the signal passing through the cable. For example, it will cause attenuation of the signal passing through the cable. At higher frequencies, attenuation increases significantly due to the resistance of copper conductors, and this is an essential factor to be considered when combining high power with a high data rate on the cables. According to [14], Category 5e and 6 U/UTP cables may not be sufficient to handle the imminent high-frequency operations under the worst case of cabling-bundling conditions.

1.2.2 Concerns on the effects of thermal variation on Ethernet cable performance

In some normal PoE operating environments such as stadiums, airports and shopping malls, the ambient temperature of the cable is not always constant. Coupled with the effect of the Joule heating of the cable, the changes in the user density on the networks can trigger a rise in temperature on the cable. Also, from the commercial point of view, some businesses adopt auto shutdown or standby of equipment at the end of the business day. Some seasonal businesses even shut down the power completely during “off” seasons. This means that the balanced twisted pair cables used for

supplying the power are not continually drawing power [13]. The thermal variations on the cable based on the time-dependent power transmission can create a dynamic behaviour of the cable, a phenomenon that the network owners and cable designers must understand to effectively design cable and avoid failure.

Additionally, WAPs will be required to function in increasingly remote locations and harsh environments. Variation in ambient temperature can influence the mechanical behaviour of the cables reaching them. Moreover, the installation of WAPs in ceiling spaces sometimes necessitates that cables are passed through framed walls, ceiling voids or risers, etc. where the heat dissipation is minimal, due to limited ventilation. The walls are usually constructed with an insulating material, so the temperature rises. Over a long time, the thermal variation on the cables can change the dielectric properties of the cabling, and this can lead to deviation from the designed transmission parameters of the cable. For example, a change in the dielectric properties as a result of thermal variation can cause impedance variation along the length of the cable and subsequent reflection of the signal. Furthermore, when the medium in which the signal propagates changes, the speed of the signal is likely to change. The stability of the electrical length of the cable under various environmental conditions is paramount to maintain Ethernet signal integrity because, in Gigabit Ethernet, the bits are distributed across several pairs, and timing is important. The twist lengths of any two twisted pairs must differ to reduce crosstalk; therefore, the cable lengths will differ, so the speed on the twisted pair must be corrected by cable parameters. Any deviation from the designed dielectric properties during usage may affect signal integrity. For these reasons, there is a strict requirement of the electrical properties of the cables for the future PoE [15].

1.2.3 Concerns on the effects of installation conditions on Ethernet cable performance

In general, changes in conductor dimensions may occur as a consequence of thermal variation. These changes in the geometry and properties of the material can cause the cable's transmission parameters such as Return Loss and Attenuation, to drift over time. Moreover, since the cables may pass through insulated areas between the telecommunication rooms and the individual equipment, localised heating can place a segment of the cable conductors under thermal stress. It is also possible for the twisted pairs at that insulated portion to nest together or separate unequally due to excessive heating, causing the asymmetry of the conductor pairs, changing the crosstalk performance. Since the installed base of PoE is predominantly unshielded balanced twisted pair cables, any noise

induced in the cable (particularly in a wireless environment) can affect the quality of the signal passing through the cable.

Balanced twisted pair cables transmit in a differential mode, so any small amount of asymmetry along the transmission path will cause, a common-mode noise signal propagating along the cable [17] to convert to differential signal, with a detrimental effect on the quality of the received signal. According to [18], mode conversion is a source of Electromagnetic Interference (EMI). Signal reflection and crosstalk are the sources of the internal channel noise, and these contribute to a reduction in the noise margins of a channel. To achieve more channel capacity, the electromagnetic noise experienced by the channel must be limited. Although Ethernet physical layer devices use sophisticated signal-processing techniques to predict and cancel the effects of internal noise sources to maintain the channel capacity, this is at the cost of higher power consumption, which results in more heat.

1.3 State of the art

Based on some of the challenges highlighted in section 1.2, the PoE installed base, having the old cables with limited bandwidth and power capabilities may not cope with the demand in the upcoming network connectivity [14]. Also, because most cables in the present PoE installed base is deployed behind walls for desktop applications; they are difficult to replace. To support the upgrade to multi-gigabit Wi-Fi, a minimum of two permanent link connections is to be deployed to each WiGi WAP in order to support link aggregation [19]. It is appropriate to mention that more cable runs will lead to larger cable bundles. Additionally, there are concerns that large cable bundles installed in environments like the data centres and wiring closet experience localised heating that may easily result in high operating temperatures. Given this, there have been some debates in the standard community about the most appropriate method for measuring the temperature rise due to CB heating [20 - 22]. Furthermore, some mitigation strategies for the CB overheating have been put in place [20] for the present (brownfield) and future (greenfield) PoE installed base. The mitigation strategies specified for the brownfield include: (i) the use of half of the cables in a bundle for remote powering while the other half is used for applications that do not require remote power, (ii) the use of air-conditioning over cabling segments that are exposed to high temperature, and lastly, (iii) separation of larger cable bundles into smaller bundles to allow free heat dissipation when the cables are used in transmitting high electrical power. In addition, the heat mitigation strategy specified for the green fields involves the use of shielded and unshielded cables with

improved thermal characteristics and electrical properties. This will mean that the cable's components, such as its electrical insulation will need to have a high heat transfer coefficient.

Furthermore, the speed of the current WAP (IEEE803.11ac wave 1) is 1.3Gbs, and its successor, which is IEEE 802.11ax – is expected to be 10Gbs when ratified. To cope with the emerging applications while cables are bundled and operating at a high-power level such as 100 W in different installation environments, the recommendation in the TIA TSB-162-A is to deploy cables with more transmission bandwidth which is a Class EA cabling (Category 6A) or higher-performing shielded cabling to support higher data rates and increased power delivery [23]. Category 6A cable has been designed to minimise external noise because of its internal foil shielding. It can also support the full implementation of the multi-gigabit Wi-Fi and Ethernet uplink speed of 1 Gbps to 10 Gbps. Since the shielded and unshielded cables with improved thermal characteristics and electrical properties have been recommended for the high-power PoE systems, network owners and end-users also have questions regarding the reliability of the insulating materials, and overall performance of balanced twisted cables under variable thermal conditions [24]. For this reason, field testing will be vital in the investigation of the long-term performance of the shielded and unshielded balanced twisted cables to establish the longevity of the cables when used for high power and high-frequency operations.

1.4 Research questions

In view of the current and project levels of the application of PoE, some research questions are recurring, and they include:

1. Considering the effect of cable bundling and installation conditions, can the existing cabling infrastructures perform optimally in different installation environments?
2. Currently, the installed base of PoE is predominantly with category 5e and 6 unshielded twisted Pair cables due to cost, weight and compactness. Therefore, can the installed base cope with high power deployment or is there a need to move to Category 6A as recommended by the TIA, or to new technologies?
3. If Category 6A cables are to be deployed, can the specified temperature limit of 60°C have a long-term effect on the cable performance due to the effects of thermal variation and localised heating? If yes, how can the changes in the cable parameters be reliably measured, quantified, and validated?

4. Do Ethernet cable dielectric properties change with temperature and thermal variation? If yes, how does dielectric degradation contribute to the changes in the electrical and transmission performance of the cables?

1.5 Aim and objectives of the research

There have been published studies on the challenges of Ethernet CB overheating and performance degradation [25 – 34], but there is very little quantitative data about the interrelationship. Specifically, there are no investigations on the direct effects of thermal variation on the performance of different balanced twisted pair cabling based on the impact of installation conditions and dielectric degradation. To combine high electrical power and high-frequency data on the balanced twisted pair cables, which are operating under thermal variation conditions, it is essential to investigate the capabilities of the cables by conducting strict performance testing based on different scenario simulations.

1.5.1 Aim of the research

This research aims to identify the root causes of the immediate and long-term performance degradation of balanced twisted-pair cabling used in remote powering applications.

1.5.2 Objectives of the research

The objectives are to:

(1) characterise cable bundle heating in terms of cable constructions, installation environments and bundle sizes at different power and current levels. Also, to validate the obtained temperature rise across the employed temperature assessment methods.

(2) investigate the effects of repeated electrical heating and high ambient operating temperature on the electrical properties and transmission parameters of Category 6A cable.

(3) externally heat full insulated unshielded cable (Category 6 U/UTP) repeatedly using the specified PoE temperature limit of 60^0C and beyond; and determine the drift in the electrical

and transmission parameters of the cable as functions of thermal cycling and installation condition.

(4) externally to heat an insulated portion of a shielded cable (Category 6A F/UTP) repeatedly using the specified PoE temperature limit of 60^0C and determine the drift in the electrical and transmission parameters of the cable as functions of intermittent and prolonged thermal cycling. Also, quantify the drift in the cable performance using the Feature Selective Validation (FSV) technique.

(5) externally heat an insulated portion of an unshielded cable (Category 6 U/UTP CMP cable) repeatedly using the specified PoE temperature limit of 60^0C and determine the drift in the electrical and transmission parameters of the cable as functions of intermittent and prolonged thermal cycling.

(6) design a dielectric measurement method that will allow the characterisation of the baseline dielectric properties of dielectric rod samples extracted from different Ethernet cables. In particular, from the Category 6 U/UTP CMP cables, assessed in (4) based on the effect of intermittent and prolonged thermal cycling.

(7) using the dielectric measurement results and obtained cabling secondary parameter of the Category 6A F/UTP assessed in (5), develop a Transmission Line Model (TLM) to predict the cabling primary line parameters. Identify and relate the contributions of the changes in the dielectric constant to the measured changes in the long term-term performance of the cable.

(8) thermally cycle a short length of twisted pair sample extracted from the Category 6A F/UTP assessed in (5) and investigate the changes in the dimensions and elemental composition of the materials of the twisted pair sample using the Scanning Electron Microscope (SEM).

1.6 Anatomy of the thesis and contributions to knowledge

1.6.1 Anatomy of the thesis

In Chapter 1, the evolution of the Ethernet technology to remote powering, its current application and emerging applications and challenges are discussed with a view of determining the critical research questions. Issues identified include the concerns on the effects of high-power deployment and cable bundling, the possible effect of the installation environment and thermal variation on Ethernet cable performance. Following a detailed review of the state of the art of Ethernet technology, the aim and objectives of this doctoral research work were defined, and the expected contributions to knowledge were identified.

Chapter 2 critically reviewed the literature to document previous research work on the Ethernet technology and identify the research gaps that could be covered in this thesis. A detailed review was carried out on a twisted pair as a balanced transmission medium. This was followed by the classification of Ethernet cables based on configurations, bandwidths, cable construction, installation environments and application environments. Also, reviews were carried out on telecommunications standards groups, cable properties and factors affecting the performance of remote powered Ethernet channels.
In addition, different methods of assessing temperature changes in Ethernet cable bundle during use, which included the resistivity measurement approach, thermocouple sensor approach, and mathematical modelling techniques, were appraised. Furthermore, different methods of assessing balanced twisted pair performance, which including Time Domain Reflectometry, Two-Port Network Analysis, Transmission Line Modelling, Feature Selective Validation (FSV) technique and Scanning Electron Microscopy (SEM) were looked into. Finally, a detailed review of dielectric materials, factors affecting their performance and methods of assessment of dielectric properties were carried out.

Chapter 3 presents the test methodologies for assessing the cable bundle heating. Also, the possible rise in temperature on different categories of balanced twisted pair cabling was investigated based on different power and current levels as well as installation conditions, cable construction and bundle sizes. In Chapter 4, the detail results of the temperature rise measurements, predictions and validations were presented. Moreover, the power carrying capacities of bundled Ethernet cables, assessed in the ventilated and non-ventilated environments and at three power levels are presented;

followed by the characterisation of the impact of cable construction on the heat generation and dissipation in bundled Ethernet cables. Furthermore, the results from the assessments of temperature rise in two sizes of Ethernet cable bundles are presented. The last set of results in Chapter 4 was the validation of the maximum temperature rise in a 24-cable bundle and the validation of the temperature distribution across 37-cable bundle.

In Chapter 5, 6 and 7, the effects of intermittent and prolonged thermal cycling are assessed on the electrical properties and transmission parameters of different PoE permanent links (PLs). The assessments are based on the investigation of the effects of electrical heating and non-electrical heating, both within the specified operating range and beyond the levels expected, to account for the extreme situations where high temperature, fluctuations in external temperature and localised heating could stress the cables and cause a drift in the performance of the links over time.

Chapter 5 detailed all the methodologies used for the assessment of the effects of repeated electrical heating and non-electrical heating tests, while chapters 6 and 7 present the results of the assessments. In chapter 6, the changes in the electrical properties and transmission parameters of the Category 6A F/UTP PL measured under two installation conditions (ventilated and non-ventilated) under low and high temperatures are presented, whereas in chapter 7, the immediate and long-term effects of thermal variation on the performance of the fully and portion (partly) insulated balanced twisted pair cables are presented. The impact of thermal cycling within $+20^0$C to $+70^0$C was presented first, followed by the thermal impact of an extended temperature of about 120^0C (sections 7.1). Moreover, sections 7.2 and 7.3 present the immediate and long-term effects of thermal variation on the portion insulated Cat 6 U/UTP CMP and Cat 6A F/UTP cables. In section 7.2, the effects of the first thermal cycle with the cyclic behaviour in the performance of the Category 6 U/UTP CMP PL are presented first, followed by the long-term effects of thermal variation on the cable. Section 7.3 also discusses the long-term effects of thermal variation on the performance of the Cat 6A F/UTP cables along with the measured drifts in the RL and IL performances of PL. In addition to the results presented in section 7, the validation of the drifts in the RL and IL performances of the portion insulated Category 6A F/UTP cable is presented (section 7.4). This was followed by the discussion of the long-term changes in the impedance profile of the Category 6A F/UTP cable and the extraction of the primary line constants. Chapter 7 ends with the presentation of the changes in the dimensions of a twisted pair sample. The changes in the electrical characteristics and drifts in the transmission parameters of the balanced twisted pair cables under

study were observed in response to the effects of the intermittent and prolonged thermal cycling as well as the effects of thermal insulation and localised heating.

Having established the immediate changes in the electrical parameters and drifts in the transmission parameters of the balanced twisted pair cables under study in chapter 7, the immediate changes and drifts in the dielectric properties of the FEP sample extracted from Category 6 U/UTP CMP are also investigated as functions of the intermittent and prolonged thermal cycling. Correlations between the drifts in the transmission parameters of the cable and its dielectric properties are drawn and established and are presented in Chapters 8 and 9. The developed method for the assessment of dielectric properties is captured in Chapter 8, while Chapter 9 detailed the results of the dielectric measurements. Chapter 8 starts with the presentation of the theoretical analysis of a 2.4 GHz Rectangular Resonant Cavity (RRC) design followed by the modeling and actual fabrication of the cavity. To ensure accurate characterisation of the Ethernet cable dielectrics, the verification and validation of the accurate sample position inside the simulated and fabricated cavities were carried out. Furthermore, the baseline dielectric properties of different Ethernet cable dielectrics were implied. The last study in chapter 8 and 9 is the assessment of the drifts in the dielectric constant ($\boldsymbol{\varepsilon_r}$) and ($\mathbf{tan}\boldsymbol{\delta}$) of the extracted FEP sample based on the effects of intermittent and prolonged thermal cycling.

Chapter 10 presents the summary and conclusions of the research work. Implications for end users, network owners and cables manufacturers are presented, while further studies are suggested.

1.6.2 Contributions of the research to knowledge

This research has been able to advance knowledge in the following areas:

Cable bundle heating sections

1. Appropriately compared three methods, which include two measurements and a modelling approach to establish their validity and applicability in quantifying the increase in temperature due to cable bundle heating in PoE. Results showed that the thermocouple approach compared favourably well with the output of the mathematical model with less than 1^0C difference.

2. The study established the temperature (~140^0C) at which the unshielded cables failed in response to an increase in temperature due to cable bundle heating. This point represents

a point at which the extruded dielectric becomes soft enough to mechanically fail and cause a short circuit between the copper conductors.

3. The study succinctly showed the interrelationship of cable construction (material and size) as well as installation environments on heat generation and dissipation in Ethernet cable bundles.

Cable performance sections

4. The study established that both repeated resistive and non-resistive heating have adverse effects on the electrical and transmission parameters of balanced twisted pair cables with their severity depending on:

    - Installation environment
    - Temperature range
    - Number of thermal cycles
    - Phase (heating or cooling phase)

5. The result obtained has provided better insight into how and why cable performance changes over time in Ethernet cable bundle used in PoE applications. Comprehensive knowledge on how thermal variation affects different transmission parameters of the cable has also been documented.

6. A method for extracting the electrical properties of the cable based on the measured changes in the characteristics of the link has been demonstrated.

7. The study has been able to show that electrical length mismatches occur due to thermal variation and installation condition and these were further accentuated with SEM images obtained on a twisted pair sample. The consequences of mode conversion in Category 6 U/UTP CMP cable were equally illustrated

Dielectric sections

8. In addition, the adequately measured baseline dielectric properties demonstrated the potential of using the developed dielectric measurement method in validating the Velocity Factor (VF) supplied by Ethernet cable manufacturers.

9. This body of knowledge has been able to show the interrelationship between the changes in Balanced Twisted Pair Cable transmission performance and dielectric properties. Using Category 6 U/UTP CMP as an illustration. Immediate performance of the cable correlates with the immediate performance of Ethernet cable dielectric. Furthermore, correlations between the drifts in the cable performance and its dielectric (FEP) properties are drawn as functions of intermittent and prolonged thermal cycling.

10. The study has shown a method for measuring the phase change in a twisted pair Ethernet cable. It has been shown experimentally that thermal variations result in phase changes in balanced twisted pair cables. It was further shown that phase drifts can occur with thermal variation due to changes in the mechanical dimension and dielectric constant.

It is believed that the information provided in this doctoral research will help the polymer manufacturers in putting robustness into the processing methods of polymers used in data grade cables. The set of results presented in this thesis could serve as a guide to cable manufacturers in the design stage of balanced twisted pair cables and connectors. For instance, robustness can be put into the chemical constituents of Ethernet cable dielectrics to prevent hysteresis, eliminate or reduce crosstalk attenuation and prevent immediate performance degradation.

CHAPTER 2 - LITERATURE REVIEW

The transmission of information over the Ethernet requires transmission media, which are classified as guided and unguided. Examples of guided media are copper cables (twisted pair, twinax and coaxial cables) and fibre-optic cables. The unguided medium includes the air or free space that carries radio frequency (RF) or infrared (IR) light signals. In this research work, the study of signal transmission through a guided medium such as twisted pair copper cable is the focus. The unguided medium is out of the scope of the research.

In the early days of Ethernet development, various grades of coaxial cables have been used, but they are being replaced in most applications by twisted pair copper cables due to cost and bandwidth inadequacy. Recently, Fibre optic cables are gaining ground due to their bandwidth advantage and the ability to provide reach and throughput. Thus, they are becoming dominant as backbone cabling and are mostly deployed for applications in the data centres. Also, fibre cabling to the home is now becoming common, but twisted pair copper cabling is known to have more economic benefits particularly when deployed for short-distance connections within and outside the data centres. Moreover, twisted pair copper cable has kept pace with the demand in speed requirements over the years, despite the gradual domination of the optical cabling at very high data rates. Thus, it is widely used in Gigabit Ethernet networks and Radio Frequency backhaul [35]. As stated in [36], in the next five years, twisted pair cables are anticipated to replace the coaxial jumper cables used in indoor distributed antennas. Moreover, the adoption of balanced twisted pair cabling in Power over Ethernet (PoE) Technology and its relatives is an excellent opportunity for copper to retain relevance in the modern world. With the need for many powered devices in the upcoming generation of mobile networking technology (5G) and the Internet of Things (IoT), balanced twisted pair cables are likely to continue to be in high demand. Hence, there is still a very strong interest in the performance of copper cables in terms of their reliability and lower manufacturing and installation costs.

2.1 Twisted pair as a balanced transmission medium

A core of the Ethernet cable (figure 2.1) consists of a single copper conductor with a small air gap around it and the insulating material. However, two insulated copper conductors are twisted to form a pair, which is driven in a balanced way (figure 2.2). The uniform twisting of the wires ensures a uniform distribution of capacitances along the length of the cable. It also allows the capacitance to ground and to extraneous sources to be balanced. Twisted pair is particularly useful for reducing

low-frequency magnetic pick-up because the effective magnetic loop area is reduced to almost zero [37]. Also, each twisted pair in the cable has an intentionally different lay length to minimise noise coupling between them [38]. As a result of the difference in the length of the twisted pair, the DC loop resistance of each twisted pair is also slightly different from each other.

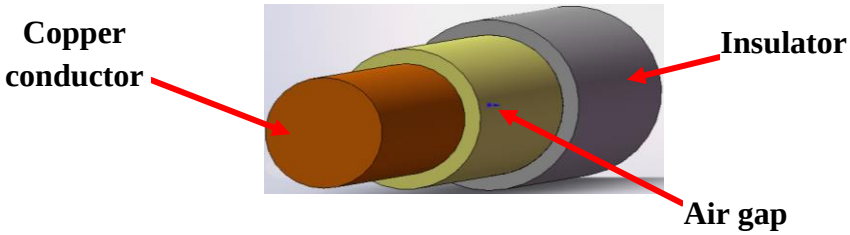

Figure 2.1: Simplified model of a single copper wire

Figure 2.2: Simplified model of a Balanced Twisted Pair (BTP)

2.2 Classification of Balanced Twisted Pair Cables or Ethernet cables

Ethernet cables are classified according to their:

(i) construction
(ii) bandwidth of operation
(iii) installation environment
(iv) application environment

2.2.1 Classification of Ethernet cables based on their constructions and bandwidths

Twisted pair copper cables consist of four twisted pairs with an outer layer jacket. Hence, the configuration referred to as an Ethernet cable. Ethernet cables are classified as shielded and unshielded cables and come in a variety of constructions, but the unshielded Ethernet cables are the most common ones and are less expensive. Shielded cables though relatively expensive, can support higher bandwidth of operations because of the effectiveness of its shield and the tighter twist of its conductor pairs, which provide noise immunity. Table 2.1 presents the specifications for the two configurations shielded and unshielded cables. As noticeable in the table, Category 5e is usually an unshielded twisted pair cable, whereas Category 6 cables come in both shielded and unshielded form. Category 7 and 8 are specified to be shielded cable type.

Table 2.1: Classification of Ethernet cables

Cable configurations	Categories of cable	Classes of cable	Transmission bandwidth	Transmission speed
Unshielded	5e	D	100 MHz	1 – 2.5 Gps
Unshielded	6	E	250 MHz	1 – 5 Gps
Shielded	6A	EA	500 MHz	1 – 10 Gps
Shielded	7A	FA	1000 MHz	1 – 10 Gps
Shielded	8 (8.1 and 8.2)	I	2000 MHz	1 – 40 Gps

All the wire pairs in the unshielded cables (figures 2.3 and 2.4) are twisted for noise cancellation and have no overall metallic shield at present, which makes them more susceptible to external electromagnetic interference.

The shielded twisted pair cables such as Category 6A F/UTP, Category 7A S/FTP and others may consist of an aluminium foil used as a shield in the cable. They also consist of more twists per meter; so, the cables radiate less effectively. Tighter twists result in less crosstalk and a better-quality signal. Also, screening each pair individually removes capacitive coupling between pairs, which makes the cables more suitable for Gigabit Ethernet applications. However, mutual capacitance between each pair to its screen and mutual capacitance between screens will still be present in the cable. Screening with braids does not provide 100 % coverage. As a result, a small amount of capacitance through the gaps in the braids will be present in the cable. In general, the purpose of the braid and screen is to reflect, attenuate and conduct any induced noise to ground.

The schematics and description of unshielded and shielded twisted pair cables with different constructions are given in figures 2.3 - 2.4 and 2.5 - 2.6, and the following abbreviations summarise the description of different types of constructions used in Ethernet cabling.

U = No form of metallic shielding present in the cable

F = Foil metallic shielding present in the cable

F_1 = Reversed metallic foil shielding present without having to fold back the foil during termination. The advantage of this is that it provides an instant 360° grounding contact to ensure the noise immunity of the channel or permanent link.

F_2 = Reversed double global metallic foil shielding. For example, in F_2/UTP cables, this means that there is a double global metallic foil shielding over all the four pairs in the cable without the need to fold back the foil to establish contact with the connector. This type of construction

contributes to the optimal Electromagnetic Compatibility (EMC) performance of the channel and increases installation efficiency.

S = Woven mesh of tinned copper wires. Presence of braid in the cable

S/F = Both a foil and a braid are present in the cable to provide dual shielding layers to the overall pairs in the cable.

(1) Unshielded twisted pair cable - Category 5e U/UTP and Category 6 U/UTP

Category 5e and 6 U/UTP are both unshielded cable types but differ in their conductor sizes. Category 5e has conductor size of American Wire Gauge (AWG) 24 while Category 6 has AWG 23. Category 3 cable was replaced by Category 5 with a similar cable construction but with more twists per meter. However, Category 5e cable is an enhanced Category 5 cable. Although Category 5 cable has the same transmission bandwidth of 100 MHz as that of Category 5e, it was designed to operate at a transmission speed of 10 or 100 Mbps whereas Category 5e cable can transmit at speed up to 2.5 Gb/s [14]. Category 6 U/UTP, on the other hand, was developed after Category 5e for a better transmission performance and bandwidth extension from the 100 MHz of Category 5e to 250 MHz. The schematics of Category 5e and 6 U/UTP are shown in figures 2.3 and 2.4, respectively. Figure 2.4 shows that the twisted pairs in most Category 6 cables are formed around a crossweb or pair separator. The purpose of the crossweb is to provide physical and electrical separation to the twisted pairs [39]. Although the crossweb can be designed differently depending on the manufacturer's preferences, the material used for the crossweb is chosen to mimic the type of dielectric used for the conductor insulation [39].

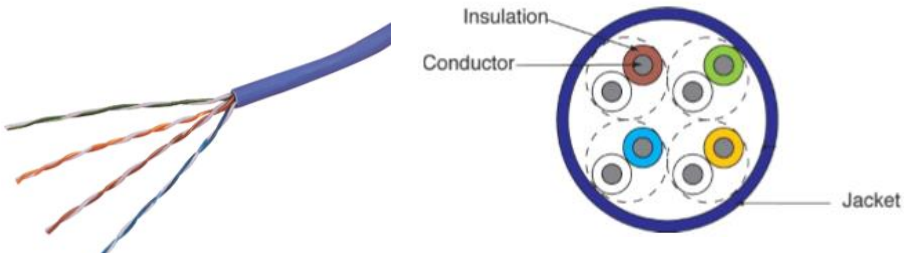

Figure 2.3: Sideways view (left) and cross section (right) of Category 5e U/UTP [40]

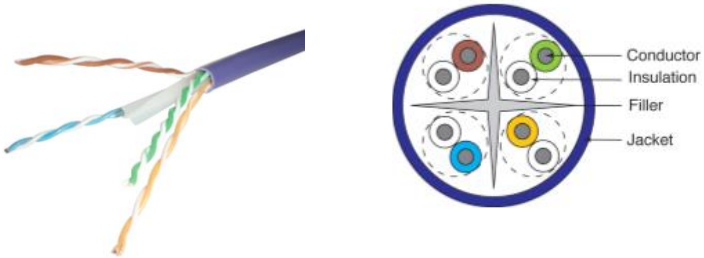

Figure 2.4: Sideways view (left) and cross section (right) of Category 6 U/UTP [40]

(2) Shielded cables - Cat 6 F/UTP, Cat 6 F/FTP, Cat 6A F/UTP, Cat 7A S/FTP and Cat 8 cables

Although the installed base of PoE is dominated with the unshielded twisted pair cables, the preferred cable construction for the "greenfield" is the Pairs in Metal Foil (PiMF) cables. The PiMF cables include Category 6A F/UTP, Category 6 F/FTP, Category 7A S/FTP and Category 8 cables.

Category 6A F/UTP

Category 6A F/UTP cable is foiled screened. It consists of an insulated copper conductor of 23 AWG, a drain wire, a ripcord, overall Aluminium foil and a central 'X' crossweb. Depending on the application requirements, the copper conductor insulation and the central 'X' crossweb are made from different types of polymers. Sometimes, they are made from polyethylene (PE) or Fluorinated Ethylene Propylene (FEP). The central 'X' crossweb and all the four twisted pairs in the cable are wrapped with a clear Mylar tape first, followed by the overall foil screen tape. Figure 2.5 presents the construction of a Category 6A F/UTP cable.

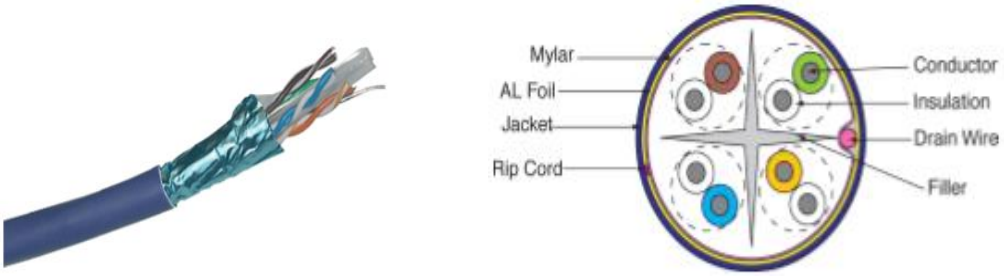

Figure 2.5: Sideways view (left) and cross section (right) of Cat 6A F/UTP cable [40]

Category 6 F/FTP

Category 6A F/FTP is an augmented Category 6A F/UTP cable. Each twisted pair in the cable is wrapped with an aluminium foil tape to provide screening for the twisted pair as well as ensuring separation from other twisted pairs in the cable. After the individual screening of each twisted pair, all the four twisted pairs in the cable are then wrapped in another overall foil to enhance the performance of the cable. In some F/FTP cables, two twisted pairs are wrapped in a foil instead of the individual pair wrapping to reduce the overall diameter and the weight of the cable. The benefit of the smaller cable diameter is that the bundled Ethernet cables occupy less space in the containment, which has an additional benefit of increased airflow in underfloor installations. The reduction in the weight of the cable also means that the cable containment can be of lighter construction, which makes the handling of the cable easier.

Category 7A S/FTP

Category 7A S/FTP cables are screened and foiled cables. Each twisted pair in the cable is wrapped with an aluminium foil tape first to provide an individual screening for the twisted pair. After that, an overall braid screen is applied to all the four twisted pairs to conceal outside noise and prevent any risk of alien crosstalk. The difference between Category 7A S/FTP and Category 6A F/FTP cables is that Category 6A F/FTP cable contains an individual foil pair wrapping as well as overall foil wrapping whereas, Category 7A S/FTP cables are screened and foiled cables. Notwithstanding, the common element in most foiled shielded cables is the presence of a drain wire of ~24 AWG, which is placed on the overall foil tape inside the cable before the cables' jacketing material. The purpose of the drain wire is to provide an electrical connection between the foil and the connector shell. Also, to ease the termination of the cable shield. The schematic of Category 7A S/FTP construction is presented in figure 2.6.

Category 8 cable

Category 8 cables are in two different forms: Category 8.1 and 8.2. The minimum specified construction types for Category 8.1 and 8.2 are F/UTP and F/FTP or S/FTP. They are constructed to provide additional transmission bandwidth for copper connectivity by a factor of 4 when compared to the transmission bandwidth of Category 6A cables. That is, from 500 MHz (Category 6A) to 2000 MHz (Category 8). Category 8 was designed to support emerging IEEE 25 GBase-T, and 40 GBase-T for server-to-access-switch interconnect applications within a distance of 30 m. In practice, the two Category 8 cable types use other connector types such as TERA and ARJ45 connectors in addition to the RJ45 connector. The difference between the RJ45 and ARJ45 connectors is that the RJ45 connector uses a compensation method for controlling differential Near End Crosstalk (NEXT) while ARJ45 connector uses isolation method.

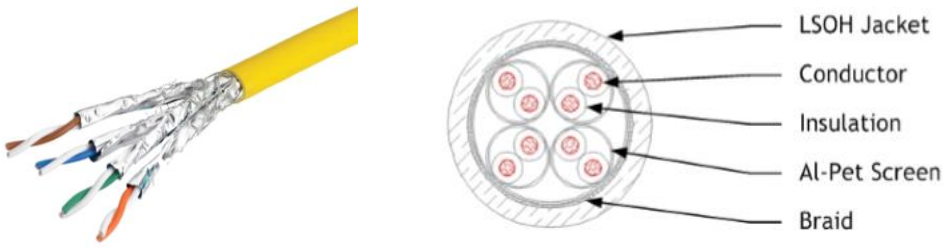

Figure 2.6: Sideways view (left) and cross section (right) of Cat 7A and 8 S/FTP cables [40]

2.2.2 Classification of Ethernet cables based on installation environments

Since the evolution of Category 5 cabling in 1991/1992, Ethernet cables have been referred to as structured cables based on their hierarchical structure within the network systems. The structure of the generic cabling system in a building or campus is defined in ISO 11801-6 [41]. Figure 2.7 shows a typical architecture of both premises and data centre cabling systems.

The premises cabling system consists of three subsystems:

(i) Campus Backbone Subsystem,

(ii) Building Backbone Subsystem and

(iii) Horizontal subsystem.

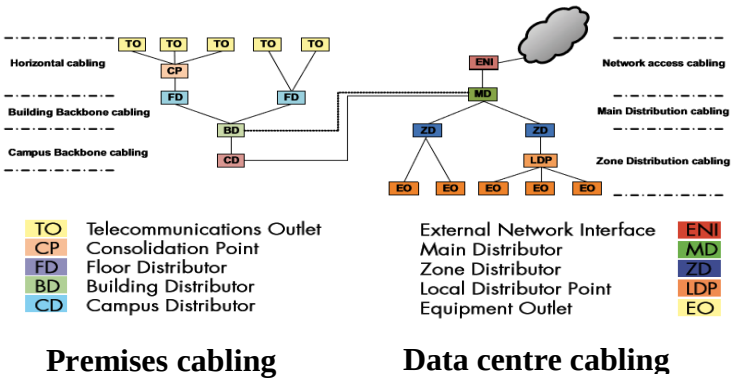

Figure 2.7: Architecture of premises and data center cabling systems [42]

(i) Campus backbone cabling subsystem

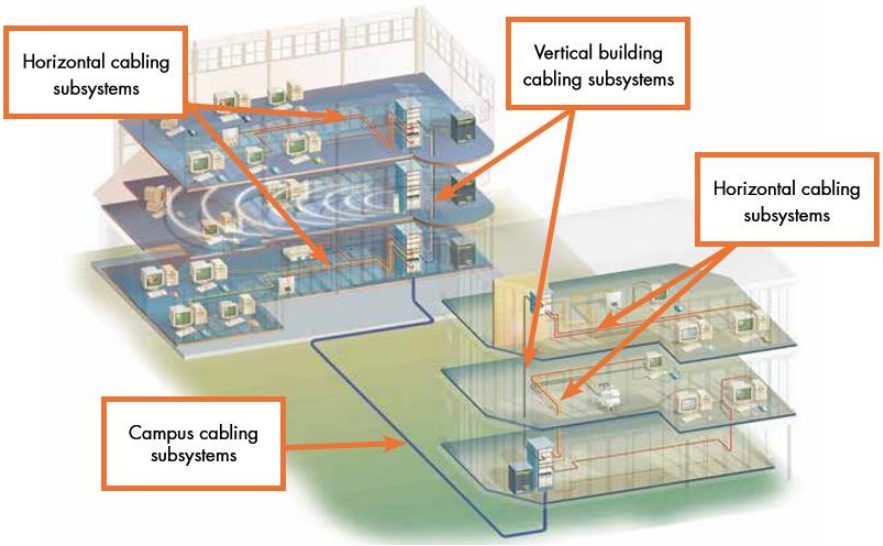

Figure 2.8: Architecture of premises cabling system [42]

The campus backbone cables link the main Campus Distributor (CD) to every Building Distributor (BD). Structured cabling infrastructure installed as inter-building cables (campus cabling subsystems) would typically be installed in some pathway systems such as conduits (plastic pipes) and be buried or installed on a floor raceway pathway system (underfloor) usually found between the building entrance facilities. If the distance between the buildings is more than 100 m, single mode or multimode fibre optic cables are usually installed.

Buried inter building backbone cables

Floor raceway pathway system

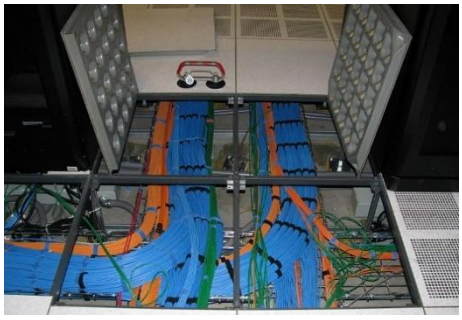

Figure 2.9: Inter-building backbone cables [42]

(ii) Building backbone cabling subsystem

The building backbone subsystem links the BD of a building to all the Floor Distributors (FD) in the same building. In other words, the intra-building backbone cabling infrastructure comprises of all the Ethernet cables between the telecommunications rooms, local distribution centres, and the entrance facilities. The intra-building backbone cables are usually in several bundles, installed in conduits (figure 2.10a) and wooden wall cabinets. They are also sometimes guarded with sleeves (figure 2.10b) upon entry to a floor to create fire barriers.

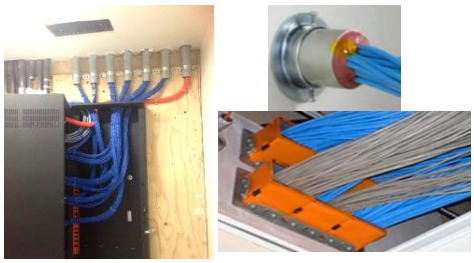

(a) (b)

Figure 2.10: Intra-building backbone cables (a -Vertical conduits) (b - Guarded CB)

(iii) Horizontal cabling subsystem.

Horizontal cables are usually in several bundles; linking the FD to all the Telecommunication Outlets (TO) of the concerned floor. As illustrated in figure 2.11, the horizontal subsystem comprises of both permanent links and communication channels. The permanent Link (PL) consists of a fixed horizontal cable and connecting hardware such as RJ45 connectors placed at the two ends of the PL. The RJ45 connectors are used for connecting the PL to both the patch panel and TO.

As shown in Figure 2.12, cables installed as PLs can be in several bundles, placed loosely on the wire basket trays and installed in the ceiling voids or be passed through wooden wall cabinets before branching off to individual TO.

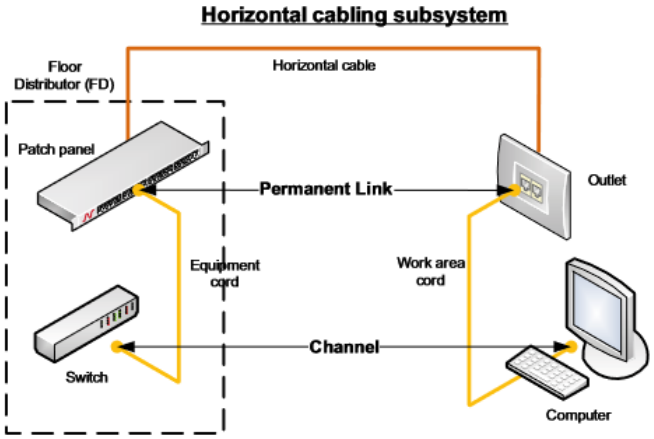

Figure 2.11: Design topology for the horizontal cabling subsystem [42]

Figure 2.12: Permanent links installed in the ceiling voids

The horizontal cabling subsystem requires active equipment such as an Ethernet switch, an equipment cord, a permanent link, and a work area cord to form a complete communication channel (figure 2.13). The equipment cords (patch cords) are non-permanent; they are cables with stranded

conductors. Whereas permanent links are permanently installed cables, and their copper conductors are usually solid cores. Although 1- 3 m length of work area cord or equipment patch cord are common for desktop applications, the physical length of a work area cord or equipment patch cord is restricted to ~10 m when connected to the network to maintain the specified 19 Ω DC loop resistance for a link. However, the maximum physical length of a channel as specified by the cabling standard is ≤100 m (328 feet) while that of the permanent link is limited to ≤ 90m (295 feet).

2.2.4 Classification of Ethernet cables based on application environments

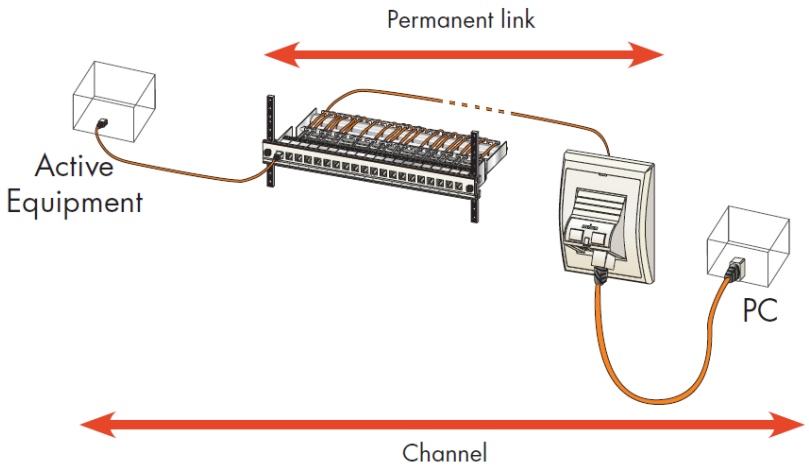

Figure 2.13: Communication paths between an Ethernet switch and a work area device [42]

Plenum rated (CMP) cables vs riser rated (CMR) cables

Based on application environments, Ethernet cables are also rated as a plenum (CMP) and riser (CMR) cables. Work area cords are usually CMR cables because they are installed in ventilated environments. However, horizontal cables can be either CMR or CMP. CMP cables are installed in restricted air circulation environments such as inside walls and ceilings above drop ceilings because their polymers have been designed to cope with the heat in such environments. Moreover, standard CMR cables are jacketed with PVC (Polyvinyl Chloride); PVC can burn quickly and release toxic fumes (Hydrochloric Acid and Dioxin) in the air. Plenum rated (CMP) cables are installed through the plenum air return spaces instead of the CMR cables to avoid circulation of toxic fumes in the environment. CMP rated cables are more expensive because of their high fire rating. Additionally, they are designed with fire-retardant jacketing material which can be a Low-Smoke Zero Halogen

(LSOH) PVC or FEP. CMP cable conductors are insulated with FEP while CMR cable conductors are insulated with High-Density Polyethylene (HDPE).

2.3 Balanced Twisted Pair Cabling Standards and Parameters

2.3.1 Balanced Twisted Pair Cabling Standards

Transmission performance of balanced twisted pair cabling is specified according to international standards to ensure structured cabling and connectivity and optimal performance in the different applications. This also ensures backward compatibility and interoperability of different components of the Ethernet channel. The standards are developed by various standards development committees such as the International Standard for Organization (ISO), International Electrotechnical Commission (IEC), International Telecommunication Union (ITU), American National Standards Institute (ANSI), Telecommunications Industry Association (TIA), Japanese Standards Association (JSA), Canadian Standards Association (CSA) (European Committee for Electrotechnical Standardization (CENELEC) and Institute of Electrical and Electronics Engineers (IEEE).

The IEEE is an Engineering application standard, which references the cabling standards [43] but ISO and IEC are International Standards. The standard bodies are responsible for the implementation of standards in the manufacturing and quality control procedures, as well as electrical distribution and related technologies such as telecommunications cabling system. The main task of the IEC is to promote and publish International Standards such as the Technical Specifications, Technical Reports, Publicly Available Specifications [44] and Guides. When appropriate, the IEC collaborates closely with the ISO to ensure International Standards fit together seamlessly [44]. An example of the ISO/IEC standard is the ISO/IEC 11801, an International Standard, used for generic cabling of customer premises and is used for both balanced copper cabling and optical fibre cabling. It reflects the requirements for commercial buildings, office premises, industrial premises, home; data centre, and distributed building services.

There are also subcommittee standards under the International Standards. For instance, the ISO/IEC JTC 1/SC 25 [45] is a standardisation subcommittee of the joint technical committee of the ISO and IEC, and responsible for developing and facilitating Standards within the interconnection of Information Technology equipment. Moreover, the standardisation of cables and

connectors is conducted within the technical committees of the IEC and ISO. The ISO/IEC JTC 1/SC 25 consist of three working groups and one task group. Each of the working groups is responsible for specific tasks in the development of standards within the field of the interconnection of information technology equipment. For instance, the purview of the ISO/IEC JTC 1/SC 25/WG 3 involves characterisation of cabling systems for customer premises, which include test procedures, and planning and installation guides.

ANSI is responsible for the standardisation, harmonisation and adoption of national standards within the United States. It represents the United States at ISO technical meeting. The North American end-users specify the TIA Standards, but the authorisation of the standards is by the ANSI. The activities of the TIA involve the development of cabling standards for structured cabling system design and installation and support of a wide range of applications as well as meeting the future high-speed requirements. For instance, the ANSI/TIA-568- C.0 - C.2 is a family of standards for Balanced Twisted-Pair Telecommunications Cabling and Components. The Standards provides requirements for 100 m length of Category 3, 5e, 6, and 6A balanced twisted-pair cabling and components and as well as field test procedures used in verifying the performance of installed cabling.

In addition to TIA and ISO, other known standards groups although region include JSA, CSA and CENELEC. The role of these regional cabling standards groups falls within their country's ISO technical advisory committees and their published standards concord with that of TIA and ISO. For instance, CELENEC EN50173-1 is the accepted standard for installing structured cabling systems in countries within the European Union.

2.3.2 Balanced Twisted Pair Cabling Parameters

The standards define the electrical and transmission parameters of each of the components of the data channel. Some of the parameters used for measuring the electrical characteristics of the channel include the DC resistance, electrical length and characteristic impedance while the parameters for measuring the transmission characteristics are categorised as in-channel and between channel parameters. Some of the parameters used for measuring the internal (in-channel) performance of the balanced twisted pair cables include Insertion Loss (IL), Return Loss (RL), Near End and Far-End Crosstalk (NEXT and FEXT) and Attenuation to Crosstalk Ratio (ACR). While, those used for the between channels performance or the impact of external influences on the signal passing through the cable include Power Sum Alien Near End Crosstalk (PSANEXT), Power Sum Alien Equal Level

Far-end Crosstalk (PSAELFEXT), Power Sum Alien Attenuation to Crosstalk Ratio (PSAACRF) among others. In addition, mode conversion parameters specified to understanding noise coupling mechanisms in balanced twisted-pair cabling [46] include Transverse Conversion Loss (TCL), Equal-Level Transverse Conversion Transfer Loss (ELTCTL), Longitudinal Conversion Loss (LCL) and Common-Mode to Differential-Mode Near-End Crosstalk (CDNEXT). Other parameters such as the High-Definition Time Domain Reflectometer (HDTDR) and High-Definition Time Domain Crosstalk (HDTDX) Analyzer are non-frequency-based; used in measuring the performance of the cable in the time domain. More explanation on the HDTDX and HDTDR is given in section 2.6.2.

(i) Parameters for measuring the electrical characteristics of twisted pair cables

DC resistance

The DC resistance, also known as ohmic resistance is a function of the conductor's cross-sectional area, its length and temperature (2.3.1).

Figure 2.14: Showing the length and area of a copper conductor

$$R = \frac{\rho(T)A}{l} \qquad (2.3.1)$$

Where ρ is the resistivity of copper, which is a function of temperature. A is the area (wire gauge) of the copper and l is the length of the copper (figure 2.14). The DC resistance of a conductor is also a function of the conductor material. The conductors of balanced twisted pair cables are mostly made of copper except in rare cases where copper-clad aluminium conductors are used. Given the same conductor diameter, aluminium has 60 % of the conductivity of copper [47], which makes its resistance higher than that of copper. The DC loop resistance for a 100m length of any twisted pair is specified to be ~19 Ω while an unbalance resistance between any twisted pair is specified to be $\leq$ 5 %, both measured and corrected to a temperature of 20^0C [48]. Moreover, because attenuation is a function of the DC loop resistance, the length of the twisted pair cable is specified to be ~100 m.

Length of the balanced twisted pair cable

The length of the balanced twisted pair cable is defined in three forms, which include the sheath length, physical length and electrical length. The sheath length of the cable is the length commonly found on the outside jacket of the cable while the physical length is the length of the copper conductors. The physical length is slightly longer than the sheath length due to the twisting of the copper conductors. Moreover, the electrical length corresponds to the number of wavelengths $\lambda = v_p/f$ at a given frequency. To measure the electrical length of a cable using a field tester, a pulse signal is transmitted into the cable by the field tester, and when the pulse reaches the far end of the cable, it reflects. By measuring the time taken by the pulse to travel and reflect (propagation delay) and knowing the Nominal Velocity of Propagation (signal propagation speed) of the conductor insulation, the cable tester determines the electrical length of the cable (2.3.2).

$$Electrical\ length = propagation\ speed * \ propagation\ delay \qquad (2.3.2)$$

Nominal Velocity of Propagation

Assuming frequency independence, the Nominal Velocity of Propagation (NVP) or velocity of propagation (v_p) measures how fast the signal travels on a twisted pair relative to the speed of light in a vacuum.

$$Propagation\ speed = (NVP)c \qquad (2.3.3)$$

The typical NVP value for the unshielded twisted cables maybe around 69 %. Sometimes, the NVP value is expressed as the Velocity Factor (0.69) [49]. The v_p of signal in media other than vacuum is characterised by the relative permittivity (ε_r) and permeability (μ_r) of the media (2.3.4).

$$v_p = \frac{c}{\sqrt{LC}} \qquad = \frac{c}{\sqrt{\mu_r \varepsilon_r}} \qquad (2.3.4)$$

For most materials, μ_r is 1 $\qquad \therefore v_p = \frac{c}{\sqrt{\varepsilon_r}} \qquad VF = \frac{1}{\sqrt{\varepsilon_r}}$ (2.3.5)

Propagation delay

Propagation delay (t_p) or phase delay, which is a measure of the time taken by a signal to propagate from one end of the twisted pair to the other varies slightly among the four twisted pairs in a cable due to the differences in the twist rate of the twisted pairs and the v_p of signals on the twisted pairs.

$$Electrical\ length\ (l) = physical\ length \times \sqrt{\varepsilon_r} \quad \text{(m)} \qquad (2.3.6)$$

From (2.3.5) and (2.3.6), $t_p = \frac{l\sqrt{\varepsilon_r}}{c}$ (ns) (2.3.7)

From (2.3.5) and (2.3.60, it can be observed that the change in the value of ε_r is a contributing factor to the change in the speed and electrical path of the propagating signal. Also, from (2.3.7), variation in the electrical length of the twisted pairs or the dielectric permittivity of the propagating medium will cause the t_p of the signal to vary. The typical value of the t_p for a 100 m length (l) of a Category 6A cable, having conductor insulation with $\varepsilon_r = 2.1$ will be ~ 483 ns. Any variation in the t_p of a signal on the twisted pairs will cause the delay skew of the cable to change; a scenario defined as the difference in propagation delay between the shortest pair and any pair in the same cable.

Characteristic impedance

Characteristic impedance (Z_0) of the twisted pair cable is a function of the capacitance and inductance distributed along the length of a twisted pair. The impedance which decreases as frequency increases is due to capacitive reactance ($\frac{1}{2\pi fC}$), and that which increases at high frequency is due to inductive reactance ($2\pi fL$). The following parameters are used to determine the precise impedance of a twisted pair: the ε_r of the conductor insulating material, the diameter of copper conductor, the diameter of the insulation, the centring of the copper within the insulation and the precision at which the two insulated wires are twisted together [50]. If any or all of these factors vary due to a thermal variation on the cable, the impedance will vary along the length of the twisted pair.

(ii) Parameters for measuring the transmission characteristics of twisted pair cables

Attenuation or Insertion Loss

Attenuation or Insertion Loss (IL) is a measure of the loss of the signal strength during transmission over a channel or permanent link. IL is affected by the material and geometry of the twisted pair through impedance mismatches, skin effect, conductor and dielectric loss. The lower the IL, the better the strength of the received signal and the higher the information carrying capacity of the channel. Given this, the strength of the received signal must be sufficiently high to be detected and interpreted by the electronic circuitry in the receiver. In general, IL is defined according to (2.3.8).

$$IL = -10 * \log\left(\frac{P_{out}}{P_{in}}\right) \qquad \text{(dB/m)} \qquad (2.3.8)$$

Where P_{out} is the power delivered to a load and P_{in} is the power transmitted? Attenuation can also be defined as 20*Log |T|, Where T is the transmission coefficient.

Return loss and Voltage Standing Wave Ratio

Return Loss (RL) and Voltage Standing Wave Ratio (VSWR) are the two parameters for measuring the amount of reflection on a Transmission Line (TL) such as a twisted pair. RL is defined as the ratio of the incident power to the reflected power. $RL = 10 \log \frac{P^+}{P^-}$. where P^+ is the reflected power and P^- is the incident power. The magnitude of the RL can also be expressed as RL = 20*log |Γ|. Where Γ is the reflection coefficient. The better the impedance matching on a communication link, the lower the reflected energy and the higher the return loss. The major factors affecting the RL performance of a channel or permanent link are the impedance mismatches and discontinuities. Impedance mismatches are from variations in the material and construction of the link, whereas discontinuities occur at the mated points of the plugs or jacks and within the plug or jack connection itself. Discontinuities also occur due to the sharp bending of the cable and kinks in the cable. The VSWR characterises the impedance matching of the load at the end of a TL to the characteristic impedance (Z_o) of the TL. The characterisation is necessary because matched impedance is required to minimise signal overshoots and undershoots caused by reflections at the end of the TL; also, to ensure maximum power transfer to the load.

Analysis of a basic transmission line

From figure 2.15, consider two parallel conductors of a TL with infinite lengths, by applying a sinusoidal voltage (V_s) across the conductors of the pair, equal and opposite currents (I) flow forever in the conductors. The current flowing creates a forward voltage wave, which travels along the conductors. Based on the sinusoidal nature of the voltage wave, it consists of both magnitude and phase. The ratio of the voltage (V_{out}) across the conductors to the current (I_{out}) flowing through the conductors (V_{out} /I_{out}), defines the Z_o of the conductor pair. The magnitude of V_{out} is determined by a series combination of the source impedance (z_s) and the Z_o as a voltage divider (2.3.9).

$$V_{out} = V_s * \left(\frac{Z_0}{z_s + Z_0}\right) \qquad (2.3.9)$$

Also, suppose the V_s is placed across a perfect lossless TL with a finite length and uniform impedance from source to load, all the power transferred through the line is fully absorbed by the load because there is no mismatch on the line and at the end of the line. Therefore, there is no reflection of the signal on the line.

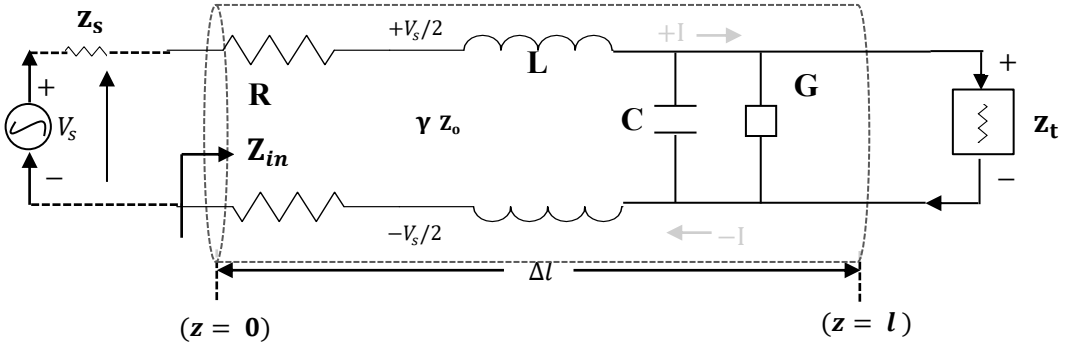

Figure 2.15: Showing a unit length of a transmission line

In this case, the source impedance (z_s) is equal to Z_o. Also, Z_o is equal to the termination impedance (z_t). The impedance at any point on the line looking towards the load is the input impedance (Z_{in}); Such that Z_{in} = Z_o. The reflection coefficient, Γ = 0 (2.3.10) and the VSWR = 1 (2.3.11).

$$\Gamma = \frac{z_s - Z_o}{z_s + Z_o}, \qquad \Gamma = \frac{z_t - Z_o}{z_t + Z_o}, \qquad \Gamma = \frac{100-100}{100+100} \qquad = 0 \qquad (2.3.10)$$

$$\text{VSWR} = \frac{V_{max}}{V_{min}} = \frac{I_{max}}{I_{min}} = \frac{1+|\Gamma|}{1-|\Gamma|} = 1 \qquad (2.3.11)$$

Assuming the end of the TL is short-circuited; such that $z_t = 0$, but $z_s = Z_o$, the source sees Z_o initially and voltage wave with amplitude $V_s/2$, propagating towards the load. However, when the voltage wave reaches the far end of the line and sees a short circuit, a voltage wave of the opposite polarity propagates back towards the source, cancelling the original wave. In this case, from (2.3.10) and (2.3.11), the reflection coefficient of the short-circuited line, $\Gamma = -1$, and the VSWR = ∞. Also, the short-circuit impedance (Z_{sc}) is according to (2.3.12) [51].

$$Z_{sc} = Z_{in}|_{Z_{t=0}} = jZ_o \tan(\beta length) \qquad (2.3.12)$$

Where β is the phase constant and $length$ is the electrical distance between the source and the load.

Moreover, if the end of the line is an open circuit; such that $z_t = \infty$, a reflected signal of equal magnitude and same polarity as the original voltage propagates backwards towards the source, adding to the original voltage. In this case, the reflection coefficient of the open-circuited line, Γ = +1. The VSWR is ∞ and the open-circuit impedance (Z_{oc}) is according to 2.3.13 [51].

$$Z_{oc} = \lim_{z_t \to \infty} Z_{in} = \frac{Z_o}{jtan\,\beta l} = -jZ_o \cot(\beta length) \qquad (2.3.13)$$

In practical transmission lines, z_s and z_t are complex; also different from Z_o. In this case, the magnitude of the pulse reflections will be according to the source (Γ_s) and load (Γ_L) reflection coefficients (2.3.14) and (2.3.15).

$$\Gamma_s = \frac{Z_s - Z_o}{Z_s + Z_o} \qquad (2.3.14)$$

$$\Gamma_L = \frac{Z_L - Z_o}{Z_L + Z_o} \qquad (2.3.15)$$

Furthermore, in a case where only one mismatch occurs at the termination end of the TL due to the complex or an arbitrary load attached to the end of the line, the relationship between the Z_{in}, Z_o and z_t is given according to (2.3.16) [52].

$$Z_{in} = Z_o \left[\frac{z_t + Z_o \tanh(\beta length)}{Z_o + z_t \tanh(\beta length)}\right] \quad (2.3.16)$$

In addition, when z_t is not equal to the Z_o of the line, the line may appear like a resonant circuit or reactive circuit to the generator input, depending on the electrical length of the line. Consequently, the Z_{in} of the line will vary as a function of the electrical length and the frequency of the propagating signal. In this case, the line is said to be resonant.

Near End and Far-End Crosstalk

Crosstalk in a multipair Ethernet cabling can be measured as a Near-End Crosstalk (NEXT) or Far-End Crosstalk (FEXT). The portion of the transmitted signal that couples back into the received signal at the near end of the transceiver is termed NEXT (Figure 2.16 a). However, if the source of the transmitted signal and the point of the crosstalk measurement are located at the far end of the line, then, the crosstalk attenuation measured is referred to as FEXT.

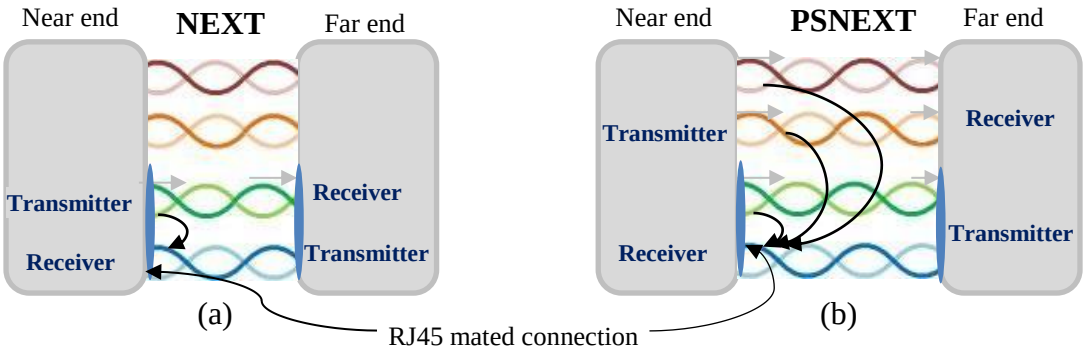

Figure 2.16: (a) NEXT and (b) PSNEXT in a twisted pair cable

NEXT is measured in dB but calculated as the difference in amplitude between a transmitted signal on one pair and the crosstalk received on one of the other twisted pairs in the same cable. Power Sum Near-End Crosstalk (PS-NEXT) is the summation of the individual NEXT effects on one

twisted pair from the other three twisted pairs in the same cable (Figure 2.16 b). Higher values of NEXT and PS-NEXT correspond to less crosstalk and better cabling performance.

Attenuation to Crosstalk Ratio

Attenuation-to-Crosstalk-Ratio (ACR) represents the signal to noise ratio for the balanced twisted pair cable. It is one of the key parameters, for measuring the transmission performance of a cabling system. ACR value is calculated as the difference in values between NEXT and attenuation of the signal being transmitted. A higher value of the ACR means that the received signal is more than the crosstalk signal from one pair. Similarly, a higher Power Sum Attenuation-to-Crosstalk-Ratio (PSACR) value means that the received signal is much larger than the combination of the crosstalk from the other three twisted pairs in the same cable.

(iii) Parameters for measuring the balance of twisted pair cables

Transverse Conversion Loss and Equal Level Transverse Conversion Transfer Loss

Transverse Conversion Loss (TCL) and Equal Level Transverse Conversion Transfer Loss (ELTCTL) are both pair balance parameters for measuring the amount of differential-mode signal converted to a common mode signal. That is, they are both measures of mode conversion within a twisted pair, but TCL measures the degree of unbalance at the near end of the cable [46, 53] while the mode conversion at the far end of a link is quantified using the ELTCTL. The two parameters are particularly important for evaluating the performance of communication links installed in industrial areas because of the high level of noise caused by industrial equipment. Also, because of the problems that EMI causes in networking equipment. The TCL value is calculated as the ratio (in dB) of a common-mode voltage (V_{cm}) measured on a twisted pair relative to a differential-mode voltage (V_{dm}) applied to the same end of the twisted pair (2.3.17). The calculated value indicates how well the impedances of the paired conductors are balanced.

$$\mathrm{TCL} = 20 \log_{10} \left(\frac{V_{cm}}{V_{dm}}\right) \quad \text{(dB)} \qquad (2.3.17)$$

Table 2.2 illustrates how TCL values are calculated. For illustration purpose, a common mode voltage is induced on each conductor of a twisted pair relative to ground by nearby Electromagnetic fields. Assuming the induced common mode voltage (V_{cm}) is 1V, a TCL value of 60 dB means that 0.1 % (1mV) of the induced 1V is converted to differential mode voltage while a TCL value of 20 dB means that 10 % (100mV) of the induced voltage is converted to differential mode voltage. Given this, a high TCL value means that the impedances of the conductors relative to the ground are almost equal, which corresponds to a better noise immunity of the cable and lower emissions from the cable. Hence, a higher TCL value of 40 dB should achieve a better-twisted pair balance [46].

Table 2.2: Calculated differential mode noise voltage (V_{dm}) for different TCL values

TCL (dB)	$V_{dm}\ (mV)$	$V_{cm}\ (V)$
20	100	1
30	31.6	1
40	10	1
50	3.16	1
60	1	1

Longitudinal Conversion Loss

The Longitudinal Conversion Loss ***(***LCL) of a cable system is a measure of the amount of common mode signal that is converted into an unwanted differential mode signal at the interface of a cabling system. It is also a measure of the quality of the cable construction or the physical balance of a twisted pair cable. LCL is measured according to figure 2.17 but calculated as the ratio (in dB) of a common-mode signal (E_L) applied on a twisted pair relative to an unwanted differential-mode voltage (V_T) measured at the interface of the system (2.3.18) [54]. The lower the LCL value, the higher the level of the interference that is created.

$$\mathrm{LCL} = 20\log_{10}\left|\frac{E_L}{V_T}\right| \quad \text{(dB)} \qquad (2.3.18)$$

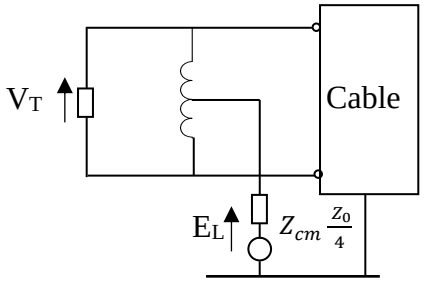

Figure 2.17: LCL at the interface of a cabling system [54]

Common-Mode to Differential-Mode Near-End Crosstalk

Common-Mode to Differential-Mode Near-End Crosstalk (CDNEXT) is the difference in amplitude between the common mode signal generated on one twisted pair and the differential mode signal measured on a different twisted pair at the same end of the cable. Higher CDNEXT value corresponds to a better noise immunity of the cabling system. According to [55], the main source of mode conversion for balanced twisted pair cabling is the mated point of the 8-pin RJ45 modular plug and jack. This is because the blades of the plug are inherently unbalanced, which can result in a significant amount of mode conversion. Additionally, the split pair pins have the largest distance between its conductors and may, therefore, have the largest difference in the crosstalk received. Since CDNEXT occurs mostly at the termination point of the cabling system, it is a measure of the quality of the connector design and the efficiency of the termination.

2.3.3 Twisted pair as a balanced transmission line

An ideal twisted pair copper cable is referred to as a balanced twisted pair cable because each pair in the cable is a differential line; the two insulated conductors of a pair have equal impedances along their length, to ground and other circuits. The twisting of the wire pairs allows the opposing electromagnetic fields in the two adjacent half-twists to cancel each other [56]. The tighter the twist of the conductor pairs, the more effective the cancellation of the field induction and the higher the data rate supported by the cables [57]. The uniform twisting of the wires ensures a homogeneous distribution of the unit capacitances along the length of the cable, which also enables high common-mode rejection. Balanced twisted cables are designed to operate using differential mode (DM) signals in a balanced transmission circuit. Differential mode means that signal flows in one direction on a conductor of a pair and reverses direction along the other conductor. It also implies that the applied voltage (+V and -V) splits evenly on the twisted pair due to the symmetrical nature of both conductors in the twisted pair unlike the common mode signal, which flows equally in the same direction along each conductor in the cable, including the cable shield if it is present. Common mode signals on a cable do generate a net magnetic field around the cable. According to [58], a small common mode current can result in large emitted signals. The benefit of representing a differential signal by the difference of voltage between a ground-isolated twisted pair is that the effect of capacitive and inductive coupling on the signal being transmitted is minimal. Also, Electromagnetic fields from outside sources cause voltages that have the same amplitudes and

polarities (common-mode voltages) on each wire in the pair, leaving the differential signal unchanged (figure 2.18).

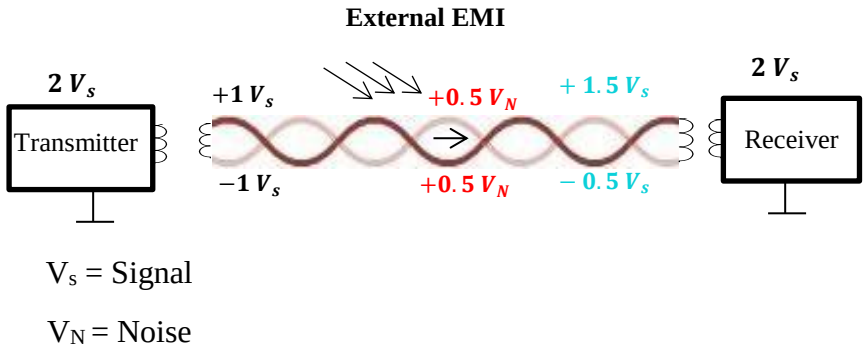

Figure 2.18: Illustrating the balanced transmission of Ethernet signal in an EMI environment

2.4 Factors affecting the performance of remote powered Ethernet channels

The quality of the signal being transmitted over the PoE channel depends on the performance of all the components of the channel and the environment in which the cables are deployed. That is, good performance of the Ethernet cable dielectrics, the balance of the cables and connecting hardware are necessary to achieve high data rate, especially with the increasing use of short electrical pulses in data transmission. If the balance of the cables and connectors (which serve as interfaces to the network) is compromised, the electrical signal being transmitted over the Ethernet can radiate and can be distorted. The distortion of the electrical signal is due to attenuation, delay, reflections and noise while radiation is caused by ringing effects [59] and the imbalances in the transmission circuit. Moreover, the degradation of Ethernet signal on PoE channels arises mainly from four general factors: overall temperature and thermal variation, handling effects and installation conditions. Given this, the focus of this section is to appraise the main factors affecting the performance of remote powered Ethernet channels. The factors contributing to the heat generation in powered balanced twisted pair cables are discussed first, followed by the analysis of the performance of high powered PoE links which are bundled in several dozens and are subject to thermal variation when passing through walls, ceiling spaces, riser shafts, and so on. In these types of installation condition, the temperature on different portions of the cable can vary. Hence, the potential adverse effect of thermal variation on Ethernet signal integrity is an area of concern. The

adverse effects of such installation conditions on channel performance are discussed by relating the possible changes in the primary line constants to the transmission parameters of the cable.

2.4.1 Factors contributing to the heat generation in powered twisted pair cables

Theoretically, the amount of power loss in form of heat generated in the cable is proportional to the square of the current passing through the cable and the resistance of the cable (2.4.1). Thus, the higher the current passing through the cable, the greater the heat generated.

$$Power\ loss = I^2R \qquad \text{(J/sec)} \qquad (2.4.1)$$

Additional to the high thermal loadings on the cable, other factors contributing to the heat rise in the cable include the number of energised twisted conductors, the size of the cable bundle, type of installation condition, type of pathway (cable tray or conduit) system, ambient operating temperature, fire stopping, the construction of the cable such as the conductor and its insulating material, screening, copper conductor and its insulation diameter (Figure 2.19).

Power Level

The amount of current flowing through the cable.

Other factors

- Environmental factors
- Number of pairs used
- Quality of the insulating materials
- Processing method employed
- Cable construction
- Cable bundle size
- Installation conditions
- Installation practice

Figure 2.19: Factors affecting the heat generation and dissipation in bundled Ethernet cables

The heat generated by the unshielded cables is higher when compared with that from shielded cables due to the smaller conductor size and the lack of screening, which could have helped with

the dissipation of the heat generated [44]. The lower categories of cable (unshielded cables) have copper with smaller conductor sizes. Therefore, their DC loop resistance per unit length is higher than that of the higher categories (shielded cables). As a result of the high current transmission in the cables, the conductors heat up and dissipate the heat by convection, radiation, and conduction. Depending on the type of insulating materials and cable jacketing materials, the heat dissipation is slightly different for different types of cable.

Another component which helps with the heat dissipation is the crossweb or filler. The compounds used for the fillers turn the fillers to a heat sink which, helps with uniform heat dissipation to the surface of the cable. Furthermore, insulating material with high dielectric constant and dielectric loss also contributes to the heat generation in the cable, unlike the insulating material with low loss, which provides reduced attenuation and heating in a circuit.

In a typical installation where cables exist in several bundles, they experience the proximity of heat sources, and that could lead to an excessive temperature rise within the cable itself and surrounding cables. Heat dissipation is reduced in such installation conditions, due to the lack of proper airflow. According to the study presented in [31], excessive heat within the cable bundle (CB) contributes to the heat-ageing of the cable polymers. Larger CBs which are fully insulated and installed under the floor or inside walls may generate a temperature rise that is high due to reduced heat dissipation and lack of airflow in the environment.

High ambient temperature also limits the current carrying capability of the wire by restricting the amount of self-healing that can be accommodated before the maximum temperature rating of the insulation is reached. Ideally, copper conducts heat at a high temperature before melting, but long before it reaches the melting point, the insulators would have melted and caused a short circuit. According to [47], the temperature at which the insulation degrades is often more limiting than any effects of temperature on the conductor.

2.4.2 Effects of temperature on the performance of balanced twisted pair cables

The degradation of the signal passing through the PoE channel mainly arises from the changes in the material properties and deformation of the twisted pair geometry through impedance mismatches, skin effect, conductor and dielectric loss. Moreover, the cables may be subjected to high temperature and thermal variation and hence fail to transmit the whole signal or part of the

signal from source to load as intended. In this case, the loss of the signal strength on the channel is termed attenuation or insertion loss. Attenuation increases due to the effect of temperature, and this causes the bandwidth of the cable to reduce, leading to the lower achievable data rate. According to [60], the IEEE 802.3ch has been working on a 1.0 dB improvement in the attenuation margin, which is believed to be critical in ensuring a 10^{-12} bit error ratio, which will be needed to achieve reliable operation of multi-gigabit Ethernet. Attenuation is a function of multiple parameters. From (2.7.3), attenuation depends independently on the resistance (R), characteristic impedance (Z_0), and conductance (G) of the twisted pair at various temperatures and frequencies.

A. Attenuation (α) due to conductor loss (αc)

Based on the application of twisted pair cables in remote powering operations, attenuation due to conductor loss increases with an increase in the resistance (R) of the cable. From the approximation of αc stated in (2.4.2), the total resistance of the cable comprises of both the DC and AC resistance components (R_{dc} and R_{ac}).

$$\alpha c = \frac{R}{2Z_0} \qquad (2.4.2)$$

The R_{dc} (DC resistance) component represents the resistance to the flow of the current passing through the entire bulk of the copper conductor while the R_{ac} (AC resistance) component represents the resistance to the current flowing near the surface of the copper conductor, caused by the skin effect. The R_{dc} is a function of temperature while R_{ac} is a function of frequency and temperature.

As the cable temperature rises above ambient, R_{dc} increases, leading to an increase in the power dissipation (attenuation) on the cable (figure 2.20). The amount of the signal power loss depends on the temperature, which also depends on the type of conductor and the resistance of the conductor. The most obvious of these is that real conductors are not perfect conductors. They have a non-zero resistivity, which causes some signal power to be dissipated and lost, with temperature on the cable. For instance, the resistivity of copper at room temperature is 1.72×10^{-8} Ωm while that of aluminium is 2.65×10^{-8} Ωm. At any given frequency and temperature, attenuation of any cable with copper conductors is smaller than the attenuation of the identical cable with Copper-Clad Aluminium (CCA) conductors because aluminium generates more heat than the pure copper conductor.

The electrical conductivity of copper conductor decreases at elevated temperatures but increases with an increase in frequency. At a steady-state of heating where the diameter of the copper remains the same, a marked increase in the low-frequency loss is due to low conductivity, which is due to

the wires having a much higher DC resistance. However, at higher frequencies, attenuation increases significantly due to the AC resistance of the copper conductors because of skin effects. This is because the skin depth of the copper conductor substantially reduces at high frequencies, which causes the effective cross-section of the wire to decrease. The smaller the effective cross-section of the wire, the better the conductivity. Given this, the conductivity of copper increases with an increasing frequency. However, above 100 MHz, conductor losses are proportional to the square root of signal frequency. Moreover, further degradation of cable performance can be expected when the skin depth of the copper conductor reaches the surface roughness of the conductors. This scenario increases the path for currents, and effectively reduces the surface conductivity of conductors and increases attenuation.

Coupled with the AC resistance of the copper conductors, which increases due to skin effects, the placement of a screen in the proximity of a twisted pair carrying electrical signal results in eddy current induction, which causes the loss of the propagating signals [50, 84]. The total unit resistance of the shielded cable represents all conductor related losses in the cable, including losses in the screen (due to eddy currents) [50]. For the unshielded twisted pair cable, losses are because of the skin effect and proximity effect only. No eddy current losses are considered as there is no shield present in the cable.

B. Attenuation (α) due to dielectric loss (αd)

The temperature of a material has a significant effect on the dielectric properties. Generally, dielectric loss increases with increasing temperature at low frequencies due to the ionic conductance but decreases with increasing temperature at high frequencies due to free-water dispersion [61]. According to [62], the dielectric loss of twisted pair is mainly derived from conduction loss caused by DC divulge current in insulation, interlayer polarisation loss caused by space charge, loss caused by a partial discharge under high electric field and, relaxation polarisation loss caused by dipole orientation. Furthermore, all real dielectrics consist of atoms with electrons. The electrons are tightly bound to the nuclei, but they still move a little when the electric field is applied to it. At low frequency (100 Hz to 10 kHz), dielectric loss, mainly derived from conduction is minimal. Reference [62], calculated tanδ as follows:

$$tan\delta = \frac{\sigma}{\omega \varepsilon_r} \qquad (2.4.3)$$

From (2.4.3), it is shown that the loss tangent (tanδ) decreases, with the increase in the low-frequency region. However, when the electric field in a dielectric is sufficiently large, it begins to pull electrons completely out of the molecules, and the dielectric becomes conductive. The tanδ of a dielectric material describes the electrical conductivity of the dielectric. A higher tanδ means that the dielectric material is more conductive and that its insulation resistance has decreased, which means that the temperature of the material will increase as a result of the current flowing through the material, which also increases the dielectric losses. Moreover, the less obvious problem is that the dielectric material between the conductors will also tend to 'leak' slightly due to the reduction in insulation resistance of the cable dielectrics. The conductance (G) represents the current leakage through the insulation between the conductors.

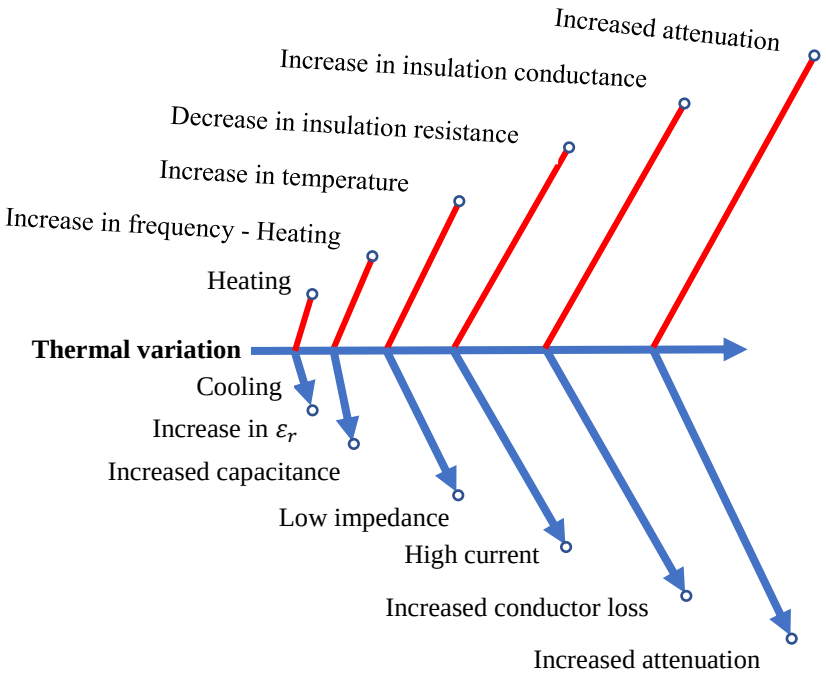

Figure 2.20: Causality of the attenuation of Ethernet signal due to thermal variation

Apart from the contributions of the resistance (R) and conductance (G) to attenuation, another factor influencing attenuation is the characteristic impedance (Z_0) of the twisted pair.

$$\alpha d = \frac{GZ_0}{2} \qquad (2.4.4)$$

The impact of the increase in Z_0 due to the changes in the dielectric constant of dielectric materials is discussed in the next section.

2.4.3 Effects of thermal variation on the performance of twisted pair cable

Most balanced twisted cables used in remote powering applications are designed with conductors and insulation of uniform sizes and materials. Also, the twisting of the insulated conductors is assumed to be uniform over the entire length of the twisted pairs in the cable. For illustration purpose, a uniform cable shown in figure 2.21 is the one with uniform materials and geometry over its entire length. Also, changes in the conductor dimensions are expected to occur due to the mechanical effects arising from temperature fluctuations.

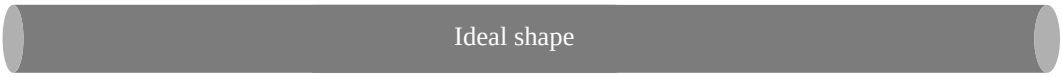

Figure 2.21: Ideal cable segment of a permanent link without geometrical deformation

However, the peculiarity of the temperature rise from PoE power levels, and the cyclic temperature variations from time-dependent power demand as well as the installation condition can lead to the geometric distortion and dynamic behaviour of the cable. For poorly manufactured cables, the twisted pairs often flex and move inside the jacketing material when under temperature fluctuations. Also, the friction between the shield and conductors of the shielded cables may generate heat, which contributes to the reduction in the flex life of the cable. As explained in [63], the resistance of copper conductors and the foil shield increases as the conductors and the foil flex under thermal cycling, and that contributes to the insertion loss of the cable. In addition, the higher the friction between the conductors and the foil shield, the more brittle the conductors and the foil shield become.

Furthermore, in an installation environment where larger cable bundles pass through insulated walls, ceilings and are operating at 100 watts DC power level; they are subject to localised heating that is likely to change the dimension of the twisted pair and the composition of the conductor insulation at that various location on the cable (figure 2.22). In this case, reflection (see R_1 to R_4 in figure 2.22) will occur at those various locations because of the changes in the characteristic impedance (see Z_1 to Z_4 in figure 2.22) of the cable.

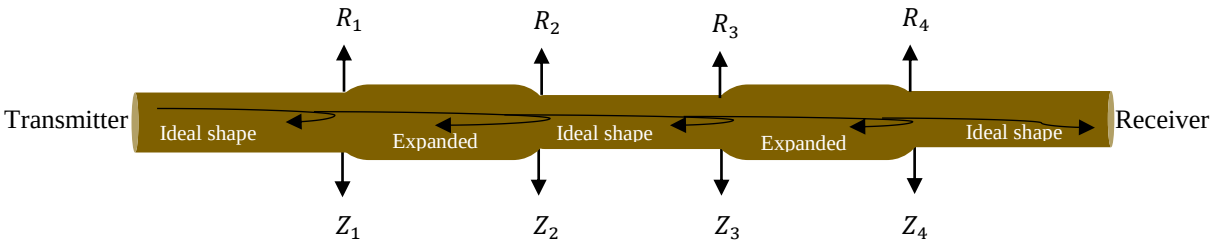

(a) Showing a PL with segments deformation due to thermal variation (heating)

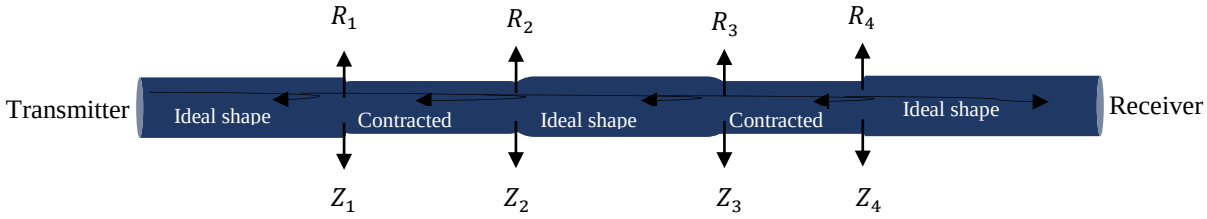

(b) Showing a PL with segments deformation due to thermal variation (cooling)

Figure 2.22: Deformation of cable segments due to the effect of thermal variation

Moreover, the characteristic impedance of a low loss transmission line depends on inductance and capacitance. The mutual capacitance of a twisted pair is specified in the cable's datasheet, but the mutual capacitance measured in practice depends on the dielectric constant of the insulator between the two conductors and the proximity of the conductors. If the heating of the cable increases the separation distance between the conductors of the twisted pairs, the capacitance (2.7.0) of the twisted pairs will decrease and vice versa. Moreover, if the dielectric constant of the conductor insulation around the insulated portions of the cable changes differently from every other part of the cable segment that is ventilated, the capacitance of the cable will vary. Then, the characteristic impedance of the cable will vary because of the non-uniformity of the twisted pairs. Moreover, any changes to the characteristic impedance result in variations in other transmission parameters of the channel that are not measured but determined indirectly from the impedance. For instance, attenuation and return loss are sometimes determined from the impedance.

Furthermore, the conductor diameter of the shielded cables is usually made bigger to reduce attenuation. However, if the conductor diameter contracts due to the cooling (during the winter period) of the cable, the overall diameter of the conductor insulation will decrease. The decrease in the overall diameter of the conductor insulation as a consequence of thermal variation will cause the ε_r of the conductor insulation to increase, which will cause the capacitance of the cable to

increase (2.7.0), and the impedance to decrease. At high frequencies, the capacitance of the cable causes a significant current to be drawn [64]. Moreover, low impedance implies high current, which increases the cable attenuation.

Furthermore, from (2.3.6), if the electrical length of the transmission-line increases due to an increase in the ε_r of the conductor insulation, the time taken for the signal to propagate through the cable will increase. Moreover, due to the heating of the cable, the length of the conductor is expected to increase because the resistance (R) of the conductor depends on temperature. If the capacitance (C) and resistance (R) of the twisted pair increase, the effective speed of the cable will be limited by the RC delay.

2.4.4 A brief review of Insertion Loss Deviation

In addition to the previously described losses, there could also be an Insertion Loss Deviation (ILD), which is caused by component mismatches. Figure 2.23 illustrates a channel with different components such as patch cords, a cable segment and some connectors.

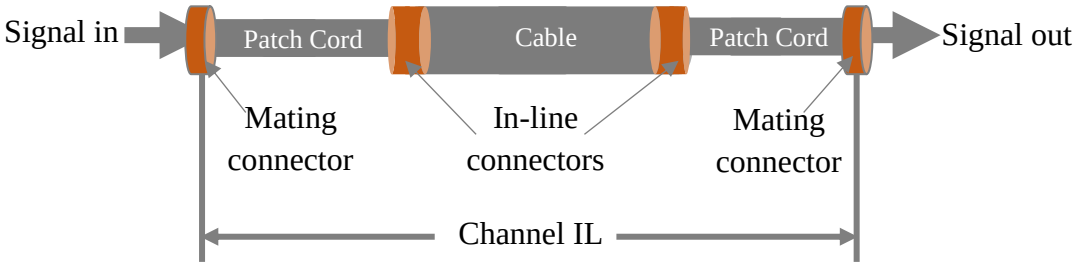

Figure 2.23: Illustrating the loss of the signal power between the input and output of a channel

Typically, the nominal characteristic impedance of the connectors, patch cords and cables used in Ethernet channels is specified to be ~ 100 Ω ($\pm$ 15). In practice, however, the value can be slightly different because the channel components are manufactured independently, and there is no guarantee that manufacturers' tolerances will be the same. Additionally, installation variances, such as pigtail connections at every termination point on the channel create a non-homogenous transmission channel as a result of the pigtail inductance and capacitance [65, 83]. Any variation in the characteristic impedance of the cable segment will affect the return loss performance of the link. Another source of return loss is the reflections from inside the link, mainly from the connectors if the connections to them are malformed. Also, according to [66], the major contributor to ILD at

high frequencies is the connector impedance mismatch. This is because among the eight pins of the RJ45 modular connector, pin 3-6, which are the split pair pins, have a higher impedance mismatch because the pins in the termination plug are further apart. Thus, if a mismatch occurs at the mating of the RJ45 plug and jack, a proportion of the incident signal will be reflected towards the transmitter while the remainder of the signal will propagate through the link. The reflected signal contributes to the loss of the channel, and it is termed mismatch loss. Any further imperfections along the link such as discontinuities at other in-line connectors will cause part of the reflected signal to be re-reflected to mix in with the original signal. According to [87], the re-reflected signal is called ILD.

The total Insertion Loss (IL) of a channel was evaluated in [87], using (2.4.5).

Channel insertion loss (IL_{CH}) = $\Sigma_{i=1}^{n} IL_i$ for an n component link. (2.4.5)

ILD is most severe at high frequencies because Ethernet signals are more susceptible to noise at high frequencies. Moreover, the re-reflected signal is also a noise source because it is delayed by a certain amount of time before propagating through the twisted pair again. Consequently, the superposition of the noise on the transmitted signal can lead to a distorted signal.

2.4.5 Factors contributing to the distortion of the transmitted signal

A. Impact of Return Loss on data transmission

Signal reflection from both the transmitter and receiver also causes severe ringing and spurious transition, which can affect the data being transferred through the cable. Excessive reflections on the TL also cause electromagnetic interference and false triggering that may prevent the full functionality of devices when operating under thermally varied conditions. Normally, the measured signal attenuation of a cable is a smooth line. However, the return loss echoes, arriving at the receiver, in phase at various frequencies and out of phase with others, cause the attenuation plot to be wavy. In other words, signal jitter causes the edge of a signal, representing a data bit to be shifted slightly in time, misleading the receiver circuit in such a way that the receiver circuit classifies the signal as a binary 1 when it should have been a binary 0 during sampling, or vice versa. Moreover, signal jitter causes the data signal to become misaligned with reference to the clock leading to a decoding error. In addition to the ringing, spurious transition and signal jitter, impedance mismatch

also causes reflection that leads to a phase shift of the transmitted signal. However, the phase shift of a signal may cause interference to occur, leading to the phase distortion of the received pulse signal. Moreover, phase distortion causes the asymmetry of the received pulses and inter-symbol-interference at high frequencies.

B. Impact of noise

Another factor contributing to the distortion of signals being transmitted is noise. Depending on the nature and the source of the noise, the received signal can be buried by excessive noise in the transmission system. Noise comes from everywhere, from internal and external sources. An example of noise from an external source is an impulse noise, which is in the form of a sharp spike on the transmitted signal. It could be generated from external EMI such as lightning. Moreover, while external noise can be mostly excluded from the transmission systems, some internal noise sources are inherent in the systems, hence cannot be totally eliminated. Some examples of intrinsic noise are intermodulation noise, contact noise and thermal noise. Intermodulation noise is generated as a result of the nonlinearity in the transmission system while contact noise is caused by the fluctuating conductivity of an imperfect joint between two conductors. Contact noise is called a low-frequency noise ($\frac{1}{f}$ noise) because its magnitude can become very large at low frequency. Thermal noise, on the other hand, arises from the random motion of electrons in all elements containing resistance and operating above 0 Kelvin. According to [67], a non-periodic voltage exists in every conductor and the magnitude of the voltage is related to temperature. As stated in [67], thermal noise voltage is proportional to the square root of the system' noise bandwidth and the square root of the resistance. The magnitude of the thermal noise voltage is mathematically described in (2.4.6) [67].

$$V_t = \sqrt{4kTBR} \tag{2.4.6}$$

The V_t can equally be represented by thermal noise current (I_t) as given in (2.4.7).

$$I_t = \sqrt{\frac{4kTB}{R}} \tag{2.4.7}$$

Where k = Boltzman's constant - $1.38\ x\ 10^{-23}$ $\left(\frac{Joules}{K}\right)$, T= Absolute temperature (Kelvin),

B = Equivalent noise bandwidth of the system (Hz) and R = Resistance (Ω).

While some noise sources are inherent and external to the communication system, some noise sources are due to manufacturing defects or are structurally dependent. An example of such noise is crosstalk, which is categorised as the major impairment in any communication cabling system with more than one wire pair. Crosstalk superimposed on the desired signal is considered noise. High level of crosstalk distorts the received signal. Crosstalk occurs in twisted pair cables and depends on the distance between the twisted pairs and the relative permittivity of the dielectric material isolating the conductors of the twisted pairs. Crosstalk can be due to mutual capacitive or inductive coupling.

C. Mutual capacitive coupling

When a balanced voltage (V) is applied between two insulated conductors of the aggressor pair, which can be pair 1 in figure 2.24; the Electric field is set up in the dielectric space surrounding the insulated conductors. The E-field inside the dielectric material reduces the applied E-field through polarisation of the molecules inside the dielectric, which in turn causes the voltage to decrease ($E = -\nabla V$) and capacitance to increase ($C_m = Q/V$) for the same amount of charges on the conductors.

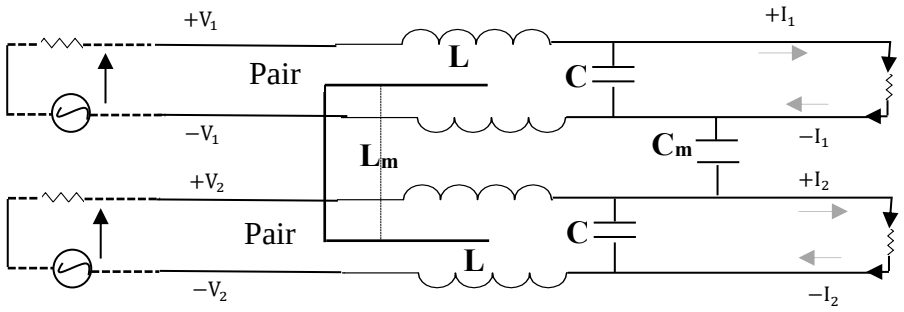

Figure 2.24: Illustrating intra-cable crosstalk [70]

D. Mutual inductive coupling

Similarly, the alternating current (I) flowing through the conductors of the aggressor pair in figure 2.24, creates a magnetic field which can couple with the conductors of the victim pair (pair 2) by mutual inductance (L_m) and induces a noise voltage (V_N) on it.

Completely balanced twisted pairs have mutual inductance and capacitance which are independently approaching zero as long as the insulated conductors are tightly twisted during manufacturing. Moreover, in the real application, the inductance (L) and capacitance (C) of a

twisted pair are related to the material properties of the twisted pair and the separation distance between the conductors of the twisted pairs. Given this, any changes in the characteristics of the twisted pair will be due to the changes in the material properties or the geometry of the twisted pair. As reported in [68], a reduction in the value of ε_r of the dielectric around the conductors of the twisted pairs causes crosstalk between the twisted pairs to decrease by decreasing the capacitive coupling.

Furthermore, if the heating of the cable changes the separation distance between the conductors of the twisted pairs, the resulting potential difference due to charge separation on the conductors will cause the capacitance of the twisted pairs to change. Although twisted pairs with tight twists may preserve their shape in the cable due to the slight heating of the cable; excessive heating of the cable can separate the twisted pairs. In addition, repeated heating and cooling of the cable may loosen the formerly tightly twisted wire. Moreover, the untwisting of the wire pairs means that the electromagnetic fields emitted by adjacent and opposite half-twists will not cancel each other entirely. As a result, the twisted pairs radiate an unwanted signal, which will be picked by other twisted pairs in the cable.

As discussed earlier, the value of the coupling capacitance depends on the separation distance (S_d) between the conductors of the twisted pairs, area of the overlapping conductors and the dielectric constant of the material between the conductors of the twisted pair (2.7.0). All other factors being equal, if the area of the overlapping conductors gets bigger during heating, the capacitance will increase due to an increased Electric field flux for a given field force. Also, if the heating of the cable changes the separation distance between the conductors of the twisted pairs, the electric field strength between the twisted pairs will change according to the inverse of the square of the distance between the twisted pairs (2.4.8).

$$E\ (\overrightarrow{r_m}) = \iiint \frac{1}{4\pi\varepsilon} \frac{(\overrightarrow{r_m} - \vec{r})}{|\overrightarrow{r_m} - \vec{r}|^3} \rho_v(\vec{r}) \partial v \qquad (2.4.8)$$

Furthermore, since the potential difference (V) between the conductors of a twisted pair is a sum of the line integral of the E-field over a distance between the twisted pair ($\Delta V = -\int \vec{E}(\vec{r}).\overrightarrow{\partial l}(\vec{r})$), the ratio of charge to the voltage will change the capacitance of the twisted pair (2.4.9) for the same amount of charge on the conductors of the twisted pair.

$$Capacitance\ (F) = \frac{Q(C)}{V(V)} = \frac{\oiint \varepsilon \vec{E}.dS}{-\int \vec{E}(\vec{r}).\overrightarrow{\partial l}\ (\vec{r})} \quad (2.4.9)$$

Moreover; in the case of an increased separation distance between the twisted pairs, the existence of the potential difference (V) between the conductors of the twisted pairs and non-zero capacitance (C_m) between the twisted pairs will cause an induced current (I_m) on the victim pair. The induced noise current is approximated to be (2.4.11).

$$\frac{dQ}{dt} = C_m \frac{dV_1}{dt} \quad (2.4.10)$$

$$I_m = C_m \frac{dV_1}{dt} \quad (2.4.11)$$

The amplitude of the induced noise current is determined by the values of the capacitances and circuit impedances, together with the rate of change of the voltage source of the aggressor pair.

If the heating of the cable separates the twisted pairs, the electric flux density between the twisted pairs will decrease because of the charge separation ($C = E\frac{dV}{dt}$), which will cause the capacitance to decrease. The reduction in the value of the coupling capacitance implies less noise coupling between the twisted pairs. On the other hand, there is a high possibility of stronger noise coupling between two twisted pairs in the cable when the cable cools down because of the close proximity of the twisted pairs. That is, if the separation distance between the twisted pairs decreases, the capacitance will increase; voltage will increase because of the concentration of the E-field between the pairs. An increase in voltage across the conductors of a twisted pair implies that the impedance will increase ($Z = V/I$). Given these, an unbalanced circuit with high $\frac{dV}{dt}$ and high impedances will be more susceptible to capacitive coupling. Although at high frequencies, capacitive coupling is a concern because capacitance offers low impedance paths to noise voltage.

Furthermore, radiation emission from the increased loop area of the twisted pairs is a concern as the cable heats up during active power operations and due to elevated environmental operating temperature. This is because a larger separation distance between the conductors due to excessive heat will result in a larger magnetic field and hence a higher inductance. According to Faraday's law, the bigger the loop area, the larger the magnetic field produced by the current in the loop.

Hence, any changes in the geometry of the twisted pair due to thermal variation and installation condition will change the crosstalk performance of the link.

The induced noise voltage on the aggressor pair by the victim pair is approximated by (2.4.12).

$$V_N = L_m \frac{dI_1}{dt} \qquad (2.4.12)$$

The induced V_N is proportional to the rate of change of current in the aggressor pair. High current implies low impedance, which implies that the inductance dominates the crosstalk between the twisted pairs. From (2.6.9) and (2.7.0), it can be noted that both mutual capacitance and inductance are affected by the change in the material properties of the twisted pair and physical separation of the source and victim pairs. As reported in [13], the effect of the change in the physical characteristics and material properties of the twisted pair can be significant on the balance performance of the cable during the initial few thermal cycles.

2.4.6 The impact of imbalance on the permanent link performance

The noise immunity performance of twisted pair cables is directly related to the balance of the cables. In particular, the balance of the screened twisted pair cables is important because of the grounding required for the screen. According to [69], screened twisted pair cables must be well manufactured and balanced to minimise the impact of common-mode noise on their performance. Also, correct termination of the screen at the connector ends is essential to achieve the screening properties of the cable. Moreover, as well as the balance of the screen at the two ends of the cable, the position and symmetry of the screen are also important to achieve a good balance of the cable. If the screen is connected to the wrong point on the termination point, common mode voltage (V_N) will be generated and conducted to the cable, and that may result in radiated emission [70].

Twisted pair cables may pick up common-mode noise from external sources, but not much of the common-mode noise will be converted to differential mode interference if the structure of the twisted pair is balanced. However, electrical degradation of the cable and its connecting hardware may cause the resistance of the permanent link to be unbalanced. Moreover, if the resistance of the conductors in a twisted pair is unbalanced, the electrical length of the twisted pair will be unbalanced; therefore, the impedance of the twisted pair will be unbalanced. In scenarios where two conductors in a twisted pair have unequal impedances to the ground, the common-mode voltage

induced on the twisted pair by nearby electromagnetic fields will be converted to differential-mode noise that could interfere with the data signal.

Furthermore, thermal variation may cause the dielectric constant of the conductor insulation of the twisted pair cable to change, leading to electrical length mismatches and asymmetry of the twisted pair. According to [70], a change in the electrical length of the cable is one of the sources of mode conversion in cables because the two signal conductors present different impedance to their environment. Moreover, as discussed in section 2.4.3, if the diameter of the conductor insulation decreases as a result of the contraction of the cable, the dielectric constant of the conductor insulation will increase. Then, the capacitance will increase while the impedance will decrease. Low impedance implies high current will be drawn. However, the noise across the capacitor, which increases as more current is being drawn through it, is a principal source of differential mode noise.

A. Radiated Emissions

The lack of symmetry in an unbalanced twisted pair causes the twisted pair to radiate an unwanted electromagnetic signal. Also, because the opposing, differential signals are not equal, they are partially converted to a common mode signal.

Another source of the common-mode signal is the internal noise voltages generated between the ground reference point and cable connection. Although good common mode rejection is achieved at the interface of the unshielded twisted pair cables with a balanced physical layout, but due to thermal variation on the cable and installation condition, some portions of the twisted pair are distorted, leaving it asymmetric. In this case, stray current induces common mode voltage (V_{cm}) on the signal conductors, which is converted to differential mode noise voltage (V_{dm}) through the imbalance of the twisted pair and equipment interface. As reported in [70], the existence of common mode currents means an imperfect cable, from the EMC point of view. Moreover, common-mode power on a wire pair produces more radiation than the same amount of power in the differential mode because the common-mode radiation from the wires does not cancel even when the wires are close together. Also, radiation which is emitted by the loop formed by the separation distance between the conductors of the twisted pair (a loop formed by the heating of the cable) can be maximised when there is 180^0 phase difference in the electrical length of the twisted pair. According to [70], radiation emitted from the whole system is more significant from 30 MHz upward, but

radiation emission at Very High Frequency (VHF) of 300 MHz tends to be dominated by cable emissions.

B. Conducted Emissions

Conducted emission from an equipment interface and power cable is usually found below 30 MHz [70]. As reported in [70], the capacitances and inductances associated with the wiring and enclosure of each unit of a system are all integral parts of the noise coupling circuit and play a significant part in determining the amplitude and frequency distribution of the common mode currents. Other common impedance coupling routes are from circuit impedances that the source shares with the victim. As suggested in [70], ground connections are the most frequent source of common impedance coupling routes. Moreover, when an interference source shares a ground connection with a victim, any current due to the output of the source flowing through the common impedance section develops a voltage in series with the input of the victim. Consider figure 2.25; the differential mode current (I_{DM}) produces the desired signal voltage across the load (R_L). The common mode current (I_{CM}) does not flow through R_L directly but through impedances Z_A, Z_B and back through the external ground. Z_A, Z_B are not circuit components, but distributed stray impedances, typically but not always, capacitive, and are determined by proximity to conducting structures in the environment.

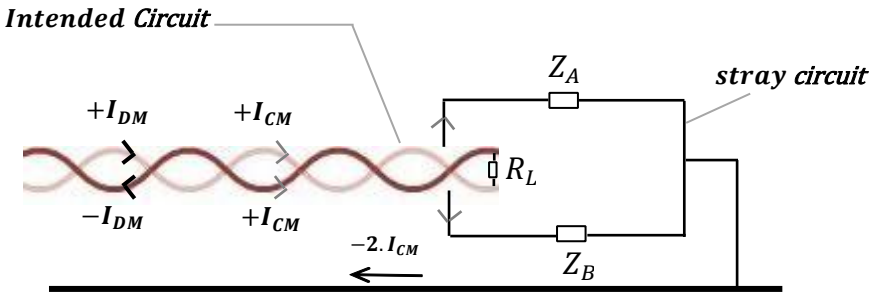

Figure 2.25: Differential to common mode conversion

If $Z_A = Z_B$ then no voltage is developed across R_L by the I_{CM}. However, any inequality in Z_A and Z_B results in such a voltage ($V_{L(CM)}$) across R_L, which is proportional to the differences in impedance (2.4.13).

$$V_{L(CM)} = I_{CM}(Z_A - Z_B) \qquad (2.4.13)$$

Furthermore, a coupling route can also be a piece of wire such as a drain wire which is used in the termination of the shield. At DC and low frequencies, the resistance of the drain wire determines the impedance. However, above a few kilohertz, the inductance of the drain wire increases the total impedance. Thus, allowing the noise current to couple more efficiently.

2.5 A review of cable bundle heating assessment methods

As a first step in assessing the heating effects on cable performance, it is crucial to measure the change in temperature of the cable, accurately. Hence, the significance of measuring the change in temperature was studied on cable bundles used in remote powering applications by quantifying the ampacity of 37 cable bundle (CB) of Category 5e [25] using different approaches. These approaches include measurement of conductor temperature by indirect measurement of direct current and resistance also called the resistivity measurement approach [20, 44], the measurement of jacket surface temperature based on the use of thermocouple sensors placed within the bundle matrix [20, 44], and 2D finite element analysis (simulation) of cable heating [71]. However, out of the different approaches that have been widely adopted for the assessment of the possible temperature rise due to cable bundle heating, the principal approaches can be summarised as follows: (1) Conductor temperature measurement by indirect measurement of direct and resistance also called the resistivity measurement approach. (2) The jacket surface temperature measurement based on the use of thermocouple sensors placed within the bundle matrix. (3) The use of the mathematical model in predicting the amount of temperature rise within different layers of the CB. The focus of this section is to review the three principal approaches and apply them (Chapter 3) to assess the level of temperature rise due to power delivery as used in the PoE, PoE+, PoE++.

2.5.1 A review of the resistivity measurement approach

The resistivity approach measures the actual temperature rise on the surface of the copper conductor due to resistive heating of the cable. That is, the temperature of the copper conductors is determined by measuring the changes in the DC resistance of the copper conductor. The first step in using this approach is to measure the initial resistance of the CB at room temperature. Alternatively, after the connection of the CB to a constant current source, the voltage across the heated pairs and the constant current passing through the CB are recorded for the calculation of the initial resistance or $R_{Measured}$. The calculation of the initial resistance of the CB is according to (2.5.1).

$$R_{Measured} = \frac{V}{I_{Test}} \quad (\Omega) \quad (2.5.1)$$

where

$R_{Measured}$ = Initial resistance measured at room or reference temperature.
V = Voltage across the heated pairs at the start of the heating process
I_{Test} = Constant current passing through the CB

Also, at the steady-state of the heating process, the heat generated in the copper conductor is obtained by calculating the temperature dependence of the conductor resistance ($R_{total\ or}$ R_{Heated}) using (2.5.2).

$$R\ (t\ ) = R(T_R) * (1 + \alpha * (T - T_0)) \quad \left(\frac{\Omega}{m}\right) \quad (2.5.2)$$

where

R (t) = Temperature dependence of the resistance of the CB (**Ω**). Also, called R_{Heated}
α = Temperature coefficient of the resistance of copper conductor
T_0 = Initial room (reference) temperature for the conductor resistance (^oC)
T = Conductor temperature at steady state (^oC)
R (T_R) = DC loop resistance of the copper conductors at room temperature (**Ω**)

Also, at the steady-state of the heating process, the heat generated in the copper conductor is obtained by calculating the temperature dependence of resistance (R_{Heated}) using (2.5.3).

$$R\ (t\ ) = R(T_R) * (1 + \alpha * (T - T_0)) \quad \left(\frac{\Omega}{m}\right) \quad (2.5.3)$$

where

R (t) = Temperature dependence of resistance of the CB (**Ω**). Also, called R_{Heated}
α = Temperature coefficient of the resistance of the copper conductor
T_0 = Initial room (reference) temperature for the conductor resistance (^oC)
T = Conductor temperature at steady state (^oC)
R (T_R) = DC loop resistance of the copper conductors at room temperature (**Ω**)

The change in temperature (temperature rise) is then calculated according to (2.5.4) or (2.5.5) after obtaining the resistance of the cable bundle at a steady state.

$$\Delta T = \frac{1}{\alpha} * \left(\left(\frac{R_{Heated}}{R_{Measured}} \right) - 1 \right) \quad (^{o}C) \quad (2.5.4)$$

Or

$$\Delta T = \frac{R_{Heated} - R_{Measured}}{\alpha * R_{Measured}} \quad (^{o}C) \quad (2.5.5)$$

Moreover, the conductor temperature at a steady state is according to (2.5.6) or (2.5.7).

$$\Delta T = \frac{1}{\alpha} * \left(\left(\frac{R_{Heated}}{R_{Measured}} \right) - 1 \right) + t_{room} \quad (^{o}C) \quad (2.5.6)$$

or

$$\Delta T = \frac{R_{Heated} - R_{Measured}}{\alpha * R_{Measured}} + t_{room} \quad (^{o}C) \quad (2.5.7)$$

Where

R_{Heated} = Final resistance obtained at a steady state of temperature.

2.5.2 Jacket surface temperature measurement using thermocouple sensors

Thermocouple sensors have been widely used in the industry to provide cost-effective temperature measurement with reasonable accuracy of ±0.2°C [72]. The accuracy of the most popular type of thermocouple sensor, the K-type was demonstrated in [72] with the use of the relevance vector machine in measuring the temperature profile of a resistive heating furnace. The results of the study conducted showed a correlation coefficient value of 0.9695 between the output of the K-type thermocouple sensor and the output of the relevance vector machine. Also, in [73, 74], the uncertainty in the output of the thermocouple sensor of K-type was suggested to be about ±4°F (±2.2°C). Based on the reasonable accuracy of the thermocouple sensor of K-type, the method

used to measure the jacket surface temperature is based on the thermocouple sensors placed within each layer of the CB. The approach measures the temperature rise on the outside of the conductor insulation as used in [25] or on the outside of the jacketing material [20]. Note that the description of the CB matrix when thermocouple sensors are used, is provided in section 3.1, but the layering of the CB is according to (2.5.8) [44].

$$N = \sum_{i=1}^{n} (6i) \tag{2.5.8}$$

Where:

N = is the total number of cables around the centre cable.
n = is the number of layers around the centre cable.

2.5.3 Mathematical modeling of temperature rise in a CB

This section describes the analytical modelling of temperature rise for different cable constructions, bundle sizes and installation conditions. Figure 2.26 represents a typical temperature profile of a CB, which is obtained by measured data for different cable types and installation environments.

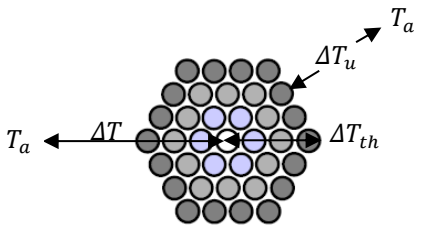

Figure 2.26: Temperature profile of a CB [20]

As illustrated in figure 2.26, T_a is the ambient temperature, whereas ΔT represents the total temperature rise between the ambient and the centre of the cable bundle. Also, ΔT_{th} is the temperature rise between the outer surface and the centre of the cable bundle. Lastly, ΔT_u represents the temperature rise between the ambient temperature and the outer surface of the bundle.
The modelling of ΔT_u, ΔT_{th} and ΔT is according to (2.5.9) – (2.6.1).

$$\Delta T_u = \frac{\rho_u * P}{\left(d * \sqrt{N} * \sqrt[4]{\frac{3}{4} * \pi^6}\right)} = \approx \frac{\rho_u * P}{(d * \sqrt{N} * 5.182)} \quad (^{\circ}C) \quad (2.5.9)$$

$$\Delta T_{th} = \frac{\rho_{th} * P}{4 * \pi} = \approx \frac{\rho_{th} * P}{12.6} \quad (^{\circ}C) \quad (2.6.0)$$

$$\Delta T = \Delta T_u + \Delta T_{th} \quad (^{\circ}C) \quad (2.6.1)$$

Where

P = Power dissipation

$$P = N * n_c * i_c^2 * R \quad (2.6.2)$$

N = Number of cables in a bundle carrying current

n_c = Number of conductors per cable carrying remote powering current (i_c)

i_c = Current per conductor (A) i. e 0.5* current delivered by a pair

R = Average DC loop resistance per unit length (Ω/m) of conductors carrying the current.

ρ_u = Constant relating to installation environments

d = Cable diameter (m)

For all cable constructions installed inside conduits or cable trays that are filled up to at least 40% capacity, the constant relating to installation environments (ρ_u) is as stated in table 2.3 [20]. Also, for all installation conditions, the constant (ρ_{th}) relating to cable constructions is as stated in table 2.4.

Table 2.3: Constant relating to installation environments

Installation environments	**Constant (ρ_u)**
Ventilated conditions	0.15
Plastic conduits or open metal trays	0.25
Closed metal trays	0.5
Insulated conditions	0.75

Table 2.4: Constant relating to cable constructions

Cable constructions	**Constant (ρ_{th})**
U/UTP cable constructions	5
F/UTP cable constructions	3
S/FTP cable constructions	2.75

Adaptation model for the total temperature rise in different CB sizes

The adaptation model in (2.6.3) describes the total temperature rise in a cable bundle based on the constant current passing through the cable bundle.

$$\Delta T\ (I, N) = \left(C_1 N + C_2\sqrt{N}\right) * I^2 \qquad (2.6.3)$$

where

ΔT_{CB} = Temperature rise (°C)

I = Current passing through the cable (A)

N = Number of cables in a bundle

C_1 = Coefficient describing the variables associated with the geometry of the cable (see table 2.5)

C_2 = Coefficient describing all the variables associated with the environmental conditions of the cable

Table 2.5: Bundling coefficients for different types of cables (all four pairs energised)

	Bundling Coefficients			
	Open-air		**Conduit**	
	C_1	C_2	C_1	C_2
0.4 mm cords	0.1445	1.7800	0.1980	2.9250
Cat 5 cables	0.1267	0.9933	0.1583	1.5300
Cat 6 cables	0.1057	0.7070	0.1206	1.1783
Cat 6_A cables	0.0857	0.6263	0.0926	0.9967
Cat 7 cables	0.0857	0.6263	0.0926	0.9967
Cat 7_A cables	0.0436	0.515	0.0555	0.841

2.6 Measurement methods for the balanced twisted pair transmission parameters

When communication cables fail in the installed base due to the ageing of the conductor insulation, poor installation condition and handling effects, it can be challenging and expensive to repair or replace the cable, if the cables are installed in difficult to reach places such as behind walls. To locate the cause of the performance failure on communication links, several techniques have been adopted for troubleshooting the links. These include the three-stake method [75] and Time-Domain Reflectometry (TDR) [76]. The use of the three-stake method may be inaccurate because of the prediction of the velocity of propagation involved in the calculation of the cable fault location.

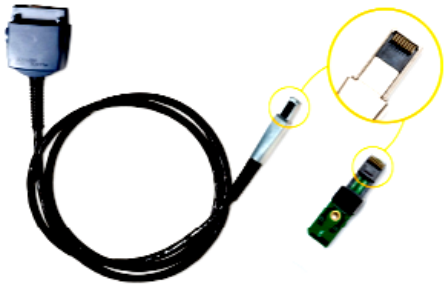

Figure 2.27: PL adapter with the adapter plug implemented on a circuit board [64]

Additionally, the method requires that the precise location of the faulty cable be known and accessible for the length marking to locate the fault on the cable. The TDR approach, however, relies on the actual velocity of propagation of the cable for the calculation of the fault location. Moreover, it has been the traditional approach for determining the changes in the electrical length of a transmission line with an accuracy of 1 %. Most test instruments have the functionalities for performing TDR measurements. For instance, the DSX 5000 Cable Analyzer, uses the High-Definition Time Domain Reflectometry (HDTDR) and High-Definition Time Domain crosstalk (HDTDX) analysis for locating the causes of RL and NEXT failures on the channel [76]. Using the HDTDR method, the test reference plane (Figure 2.27**)** is taken at the end of the RJ45 plug of the PL adapter such that the length of the test leads is automatically deducted from the measured length of the cable under test.

Also, to limit the impedance mismatches at the start of the TDR trace, most field testers have balance controls, which are used for matching the impedance of the test leads and plugs to that of the cable under test. Changes in the characteristics of the channel are measured in the frequency domain as Scattering parameters (S-parameters) with the aid of measurement devices such as a Vector Network Analyser (VNA) and Cable Analyser (handheld or portable field

tester). For instance, the signal integrity measurements with a VNA are based on S-parameter and Time Domain Reflectometry (TDR) measurements. Although most of the channel parameters are measured in the frequency and time domain, problems with the connectors are often challenging to identify in the frequency domain measurement data representing the electrical characteristics of the cable link because RL is not "cascadable". Also, the new set of modular connectors has been designed with a certain amount of crosstalk compensation to cancel NEXT. Besides, because of attenuation, some effects due to connector problems are lost in the trace. Furthermore, the patch cords, cables, jacks and plugs may respond to different frequencies and reflect some of the energy toward the transmitter. For instance, if the patch cord and cable segment have severe impedance mismatches, the resonance caused by the reflections can be as high as 5-10 dB above the baseline RL trace [78]. Also, if one component on the channel is defective or is of inferior quality, the RL response curve may be very unpredictable, with the bad component causing echoes at unexpected frequencies [78]. The TDR is widely adopted for locating faults on the cable links. However, it is associated with some disadvantages, such as the inability to identify all modes of failure and all-time domain events in the measurement data [55]. Based on the limitations of the TDR techniques, an algorithm was developed in [55] to detect a failure in the electrical cable assembly. The study described how CDNEXT measurements were utilised for connector detection. In the study conducted, a frequency domain data was obtained first using a test instrument. Then, from the measurement data obtained, an estimation of each connector location along the length of the cable was made. After that, the contribution of each connector to the cable link failure was then ranked with the aid of the algorithm.

2.6.1 Measuring the performance of Ethernet cable using Scattering parameters

The Scattering (S) parameters are used for analysing circuits at microwave frequencies where voltage and current are not well defined or are difficult to measure [79]. The conventional S-parameters are used for describing the electrical behaviour of linear time-invariant electrical two-ports (figure 2.28).

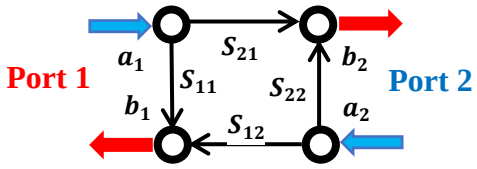

Figure 2.28: Signal flow notation for 2-port network using S-parameters [80]

To analyse the circuits, the input variables are related to the output variables of the circuit. That is the incident (a_1) and reflected (b_1) wave coefficients at port 1 are related to the incident (a_2) and reflected (b_2) wave coefficients at port 2 of the device according to the 2-port S-matrix below.

$$\begin{bmatrix} b_1 \\ b_2 \end{bmatrix} = \begin{bmatrix} S_{11} & S_{12} \\ S_{21} & S_{22} \end{bmatrix} \begin{bmatrix} a_1 \\ a_2 \end{bmatrix}$$

$$b_1 = S_{11}\ a_1 \quad + \quad S_{12}\ a_2$$

$$b_2 = S_{21}\ a_1 \quad + \quad S_{22}\ a_2$$

Although S-parameters are defined in terms of wave variables, they comprise a set of parameters that describe the scattering and reflection of the travelling electromagnetic waves in a communication channel. For the S-matrix, the trailing diagonal of a 2-port (S_{21}) and (S_{12}) represents the voltage wave transmission coefficients, while the main diagonal terms are the voltage wave reflection coefficients (S_{11}) and (S_{22}).

The S-parameters can be measured as single-ended and differential signalling to characterise the insertion loss, reflection and crosstalk performance of a system. The notation for a four pair differential signalling is given in figure 2.29 while the notation for the S-parameters measured by a conventional unbalanced network analyser is given in figure 2.30.

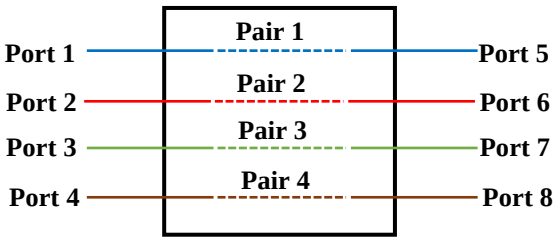

Figure 2.29: Port notation for four pair, differential signaling [80]

$$\begin{bmatrix} S_{11} & S_{12} & S_{13} & S_{14} \\ S_{21} & S_{22} & S_{23} & S_{24} \\ S_{31} & S_{32} & S_{33} & S_{34} \\ S_{41} & S_{42} & S_{43} & S_{44} \end{bmatrix}$$

Figure 2.30: Four port S-parameters measured by a conventional unbalanced network

2.6.2 Measuring the performance of permanent link using a field tester

(A) Permanent link (PL) compliance test in the frequency domain

Some channel performance assessments are set up as permanent links with the exclusion of the patch cords to limit the number of connection points and avoid complicated resonances. Figure 2.31 shows a permanent link set up using a set of field testers.

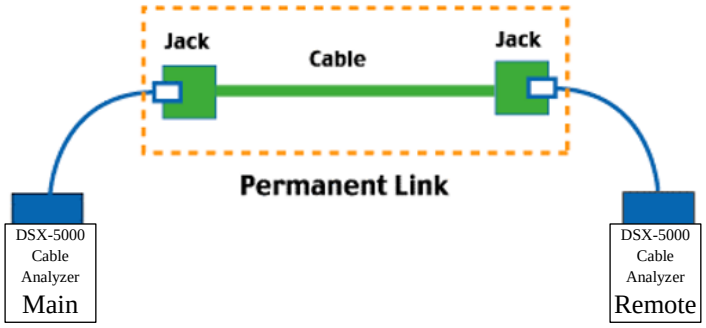

Figure 2.31: A schematic, showing a permanent link setup using field tester [68]

From figure 2.31, the main and remote units at the ends of the link have openings for the connection of the permanent link adapters attached to the cables used for the permanent link testing. The two units also consist of separate channel adapters in which the RJ45 plugs can fit when performing channel performance testing. The main and remote units can be used for cable performance testing in two ways. (1) They can both be used as active units. That is, the two units can send and receive signals at both ends. (2) One unit can be the active device (usually the main unit), controlling the testing while the remote unit been the passive device, receiving and sending back the received signal to the main unit [55]. During the automatic testing, the cable tester performs link pin-to-pin continuity and wire pairing to the correct pins according to a specific wiring standard. The pairing schemes electrically identify the specific pins connection in the 8-pin modular RJ45 connector. Although the two pairing schemes intended for use with the standard networking protocols are T568A and T568B (figure 2.32), but the T568B arrangement is more widely adopted [82].

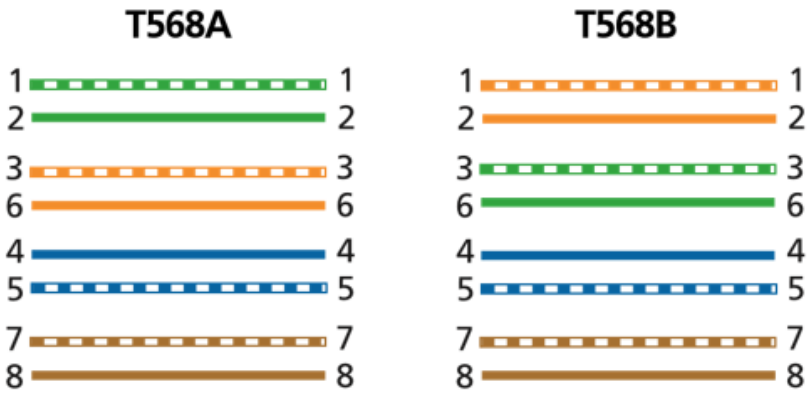

Figure 2.32: Pin numbers and wire colour of the four twisted pairs in an Ethernet cable [76]

To pass the compliance test, all measurements at each frequency in the range of the transmission bandwidth of the cable must fall within the defined performance range or exceed the limit values specified by the standard bodies. Figure 2.33 shows an example of the overall results for each test performed based on the test standard limit selected (ISO/IEC or TIA). Twisted pair cables in which all their parameters meet or exceed the specified values are reported as PASS (figure 2.33a). However, those cables in which some or all of the values of their parameters fall within the accuracy uncertainty as reported as Marginal PASS (figure 2.33b) and lastly, the cables in which some or all their parameter values fall outside the standard limits are reported as FAIL (figure 2.33c).

a (values are within the limits) b (within the accuracy uncertainty) c (values are outside the limits)

Figure 2.33: Performance tab (a – PASS), (b - Marginal PASS) and (c - FAIL) [76]

(B) Time Domain Reflectometry fault locating techniques using a field tester

To locate the cause of RL failure on a PL, the tester sends stimulus signal into the PL, and the transmitted pulse travels along a cable at a certain velocity factor, which is supplied by the manufacturer of the cable but stored in the field tester by the tester manufacturers. With no changes in the characteristics of the PL, the pulse travels along the cable with only a gradual attenuation. However, with impedance mismatches or discontinuities along the link, reflections occur. By examining the pulse width, amplitude and the time delay of the reflections, the cause and location of the imperfection on the link are reported by the reflectometer.

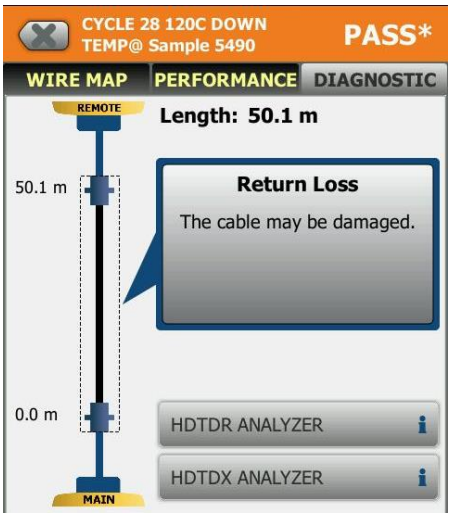

Figure 2.34: Output of the HDTDR measurement [76]

The High-Definition Time Domain Reflectometer (HDTDR) shows the locations where the change in the electrical characteristics of the link had occurred to help identify the causes of the RL failure (figure 2.34). It also reports the percentage of the signal that has reflected. Similarly, to investigate and locate the cause of crosstalk failure measured in the frequency domain, the High-Definition Time Domain crosstalk (HDTDX) analyser shows the locations and amplitudes of the crosstalk signals to help quantify the crosstalk failures. For example, the HDTDX plots shown in figure 2.35a indicate the exact location at which the worse crosstalk occurs on a Category 6 U/UTP PL due to the localised heating of the cable. It also shows the probable cause of the TCL performance failure (figure 2.35b) within the first three thermal cycles performed on the Category 6 U/UTP PL.

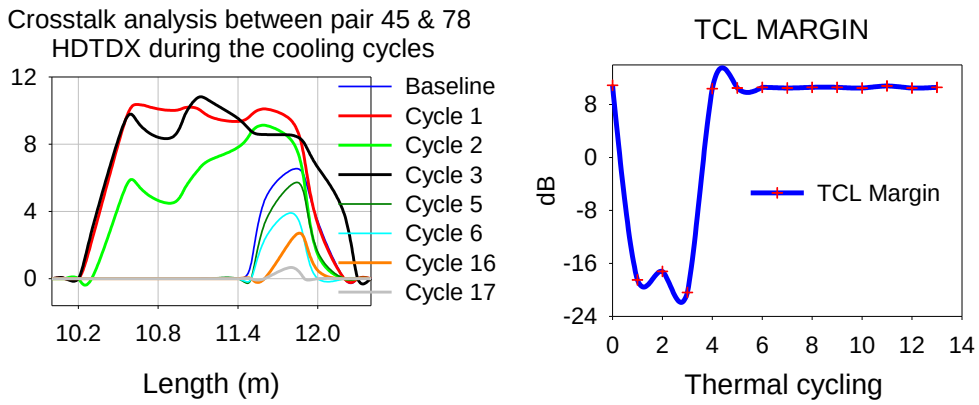

(a) Output of the HDTDX Analyser (b) TCL measurements in the frequency domain

Figure 2.35: Output of the HDTDX Analyser (a) and TCL measurements (b)

2.6.3 Modeling of cable transmission parameters using the Transmission Line Method

Long before computers were available with fast electromagnetic solvers and circuit simulators for the modelling of twisted pair cable geometry and its frequency dependent characteristics, the behaviour of twisted pair cables was mostly analysed using analytical methods. Also, the International Standards bodies mostly use empirical equations and equations obtained by curve fitting of measured data to obtain standard limits for the secondary cable parameters [83]. However, it is more appropriate to employ equations, which relate directly to the specific physics rather than observed behaviour [83]. Hence, cable designers inculcate the underlying physics into Computer-Aided Engineering (CAE) software [84 - 86], which is used in performing a sensitivity analysis of the unit parameters of the twisted pair. With this approach, the propagation delay, for example, was easy to vary by changing the dielectric constant of the conductor insulation and the physical length of the conductors. Given these, this research adopts a similar approach in analysing the changes in the characteristics of the primary line parameters of a twisted pair, to investigate the factors influencing the changes in the designed differential impedance of a twisted pair.

(i) Analysis of the primary line constants

The analysis of the secondary cable transmission parameters can be viewed from the conceptual idea of a transmission line consisting of four distributed primary parameters: the series resistance

(R) per unit length, series inductance (L) per unit length, shunt capacitance (C) per unit length and shunt Conductance (G) per unit length. The R represents the DC and AC resistance of the conductors, L, the inductance, quantifies the magnetic flux surrounding the conductors. The G represents the current leakage through the insulation between the conductors and lastly, C is due to the Electric field between conductors. An equivalent circuit of a short length of a transmission line (TL) such as a twisted pair (figure 2.36) shows all the four primary line parameters.

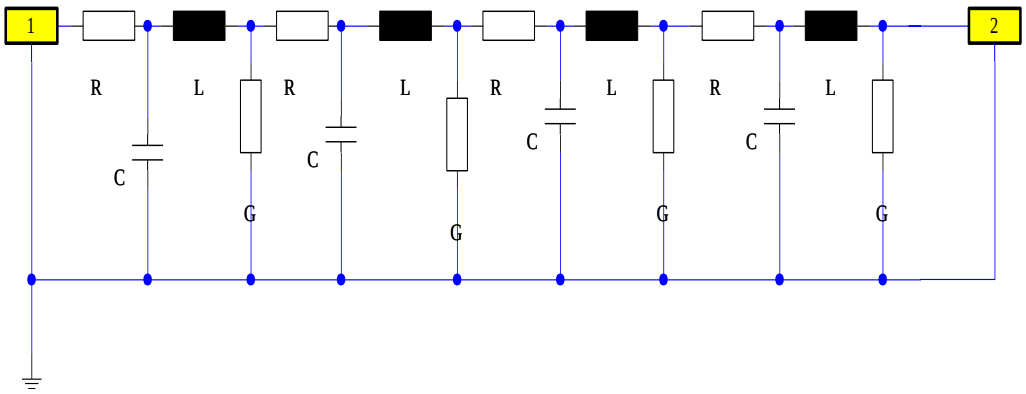

Figure 2.36: Cascaded RLCG nodes, forming a two-port model

Although figure 2.15, (Δl) consists of a set of reactive (C and L) and resistive (R and G) components, a TL may be considered as an array of small segments of the line constants (figure 2.36), representing a single pair in a cable of total physical length, l. Cascading sections of the line and visualising the circuit provides an insight into the behaviour of the line in general. However, to achieve a close prediction of the performance of the line in the frequency domain, the length of each node is made much smaller (usually $\lambda/10$) than the wavelength of the highest frequency components of the frequency of interest.

Figure 2.37 shows the cross-section of an unshielded twisted pair. Given the individual design parameters such as the dimensions of a twisted pair and its material properties, the R, L, C and G per unit length of a twisted pair can be calculated according to (2.6.7) – (2.7.1) respectively [87].

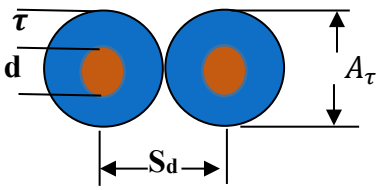

Figure 2.37: Cross-section of an unshielded twisted pair

AC resistance $$R_{ac} = \frac{2R_s}{\pi d}\left(\frac{\frac{S_d}{d}}{\sqrt{\left(\frac{S_d}{d}\right)^2 - 1}}\right) \quad (2.6.4)$$

Surface resistance $$R_s = \frac{1}{\sigma\delta} = \sqrt{\frac{\pi f \mu}{\sigma_c}} \quad (2.6.5)$$

DC loop resistance $$R_{dc} = \frac{l}{\sigma_c A} \quad (2.6.6)$$

From (2.6.5) and (2.6.6),

Total resistance of a pair $$R = R_{ac} + R_{dc} \quad (2.6.7)$$

Area of the copper conductor $$A = \pi \frac{d^2}{4} \quad (2.6.8)$$

Loop inductance $$\mathrm{L} = \frac{\mu_r \mu_o}{\pi} \cosh^{-1}\left(\frac{S_d}{d}\right) \quad (2.6.9)$$

Mutual capacitance $$C = \frac{\pi \varepsilon_r \varepsilon_o}{cosh^{-1}\left(\frac{S_d}{d}\right)} \quad (2.7.0)$$

Mutual conductance $$G = \frac{\pi \omega \varepsilon''}{cosh^{-1}\left(\frac{S_d}{d}\right)} \quad (2.7.1)$$

(ii) Relationship between the primary and secondary cable parameters

Given the four primary line constants R, L, C and G, the two important parameters used for describing the characteristics of a propagating signal are the propagation constant (γ) and characteristic impedance (Z_o): (2.7.2) and (2.7.5) [88, 89]. The complex quantity, γ, is dimensionless and frequency dependent, it consists of real (α) and imaginary (β) parts. When a signal is launched into a TL, the electromagnetic waves of the voltage signal propagate through the dielectric at the velocity of propagation(v_p), using the conductors are guides. Its amplitude and phase may vary as functions of space (z) and time (t) depending on the characteristic of the line. Moreover, for long-distance communication, the initial amplitude of the signal, P_o decays by a factor of $e^{-2\alpha z}$, such that $P = P_o e^{-2\alpha z}$ where P_o is the power at $z = 0$ and P is the power at $z = l$ (see figure 2.15). Hence, the term attenuation constant (α) in (2.7.3) is a function of the line parameters. It is a measure of the reduction in the amplitude of the signal while β measures the phase change as the signal propagates through the line. Moreover, Z_o is the ratio of the voltage to current at any point on the TL. Depending on the characteristics of the conductor pair, Z_o may vary along the length of the TL.

Propagation constant $\gamma = \alpha + j\beta \ = \sqrt{(R + j\omega L)(G + j\omega C)}$ (2.7.2)

Attenuation constant $\alpha = \left(\frac{R}{2Z_o} + \frac{GZ_0}{2}\right)$ (2.7.3)

Phase constant $\beta = \omega\sqrt{LC}$ (2.7.4)

Characteristic impedance $Z_0 = \sqrt{\frac{R+j\omega L}{G+j\omega C}}$ (2.7.5)

(iii) Approximation for the lossless Transmission Line

A lossless TL consists of uniformly distributed elements with constant impedance along its length. That is, the source impedance (z_s) is matched to the line (Z_0) and load (z_t) impedance such

that the total power transmitted is completely delivered to the (matched) load, and no reflection of signal is observed on the line; also, no power loss on the TL. Thus, the resistive term (R and G) is eliminated from (2.7.5), and the propagation constant is given as (2.7.6).

$$\alpha = 0,\ \gamma = j\beta \qquad = \sqrt{(j\omega L) * (j\omega C)} \quad = j\omega\sqrt{LC} \tag{2.7.6}$$

Also; the impedance seen by the signal is a real quantity, and no imaginary part is observed (2.7.7). Hence, in an ideal lossless transmission line, (2.7.5) can be approximated as:

$$Z_0 = \sqrt{\frac{L}{C}} \tag{2.7.7}$$

However, as the signal propagates through the line, it undergoes a phase change of 2π in a given distance of a wavelength, such that $\beta = \frac{2\pi}{\lambda} = k$. Moreover, for a distortionless TL, β must be proportional to ω. Also, the wavenumber (k) must be proportional to frequency. Given this, k is a measure of the number of cycles in a given length of a TL. Therefore, since the phase velocity or $v_p = f\lambda, \quad \beta = \frac{\omega}{v_p}$. In addition, from Fourier analysis, a pulse signal is a superposition of signals having many frequencies and many different wavelengths. For a distortionless TL, the signals travel at the same v_p and arrive at the receiving end at the same time. Thus, for a lossless line, the v_p is independent of frequency; therefore, there is no dispersion of signal on the line. Given this, the v_p for a uniform lossless transmission line, $v_p = \frac{1}{\sqrt{LC}}$.

(iv) Approximation of a low frequency, low- loss Transmission Line

Typically, Z_0 is approximated at low frequencies as resistive because capacitance depends weakly on an increasing frequency. However, based on the small significance of capacitance at low frequency, it is valid to approximate Z_o at low frequencies as being complex (2.7.8).

$$Z_0 = \sqrt{\frac{R}{j\omega C}} \quad = \frac{1-j}{\sqrt{2}}\sqrt{\frac{R}{\omega C}} \tag{2.7.8}$$

Also, conductor losses (due to R_{dc}) dominate at low frequencies when compared with the dielectric loss (due to G). Moreover, the small conductor loss causes the amplitude of the signal to vary slightly but not rapidly, causing the attenuation to change slightly. Since the L and G are small at low frequencies, the low-loss approximation for γ is given as:

$$\gamma = \alpha + j\beta \quad \cong \sqrt{j\omega RC} \quad = \frac{1+j}{\sqrt{2}}\sqrt{\omega RC} \tag{2.7.9}$$

(v) Approximation for the high-frequency, low- loss Transmission Line

For the high-frequency low-loss TL, the small loss from the resistive elements (R and G) will cause the amplitude of the signal to change slightly. Therefore, γ for the high frequency, low- loss TL is given in (2.8.0). Note that in this case, the small loss introduced to the line does not change the phase of the propagating signal significantly and that the dispersion of signals on the line does not cause much distortion.

$$\gamma = \alpha + j\beta \quad = \quad \frac{1}{2}\left(R\sqrt{\frac{C}{L}} + G\sqrt{\frac{L}{C}}\right) + j\omega\sqrt{LC} \tag{2.8.0}$$

Furthermore, at high frequencies, R and G are much smaller than L and C. Therefore, R and G can be ignored such that Z_o is approximated as the Z_o in the lossless case (2.7.7). Moreover, it appropriate to mention that only the external inductance (L_{ext}) is considered in this case. The internal inductance (L_{in}) is negligible at high frequency because of skin effect.

(vi) Approximation of the lossy Transmission Line

For a severe lossy TL, where there is small-signal transmission to the load, and small phase variation of the signal, the resistive term (R and G) is used for the estimation of the losses on the line. The γ is approximated to a real quantity as given in (2.8.1).

$$\gamma = \alpha + j\beta \quad \approx \sqrt{RG} \tag{2.8.1}$$

Similarly, since the resistive term R and G are much larger than the reactive elements L and C, the Z_o of the lossy line is approximated as (2.8.2).

$$Z_0 = \sqrt{\frac{R+j\omega L}{G+j\omega C}} \qquad \approx \sqrt{\frac{R}{G}} \tag{2.8.2}$$

$$\beta = \left[\omega\sqrt{LC} - \frac{RG}{4\omega\sqrt{LC}}\right] \tag{2.8.3}$$

Therefore, insertion loss depends on the impedance mismatch between the load and the characteristics of the network. Also, for a lossy line, the v_p is a function of frequency (ω).
The energy of the signal and its information content are spread across many frequencies. Thus, if the different frequencies in a signal travel at different velocities, the signals will arrive at the end of the transmission line at different times and distorted. Therefore, a lossy line is a dispersive TL.

2.7 The Feature Selective Validation (FSV) Method

The focus of this section is on the review of the validation tool employed for the validation of the long-term effect of thermal variation on the performance balanced twisted pair cable.

The brain is the best-known pattern recognition device; as such, it has been used historically in combination with visual evaluations for data analysis. However, human vision is often affected by physical and psychological influences. Also, age has a significant impact on the visual evaluation of the results of different subjects. Hence, visual impairment can lead to a wrong judgement when comparing two data sets. Furthermore, the fatigue associated with the evaluation of complex data often leads to inadequate data analysis [90]. Moreover, while there are other methods such as correlation methods [90], Kolmogorov-Smirnov (KS) test, Mean Absolute Prediction Error (MAPE) [87, 91] for data comparison, data quantification and evaluation of the level of accuracy in data predictions, the Feature Selective Validation technique (FSV) is a robust method used for determining the agreement between data sets with a consistent level of accuracy. The first version of the FSV standard (IEEE 1597.1) was ratified in 2008 [92, 93], while the second version (IEEE

1597.2) [94], which is useful in the interpretation of the validated data was ratified in 2010. The IEEE 1597.2 has the capability for validating measurement results against the results obtained using analytical methods. It is also used to cross-compare techniques to determine a level of agreement. Based on human expertise in a problem domain, one is subjective in decision making on two traces as a result of the pre-knowledge of the subject area. However, FSV method removes the human subjectivity and allows the comparison to be drawn objectively. That is, it removes the element of individual subjectivity from the decision-making process.

Short description of the FSV process

In the first instance, using the FSV allows the detection of the similarities and dissimilarities between two data sets and identifies the overlapping portions of the data sets. Then, the overlapping portions are interpolated in such a way that the data points align at the same points on the x-axis. After that, the data sets are Fourier Transformed and filtered into a Low Pass (DC offset), Bandpass (Lo) and High pass (Hi) information (six output, three for each data set). The low pass and Bandpass contents present the offset and trend information in the data sets, while the Hi-pass contents give the features in the two datasets. The six outputs (DC, Lo and Hi for the two data sets) are then inverse transformed to produce three final components. These components are the Amplitude Difference Measure (ADM), the Feature Difference Measure (FDM) and the Global Difference Measure (GDM). ADM, which compares the envelopes of one data set to the other is constructed from the DC and Lo contents, while the FDM, which compares the fine details in the data sets is constructed from the Lo and Hi contents. However, the ADM and FDM are combined to produce the Global Difference Measure (GDM). The GDM quantifies an acceptable level of agreement between the two data sets. Also, by obtaining the mean value of the ADM, FDM and GDM, a single value is produced with its associated Grade and Spread. This single value is used for decision-making on the quality of data comparison and can be described with a natural language as set out in table 7.9. (See section 7.4).

The GRADE is also a direct interpretation of the quality of the comparison. A smaller number of the GRADE indicates a better comparison of the data sets, while the SPREAD is used to judge the reliability of the outputs. The smaller the SPREAD, the higher the reliability of the results. Note that GRADE and SPREAD are computed for each ADM, FDM, GDM output. For the visual interpretation of the level of the agreement between the data sets, the ADM, FDM and GDM results are also displayed using the confidence histograms that are referred to as ADMc, FDMc and GDMc

respectively. To further understand the origin of the contributors to the ADM, FDM and GDM output, FSV tool performs point-by-point comparisons of the amplitude differences, the feature differences and the global differences and output the results as ADMi, FDMi and GDMi. These new three outputs are then used to analyse the results in more details.

2.8 Scanning Electron Microscopy (SEM)

Different techniques have been used in materials science to evaluate the elemental composition of different materials and to obtain information on the topology and morphology of different samples. These include Energy-Dispersive X-Ray Spectroscopy (EDX), Transmission Electron Microscopy (TEM), and Scanning Electron Microscopy (SEM) among others. The EDX is a chemical Microanalysis technique. It detects the X-rays emitted from the sample under test during a bombardment of an electron beam to extract the elemental composition of a sample. Using the EDX or EDS, features that are as small as 1 μm can be analysed. TEM is also a technique used for observing the features of small specimens. The TEM technology uses an accelerated beam of electrons, which are transmitted through a thin specimen to extract the structure and morphology of the sample. However, SEM is a powerful technique used in the examination of materials. It is widely adopted in different fields to obtain a high magnification of images, with a good depth of field [95]. When SEM is used in conjunction with other closely related techniques such as EDX or EDXA, the composition of individual crystals in a material is determined. The SEM machine has detectors for secondary and backscattered electrons, improved electron optics and electron emission guns with increased resolution when compared to the TEM, where the sample of interest is illuminated with the mobile beam.

The SEM technology is used in the study of samples from different field of studies, which includes biological samples, polymers and semiconductors. It measures the thickness and the concentration of samples, among others [96]. In the study of polymers, this technique is used to obtain information on topology and morphology, as seen in the studies of [97]. SEM is also seen to be used in the study of aluminium alloy and its chemical composition by [98]. Thus, SEM provides information on the chemical composition, electron behaviour and surface topography of samples [95].

2.9 Dielectric materials and techniques for measuring dielectric properties

Dielectric materials such as insulators play important roles in the development of humankind. Insulators are used in every electronic circuit from the charge storage (capacitor) to silicon dioxide used in microelectronics. Heating through dielectric loss is widely employed in industry for preheating plastics before moulding, for drying lumber and other fibrous materials. Electronic circuits are designed to be small and fast with suitable dielectrics to cater for the increasing number of users on the network. In Telecommunication, silica-based fibre optics are often preferred due to its high level of heat conductivity and low rate of transmission loss. In wire and cable industries, good polymers are used for Earthing and electrical insulation between conductors [99]. They also provide mechanical support (fillers and jacket) to different categories of cable. Low dielectric constant materials are used for minimising propagation delay, electromagnetic (EM) coupling and the loss of signal flowing through the cable.

Some of the base insulation resins used for insulating twisted pair copper conductors include Polypropylene (PP), Fluorinated ethylene propylene (FEP) and High-Density Polyethylene (HDPE) [100] and the base jacketing resin often used is Polyvinyl chloride (PVC). Besides, PP and HDPE are part of the polyolefin family while FEP is currently the most common polymer used among the Perfluoropolymers (PFPs). The HDPE is usually employed for the CMR cables while FEP is used for the CMP cables, but both CMR and CMP cables use compounded PVC for their jacketing. HDPE has little branch; as a result, its intermolecular forces are strong. Other properties of HDPE include its capability to perform well up to 75 °C and withstand higher temperatures of about 120°C for a short period. FEP offers an outstanding balance of properties, which includes low dielectric constant and dissipation factor with high flame retardancy. The useful temperature range for the FEP is the range of -65 °C to 175 °C [100]. According to [100], FEP has better dielectric properties, as compared to the polyolefins.

Typically, the transmission performance of balanced twisted pair cabling depends on the dielectric properties of the cable's conductor insulation. Thus, the dielectric properties of materials provide useful information on the dissipation of heat, electric and magnetic fields in the materials. The two parameters determining the electromagnetic field propagation in the material are the electrical permittivity (ε) and magnetic permeability (μ). Since different components of balanced twisted pair cables are not magnetic, the magnetic permeability of most materials is usually 1. However, electric permittivity is a material property, which affects the propagation of the electric field when an alternating voltage is applied to a material. It profoundly affects the speed of signal

propagation in the cable. An electric permittivity is a complex number, which can be obtained using the equation below (2.9.1).

$$\varepsilon = \varepsilon' - j\varepsilon'' \qquad (2.9.1)$$

The real part of dielectric permittivity (ε'), also called the dielectric constant or relative permittivity represents the amount of energy from an external electrical field stored within the material.

Dielectric constant $\varepsilon_r = \frac{\varepsilon'}{\varepsilon_0}$ (2.9.2)

where

ε_0 is the permittivity of free space ~ 8.85×10^{-12} $(F.m^{-1})$

A certain amount of energy is dissipated (loss) from the material when an external electric field is applied and is measured as the imaginary part, ε''. The dissipation factor or the loss tangent is used to quantify a material's inherent dissipation of electromagnetic energy as heat due to the charging and discharging capacitor. As stated in (2.9.3), the loss tangent represents the ratio of the imaginary part to the real part of the complex permittivity.

The loss tangent: $\tan\delta = \frac{\varepsilon''}{\varepsilon'} = \frac{\sigma}{\omega\varepsilon}$ (2.9.3)

Where σ is the conductivity of the material and ω is the angular frequency.

As shown in figure 2.38, the overall conductivity of polymers can be made up of different conduction mechanisms at low frequencies, but ionic conductivity is the most prevalent in most materials. The ionic conductivity of materials contributes to the dielectric loss.

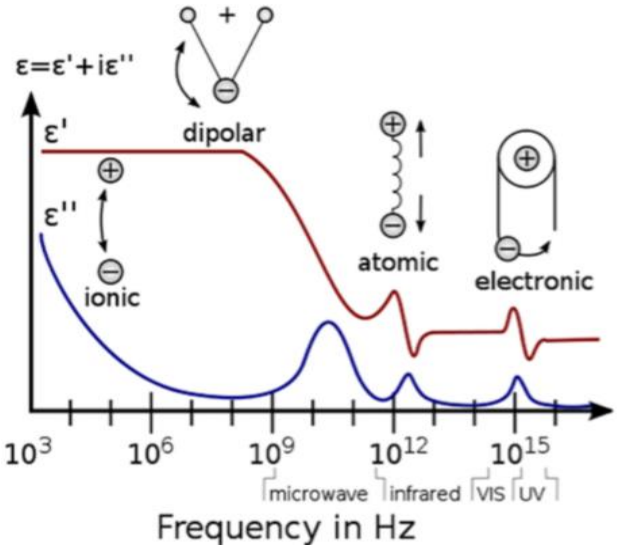

Figure 2.38: Various conduction mechanisms at different frequencies [100]

2.9.1 Thermal degradation of Ethernet cable and its polymeric materials

Many factors contribute to the performance and life expectancy of Ethernet cable and its polymeric material, some of which include: (1) the quality of the polymer employed in the manufacturing of the cable (2) the processing methods employed for making the cable and its dielectrics (3) and the application environments in which the cables are deployed. Moreover, there is a higher significance for thermal degradation of polymers during processing than in the actual application.

Polymers are generally volatile at ordinary room temperatures; however, they do degrade in an oxidative atmosphere. According to [101], oxidative atmosphere and higher temperature will increase the rate of degradation of polymers. Also, prolonged application of loads on the cables at low temperatures may result in slow plastic deformation. Hence, a slow visco-plastic deformation can occur, and the process accelerates with time under a constant load at a particular temperature, this process is termed thermal creeping. It results from the effects of strain and temperature. According to [102], it is the cause of springs loosening up with time. Thermal creeping occurs above 30 % of the melting temperature or glass transition temperature. Moreover, prolonged thermal exposure and high humidity can damage the cable polymeric materials. *"Other than having some relation to elevated temperature and humidity, the electrical wire and cable manufacturers do not completely understand why failure occurs in some installations and not in others"* [103].

Most polymers have small amounts of additives that impart their desired characteristics. For example, the addition of heat stabilisers to polymers prevents thermal degradation of the material at high temperature, whereas antioxidants are used as anti-ageing in polymers. In addition, fire and flame retardants are self-extinguishing additives and smoke suppressants. Moreover, the addition of fillers increases rigidity and creep resistance. Furthermore, stabilisers are for the phase stability of the cable and plasticisers enhance the flexibilities of polymers. The plasticiser added to the PVC resin to make it pliable may sometimes remain as individual components and held with the PVC by intermolecular forces and not firmly bound to the base resin. Giving this, some links in the polymer may be weak if the processing of the materials is inadequate, leaving the polymer unstable. According to [103], when the polymer is exposed to sufficient heat and time, the degradation of the material may start from the weak links. Also, [104] reported that the initial degradation of PVC is an increased elimination of the side group chains (HCL) attached to the backbone of the polymer and the formation of polyenes. After this initial step, the polymer remains unstable and undergoes further reaction.

Although the mechanisms behind the thermal degradation of PVC is still not very well known, [104] suggested that if an improper quantity of plasticiser is used in a PVC resin, the plasticiser may push the polymer chain apart and move from the vinyl mass before migrating to the surface of the polymer by diffusion. A study conducted on food plastics containing plasticiser reported small deformation of the plastic due to long-term repeated heating [105]. It was suggested in the study that an increase in the temperature of the material could lead to an increase in the decomposition of the additives and the breakdown of the polymer chains, which would cause some chemicals to be released from the surface of the plastic. From the observation in the study, it can be noted that the effects of temperature are linked to the migration of compounds from the polymers. It is to be noted that the same polymer from different manufacturers may have different properties because of the variations in branching and molecular weight. Also, the physical properties of polymers such as failure strain, toughness, and so on may depend on their processing history.

Another factor affecting the performance of polymers is the interfacial adhesion of copper to polymers. Interfacial adhesion is the molecular attraction between the interfaces of different materials in contact. In view of this, the state of the two surfaces brought into contact will determine the magnitude of the adhesion. According to [106], the state of energy of a surface quantifies its surface energy. The adhesion between two surfaces will be high if they show similar surface energies and vice versa. Metals exhibit high surface energy, while synthetic polymers mostly used as commercial materials have low surface energy. Thus, there is a low adhesion of these polymers to high surface energy metallic coatings. Besides the surface energies of the bodies in contact, one

other factor influencing the adhesion of two different surfaces is the roughness of the contact between the two bodies. Traditional electromigration lifetime studies were performed in [107] to investigate device reliability as a result of the drift velocity. Results indicate that the adhesion of the copper interface is directly related to the electromigration of copper conductors. As suggested, Electromigration in copper conductors is almost exclusively through interfacial or surface diffusion. In [108], the effects of wet chemical treatment and thermal cycle conditions on the interfacial adhesion energy of Cu/SiN_x thin-film interfaces were evaluated by a 4-point bending test method. The amount of Cu oxide between SiN_x and copper was found to increase after thermal cycling. The thermal stress due to the mismatch of thermal expansion coefficient during thermal cycling seemed to weaken the Cu/SiN_x interface adhesion, which led to an increased amount of copper oxide at the surface of the Cu film.

One of the significant factors affecting the properties of thermoplastics is crystallinity [109]. Crystallisation causes a significant volume of polymer to reduce during solidification because crystals may be dispersed through the material. As a result, variation in the thickness of thermoplastics during processing may cause differential contraction due to different cooling rates, which may also lead to shape distortion.

Other factors causing deformation of polymers are thermal variation and localised heating. According to [102], small temperature change causes elastic deformation that disappears when the initial temperature is recovered. However, temperature variations cause non-recoverable deformations on either free-standing or constrained materials. As suggested in [102], plastic deformation is due to slippage at the atomic level, with bond-breakage and bond-forming processes, favoured by dislocations and imperfections in the plastic.

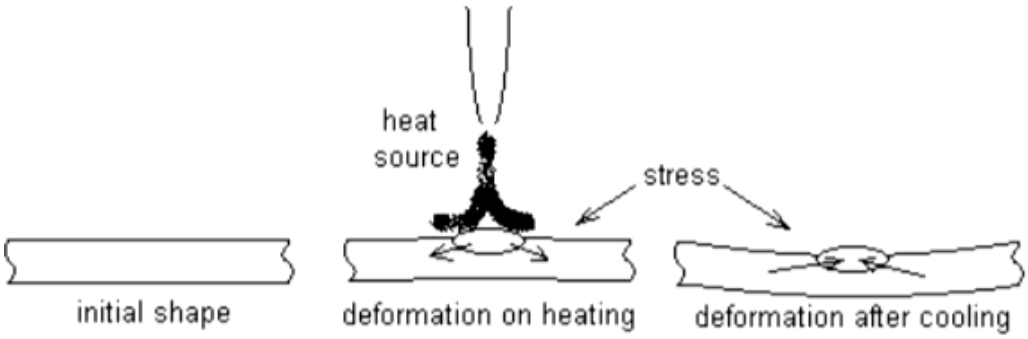

Figure 2.39: Showing thermoplastic deformation due to localised heating [102]

High temperatures cause significant mobility and easy rearrangement of matter within the polymer that, after solidification, gives rise to new stable bonds. When plastic is locally heated (figure 2.39), there is an elastic convex deformation at first, which fades out upon cooling. However, if the plastic is heated to a high temperature, a plastic concave permanent deformation occurs after cooling. Moreover, whichever way the plastic is heated, a permanent bending occurs by material shrinkage due to plastic strains from the locally heated portion of the plastic [102]. From this illustration, it can be noted that the deformation of Ethernet cable dielectric due to localised heating is an area of concern in some installation environments where a significant portion of the cables pass through insulated areas. As suggested in [110], the shrinking of the overall diameter of the dielectric will cause the ε_r to increase. An increase in the ε_r will cause the capacitance to increase. At high frequencies, the increase in the unit capacitance of the cable will cause a significant current to be drawn for the same amount of power transfer [111].

The performance of polymers is also affected by the phase transition effects at room temperature. In the study conducted in [112], a significant change (0.1 %) in the electrical length of a half wavelength Teflon cable was observed as the Teflon in the cable goes through a room-temperature chemical molecular phase transition. According to [112], the two common crystalline temperatures at which phase transition occurs in PTFE (Teflon) are 19°C and 30°C. A slight untwisting of the helical chain conformation was observed to have occurred at 19°C transition, affecting 13 to 15 CF_2 groups per 180° twist. In addition, the chain segments were disordered from a perfect lattice by small angular displacement about their longitudinal axis between 19°C and 30°C. Above 30^0C transition, the preferred crystallographic direction has been lost, and the molecular segments oscillate about their long axis with random orientation in the lattice. Although it was illustrated in [113] that phase drifts could occur with the temperature only due to changes in the mechanical dimension or dielectric constant of the conductor insulation; their experimental result suggested that the major phenomenon responsible for the phase drift in coaxial cables was due to the sensitivity to thermal variation.

In summary, regardless of the type of polymer employed for any cable, all polymers will degrade when exposed to oxidising medium like air. The degradation of the polymers will be accelerated with an increase in temperature. Temperature fluctuations and localised heating are detrimental to polymers. Combination of stresses will accelerate the degradation of cable performance. Cables with better polymer and better processing methodologies can last longer during usage and will maintain the defined transmission characteristics for an extended time. However, cables having polymers made from inadequate material composition and processing method will degrade even

within the first few days of thermal cycling. Given these, it is essential to investigate the properties of materials under different operating conditions using accurate test methodology.

2.9.2 Dielectric properties assessment methods

There are different techniques (figure 2.40) for assessing the complex permittivity of polymeric materials. These include analytical methods [114], numerical methods [115, 116] and microwave measurement techniques [117].

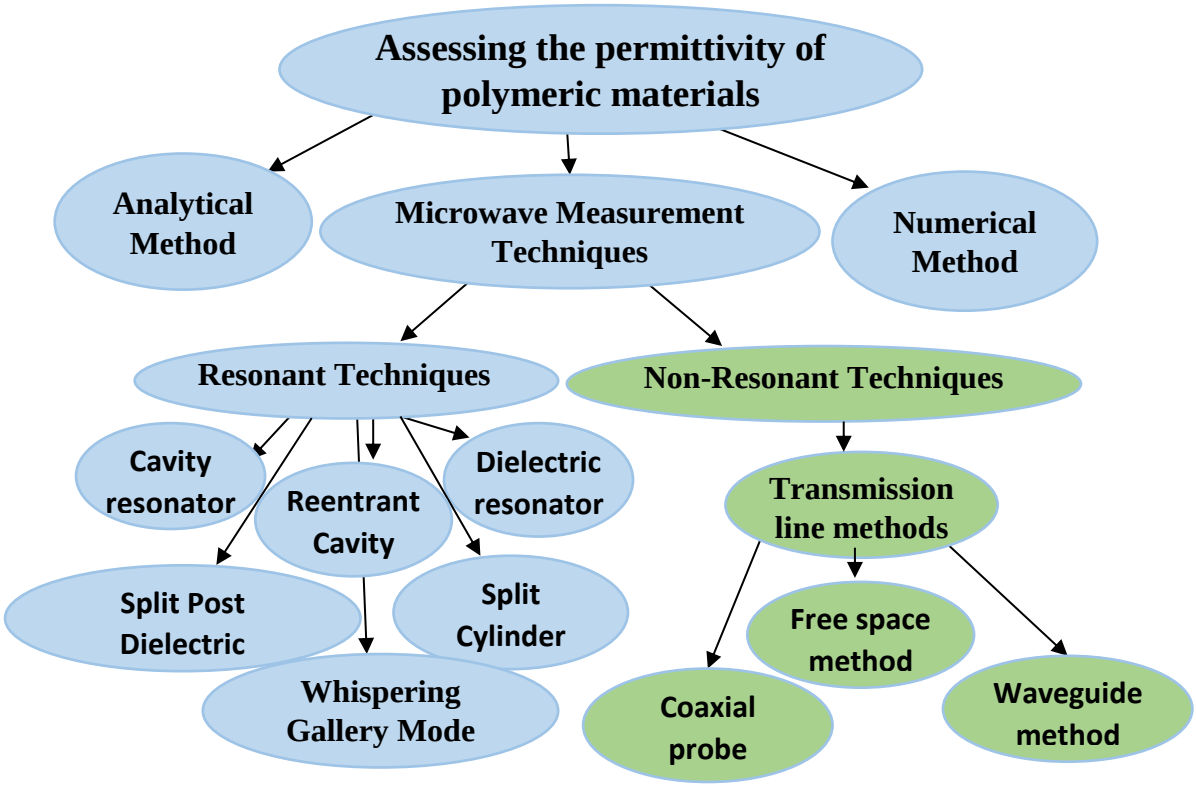

Figure 2.40: Different techniques for dielectric characterisation

The microwave measurement techniques are in two broad categories, the resonant and non-resonant techniques. The resonant techniques encompass of the cavity resonator, dielectric resonators, split-post dielectric resonators, split-cylinder resonators**,** re-entrant cavities and whispering gallery mode resonators among others. Whereas, some of the non-resonant techniques are classified into transmission or reflection line method, which includes: free space method [117], waveguide method, coaxial probe method and parallel plate method. Each of these methods is limited by the frequency at which the measurements are carried out and the type of dielectric sample that can be measured.

(A) Resonant Method

The advantage of the resonant method is the capability to measure a tiny sample. However, its disadvantage is the need for a high-frequency resolution Vector Network Analyser. Also, resonant techniques are suitable for the characterisation of material properties of different samples but measure dielectric properties at a single or few discrete frequency points [118]. With the resonance method, the resonant frequency and bandwidth of an empty cavity are measured first, as shown in figure 2.41. The f_0 in figure 2.41 is the resonant frequency, while Δf is the frequency difference at 3 dB points.

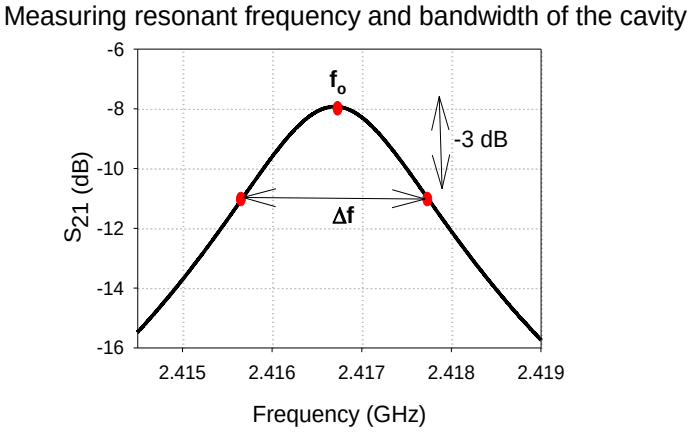

Figure 2.41: Measuring the resonant frequency and bandwidth of the cavity

After the initial measurements of the empty cavity resonance and bandwidth, the measurements are repeated after filling the cavity with the dielectric sample. Then, the complex permittivity of dielectric material under test is determined from the measurements of the resonance frequency shift, quality factor (Q) and volume of the loaded and unloaded cavities.

(i) Cavity Resonators

The cavity resonators are designed to resonate to the specific mode for which they are designed which can be in the Transverse Magnetic (TM) mode or Transverse Electric (TE) mode. For example, in cavities operating in TE_{10n} mode, electric field lines are tangential to the surface of the dielectric material. Also, there is a strong electric field at the centre of the cavity, where samples of different geometries can be placed and tested. According to [118], the volume of the perturbation sample should be relatively small compared to the volume of the cavity. The diameter of a rod sample was suggested to be 10 % or less when compared to the wavelength of the measurement

frequency. Also, the diameter of a thin sample should be $\leq 0.25a$ [119]. Studies conducted in [120] concluded that the maximum sample volume for dielectrics with different geometries follows the order of strip or disk>sphere>rod or bar. It was suggested in [121] that rod samples have an advantage of lower depolarisation effects than a flat sample. Given this, using the cavity resonator method, a thin rod sample is inserted into a hole at the centre of the cavity, and a perturbation technique [118] is used to obtain its permittivity. To obtain an accurate dielectric measurement using this technique, a correction for the hole may be necessary. Moreover, in the study conducted in [34], the effect of the air gap around the dielectric rod sample was considered by using multiple dielectric rods instead of a single rod and by considering the electromagnetic shielding of a rectangular cavity with an aperture.

(ii) Dielectric resonator

The dielectric resonator consists of a metallic cavity and a cylindrical shaped dielectric material. By using the dielectric resonator, the measured loss consists of loss from the metallic lateral walls and dielectric loss. The difference in the linear thermal expansion coefficient of the metal wall of the cavity and that of the dielectric material constitutes a problem, especially during low-temperature measurement. However, by using superconducting materials or Perfect Electrical Conductor (PEC) as the end and wall plate, the loss is minimised, and the measured loss will be from the sample under test only. The cavity perturbation method allows dielectric samples of different geometries to be tested, but the dielectric resonator method works only on samples with either rectangular or round shape. Although the CPM is suitable for low, medium to high loss material, the low loss measurement method requires materials of larger samples. Another advantage of the cavity perturbation method is its simple calculation process for obtaining the complex permittivity [118] as compared to the computer algorithm used in the dielectric resonator method. The cavity perturbation method has been very useful in the specification acceptance, manufacturing control, research, and development of different electronic components [118]. Many researchers have also adopted it for the measurements of high and low loss materials.

(iii) Split-Post Dielectric Resonators

The Split Post Dielectric Resonator (SPDR) measurement technique produces accurate dielectric measurement results. It can be designed to function in the low gigahertz region and can measure dielectric material as a function of temperature. However, it can only measure dielectric

material at a spot frequency since it is among the family of the resonant methods. This method involves inserting a thin dielectric sample between two fixed dielectric resonators and the resonator measures the dielectric permittivity in the plane of the specimen [122]. Although the quality factor of the support post is influenced by the presence of the specimen, to reduce the loss in the resonator, the dielectric resonators are supported by low-permittivity dielectric posts. The primary source of uncertainty in the measurement of relative permittivity using the SPDR is the thickness of the specimen. Typically, an uncertainty of ±0. 002 in the value of ε_r is not uncommon [123]. Whereas, the uncertainty in the dielectric loss tangent depends on the accuracy of the quality factor measurements. According to [123], an uncertainty of ±2 x 10^{-5} in the dielectric loss tangent is possible for a properly chosen sample thickness.

(iv) Split-Cylinder Resonators

The split-cylinder resonator is used to measure the complex permittivity of low-loss substrate materials at microwave frequencies. The method uses a cylindrical cavity which is separated into two halves. Generally, a substrate sample is placed in the gap between the two shorted cylindrical waveguide sections. The cylindrical cavity is excited with the coupling loops, and from measurements of the resonant frequency and quality factor, the complex permittivity of the sample is determined. The requirements for this method are the use of a flat sample and to extend the sample under test beyond the diameter of the two-cavity sections. However, the extension of the sample causes fringing fields in the sample region outside of the cylindrical waveguide sections. As a result, the uncertainty in the measurement of the dielectric constant is limited to ±0. 005 while that of the loss tangent is limited to ±5 x 10^{-5}. Moreover, the Split-Cylinder Resonator technique has been improved theoretically in [124, 125] by considering the effect of fringing fields based on the mode-matching method.

(v) Coaxial Reentrant Cavity

The reentrant cavity is used for dielectric measurement at radio and microwave frequencies. The coaxial reentrant cavity consists of a coaxial transmission line with a gap in its inner electrode [126, 127]. By inserting the sample into the gap, the cavity resonates, and the capacitance of the gap produces a frequency shift. There are two types of coaxial re-entrant cavity system based on the location of the specimen gap region (SGR): if the SGR is located at the top or bottom of the cavity, then the system is a single reentrant cavity, whereas if the location is in the middle of the cavity then is called a double reentrant cavity. The major difference between the reentrant cavity and the

conventional coaxial resonators is the variable air gap in the reentrant cavity's inner conductor. Researchers have used several methods for modelling the resonant properties of reentrant cavities over the years. In [128], lumped-element equivalent circuit models were used. Also, in [129, 130], modal analysis was the modelling technique of choice. However, due to the limited accuracy of the lumped-element equivalent circuit models, researchers turned to numerical methods such as finite element method (FEM) [131] and the finite-difference-time-domain (FDTD) [132]. Moreover, because of the long computation time required for the FEM and FDTD approaches, a study in [133] modelled the resonant properties of the entire reentrant cavity by dividing the reentrant cavity into regions where scattering parameters of each region are computed easily and combined using circuital analysis [133]. This technique was further adopted in [113] to predict the resonant properties of the reentrant cavity at fundamental and higher-order resonant frequencies. The advantage of this approach is that dielectric properties can be characterised at high frequencies using higher-order mode.

(vi) Whispering Gallery Mode Resonator

The Whispering Gallery Mode (WGM) Resonator [134 - 137], is one of the most accurate dielectric measurement methods for a very low loss dielectric material. The WGM technique is a complicated method; it requires large dielectric samples of specific shapes. At high frequencies, the conventional dielectric resonators have quite small dimensions, lower quality factor and are challenging to fabricate. However, the quality factor of the WGM resonators is high, even at high frequencies. The disadvantage of the WGM resonators is the difficulty in identifying the correct modes. As a result, knowledge of the permittivity of the sample under test is required, using another technique before the use of the WGM resonators for microwave characterisation of materials.

(B) Non - Resonant methods (Transmission Line or Reflection Line Method)

Transmission line or reflection line method is a broadband measurement method which utilises transmission line concepts and involves placing a piece of dielectric material inside a coaxial line or waveguide, and an electromagnetic wave is directed at the sample [138, 139]. Waveguides are suitable for measuring the dielectric properties of larger samples at frequencies up to 2.45 GHz. The method involves measurement of relevant scattering parameters, which are converted using a computer program to obtain the complex permittivity of the dielectric under test. Non-resonant

techniques can provide measurement capability over a wide range of frequencies, but the effects of airgap limit the measurement accuracy. Furthermore, the accuracy of the Transmission line technique also relies on the sample geometry.

(i) Free Space Method

The free space method allows measurements of dielectric samples under many environmental conditions such as high temperatures and humidity. The characterisation of the dielectric materials requires two antennas facing each other in an open space environment [140]. The reflective mirrors are set up in such a way that the diverging beams are directed onto the dielectric under test. The network analyser, which is connected to the antennas, is used to obtain the reflection and transmission coefficients. The measured reflection and transmission coefficient are further used to determine the dielectric properties by post-processing the measurements using a computer program. Free-space measurement using the transmitting and reflecting antenna is ideal for the measurement of dielectric materials up to high frequencies, but the measurement requires a large and flat sample. Additionally, the measurement performed in an open space increases the possibility of obtaining incorrect results because of the multiple reflections between the antenna and surface of the dielectric sample.

(ii) Coaxial-probe(s) method

The coaxial probes and waveguides are suitable for measuring the permittivity of samples of medium to high loss. Coaxial probe method is a non-destructive testing method used for the measurement of elevated temperature of both solids and liquids samples [141]. A coaxial line of 7 mm diameter is suitable for dielectric measurement from 1 MHz to approximately 18 GHz, whereas, a coaxial line of 14 mm diameter measures samples from 100 kHz to 2 GHz. Two coaxial probes can also be used as a two-port test device, where a specimen is inserted between the probes for the measurement of both reflection and transmission data. In this case, the measurements obtained are inverted for the calculation of dielectric permittivity.

(iii) Open-ended Coaxial Probe method

The open-ended coaxial probe is a truncated section of a transmission line. The probe is pressed against a sample, and the Electromagnetic fields at the end of the probe penetrate the sample under test. The reflected signal is obtained using a Vector Network Analyser (VNA) that is connected to

the coaxial probe, and the dielectric properties are calculated from the measured phase and amplitude of the reflected signal. The open-ended coaxial probe method is easy to use and requires no machining of the sample. After the calibration of the measurement system, the dielectric properties of a large number of samples can be routinely measured within a short time. Also, dielectric characterisation of thin materials is possible over a wide range of frequencies (500 MHz – 110 GHz). However, only reflection measurement can be performed. According to [142], one of the major issues with the use of a coaxial probe method is obtaining good surface contact with the solid material (effect of air gaps). As a result, the measured reflection may not fully represent the reflectance from the solid sample [143].

Among all the dielectric measurement methods, resonant methods are the most accurate methods for dielectric properties characterisation [144]. Also, based on the low loss nature of the rod samples required for this research, Cavity Perturbation Method was chosen to be an ideal method for the dielectric property measurements. Thus, it was adopted in this research.

CHAPTER 3 - ASSESSMENT OF CABLE BUNDLE HEATING

The test methodologies for the assessment of cable bundle heating in this research are detailed in this section. From the literature (see section 2.5), there are three principal methods of assessing the possible temperature rise in cable bundles when used in powering PoE equipment. The three approaches are:

i. *Thermocouple approach,*
ii. *Resistivity approach and*
iii. *Mathematical model.*

All the three approaches were adopted in this research to assess possible temperature rise due to cable bundle heating. Moreover, various scenarios of cable bundle heating were evaluated. In the first instance, the assessment of cable bundle heating based on different power levels was conducted (section 3.1) taking cognisance of the cabling installation environments. After that, the impact of cable construction on heat generation and dissipation in different Ethernet cable bundles was evaluated (section 3.2). Furthermore, cable bundle heating as a function of bundle sizes was characterised at five current levels (section 3.3). In the subsequent tests, the measured temperature distribution across a 37 CB (36 around 1) configuration using the thermocouple approach was compared with the prediction made using the mathematical model. Also, the temperature rise of the 37 CB assessment scenario using the three approaches was compared (section 3.4). That is, the thermocouple approach was used to validate the mathematical model and the resistivity approach.

3.1 Assessment of CB heating based on power levels and installation environments

The assessment of CB heating in two installation environments was conducted using the thermocouple approach. The two installation environments considered are: (i) ventilated ("Free air") spaces and (ii) unventilated (insulated) spaces. Also, three DC power levels were considered in total: PoE+ at 34.2 watts, UPoE at 60 watts and HDBase-T at 100 watts. To get an accurate reflection of the impact of power levels on cable performance, shielded and unshielded Ethernet cables were tested (see table 3.1). The test configurations and set-up are explained below.

Table 3.1: Categories of cable used in the CB heating assessments

Unshielded Ethernet cables	Shielded Ethernet cables
Category 5e U/UTP	Category 6 FTP
Category 6 U/UTP	Category 6 F/UTP
Category 6 CCA	Category 6A F/FTP
Reduced diameter Category 6 U/UTP	Category 7A S/FTP

Free air heating set-up

In the first stage of the assessment, a test rig was constructed to allow a bundle of 37 cables to be suspended in the free air environment. According to the procedure described in [20], a single 100 m length of cable was spooled to produce a CB with three complete layers surrounding a centre cable, as shown in figure 3.1.

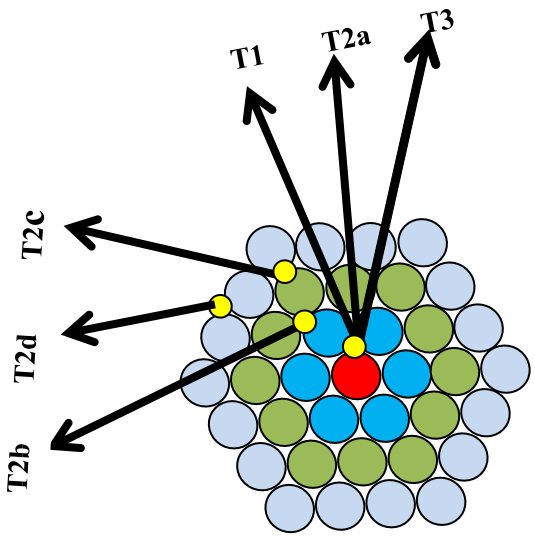

6 around 1 (7) over 12 around 7 (19) and finally, 18 around 19

Figure 3.1: Cable bundle and thermocouple locations

Thermocouple sensors of K-type for the temperature measurement (T2b, T2c and T2d) were placed on the surface of the cable jacket in each layer of the CB as indicated in figure 3.2, and in accordance with reference [20].

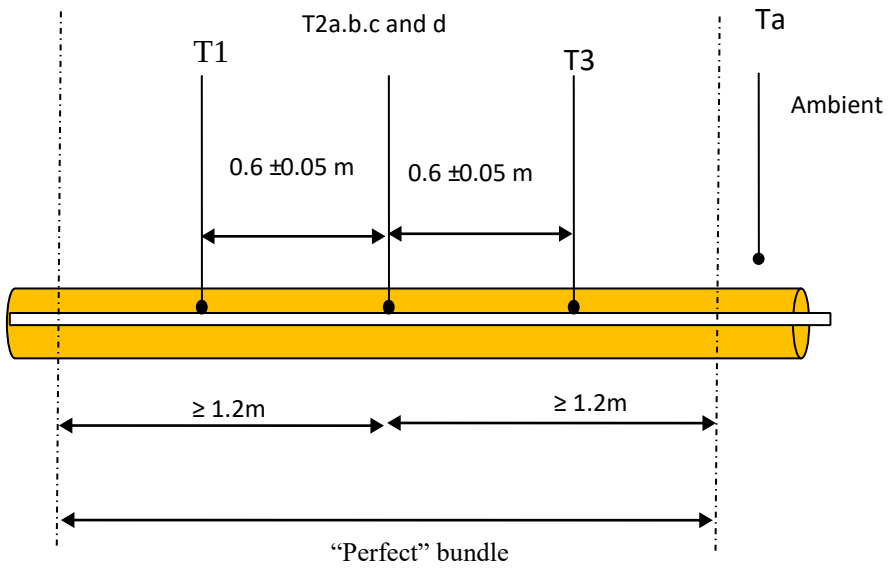

Figure 3.2: "a perfect cable bundle" and the positions of thermocouple sensors

Aside thermocouple sensors being distributed throughout the layers, thermocouples (T1, T2a and T3) were also positioned along the length of the centre cable with T3 being the thermocouple sensor near the actual source of the power. Although thermocouples were placed within 2.4 m length of the CB, each of the cables within the bundle is of 2.7 m length. After the bundling of the cable, the finished CB was suspended with a supporting frame of low thermal conductivity, in a free-air environment to achieve heat dissipation into the surrounding environment. Figure 3.3 shows the suspension of the CB in the free air environment.

Figure 3.3: Suspension of the CB in the free air environment.

Insulation heating set-up

The cable bundling and test configuration described in section 3.1 also apply to the case of the insulation heating set-up, except that polyethylene thermal insulating foam was used to insulate the unshielded Ethernet cables. Moreover, due to the larger cable diameter, the shielded Ethernet cables were insulated with a glass fibre based insulating material. Before the whole CB was connected to the power supply, thermal insulating foam spray was used to cover the two ends of the CB to limit heat transfer from both ends. Figure 3.4 and 3.5 show the insulated CBs with the dimensions of the insulating materials. Note that the covering of the two ends of the CB was to create extremes of heat build-up. That is, to produce a worst-case scenario of CB heating that should not be exceeded in 'real-life' installations.

Insulation thickness: 25mm and pipe diameter: 28mm

Figure 3.4: Insulation of the unshielded Ethernet cables

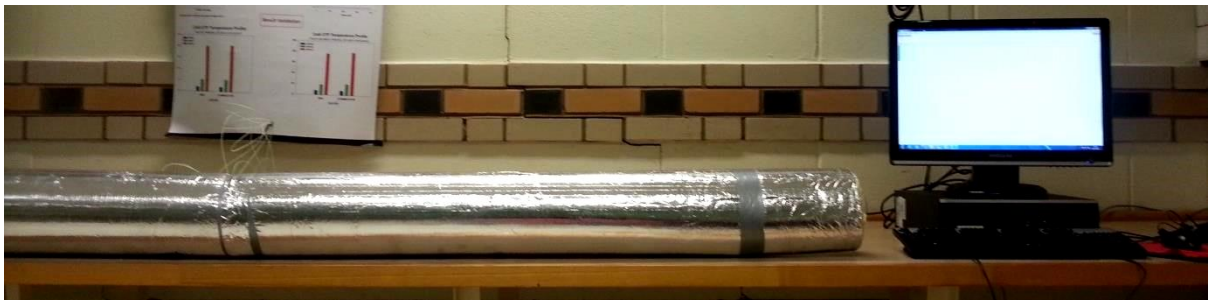

Insulation thickness: 25 mm and pipe diameter: 114 mm

Figure 3.5: Showing the insulation of the shielded Ethernet cables

The connection of the cable bundle

After the installation of the CB, the connection of all the conductors in the cable was made in series to allow the balanced pairs within them to be fed with a constant current. Figure 3.6 shows the connection of the CB.

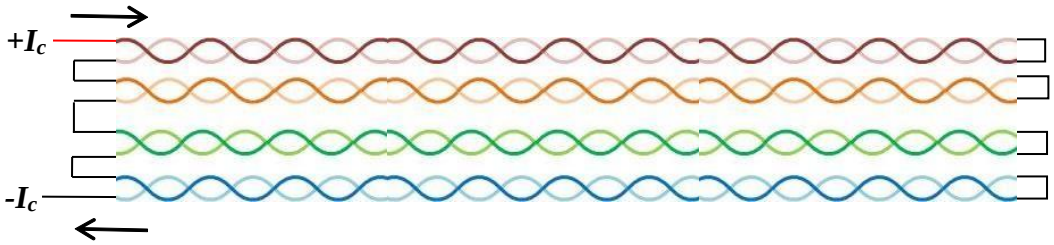

Figure 3.6: Configuration of the copper conductors inside the whole CB

Powering of the cable bundle

Flexible heavy gauge wires were connected between the CB and a DC power source to supply power to the CB. The tests were carried out over four-pair powering and with the three stated power levels: 32.4, 60 and 100 watts respectively.

Temperature Measurements

The room temperature and the temperature of each thermocouple sensor placed in different layers of the CB were automatically recorded using a temperature data logger. Final measurements were taken after the temperature of the CB had reached a steady state. It is important to mention that in every aspect of the CB heating assessment, importance was placed on the temperature rise in the centre of the mass (T2a - the centre of the CB), temperature distribution across the CB and the stability of temperature rise with respect to time.

3.2 Assessment of cable bundle heating based on cable constructions

3.2.1 Assessment of cable bundle heating based on cable conductor sizes.

Using the set-up in Section 3.1, the first part of the assessment of the impact of cable conductor sizes on cable bundle heating compared the temperature performance of a standard Category 6 U/UTP AWG 23 against that of the reduced diameter Category 6 U/UTP. The rationale for the comparison was to establish the effect of conductor size on possible heat generation in the two cables. Also, to investigate the performance of the reduced diameter Category 6 cable as it is claimed to offer 100-meter channel performance of Category 6 U/UTP while having physical characteristics closer to that of Category 5e U/UTP. To this effect, the DC loop resistance values of the two cable types were examined and compared. However, the second part of studies compared the temperature performance of two Category 7A S/FTP cables based on their conductor sizes. The first Category 7A S/FTP cable has conductor size of AWG 22 while the second Category 7A S/FTP is of AWG 23. The results of the assessment in this section are presented in section 4.2.1.

3.2.2 Assessment of cable bundle heating in terms of material types

Based on the heating set-up described in section 3.1, the impact of cable construction, such as the material of the crossweb, conductor material, the quality of the conductor insulation and cable screening was examined.

In the first instance, the impact of conductor size and polyethylene based crossweb on heat generation and dissipation was assessed. Category 5e U/UTP and Category 6 U/UTP were used for the analysis. Results of the analysis are presented in section 4.2.2. Secondly, the investigation of the impact of conductor material on heat generation was conducted using the temperature performance of Category 6 U/UTP (Copper Clad Aluminium) and Category 6 U/UTP copper cabling for the analysis (see section 4.2.3 for the results). The last study in this section evaluated the impact of individual screening of conductor pairs on heat dissipation by comparing the performance of Category 6A F/FTP against that of Category 6 F/UTP. The results of this last assessment are in section 4.2.4.

3.3 Assessment of cable bundle heating based on cable bundle sizes

The possible temperature rise of the 24 (24 cables in a bundle) and 37 CBs of Category 6A F/UTP was assessed in two installation environments using six current levels: 0.3A, 0.45A, 0.6A, 0.75A, 0.9A, and 1A respectively (values of current below and above the specified 0.6A of the IEEE 802.3at). Figure 3.7 shows the configuration used for the 24 and 37 CBs. In addition to the temperature rise measurements, using the thermocouple approach, the adaptation model equation described in section 2.6.3 was further used to predict the temperature rise of the 24 CB size using the six current levels.

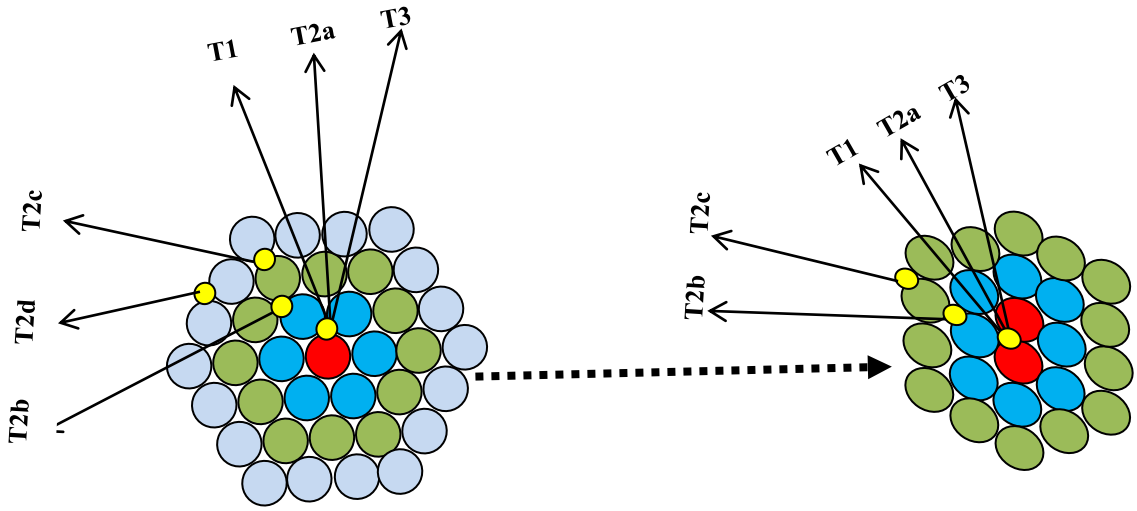

37-cable bundle and thermocouple locations - 6 around 1 (7) over 12 around 7 (19) and finally 18 around 19 (37)

24-cable bundle and thermocouple locations - 8 around 2 (10) over 14 around 10 (24)

Figure 3.7: Configuration of the 24 cables in a bundle and 37 cables in a bundle.

The configuration and the insulation of the 37 CB were as described in section 3.1. However, for the 24 CB size, the T1, T2a and T3 in figure 3.7 represent the thermocouple sensors placed in the axial direction of the 24 CB while T2b, T2c were the thermocouples sensors placed within the bundle layers in a radial direction. The maximum temperature rise on the 24 and 37 CBs using the thermocouple approach was compared first. Then, the maximum temperature rise on the 24 CB using the thermocouple approach was compared with the prediction of the total temperature rise using the adaptation model. The results of the studies in this section are presented in section 4.3.

3.4 Comparisons between the three cable heating assessment methods

This section validates the maximum temperature rise and temperature distribution across a 37 CB using the thermocouple approach. The set-up described in section 3.1 is also applicable to the studies made in this section except for the five current levels: 0.3A, 0.45A, 0.6A, 0.75A and 1A that were used instead of the power levels. Also, only Category 6A F/UTP was assessed as it represents one of the recommended cables for the future PoE installed base.

In the first part of the assessment, the measured temperature distribution across a 37 CB (36 around 1) using the thermocouple approach was compared with the prediction made (ΔT_u and ΔT_{th}) (2.5.9 - 2.6.1) using the mathematical model. After that, the maximum temperature rise of the 37 CB using the thermocouple approach was validated against the output of the mathematical model (ΔT) first and then against the results of the resistivity approach. The results of the comparisons in this section are presented in section 4.4.

CHAPTER 4 - CHARACTERISATION OF ETHERNET CABLE BUNDLE HEATING

The first set of results in this section shows the power carrying capacity of bundled Ethernet cables assessed in two different installation environments and at three power levels (section 4.1). This is followed by the characterisation of the impact of cable construction on the heat generation and dissipation in bundled Ethernet cables (section 4.2). Furthermore, the results from the assessments of the temperature rise in two sizes of Ethernet cable bundles are presented (section 4.3). The last set of results in this section presents the validation of temperature distribution across 37 cable bundle (CB) and then the validation of the maximum temperature rise (section 4.4).

4.1 Characterization of CB heating based on power levels and installation environment

Figure 4.1 shows the results of the free air heating test, while the result obtained during the insulation heating test is presented in figure 4.2. The maximum temperature rise above ambient temperature was obtained from the centre (T2a) of each CB under test. Note that the steady-state temperature gradient across the CBs is given in the appendix A and B. Comparing the results in figure 4.1 and 4.2, the CBs heated in the free air environment generated less temperature rise than the CBs under-insulated heating. Furthermore, in both heating tests, the resistance of the CBs increased due to heating, and the magnitude of the increase was directly proportional to the temperature rise in all the CBs. The resistance increase has always been known to be a contributing factor to the scale of attenuation of the signal on a channel (2.7.3). The effect of resistance increase on high-frequency cable parameters is discussed in section 2.4.

(i) Free air heating

Within the accuracy of the thermocouple sensors, it can be seen from figure 4.1 that the temperature rise on all the cable bundles was within the IEEE and TIA limits at PoE+ (~30 watts) power level but not at UPoE (60 watts) and the HDBase-T (100 watts) levels. However, when the specified operating temperature (60˚C) for the PoE application environments is considered, the temperature rise on all the CBs was within the acceptable power levels of PoE+, UPoE and HDBase-T except for the unshielded twisted pair cables in which their temperature rose by ~42^0C rise above the ambient temperature of ~23^0C at 100 watts power level. Combining the

42^0C temperature rise and the ambient temperature of ~23^0C, result in a temperature value (i.e. 65^0C) that is higher than the specified operating temperature of 60˚C stated within the cable construction standard of [145]. However, it is important to recognise that the temperature rise for the shielded cable bundles was within the specified 60^0C at all power levels.

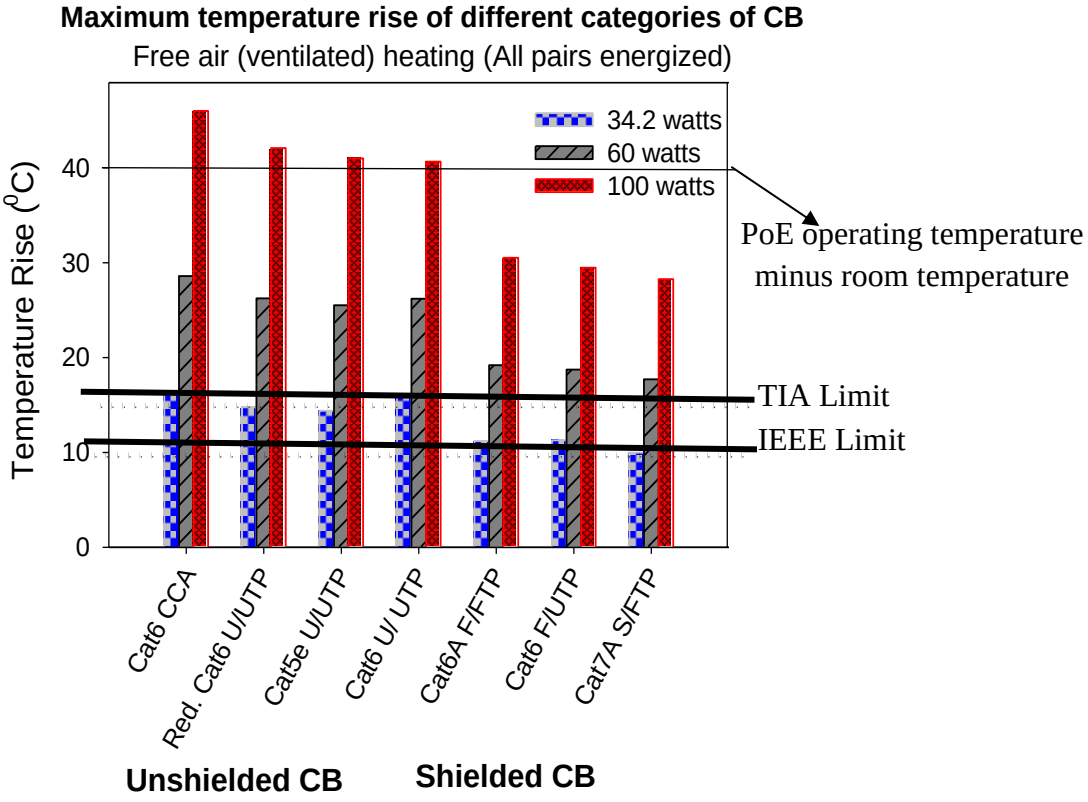

Figure 4.1: Maximum temperature rise (T2a) for the free air heating tests

(ii) Insulation heating

Figure 4.2 shows the impact of high-power deployment on bundled Ethernet cables that are installed in non-ventilated (restricted heat dissipation) environments. The temperature rise on all the CBs was within the 60^0C limit at PoE+ power level but increased beyond the 60^0C limit at UPoE power level; the worst-case scenario of cable bundle heating adopted for the insulation heating tests.

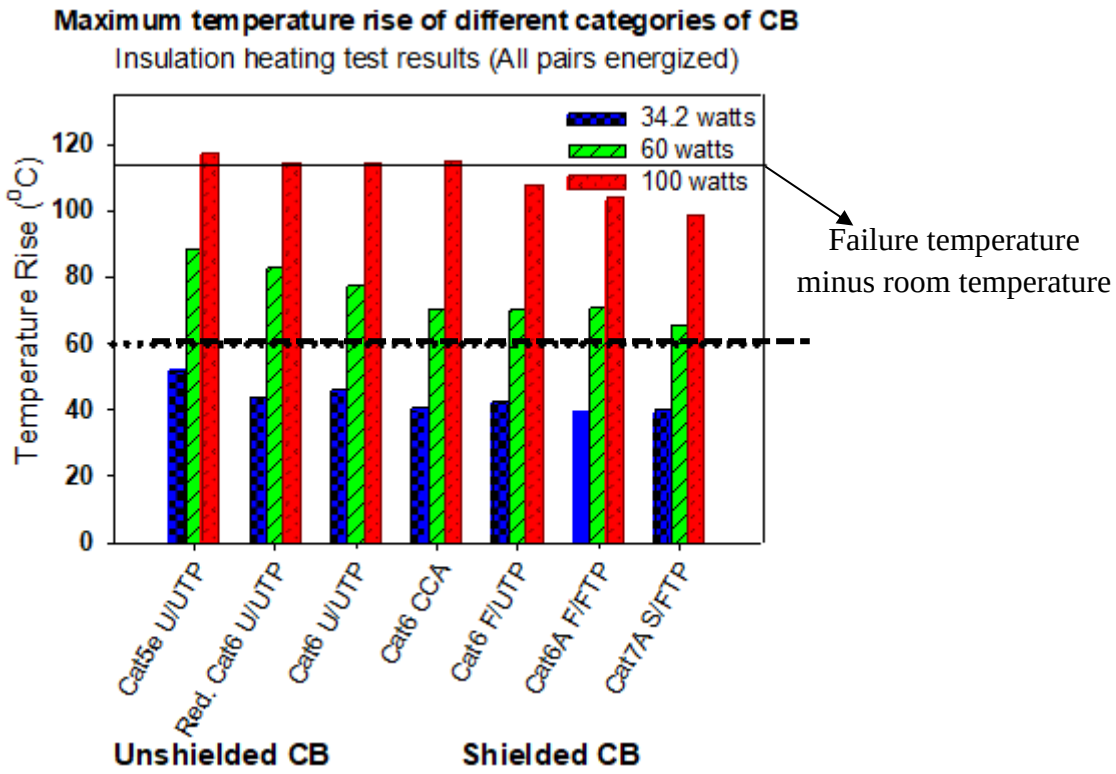

Figure 4.2: Maximum temperature rise (T2a) for the insulation heating tests

At 100 watts, all the unshielded cable bundles (CBs) failed because the increase in temperature was beyond the specified limit of 60^0C. Also, due to the worst-case scenario of CB heating. Figure 4.3 – 4.5 show the points at which the insulated unshielded CBs physically failed at 100 watts.

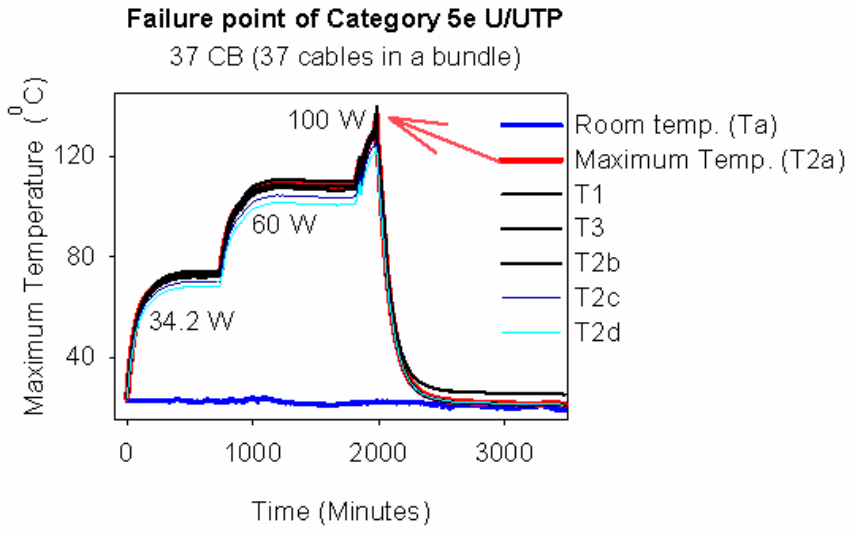

Figure 4.3: Physical failure of the insulated Cat5e CB at 100 watts

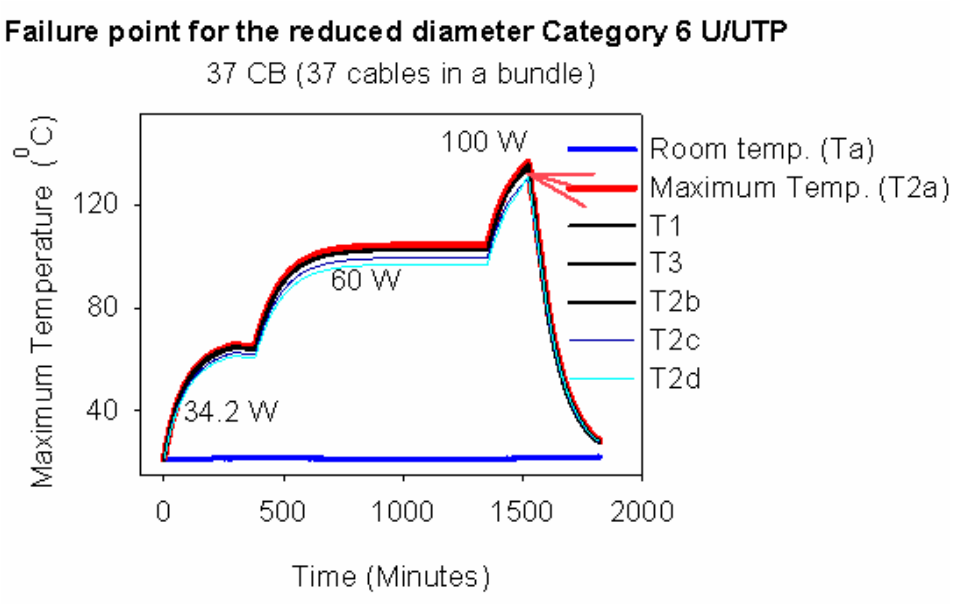

Figure 4.4: Physical failure of the reduced diameter Cat6 CB at 100 watts

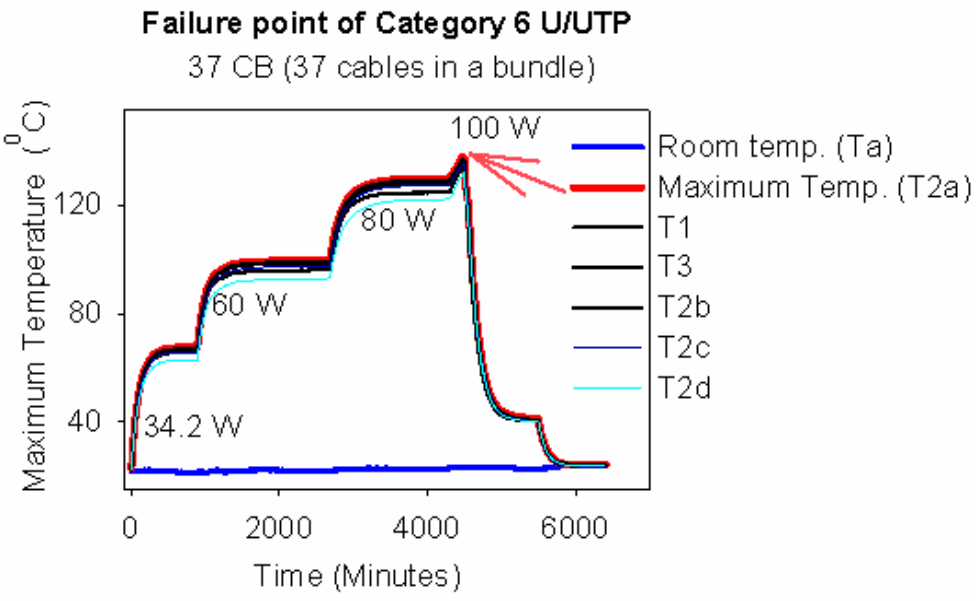

Figure 4.5: Physical failure of the insulated Cat6 CB at 100 watts

Table 4.1: Critical temperatures and the time to fail for the unshielded CBs

Free air heating test results - Maximum temperature rise (T2a) at 100 watts				
Unshielded twisted pair cables	**Category 5e U/UTP AWG 24**	**Reduced diameter or HD Category 6 U/UTP**	**Category 6 CCA AWG 23**	**Category 6 U/UTP AWG 23**
Time to fail (minutes)	1979	1521	3794	4472
Critical Temperature (^{0}C)	**137.67**	**136.31**	**138.21**	**137.68**
DC loop resistance at room temp (Ω/100 m)	19.70	16.40	22.25	15.00
DC loop resistance at steady state (Ω/100 m)	26.69	22.39	30.36	20.40
Conductor diameter (mm)	0.51	0.52	-	0.58
Cable diameter (mm)	5.2	5.40	-	6.2

As noticeable in table 4.1, the common critical temperature for the failure in the cable bundle was at about 140˚C (plus the room temperature). This temperature represents a point at which the extruded dielectric becomes soft enough to mechanically fail and cause a short circuit between the copper conductors.

It is to be noted that the insulated unshielded cable bundles failed due to the extreme heat build-up at 100 watts, but the insulated shielded cable bundles met the PoE operating temperature limit at 802.3at power level and did not fail at 100 watts. The maximum temperature at the steady-state and the time to reach the steady-state for the insulated shielded cable bundles are stated in Table 4.2. It can be seen from figure 4.2 and table 4.2 that the maximum temperature for the insulated shielded cable bundles never reached the point of failure because of their constructions.

Table 4.2: Maximum temperature at steady state and the time to reach the steady state

Insulation heating test results - Maximum temperature rise (T2a) at 100 watts			
Shielded twisted pair cables	**Category 6 F/UTP AWG 23**	**Category 6A F/FTP AWG 23**	**Category 7A S/FTP AWG 23**
Steady state time (minutes)	7811	3297	3181
Temperature at steady state (^{0}C)	**130.98**	**126.79**	**122.00**
DC loop resistance at room temperature (Ω/100m)	15.90	13.95	11.00
DC loop resistance at steady state (Ω/100m)	21.16	18.35	14.31
Cable diameter (mm)	7.2	6.9	7.8

Summary of results

In summary, the physical failure of the unshielded cable bundles shows the impact of high-power transmission over the bundled Ethernet cables installed in non-ventilated (restricted heat dissipation) environments. However, it is essential to emphasise that the insulation heating test carried out in this study was a worst-case scenario of restricted heat dissipation, because of the type of materials used for the insulation of the CBs. Also, the CBs were used as loads to dissipate all the power instead of delivering most of the power to intended loads such as WAPs. The worst-case scenario of cable bundle heating was chosen because, in some typical hidden insulated pathway systems, the cable bundle will generally be larger than a 37 CB and installed inside a conduit before being placed under the floor or ground or in the ceiling spaces and so on. Also, as climatic conditions and installation environments vary all over the world, knowing the results of the worst-case scenario, the effects of a higher power in restricted heat dissipation environments can be considered or avoided. Furthermore, as the temperature rise of the shielded cables met the standard limit of 60 ^{0}C at 802.3at power level and did not fail using the worst-case scenario of cable bundle heating, it can be inferred that cable constructions and installation environments play pivotal roles in the dissipation of the generated heat. The next section expatiates further on the impact of cable construction on the heat generation and dissipation in bundled Ethernet cables.

4.2 Effects of cable constructions on heat generation and dissipation in CBs.

The impact of material and cable dimensions on the heat generation and dissipation behaviour of the bundled Ethernet cables is analysed in this section. Different combinations of the cables' temperature performances are used for the analysis.

4.2.1 Impact of conductor size on the heat generation in powered cable bundles

Standard Category 6 U/UTP AWG 23 vs Reduced diameter or HD Category 6 U/UTP

The reduced diameter or HD cable is classed as Category 6 U/UTP, and it is expected to offer 100-metre Category 6 channel performance but has physical characteristics of Category 5e U/UTP. Furthermore, its conductor size of 0.52 mm and overall cable diameter of 5.4 mm are closer to that of the 24 AWG. Also, its DC loop resistance is less than that of the standard Category 6 U/UTP AWG 23 (table 4.1).

The first observation about its performance was the time taken to reach a steady state. This time was less than half of the time taken by the standard Category 6 U/UTP 23AWG to reach the steady-state. Also, the reduced diameter cable failed before the regular Category 5e cable failed (figure 4.3 and 4.4). However, amongst all the unshielded CBs that experienced the physical failure, Category 6 U/UTP AWG 23 lasted much longer before it failed. These results show a distinct temperature performance benefit of the standard Category 6 U/UTP cable over the reduced diameter Category 6 U/UTP cable and other unshielded cables under test.

Category 7A S/FTP AWG 22 vs Category 7A S/FTP AWG 23

It should be noted that the two Category 7A S/FTP cables described in this section are different from the Category 7A S/FTP described in section 4.1; because they were sourced from different manufacturers. However, the two Category 7A cables analysed in this section are both four pair S/FTP cables with an overall braid as well as individual pair foil. One of the Category 7A S/FTP cables has copper conductor size of 22 AWG while the other has AWG 23. The temperature profile for the two cables was assessed using six current levels. As shown in figure 4.6, the Category 7A S/FTP cable with a larger conductor size (22 AWG) generated less temperature rise in comparison

to the Category 7A S/FTP cable with a smaller conductor size (23 AWG). These sets of results show the impact of heat generation in Ethernet cable bundles used in remote powering operations.

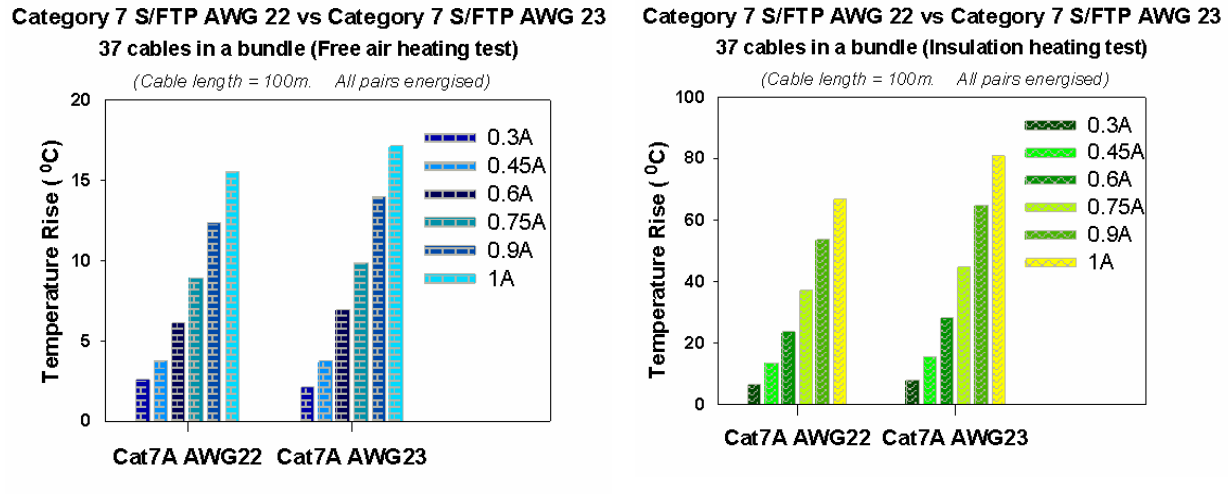

Figure 4.6: Free air and insulation heating test results (AWG 22 vs AWG 23)

Also, from table 4.3, Category 7A S/FTP AWG 22 generated less temperature rise at all current levels, both for the free air heating test and insulation heating test due to its larger conductor size.

Table 4.3: Comparison of temperature profile - Category 7A S/FTP (AWG 22 vs AWG 23)

Energized current	**0.3A**	**0.45A**	**0.6A**	**0.75A**	**0.9A**	**1A**
	Maximum temperature rise for the free air heating test (^{0}C)					
Category 7A AWG 22	2.59	3.77	6.11	8.93	12.36	15.56
Category 7A AWG 23	2.13	3.76	6.96	9.88	14.02	17.14
	Maximum temperature rise for the insulation heating test (^{0}C)					
Category 7A AWG 22	6.41	13.45	23.59	36.99	53.62	66.69
Category 7A AWG 23	7.80	15.55	28.11	44.65	64.87	80.80

4.2.2 Impact of conductor size and cross filler on heat dissipation in cable bundles

Category 5e U/UTP vs Category 6 U/UTP

To analyse the impact of conductor size and additional properties such as polyethylene based cross filler on heat generation and dissipation in Ethernet cables, the temperature performances of Category 5e U/UTP and Category 6 U/UTP are compared. Category 5e U/UTP and Category 6 U/UTP were of Standards compliant construction, four pairs contained within an LSOH sheath, with their conductor insulation made from the polyethylene-based compound. However, the difference between Category 5e and Category 6 U/UTP under tests is that Category 5e has a conductor size of 0.51 mm (24 AWG) whereas Category 6 U/UTP has a larger conductor size of (23 AWG) and additional polyethylene cross filler.

The result showed that Category 5e had a short circuit within 1979 minutes after 100 watts was introduced in the cable. Whereas, Category 6 U/UTP conductor had a short circuit after 4472 minutes of 100 watts powering (table 4.1). Firstly, the larger conductor diameter of Category 6 U/UTP helped reduced Joule heating of the cable because of its lower resistance as compared to that of Category 5e cable bundle. Additionally, the polyethylene cross filler in the Category 6 U/UTP cable helped by slowing down the time to reach the failure point.

4.2.3 Impact of conductor material on heat generation in Ethernet cables

Category 6 U/UTP (Copper Clad Aluminium) vs Category 6 U/UTP copper cabling

The performance of Category 6 CCA cable and standard Category 6 copper cabling are compared in this section to understand the effect of conductor material on the heat generation in the cable. Category 6 CCA cable and standard Category 6 copper cabling are both U/UTP of 23 AWG. However, Category 6 CCA cable had a DC Loop resistance of 22.25 Ω/100m at room temperature, which was compliant with the standard limit of 25 Ω before the heating of the cable. However, as shown in table 4.1, the resistance of the CCA cable increased up to 30.36 Ω at the steady state of 100 watts powering. While the resistance of the Category 6 CCA cable increased beyond the standard limit, the resistance of the standard Category 6 U/UTP was 20.40 Ω at the peak temperature of 100 watts powering. Furthermore, despite the similarity of the conductor diameter, the change in the resistance of Category 6 CCA CB was as much as 8%, while that of the standard Category 6

U/UTP CB was just 5%. The details of the change in the resistance of the CCA cable may be attributed to the Aluminium coating of its copper conductor, and this further explains the risks attached to the deployment of CCA based cables for high power PoE.

4.2.4 Impact of individual screening of conductor pairs on heat dissipation

Category 6A F/FTP vs Category 6 F/UTP

Category 6A F/FTP and Category 6 F/UTP contain both overall foil around their cable pairs, but each pair of Category 6A F/FTP has an individual foil around it. Also, Category 6 F/UTP conductor insulation was made with Fluoropolymer based compound. From the results presented in figure 4.1 and 4.2, the temperature rise on Category 6 F/UTP was slightly higher than that of Category 6A F/FTP during the Free Air heating test. However, the temperature rise in Category 6A F/FTP was lower than that recorded in Category 6 F/UTP during the insulation heating test. This is possibly due to reduced conduction (since each cable has foil separation). Although the overall diameter of the Category 6A F/FTP cable (6.9 mm) was slightly smaller than that of Category 6 F/UTP, the combination of the overall screening, individual pair screening and lower conductor resistance helped with its lower generation of heat.

Summary of results

In summary, the analyses of the cable bundle heating test results in sections 4.1 and 4.2 indicated that the Standards compliant Category 6 U/UTP performed better than other unshielded lower Category cables. However, all the unshielded cables failed at 100 watts, including Category 6 U/UTP during the insulation heating tests whereas, none of the shielded cables failed. The result further highlights the importance of cable constructions such as overall screening, individual pair screening and larger conductor diameter on the heat generation and dissipation properties of bundled Ethernet cables. However, if shielded cables are deployed for PoE applications in different installation environments, how will the cable bundle size affect the temperature rise on the cables? In addressing this, the next section evaluates and compares the effect of CB bundle sizes on the temperature performance of shielded twisted pair cables using Category 6A F/UTP cable as an example.

4.3 Characterization of cable bundle heating based on cable bundle sizes

4.3.1 Comparison between the temperature performances of 24 and 37 CBs

In this section, the results of the resistive heating tests conducted on the 24 CB (24 cables in a bundle) and 37 CB (37 cables in a bundle) of Category 6A F/UTP using six current levels are presented. Figure 4.7 presents the temperature rise for the free air heating of the 24 and 37 CBs, while figure 4.8 is the results of the two CBs when they are thermally insulated.

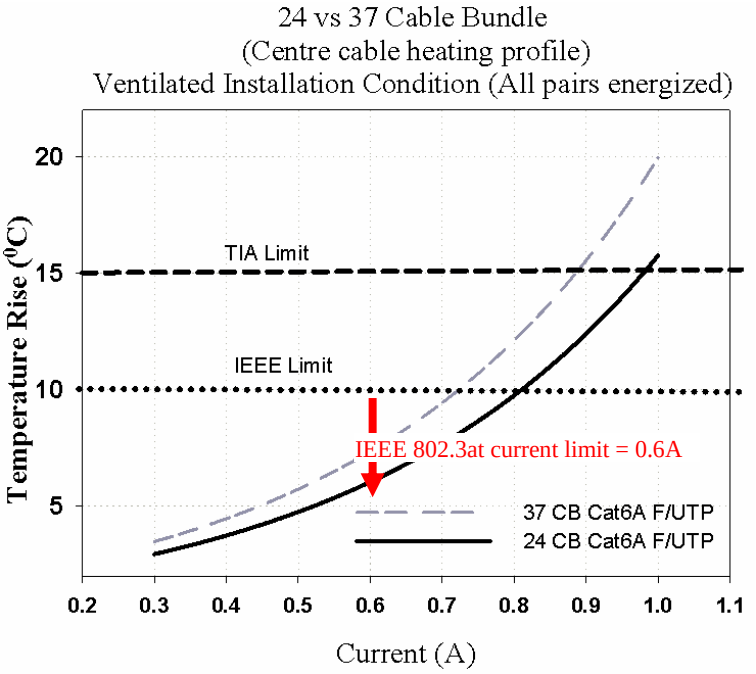

Figure 4.7: Free air heating test results for the two CB sizes of Cat6A F/UTP

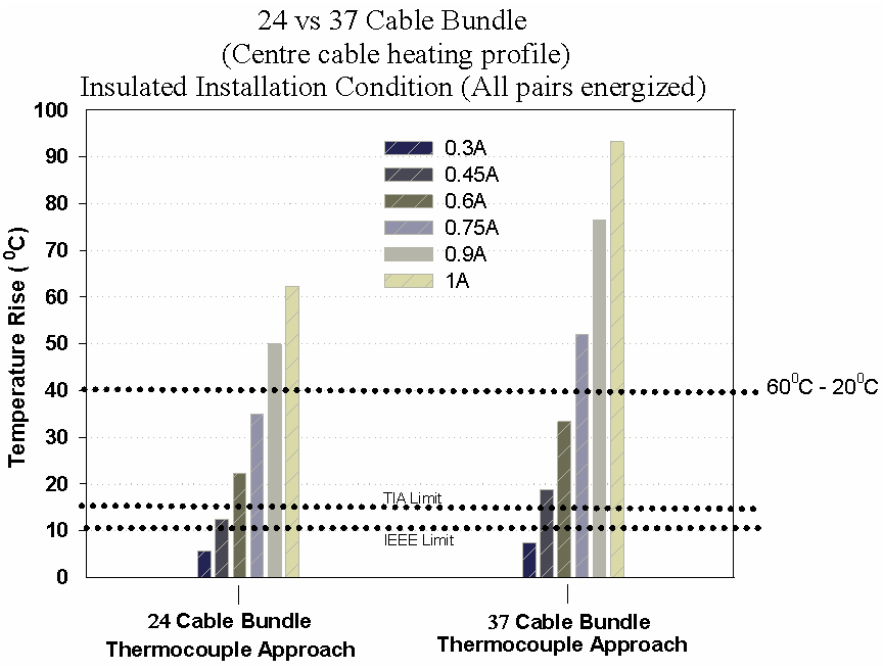

Figure 4.8: Insulation heating test results for the two CB sizes of Cat6A F/UTP.

As shown in both figures, the temperature rise in the 37 CB was higher than those recorded in the 24 CB at all current levels. Also, the rise in temperature on the CBs was more accentuated as the energised current level increased. It is noteworthy that the free air heating test results showed that the temperature rise on the two CBs met the TIA and IEEE temperature limits at the specified current level of PoE+ (0.6A) with headroom of 0.2A for the 24 CB and 0.12A for the 37 CB before the IEEE limit. However, the temperature rise on the insulated CBs exceeded the TIA and IEEE limits at the specified current level of 0.6A and a higher current of more than 0.6A (Figure 4.8). This suggests that larger CBs have an appreciable impact on the heat build-up than the smaller CBs. In particular, larger CBs installed in a non-ventilated environment (restricted heat dissipation) may promote extreme heat build-up within the CB when operating at a higher current level.

4.3.2 Temperature rise measurement vs temperature rise prediction for a 24 CB size

The measured temperature rise during free air heating of a 24 CB is compared with the predicted values for a 24 CB size in this section, and the results are presented in table 4.4. The values predicted by the adaptation model largely agree (with less than 1^0C difference) with the measured values up to a current level of 0.75 A (Table 4.4). However, for the current level of 0.9 A and 1 A, the difference between the measured and model predicted values was about 1-2^0C. Thus, it could be concluded that the temperature rise measurement results agree with the output of the mathematical model given the range of accuracy 1-2^0C of the thermocouple sensors.

Table 4.4: Free air heating results for the 24 CB size

Temperature profile for the 24 CB size. CB heated in the free air environment			
Energized current (A)	Temperature rise measurement (Thermocouple Approach) (^{0}C)	Temperature rise prediction (Adaptation Model) (^{0}C)	Differences (^{0}C)
0.3	1.98	1.85	-0.14
0.45	4.19	4.15	-0.04
0.6	7.25	7.38	0.13
0.75	10.84	11.53	0.69
0.9	15.48	16.61	1.13
1	18.26	20.50	2.24

4.4 Validation of the temperature rise and temperature distribution across a 37 CB.

In this section, comparisons of the temperature rise for a 37 CB of Category 6A F/UTP under the various cable heating assessment methods are made. Firstly, a comparison between the changes in temperature rise between the ambient temperature and outer surface of the bundle (ΔT_u) is made. Followed by the comparison of the temperature rise between the outer surface and the centre of the bundle (ΔT_{th}). Lastly, a comparison of the total temperature rise between the ambient temperature and the centre of the bundle (ΔT) was made.

In the first instance, the measurement with the thermocouple approach was compared with the predicted mathematical model outputs by analysing the ΔT_u and ΔT_{th} terms. After that, ΔT is analysed by comparing the results of the thermocouple approach against the results of the resistivity approach first and then against the output of the mathematical model.

4.4.1 Analysis of ΔT_u using the thermocouple approach and the prediction model

The temperature difference from the ambient temperature to the surface of the 37 CB (ΔT_u) of Category 6A F/UTP is given in figure 4.9. The result showed that the measured (thermocouple approach) values compared favourably well with the output of the mathematical model. The results of the two approaches agree with less than 1^0C difference.

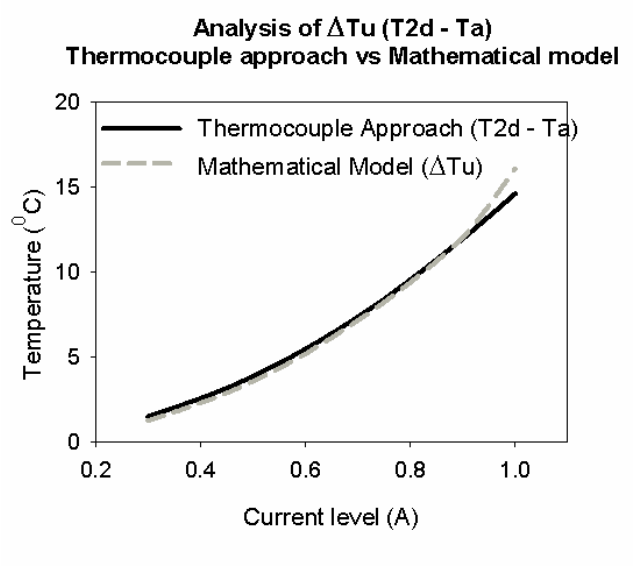

Figure 4.9: Analysis of ΔTu using the thermocouple approach and mathematical model

4.4.2 Analysis of ΔT_{th} using the thermocouple approach and the prediction model

The temperature rise between the bundle outer surface and the centre of the cable bundle (ΔT_{th}) is given in figure 4.10. The agreement between the results of the thermocouple approach and the output of the mathematical model is noticeable. The measured and predicted values agree with less than 1^0C difference up to a current level of 0.9A. However, as ΔT_u and ΔT_{th} were not the same at a steady state, it is apparent that there will be a temperature gradient on the CB. The detailed thermal variation on all the cable bundles at steady state is presented in the appendices.

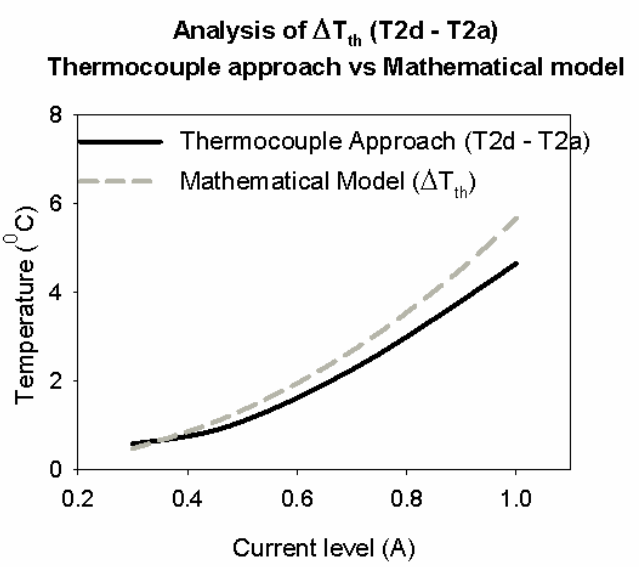

Figure 4.10: Analysis of ΔT_{th} using the thermocouple approach and mathematical model

4.4.3 Analysis of ΔT using the three cable heating assessment methods

The total temperature rise (ΔT) between the ambient temperature and the centre of a 37 CB at the 6 current levels, using the thermocouple and resistivity approach are presented in table 4.5. Then, to establish the validity of the methods, the results obtained using the three approaches are compared and presented in table 4.6.

Table 4.5: Analysis of ΔT using the thermocouple and resistivity approaches

Total temperature rise (ΔT) on 37 CB of Category 6A F/UTP cable.			
Current (A)	**Thermocouple Approach (T2a – Ta) (^{0}C)**	**Resistivity approach (ΔT) (^{0}C)**	**Difference (^{0}C)**
0.30	2.10	2.13	-0.03
0.45	4.07	4.20	-0.13
0.60	7.10	7.04	0.06
0.75	11.02	11.00	0.02
0.9	15.78	15.50	0.28
1.0	19.41	19.40	0.01

The obtained total temperature rise using both the thermocouple and resistivity approach compared favourably well.

Table 4.6: Analysis of ΔT using the thermocouple, resistivity and prediction model approaches

Current (A)	**Thermocouple Approach (T2a – Ta) (^{0}C)**	**Resistivity approach (ΔT) (^{0}C)**	**Prediction Model (ΔT) (^{0}C)**
0.30	2.10	2.13	1.80
0.45	4.07	4.20	4.08
0.60	7.10	7.04	7.33
0.75	11.02	11.00	11.62
0.9	15.78	15.50	**17.02**
1.0	19.41	19.40	**21.32**

From table 4.6, the results obtained with the three approaches agree when considering the energised current levels from 0.3A – 0.75A. The deviation of the prediction model result at 0.9A and 1A could be due to the employed empirical factors (see tables 2.3 and 2.4), which are only valid for the lower power levels.

Chapter summary

The study in this section started with the characterisation of cable bundle heating based on different power levels and installation conditions. It was found that high power (100W) deployment over the bundled insulated unshielded Ethernet cables caused an extremely high temperature on the cable bundle. Category 5e cable (which has the smallest conductor diameter) produced the highest temperature rise during the free air heating test and failed along with other unshielded Ethernet cables due to the extreme heat build-up within the cable bundle. However, shielded cables such as Category 6 FTP, Category 6A F/UTP, Category 6A F/FTP and Category 7A S/FTP did not reach a point of failure when tested in the free air and insulated environments at all power levels. Category 7A S/FTP cable with a large overall diameter and the lowest conductor resistance along with a large amount of screening generated the lowest temperature rise at 100 Watts.

From the results of these studies, it can be inferred that cables with larger conductor size with a screened construction, such as an individual screening of the conductor pairs and overall screening, will likely generate lower temperatures and take a longer time to reach the steady-state. Furthermore, conductor material and the quality of the conductor insulation (cables whose conductor insulation made from Fluoropolymers did not fail- Cat 6A F/FTP, Cat7A S/FTP where cables with conductor insulation made from polyethylene failed), as well as installation conditions will determine the amount of heat generated and dissipated by a CB. With the analysis of the effect of CB sizes, it is important to recognise that larger cable bundles tend to prevent free dissipation of heat. As this can lead to the heat ageing of the conductor insulating materials, care must be taken when deploying bundled Ethernet cables for PoE applications.

It is appropriate to mention that the average ambient temperature during the study was ~20^0C, However, if the ambient operating temperature is very high, less energy is required for the standard limits to be exceeded. For instance, if the cables are bundled in thousands, a higher

power of more than 30 Watts in restricted heat dissipation environments will have an impact even with the load attached to the end of the cable. Also, as higher power requires much higher current than the existing 0.6A of the IEEE802.3at, the cabling operating environment and cable bundling become important points of consideration.

Consequently, regardless of the amount of power transmitted through the CB, heating occurs within the cables and their surroundings due to the passage of the electrical current. Also, thermal insulation of the CB portions causes localised heating of the cable. Given these conditions, the research questions of interest include: (1) does the electrical heating, or the temperature of the installation environment affect the transmission parameters of the cable? (2) does the thermal cycling on the CB or the possible fluctuation in the temperature of the installation environment cause the cabling transmission parameters to degrade over time? (3) If Category 6A cables are to be deployed, can the specified temperature limit of 60°C have a long-term effect on cable performance? If yes, how can the changes in the cable parameters be reliably measured and compared with the baseline cable performance?

The next Chapter (Chapter 5) details the assessment methods for electrical heating and non-electrical heating tests. Moreover, chapter 6 and 7 present the immediate and the long-term effects of electrical heating and non-electrical heating on the performance of PoE permanent links constructed with horizontal shielded and unshielded Ethernet cables.

CHAPTER 5 - ASSESSMENT OF THE IMPACT OF THERMAL VARIATION ON POE PERMANENT LINK PERFORMANCE

In the previous chapter, the possible rise in temperature on different categories of balanced twisted pair cabling was investigated based on different power and current levels as well as the installation conditions. In this Chapter, the immediate and long-term effects of temperature and thermal cycling on the electrical properties and transmission parameters of different PoE permanent links (PLs) are investigated. The assessments were based on the investigation of the effects of electrical heating and non-electrical heating, both within the specified operating range and beyond the levels expected, to account for the extreme situations where high temperature, fluctuations in external temperature and localised heating could stress the cables and cause a drift in the performance of the links over time.

The first assessment investigates the effects of electrical heating on the performance of Category 6A F/UTP cable (section 5.1). However, the investigation of the effect of non-electrical heating was covered in section 5.2 and 5.3. The rationale behind the investigation of non-electrical heating is that the temperature rise and thermal cycling may induce accelerated ageing of the compounds used for the cable conductor insulation, creating progressive and permanent damage to the overall performance of the cable. Given this, isolating possible resistive heating effects will help in the identification of the effect of external temperature on the dielectric performance of the cable. Therefore, section 5.2 simulates insulated pathway systems where intra-building backbone cables are fully installed in restricted heat dissipation environments. For example, cables installed inside conduits, wooden wall cabinets, and so on. will generate a temperature rise above 60^0C as observed in the CB heating assessments section (See figure 4.2). In this case, the effect of temperature and thermal variation will have significant effects on the performance of the PoE PL. However, section 5.3 examines the performance of the permanent links in which a portion of the cables (shielded and unshielded) pass through thermally insulated areas and that portion is insulated, causing the transmission parameters of the links to drift over time, based on the effects of temperature and thermal cycling. It has been highlighted in the literature review section (See section 2.4) that if the dimensions of the cable and dielectric constant of the dielectric around an insulated portion of the cable change differently from every other part of the installed cable, the capacitance of the cable will change. Then, the designed characteristic impedance of the cable will also change because of the non-uniformity of the cable, and that will cause the transmission parameters of the channel to change. For instance, the crosstalk performance of the channel will change. Also, the RL and IL

performance of the channel will drift over time because of thermal cycling. Given these, the baseline RL and IL performance of Category 6A F/UTP PL were compared with the drift in the RL and IL performance of the link using the Feature Selective Validation (FSV) technique in section 5.4. Also, the extraction of the primary line constants such as the inductance and capacitance from the measured impedance variation of the line was conducted in section 5.5. Lastly, the changes in the dimensions and elemental composition of the material of a twisted pair sample were investigated in section 5.6.

5.1 Assessment of the resistive heating effects on the performance of Cat 6A F/UTP PL

This section investigates the effects of electrical heating on the performance of Category 6A F/UTP PL to establish the long-term effect of repeated electrical heating at high energised current levels on cable performance. The two installation conditions considered are outdoors (ventilated or "free air") and restricted heat dissipation (non-ventilated) installation environments. In both environments, the effects of thermal cycling were examined on the electrical properties, and transmission parameters of the PL using the Category 6A F/UTP cable (24 CB) tested in section 4.3.

5.1.1 Test setup for the resistive heating

As described in section 4.3, after the last heating test had been conducted on the 24 CB of Category 6A F/UTP, the ends of the cable were connectorised and the baseline transmission performance of the PL was obtained with a DSX 5000 Cable Analyzer. Figure 5.1 shows the schematic of a PL setup while figure 5.2 shows that the baseline performance of the PL met the specifications of the TIA Category 6A PL performance.

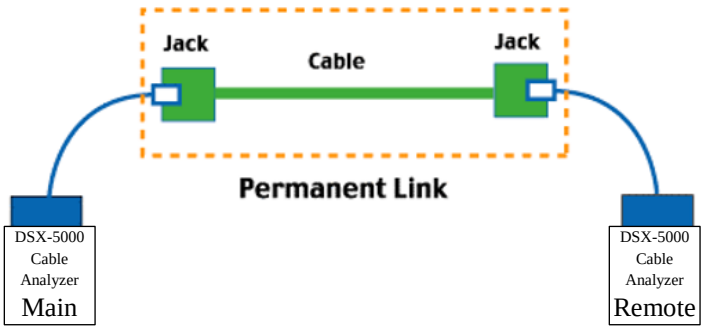

Figure 5.1: Schematic describing the experimental set-up

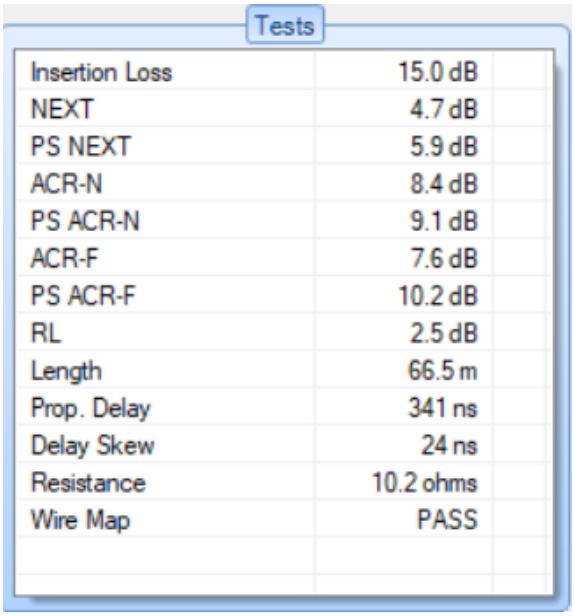

Figure 5.2: Baseline headroom of Category 6A F/UTP PL performance at 23^0C

After the baseline performance of the PL had been established, the connectors at the ends of the cable were removed, and the Category 6A cable under test was energised with five current levels: 1.15 A, 1.25 A, 1.35 A, 1.5 A and 1.6 A one after the other. It is noteworthy that the energised current levels used in this section were higher than that of the ones used in section 4.3. The rationale for the higher current levels used in this section was to raise the temperature of the cable conductors to 60^0C while the PL was set-up in the ventilated space to address the potential concerns of heating at the extremes of cable operation.

5.1.2 Assessment of the resistive heating effects on cable performance

For each of the energised current levels except 1.6 A, the temperature of the cable was allowed to naturally cool from the peak temperature to the near room temperature before the ends of the cable were connectorised again for the assessment of the PL performance. In essence, when the temperature on the CB had reached a steady-state, the power supply unit was turned off. Then, the ends of the CB were connectorised with the standard Category 6A F/UTP jacks and measurements were taken with a DSX 5000 Cable Analyser, using the TIA Category 6A PL test standard. Besides, the performance of the Category 6A F/UTP PL was assessed with an energised current level of 1.6 A when the cable was installed in the ventilated space first, and then when it was insulated with an aluminium foil lagging. The performance of the PL was measured, as the temperature of the cable bundle was gradually returning to the room temperature after the steady-

state. The measured changes in the electrical properties and transmission parameters of the PL are presented in chapter 6. Note that the VF and ε_r of the conductor insulation were calculated from the measured changes in the electrical characteristics on the PL using (8.18 – 8.20). Also, changes in the crosstalk, RL and IL performances of the PL were used for the analysis of the PL performance degradation as functions of installation conditions and thermal cycling.

5.2 Assessment of the performance of Cat 6 U/UTP (full insulation)

The immediate and long-term effects of thermal cycling were examined on the electrical properties and transmission parameters of a standard Category 6 U/UTP PL. The PL was constructed with 50.5 m length of a Standard Category 6 U/UTP cable. As stated earlier, the study in this section simulates cable installed inside the conduits, wooden wall cabinets, etc. where the installed cable is thermally insulated and under varying thermal conditions. Moreover, the assessment was carried out in two phases: (1) the tests thermally cycle the cable from ambient of +20 ^{0}C up to an ambient of +70 ^{0}C to see if there is any substantial 'knee point' in the performance of the cable (2) the thermal cycling was extended to about 120 ^{0}C to assess the impact of high temperature on the performance of the Category 6 U/UTP PL. In high power PoE systems, the CBs would generally be operating at high power levels and at the same time experiencing contributions from heat sources from the environment. However, the cable examined in this section was not energised as explained earlier but was heated externally in a constructed heat chamber to isolate the effects of resistive heating from external heating effect. The schematic describing the heat chamber is shown in figure 5.4.

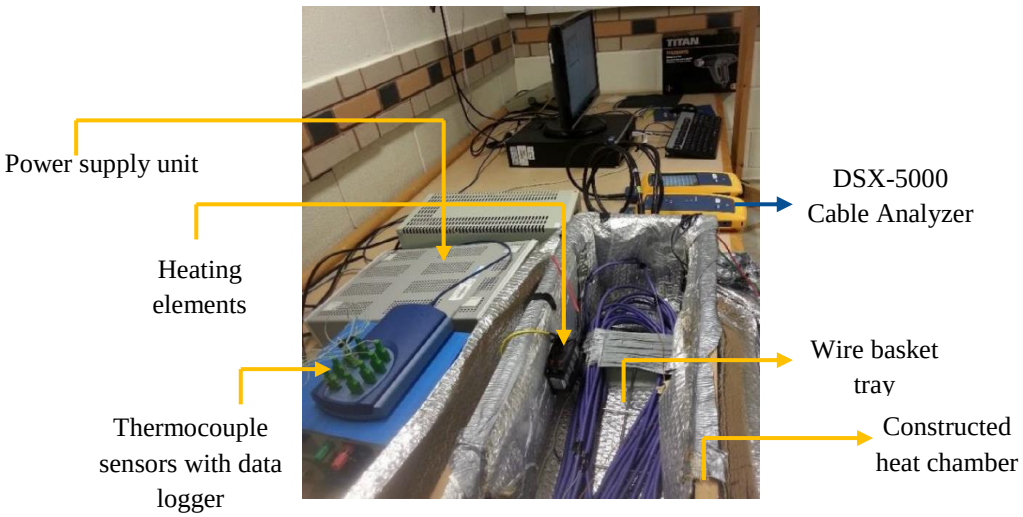

Figure 5.3: Experimental set-up for the full cable insulation test

As indicated in figure 5.4, the heat chamber is about 2 m in length and was constructed using a wooden box with a lid. Moreover, the heat chamber has two small circular openings and one square opening on its sides. The circular openings were used to situate the thermocouple sensors on different positions on the cable under test, while the square opening was used for the mounting of a faceplate that housed the RJ45 jacks. The internal surface of the chamber was lined with a thermal insulating foil to provide extra insulation and reflect any form of radiation. The wire basket tray (shown in figure 5.3) was raised off the bottom of the chamber with a small piece of wood at different locations in the chamber to limit the amount of heat transfer between the wire basket tray and the aluminium foil.

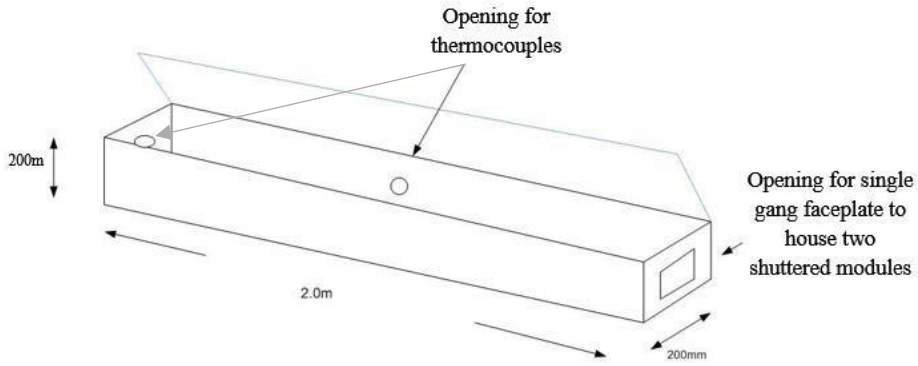

Figure 5.4: Schematic describing the dimensions of the heat chamber

Description of the test setup for the non-electrical heating tests

The experimental setup shown in figure 5.3 consists of a DSX-5000 Cable Analyzer with the appropriate permanent link adapters, a set of thermocouple sensors, a wire basket tray, a temperature data logger for the automatic temperature readings from the thermocouple sensors, some heating elements for heating the cable externally, Power Supply Units (PSU) that were used for powering the heating elements, a constructed heat chamber and the cable under test.

Description of the general test procedure

The cable under test was spooled loosely on the wire basket tray to avoid tight cable bundling, and six thermocouple sensors (named as cable temperature 1-6) were placed in various locations on the cable jacketing material. The cable was left in place, in the heat chamber and without any movement throughout the test period. The measurement ends of the cable were connectorised with

standard RJ45 jacks. Before the testing began, the main and remote ends of the Cable Analyzer were connected using the appropriate permanent link and channel link adapters to set a reference point for the measurements. After that, appropriate test limits and cable type were selected to ensure measurements were made in the required frequency range and that the actual Velocity Factor (VF) or Nominal Velocity of Propagation (NVP) value for the cable under test, is obtained. Also, before the heat cycling test began, the automatic data logger was set to record the baseline cable temperature and the subsequent temperatures in real-time. However, the baseline performance of the permanent link was obtained manually at the start of the test.

It should be noted that the setup described in this section applies to the investigations conducted in sections 5.3.1 and 5.3.2 except that different lengths of cables were used. Also, different test limits, cable types and RJ45 jacks were used for the other PLs. However, in all the assessments, the PLs were carefully installed in such a way that the symmetry of all the components of the links was not compromised. For example, the sharp bending of the cables was avoided. Also, shielded cables were terminated correctly at both ends with the appropriate connectors.

Phase 1 – Thermal cycling of the fully insulated Category 6 U/UTP cable from +20^{0}C to +70^{0}C

The performance of the standard Category 6 U/UTP PL was obtained first before the heating of the cable began using the ISO11801 PL class E test Standard. Figure 5.5 shows that the PL performance met the specifications of the ISO test limits. Moreover, figure 5.6 shows that there was no DC resistance contact issue.

Figure 5.5: Baseline marginal values for the fully insulated Category 6 U/UTP cable

Figure 5.6: Baseline resistance profile for the standard Category 6 U/UTP PL

During the first heating of the cable, the performance of the PL was obtained again when the temperature of the cable had reached ~70^0C. After that, the cable was allowed to cool naturally by turning the PSU off and by taking the lid of the heat chamber off. When the temperature of the cable had returned to ambient, the performance of the permanent link at room temperature was also measured. After the first cooling of the cable, the second heating cycle started, and this process was repeated for ten heating cycles. However, after a trend in the cable performance had been observed during the ten daily heating cycles, another two weekly heating cycles (cycle 11 and cycle 12) were carried out using the previous process but with prolonged heating time (weekly heating) to differentiate the effects of intermittent heating from the effects of prolonged thermal cycling on the cable performance.

Moreover, another thirteen thermal cycles were carried out after the initial twelve cycles to gain adequate information on the effects of long-term repeated thermal cycling. Figure 5.7 shows the heating profile of the last thirteen successive thermal cycles. It also shows that the temperature rating of the cable dielectrics was not exceeded. The results of this phase of the thermal cycling tests are presented in section 7.1.

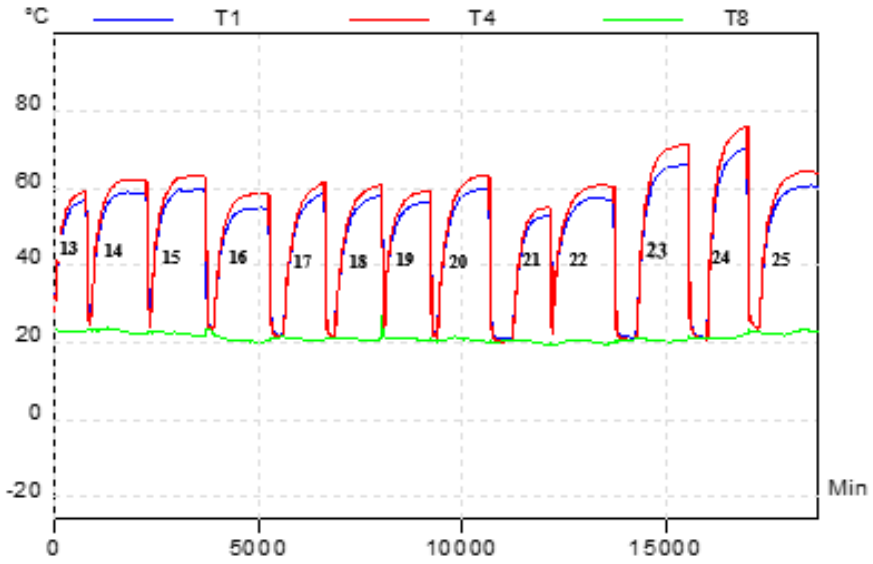

Figure 5.7: Temperature profile for the thermal cycling test (+20^{0}C to +70^{0}C)

Phase 2 – Thermal cycling of the fully insulated Category 6 U/UTP cable from +20 ^{0}C to +120^{0}C

In the second phase of the thermal cycling tests, the cable under test was heated and cooled repeatedly again from an ambient of +20^{0}C up-to a maximum temperature of 120 ^{0}C to investigate the effects of the observed high temperature in section 4.1 (see figure 4.5) on the transmission performance of the cable. After the heating of 120^{0}C, all the power supply units were switched off except for the one connected to the heating element, where the thermocouple sensor named as "cable temperature 6" was located (see the red arrow and the legend in figure 5.8). That is, the Category 6 U/UTP under test was subjected to a localised heating at one spot.

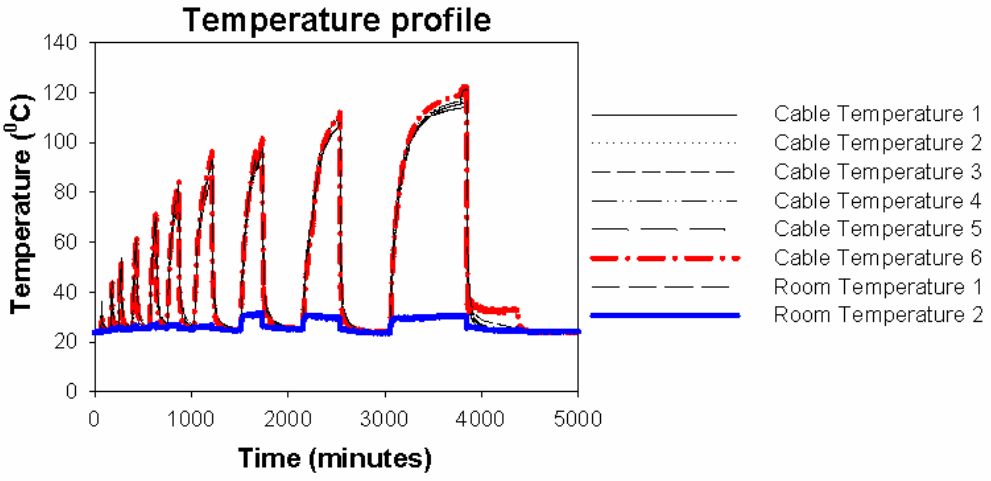

Figure 5.8: Temperature profile for the thermal cycling test (+20^{0}C to +120^{0}C)

This was purposely left on to subject the cable to localised heating. After heating the cable locally for 9 hours, the temperature around the heating element, at cable temperature 6 was about 30 ^{0}C, but the temperature on the other parts of the cable was around 24 ^{0}C. The performance of the PL at this point was measured and then measured continuously after the heating element at cable temperature 6 was turned off. Moreover, the last measurement was taken when the temperature of every part of the cable was near the room temperature. The RJ45 plug was inserted into the jack before each thermal cycle and removed from the jack after each thermal cycle. The result of the multiple insertion and removal of the RJ45 plug from the jack is an open connection which is reflected in figure 5.9. The detailed results of this phase of the thermal cycling tests are presented in section 7.1.

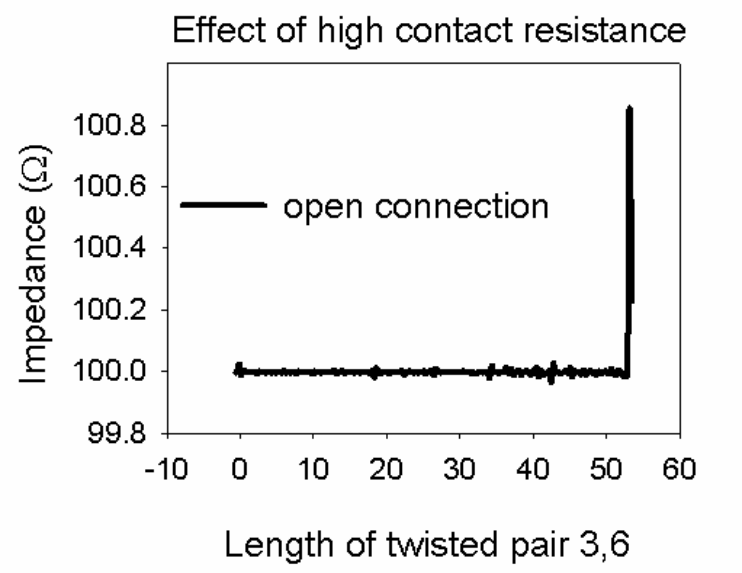

Figure 5.9: Long-term effects of insertion and removal of RJ45 plug from the jack

5.3 Assessment of the performance of the portion insulated Cat 6 and Cat 6A cables

The performance of the permanent links in which portions of the cables (shielded and unshielded) pass through thermally insulated areas is assessed in this section. Figure 5.10 represents the experimental setup for the Category 6 U/UTP and Category 6A F/UTP PLs under study. A substantial portion of Category 6 U/UTP and Category 6A F/UTP PLs was subject to thermal variation conditions by performing several thermal cycling tests on the insulated portion of the cables.

Figure 5.10: Experimental set-up for the cable portion insulation test.

5.3.1 Assessment of the performance of Cat 6 U/UTP cable (portion insulation)

Using the general test procedure described in section 5.2, the performance of a 56.6 m length of a plenum rated (CMP) Category 6 U/UTP cable was tested within the PoE operating temperature. The cable under test was tested as a General Cable 6000 CMP cable type and as a Standard Category 6 U/UTP cable type using the ISO 11801 PL Class E (+All) test standard to investigate the supplied VF of the cable for comparison with the obtained VF of the extracted dielectric rod sample from the cable under test (see section 9.1.4). In this study, twenty-four heating and cooling cycles were performed.

Firstly, ten intermittent (daily) thermal cycles were performed, followed by another ten-consecutive prolonged (weekly) thermal cycles. After that four thermal cycles were conducted on a monthly basis. In all the thermal cycling tests, the CMP cable was heated from the room temperature up to a temperature of ~65 ^{0}C. Figure 5.11 – 5.13 show the heating profile of the daily, weekly and monthly thermal cycles.

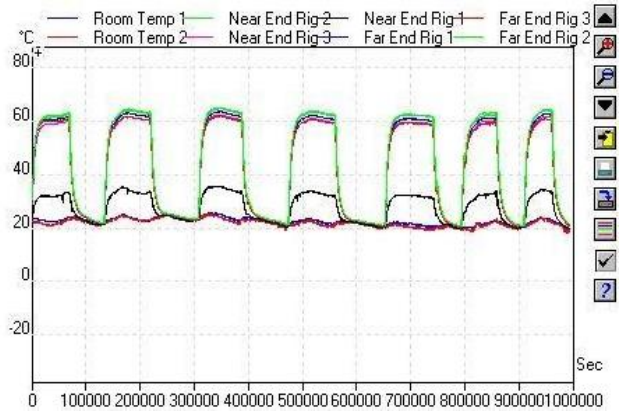

Figure 5.11: Temperature profile for the daily thermal cycling

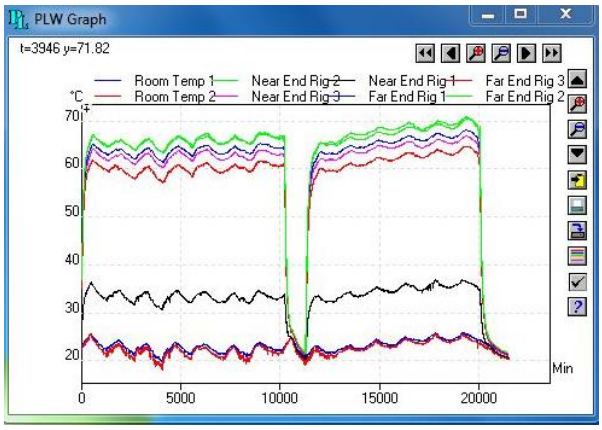

Figure 5.12: Temperature profile for the weekly thermal cycling

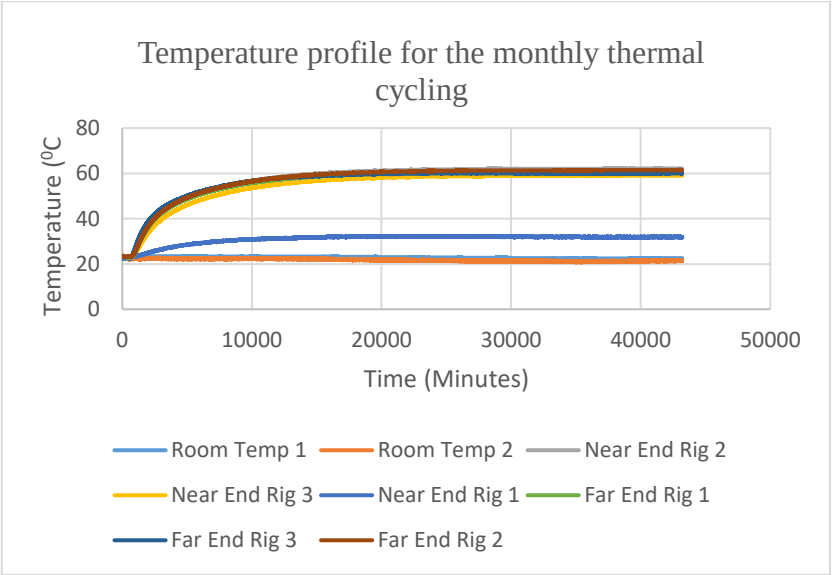

Figure 5.13: Temperature profile for the monthly thermal cycling

The baseline transmission performance of the Category 6 U/UTP PL was obtained at the beginning of the assessment (figure 5.14). Then, for each of the thermal cycles, the performance of the PL was monitored as the temperature of the cable portion was rising to the peak temperature and when the temperature was returning to near the room temperature. Furthermore, the VF and ε_r of the cable's conductor insulation were calculated from the obtained electrical features of the PL using (8.18 – 8.20). The baseline VF was validated against the VF obtained through dielectric measurements (see section 9.1.4) and the VF reported by the manufacturer of the cable under test.

Obtained with ISO 11801 PL Class E test standard
Cable type**: CMP** Category 6 U/UTP

Insertion Loss	13.0 dB
NEXT	4.8 dB
PS NEXT	6.9 dB
ACR-N	11.4 dB
PS ACR-N	12.5 dB
ACR-F	11.0 dB
PS ACR-F	13.7 dB
RL	0.8 dB
TCL	7.6 dB
CMRL	
CDNEXT	
ELTCTL	23.6 dB
Length	56.6 m
Prop. Delay	278 ns
Delay Skew	16 ns
Resistance	8.60 ohms
Resistance Unbalance	0.035 ohms
Resistance P2P Unbala...	0.055 ohms
Wire Map	PASS

Obtained with ISO 11801 PL Class E test standard
Cable type: **Standard** Category 6 U/UTP

Insertion Loss	13.0 dB
NEXT	5.1 dB
PS NEXT	7.1 dB
ACR-N	10.6 dB
PS ACR-N	12.3 dB
ACR-F	9.6 dB
PS ACR-F	11.6 dB
RL	0.7 dB
TCL	7.2 dB
CMRL	
CDNEXT	
ELTCTL	23.6 dB
Length	54.2 m
Prop. Delay	278 ns
Delay Skew	16 ns
Resistance	8.64 ohms
Resistance Unbalance	0.033 ohms
Resistance P2P Unbala...	0.055 ohms
Wire Map	PASS

Figure 5.14: Baseline marginal values of Category 6 U/UTP PL at 22.5^0C

5.3.2 Assessment of the performance of the portion insulated Cat 6A F/UTP cable

The thermal cycling of a portion of the 30.8 m length of Category 6A F/UTP permanent link follows the same procedure as that of the Category 6 U/UTP (CMP cable) PL except that the Category 6A F/UTP PL was tested as F/UTP cable type using both the ISO 11801 PL2 Class Ea (+All) and TIA Cat 6A Permanent Link (+All) test Standards. Also, in this investigation, 40 heating and cooling cycles were performed. The first twenty thermal cycles were conducted daily while the last 20 cycles were on a weekly basis. The reason for this was to study the effects of the intermittent and prolonged thermal cycling on the performance of the link.

The baseline transmission performance of the Category 6A F/UTP PL was obtained at the beginning of the assessment (figure 5.15), at the peak temperatures and at near the room temperature. Moreover, the VF and the ε_r of the cable's conductor insulation were calculated from the obtained electrical characteristics of the PL using (8.18 - 8.20). Moreover, the baseline VF was validated

against the VF obtained through dielectric measurements (see section 9.1.3) and the VF reported by the manufacturer of the Cat 6A cable under test.

ISO 11801 PL2 Class Ea (+All) test Standard
Cable type: F/UTP

Insertion Loss	27.3 dB
NEXT	2.7 dB
PS NEXT	4.4 dB
ACR-N	19.6 dB
PS ACR-N	20.0 dB
ACR-F	8.9 dB
PS ACR-F	10.8 dB
RL	5.1 dB
TCL	6.8 dB
CMRL	
CDNEXT	
ELTCTL	20.4 dB
Length	30.8 m
Prop. Delay	158 ns
Delay Skew	11 ns
Resistance	4.7 ohms
Resistance Unbalance	0.03 ohms
Resistance P2P Unbala...	0.06 ohms
Wire Map	PASS

TIA Cat6A Perm. link (+All) test Standard
Cable type: F/UTP

Insertion Loss	29.4 dB
NEXT	2.7 dB
PS NEXT	4.4 dB
ACR-N	13.0 dB
PS ACR-N	13.1 dB
ACR-F	9.9 dB
PS ACR-F	11.8 dB
RL	5.1 dB
TCL	6.5 dB
CMRL	
CDNEXT	
ELTCTL	20.5 dB
Length	30.8 m
Prop. Delay	158 ns
Delay Skew	11 ns
Resistance	4.7 ohms
Resistance Unbalance	0.03 ohms
Resistance P2P Unbala...	0.06 ohms
Wire Map	PASS

Figure 5.15: Baseline marginal values of the Category 6A F/UTP PL at 18.4^{0}C

5.4 Quantification of the drifts in the performance of Cat 6A F/UTP cable

The aim of the study conducted in section 5.3.2 was to thermally cycle shielded cable in order to determine the drift in the transmission parameters of the cable as a function of thermal cycling. The results from the analyses were fed into the FSV tool for the quantification of the drift in the PL performance. That is, the FSV tool was used for comparing the baseline transmission parameters of Category 6A F/UTP PL with the degradation in the PL performance. The detailed results of the study conducted in this section can be found in section 7.4.

5.5 Extraction of the primary line constants from the measured impedance variation

As discussed in the literature review section, the performance of a transmission line (TL) such as a balanced twisted pair depends on the symmetry along the length of the line and its associated components. However, if the balance of the line is compromised in any form, the designed primary line constants will change. For instance, if the dielectric constant of the conductor insulation increases, the capacitance will increase. Moreover, when the heating of a portion of the cable separates the pair, the capacitance of that portion of the pair will decrease, and inductance will increase. As any of these scenarios can change the impedance profile of the TL and the quality of the received signal, analysing the TL behaviour using an analytical approach can provide insight into the contributing factors to the observed changes in the PL performance. Moreover, as a first-order assessment of the analysis, the variation in the impedance profile of the Category 6A F/UTP PL as a function of thermal cycling was computed first from the measured HDTDR data of the line to establish possible changes in the impedance profile of the line (see section 7.3.2). After that, the primary line parameters were extracted from the variation in the impedance of the PL using the TLM approach implemented in Matrix Laboratory (MATLAB) software [146]. The results of the extraction of the primary line parameters can be found in section 7.5.

5.6 Investigation of the changes in the properties of a twisted pair sample using SEM.

To investigate the impact of heating and cooling on the dimensions and elemental composition of a twisted pair, SEM was used for the examination of the changes in the dimension and elemental composition of a short length of a twisted pair obtained from Category 6A F/UTP cable.

The dimension and elemental composition of the short length of a twisted pair were examined first using the SEM. After that, the sample was heated once up to 60^0C inside an oven with automatic temperature control. Then, after the heating had reached a maximum temperature of 60 ^{0}C, the temperature of the twisted pair was allowed to return to the room temperature naturally. Then, the dimensions and elemental composition of the twisted pair sample were investigated again using the SEM. The results of the study in this section are presented in section 7.6.

CHAPTER 6 – LONG - TERM EFFECTS OF REPEATED RESISTIVE HEATING ON THE PERFORMANCE OF CAT 6A F/UTP

This section presents the results on the simulated long-term effect of repeated electrical heating on the performance of Category 6A F/UTP PL. The changes in the electrical properties of the PL measured under two installation conditions (ventilated and non-ventilated) are presented in section 6.1 whereas section 6.2 presents the changes in the transmission performance of the PL for both installation conditions.

6.1 Effect of repeated resistive heating on the electrical properties of Cat 6A F/UTP

The baseline electrical properties and degradation in the electrical properties of Category 6A F/UTP PL are presented in table 6.1 whereas figures 6.1 – 6.6 present the traces for the measured electrical performance against the cable temperatures. The actual values of the changes in the electrical properties of the link are presented in table 6.1 while the difference between the baseline values of the electrical properties and the last measured changes are presented in table 6.2.

Table 6.1: Effects of resistive heating on the electrical properties of Category 6A F/UTP PL

	Effects of resistive heating on the electrical properties of Category 6A F/UTP permanent link Obtained at room temperature after performing several thermal cycling on the cable.								
Twisted pair colour codes	Pair No.	**Baseline** electrical properties (23^0C)				Electrical properties obtained after the **insulation heating** test (24^0C)			
		Initial Length (m)	Propagation delay (ns)	Delay skew (ns)	**Initial resistance (Ω)**	Increased length (m)	Increased propagation delay (ns)	Changes in delay skew (ns)	**Final resistance (Ω)**
Green pair	3,6	71.6	341	24	**10.2**	73.4	350	25	**10.2**
Blue pair	4,5	70.3	335	18	**9.9**	71.6	341	16	**10.0**
Brown pair	7,8	68.2	325	8	**9.7**	69.9	333	8	**9.8**
Orange pair	1,2	66.5	317	0	**9.6**	68.2	325	0	**9.6**

6.1.1. Effect of repeated resistive heating on the electrical resistance of Cat 6A F/UTP

There was no clear difference in both the initial and the final DC loop resistance of each pair in the cable (Table 6.1). The increase of 0.1 Ω in the final loop resistance of pair 4,5 and 7,8 could be due to the resistance unbalance between the pins of the RJ45 connection which was not monitored for this study. Moreover, the DC loop resistance measured for each cycle is presented in figure 6.1. The figure showed that the resistance of each pair increased and decreased in response to the increase and decrease in cable temperatures. The significance of this is that cable bundles operating with high power such as 100 W or more will generate high temperature which may cause the resistance of the cable to increase and eventually limit the maximum available power to the end device and the attenuation of the signal power.

Table 6.2: Absolute changes in the electrical properties of Category 6A F/UTP PL

Effects of resistive heating on the electrical properties of Category 6A F/UTP PL Obtained at room temperature after several thermal cycling						
	Ventilated -Free air heating test			Non-Ventilated - Insulation heating test		
Pair number	**Decrease in length (m)**	Decrease in propagation delay (ns)	Increase in delay skew (ns)	**Increase in length (m)**	Increased propagation delay (ns)	Change in delay skew (ns)
Pair 3,6	**0.2**	1	1	**1.8**	9	Increased by 1 ns
Pair 4,5	**0.4**	2	0	**1.3**	6	Decreased by 2 ns
Pair 7,8	**0.4**	2	0	**1.7**	8	0
Pair 1,2	**0.4**	2	0	**1.7**	8	0

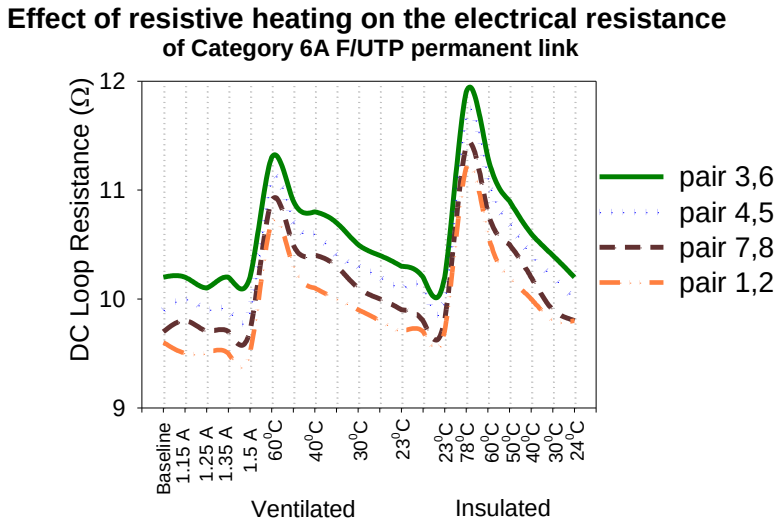

Figure 6.1: Effect of resistive heating on the electrical resistance of Category 6A F/UTP PL

6.1.2. Long-term effect of repeated resistive heating on the electrical length of Cat6A

Table 6.2 shows that the electrical length of each pair in the cable decreased due to the effects of repeated resistive heating in the ventilated environment. However, the electrical length of each twisted pair increased permanently due to the effect of prolonged thermal cycling. As observed in figure 6.1, the DC loop resistance of the twisted pairs decreased with a decrease in temperature during the insulation heating test. The trend in the DC loop resistance of the cable can be expected as the resistivity of copper depends on temperature. However, figure 6.2 shows that the electrical length of all the twisted pairs in the cable increased permanently as the cable temperature was decreasing. Given these, it could be assumed that the permanent increase in the electrical length was because of the increase in the dielectric constant of the conductor insulation as a result of the thermal ageing of the conductor insulation when the cable was tested using the thermal insulating material.

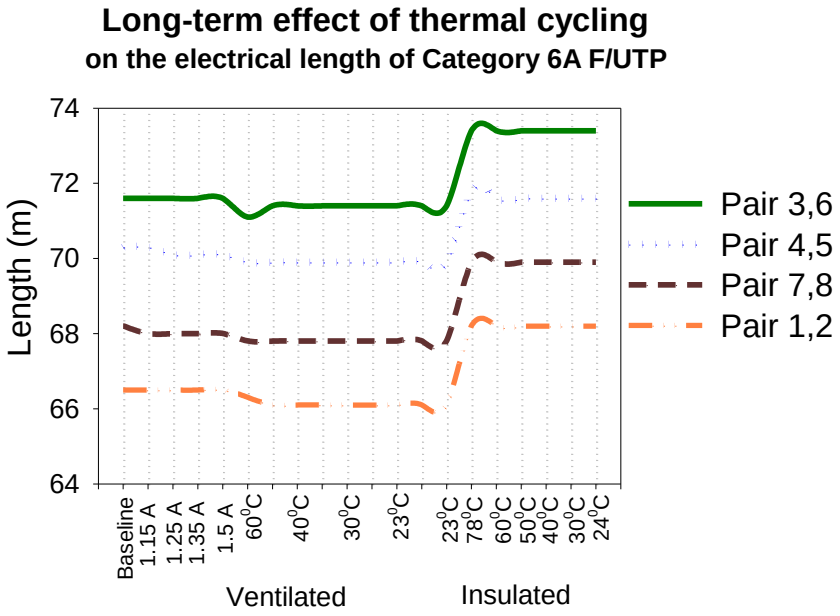

Figure 6.2: Effect of repeated resistive heating and thermal insulation on the electrical length

6.1.3 Long-term effect of resistive heating on the propagation delay of Cat 6A F/UTP

The changes in the electrical length of each twisted pair in the Category 6A F/UTP cable also caused a proportionate change in the end-to-end propagation delay of the signal on each twisted pair (figure 6.3).

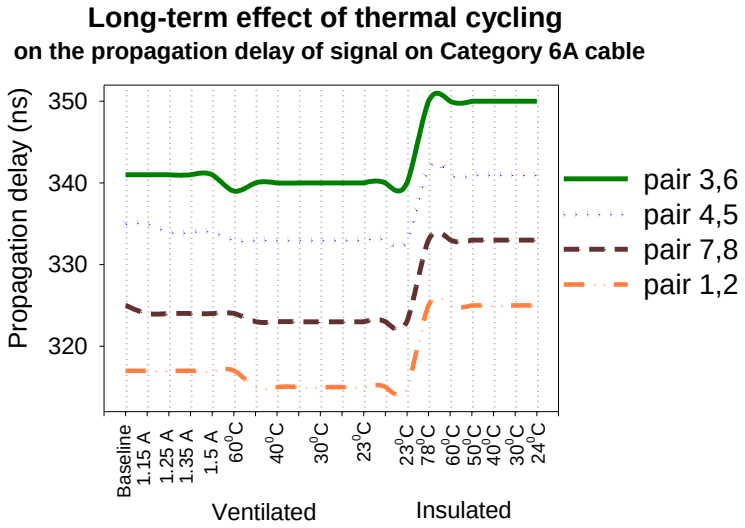

Figure 6.3: Long-term effect of repeated resistive heating (propagation delay of Cat 6A)

As stated in table 6.1, the measured baseline propagation delay of pair 3,6 was ~ 4.763 ns per meter. Therefore, a change of 0.2 m in the route length of a signal as a consequence of the change in the dielectric constant of the conductor insulation will cause a phase delay of 1ns. As reported in table 6.2, this value corresponds to the change in the propagation delay of pair 3,6.

6.1.4. Long-term effect of repeated resistive heating on delay skew of Cat 6A F/UTP

Table 6.2 shows that the delay skew on pair 3,6 increased by 1ns (from 24 to 25 ns) based on the last measurement made during the insulation heating tests but the plot of the delay skew for all pairs in figure 6.4 indicates that the delay skew on pair 3,6 initially decreased by 1ns (from 24 to 23 ns) at 60^0C and increased permanently from 23 ns to 25 ns during the transition between 60^0C to 50^0C, upon the cooling of the cable. This can be attributed to rounding errors in the measurements (rounding to the nearest half ns), which cannot be ignored but this observation is certainly interesting and worthy of further investigation, particularly in light of other findings.

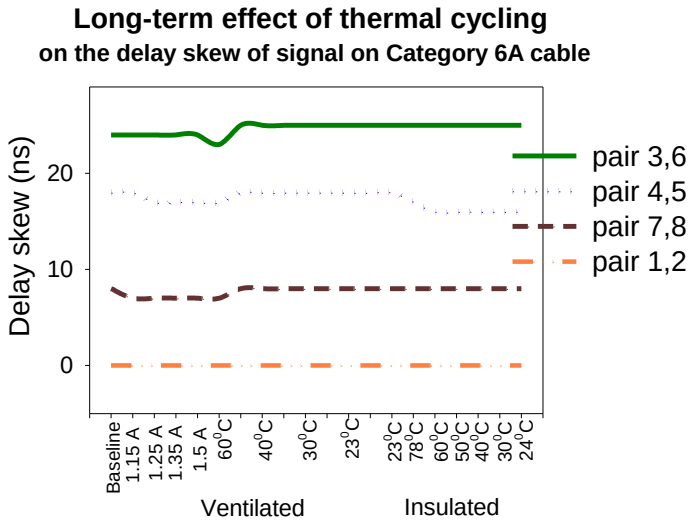

Figure 6.4: Changes in the delay skew of Cat 6A cable due to repeated resistive heating

Furthermore, the initial 1ns decrease in the delay skew of pair 7,8 (from 8 to 7 ns) during the first heating of the cable increased back by 1ns (from 7 to 8 ns) during the transition from 60^0C to 50^0C as indicated in figure 6.4. Similarly, the initial 1ns decrease in the delay skew of pair 4,5 (from 18 to 17 ns) during the first heating of the cable increased back by 1ns (from 17 to 18 ns) during the transition between 60^0C and 50^0C (figure 6.4). The delay skew of pair 4,5 later decreased again by 1ns (from 18 to 17 ns) at the peak temperature of 78^0C observed during the heating and decreased further by another 1ns (from 17 to 16 ns) during the cooling between 78^0C and 60^0C. Moreover, as shown in figure 6.4, the delay skew on the shortest pair (pair 1,2) remained unchanged throughout the free air and insulation heating tests.

6.1.5 Effect of resistive heating on the VF and ε_r of Cat6A conductor insulation

The calculated dielectric constant and velocity factor (VF) of Category 6A F/UTP conductor insulation are presented in figures 6.5 and 6.6. As discussed in the methodology section, the effective ε_r and VF were calculated from the measured changes in the electrical characteristics on the PL. The ε_r of the conductor insulation of all the twisted pairs in the cable except the green pair (pair 3,6) decreased permanently because of repeated heating and cooling of the cable (figure 6.5). However, the ε_r of the conductor insulation around pair 3,6 initially decreased but later increased permanently. The reason for this could be due to the different composition of the conductor insulation.

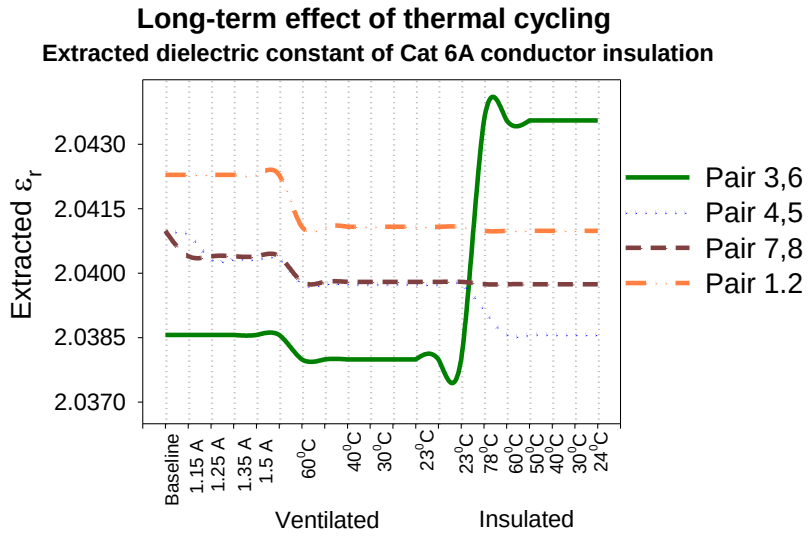

Figure 6.5: Effect of resistive heating on the $\boldsymbol{\varepsilon_r}$ of Cat 6A conductor insulation

The effects of the changes in the ε_r is noticeable on the VF of the conductor insulation around all the twisted pairs conductors (figure 6.6). That is, the lower the ε_r of the conductor insulation, the higher the VF and vice versa. The implication of the increase in the ε_r is the reduction in the speed of the signal passing through the cable. Moreover, the behaviour of pair 7,8 and 1,2 are similar but, that of pair 3,6 is distinct possibly due to a different composition of the conductor insulation that was extruded on the conductors or due to a unique twist ratio that was applied to make the twisted pair longer.

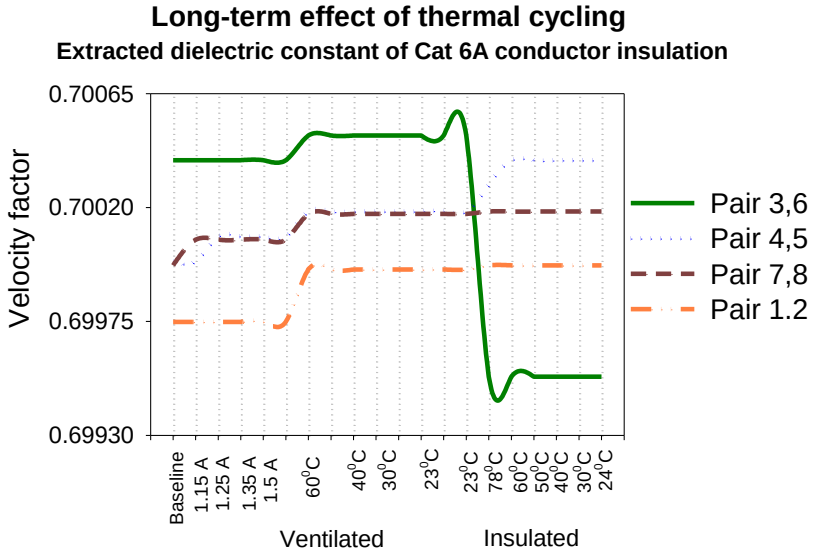

Figure 6.6: Effect of resistive heating on the VF of Cat 6A F/UTP conductor insulation

Summary of results

It has been observed that temperature affected all the twisted pairs in the Category 6A F/UTP cable differently. The distinct changes in the characteristics of pair 3,6 can be attributed to a unique twist ratio that was applied to the twisted pair, to make it about 1.8 m longer than the blue pair, ~3.5 m longer than the brown pair and ~5.2 m longer than the orange pair. Nevertheless, the VF of its conductor insulation decreased permanently during the insulation heating test because of the permanent increase in the dielectric constant of its conductor insulation. Moreover, the electrical length of all the pairs in the cable increased permanently when the cable temperature was cooling to near the room temperature. The implication of the change in the electrical length of the cable is a phase shift between the differential lines. If the phase difference becomes so large at the receiving end of the communication link, the amount of the achievable data rate on the channel will reduce as the receiver compensates for the delays.

6.2 Long-term effects of resistive heating on the transmission performance of Cat 6A PL

This section presents the effects of resistive heating on the RL, IL and crosstalk performances of Category 6A F/UTP PL. The analysis of the changes in the RL performance of the link is presented in section 6.2.1 whereas, 6.2.2 presents the IL performance of the PL. Lastly, 6.2.3 gives a detailed analysis of the crosstalk performance of the PL.

6.2.1 Long-term effect of resistive heating on the RL performance of Cat 6A F/UTP

In figure 6.7, the RL marginal values of Category 6A F/UTP PL is presented while figure 6.8 shows the RL traces obtained after the insulation heating tests. There was a decrease in the RL margin of the PL when the cable was thermally insulated. Repeated resistive heating in the ventilated environment caused the RL margin of the PL to decrease from 3 dB to 1.5 dB (figure 6.7), while thermal cycling, cable insulation and high heating temperature (78^0C) caused the RL margin of the PL to decrease beyond 0 dB.

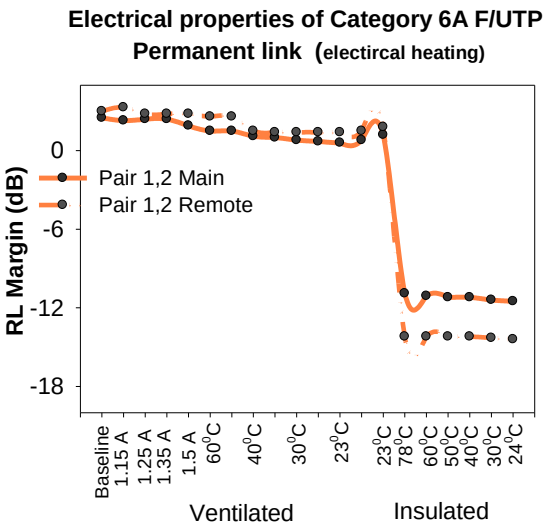

Figure 6.7: Reduction in the RL margin of Cat 6A due to repeated resistive heating

The impact of impedance mismatches along the link is apparent in figure 6.8. The worst RL performance was measured at the main side of the link around 37 MHz (on the worst pair -7,8). The cause of the RL performance can be attributed to the bends in the cable bundle due to tight bundling and heat aging of the conductor insulation when the cable was tested inside the insulation containment. The periodic non-uniformities in the cable geometry as a result of the bends in the cable created distinctive peaks in the RL characteristics of the link. The harmonics of the 37 MHz in the RL performance are also present in the IL and NEXT performances. (See figure 6.11 and 6.15).

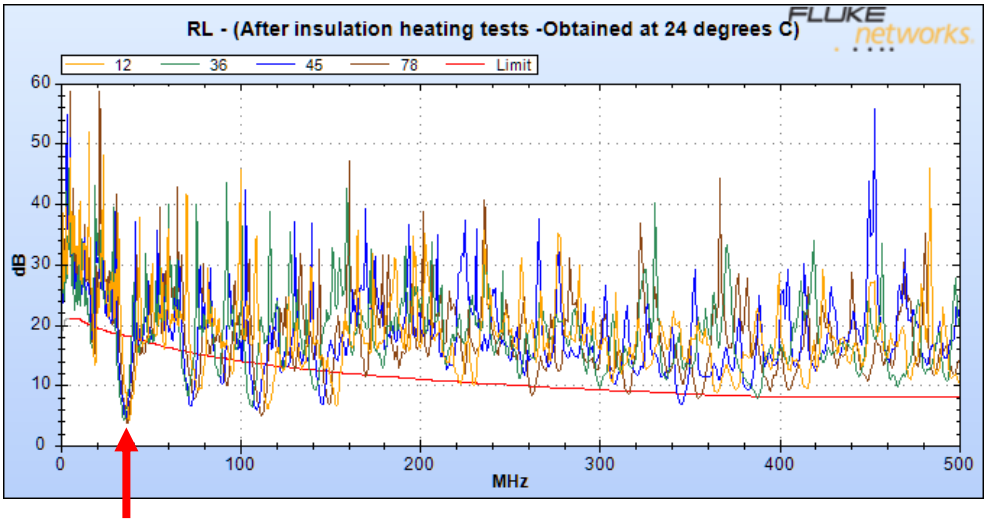

Figure 6.8: Reduction in the RL performance of Cat 6A because of repeated resistive heating

6.2.2 Long-term effect of resistive heating on the IL performance of Cat 6A F/UTP

Figure 6.9 is the baseline IL performance of Category 6A F/UTP PL at 23^0C, which shows that the IL performance of the link conformed to the TIA Category 6A PL specifications before the heating of the cable began.

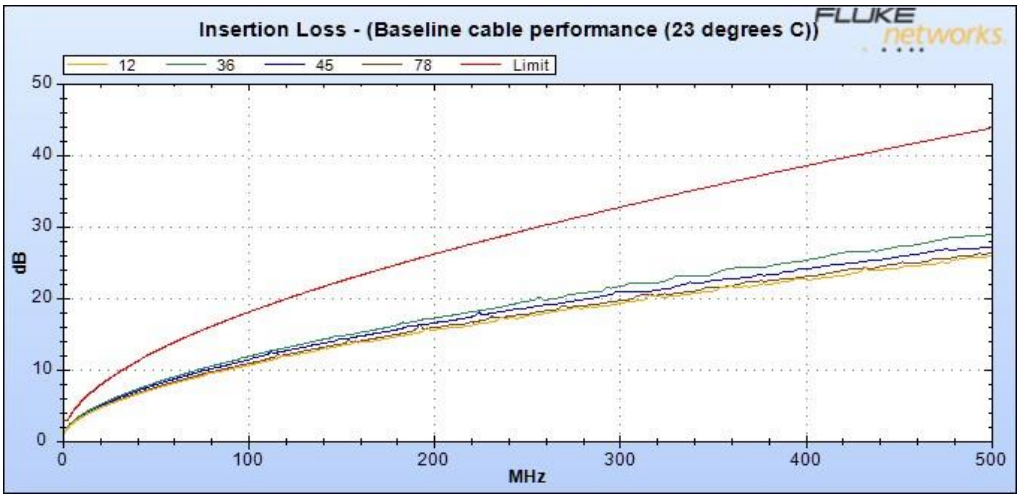

Figure 6.9: Baseline IL performance of Category 6A F/UTP PL

Figure 6.10 also shows that the IL performance of the Category 6A F/UTP PL met the TIA Category 6A PL standard limit at 23^0C after the cable had been heated and cooled repeatedly in the ventilated environment.

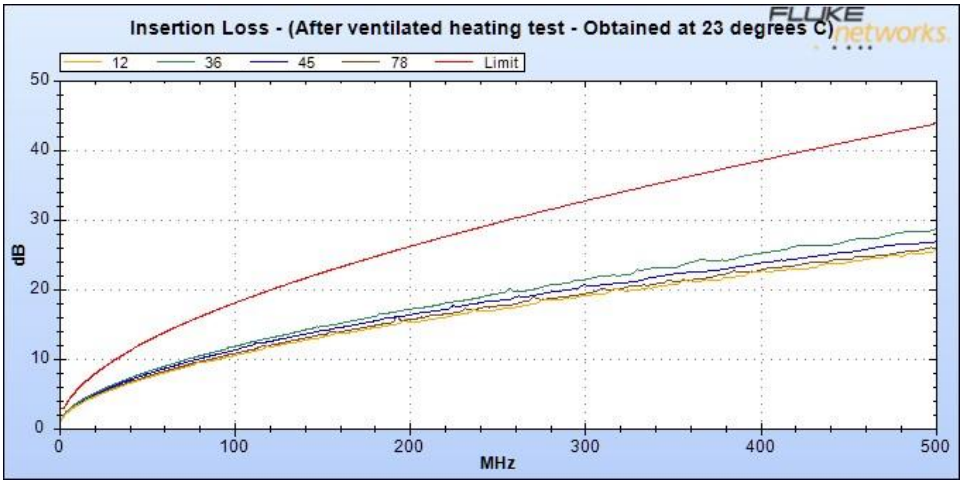

Figure 6.10: IL obtained after the heat cycling of Cat 6A cable (ventilated environment)

The IL performance obtained at 24^0C after the insulation heating tests (figure 6.11) shows that the cable failed around 35.5 MHz because of the long-term effects of repeated resistive heating at high temperature.

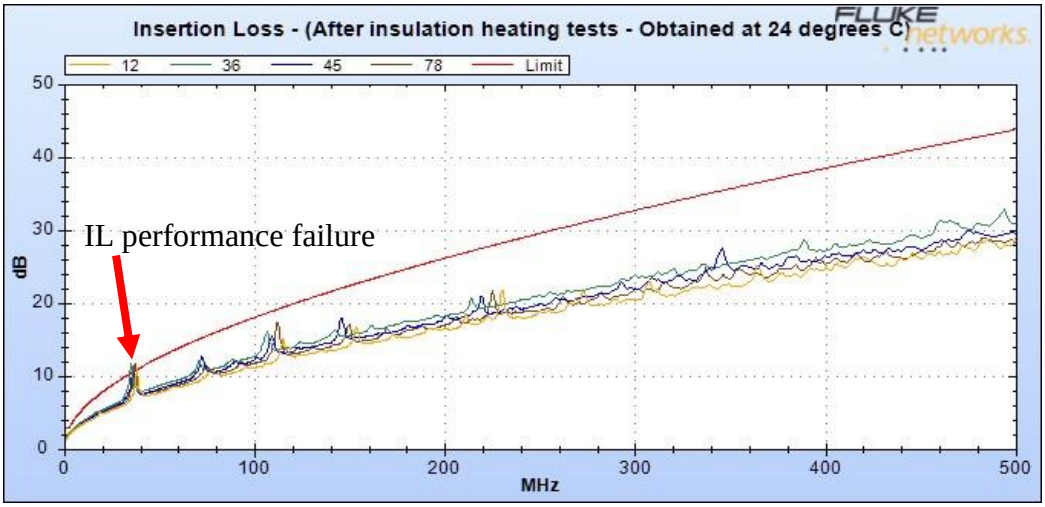

Figure 6.11: IL obtained after the heat cycling of Cat 6A cable (insulated environment)

Although IL is frequency dependent, the cause of the IL performance failure around the lower frequency range can be attributed to the impedance mismatches on the cable, caused by the heat ageing of the conductor insulation around various bends in the cable (bend losses) when tested inside the insulation containment. Also, because of the geometrical distortion of the twisted pairs around the bends (at ~3 m on the cable), caused by the thermal cycling of the cable, any induced noise in the cable will corrupt the signal passing through the cable (crosstalk attenuation) and cause the whole cabling system to fail altogether. As observed in figures 6.11 and 6.15, reflections at various interfaces (bends) in cable bundle also produced echoes at 35.5 MHz and the harmonics of the 35.5 MHz. It is appropriate to mention that crosstalk and impedance mismatch contribute to signal integrity issues.

6.2.3 Effects of resistive heating on the crosstalk performance of Cat 6A F/UTP

Figure 6.12 presents the High Definition Time Domain Crosstalk (HDTDX) analysis of the baseline measurement before the test began. The baseline performance of the PL met the specifications of the TIA Category 6A PL test limit as discussed in section 5.1. However, it can be observed in figure 6.12 that the amplitude of the baseline crosstalk was slightly high due to the

imperfections in the geometry of the twisted pairs. Moreover, the balance of twisted pairs is generally not ideal. Given this, the slight bending of the cable during bundling caused part of the energy of the transmitted signal to be converted to electromagnetic radiation which induced current in the surrounding twisted pairs.

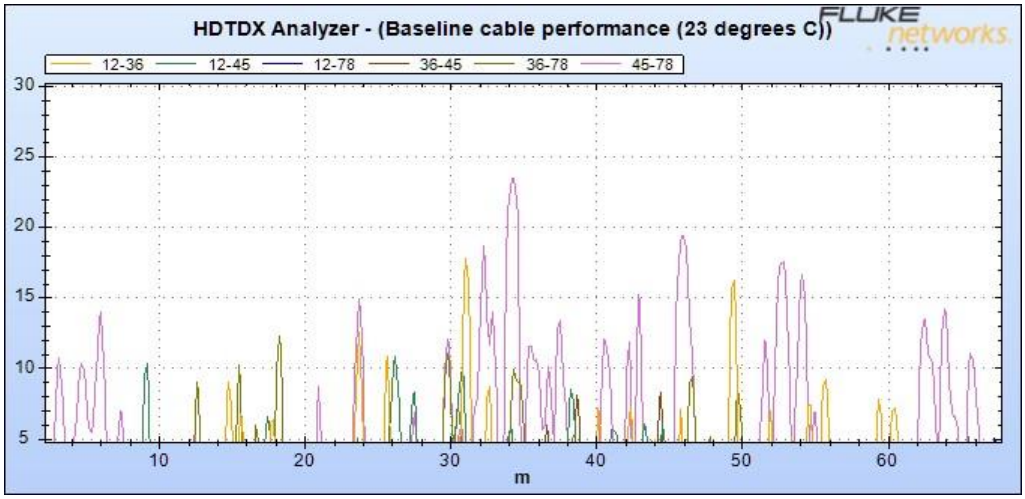

Figure 6.12: Baseline crosstalk performance of Category 6A F/UTP PL

The crosstalk performance of the PL improved slightly after the repeated resistive free air heating tests (figure 6.13).

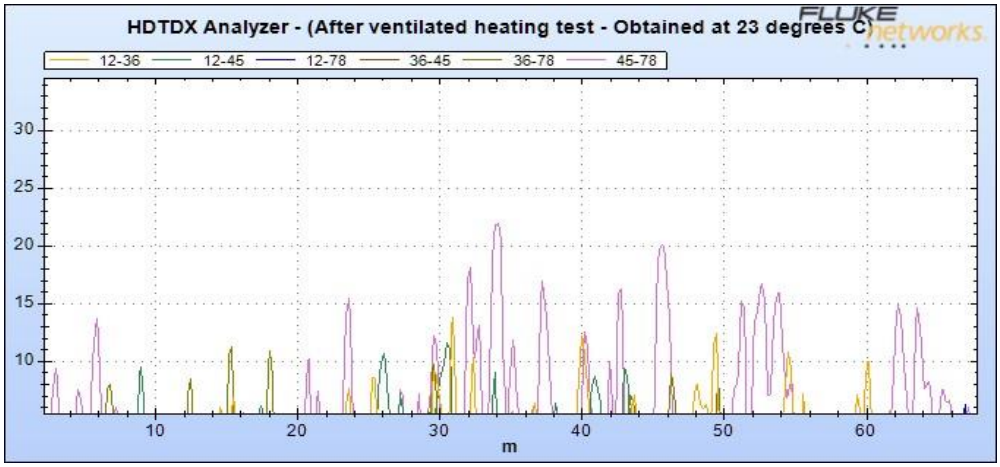

Figure 6.13: Crosstalk performance of the link after the repeated resistive free air heating

However, the spurious crosstalk signal shown in figure 6.14 reveals the impact of geometrical distortion of the twisted pairs and the inhomogeneity of the permittivity of the medium of the signal

propagation. That is, due to the asymmetry of the conductor pairs during the insulation cycling tests, severe energy coupling also occurred between the voltage modes with different velocities.

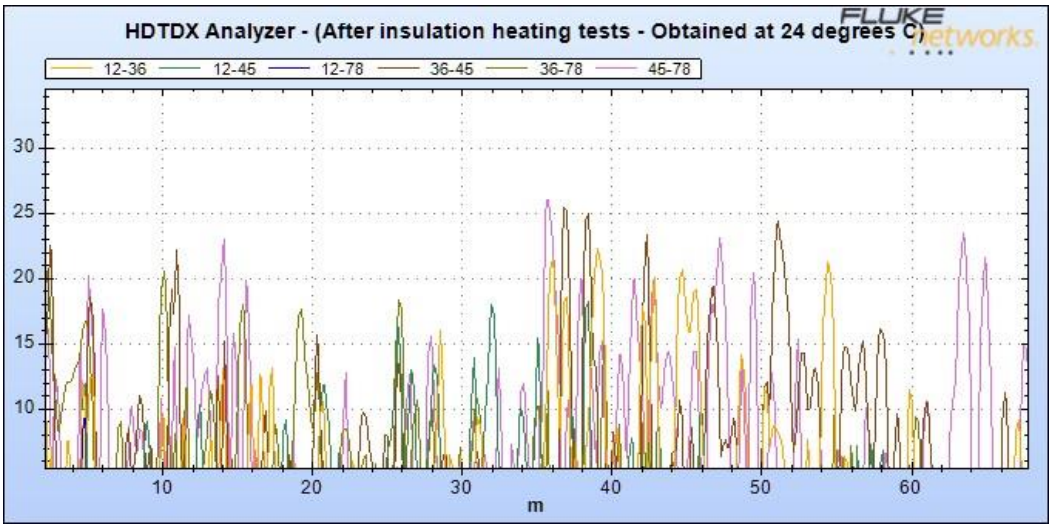

Figure 6.14: HDTDX plot of the Category 6A PL obtained after the insulation heating tests.

As indicated by the red arrow in Figure 6.15, crosstalk between pair 36-45 dominated the NEXT performance failure of the Category 6A F/UTP permanent link at 35.5 MHz.

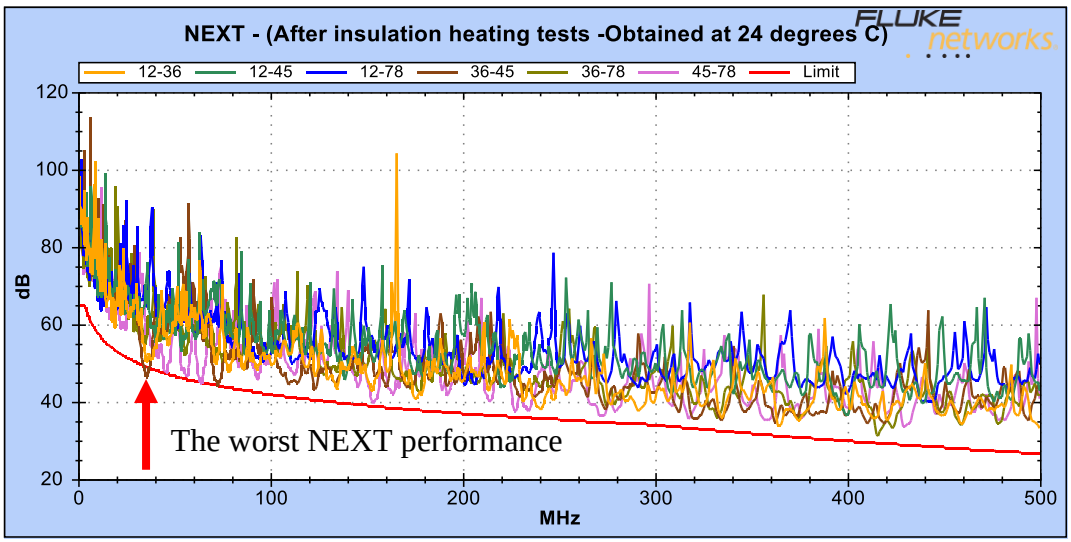

Figure 6.15: Crosstalk performance of Cat 6A PL obtained after the insulation heating tests

Summary of results

In this section, it has been observed that repeated resistive heating has an adverse effect on both the electrical properties and transmission parameters of the cable. Repeated resistive heating in the ventilated environment caused a minimal degradation to the performance of the PL whereas the insulation of the cable and the repeated resistive heating at high temperature caused severe degradation to the Category 6A F/UTP performance. Moreover, the failure of PL was dominated by the RL, IL and crosstalk performance failure. Lastly, another key observation in this section is that the heating of the cable improved the crosstalk performance slightly when the cable was heated and cooled repeated in the ventilated environment. The next chapter presents the effects of non-electrical heating on both the electrical properties and transmission parameters of shielded and unshielded balanced twisted pair cable.

CHAPTER 7 - EFFECTS OF NON-ELECTRICAL HEATING ON THE PERFORMANCE OF POE PERMANENT LINKS

In this section, the immediate and long-term effects of thermal variation on the electrical properties and transmission parameters of different PoE PLs are presented. Section 7.1 reports the immediate and long-term effects of thermal variation on the fully insulated standard Cat 6 U/UTP performance. The impact of thermal cycling within +20^{0}C and +70^{0}C is presented first, followed by the thermal impact of the extended temperature of about 120^{0}C. Moreover, sections 7.2 and 7.3 present the immediate and long-term effects of thermal variation on the portion insulated Cat 6 U/UTP CMP and Cat 6A F/UTP cables. In section 7.2, the effects of the first thermal cycling with the cyclic behaviour in the performance of the Category 6 U/UTP CMP PL are presented first, followed by the long-term effects of thermal variation on the cable. Section 7.3 also discusses the long-term effects of thermal variation on the performance of the Cat 6A F/UTP cables along with the drifts in the RL and IL performances of PL. Moreover, the validation of the drifts in the RL and IL performances of the portion insulated Category 6A F/UTP cable is presented in section 7.4. This is followed by the discussion of the long-term changes in the impedance profile of the Category 6A F/UTP cable and the extraction of the primary line constants of the PL. Moreover, this chapter ended with the presentation of the changes in the dimensions and elemental composition of the materials of a twisted pair sample.

7.1 Effects of thermal variation on the performance of the fully insulated Cat 6 U/UTP

Section 7.1.1 presents the results of the extracted and measured changes in the electrical properties of the standard Category 6 U/UTP while section 7.1.2 presents the measured transmission parameters of the PL.

7.1.1 Changes in the electrical properties of the fully insulated standard Cat 6 U/UTP

Figure 7.1 shows the DC loop resistance of each twisted pair in the standard Cat 6 U/UTP cable, which was obtained during the thermal cycling tests. Although the cable sheath length was 50.5 m, results show that the baseline DC loop resistance of each twisted pair was according to the physical length of each pair in the cable. That is, twisted pairs: 3-6, 4-5, 1-2 and 7-8 having the length of 53.4, 52.3, 51.1 and 50.5 m respectively. Moreover, the DC loop resistance of each twisted pair increased and decreased in proportional to the increase and decrease in cable temperatures. Also, it

can be observed that the orange (pair 1,2) and brown (pair 7,8) pairs having physical lengths of 51.1 and 50.5 m had lower DC loop resistance due to their similar lay lengths, in comparison to that of the green and blue twisted pairs. It can also be noted that pair 1,2 and 7,8 exhibited similar differential impedance characteristics (figures 7.7 and 7.8).

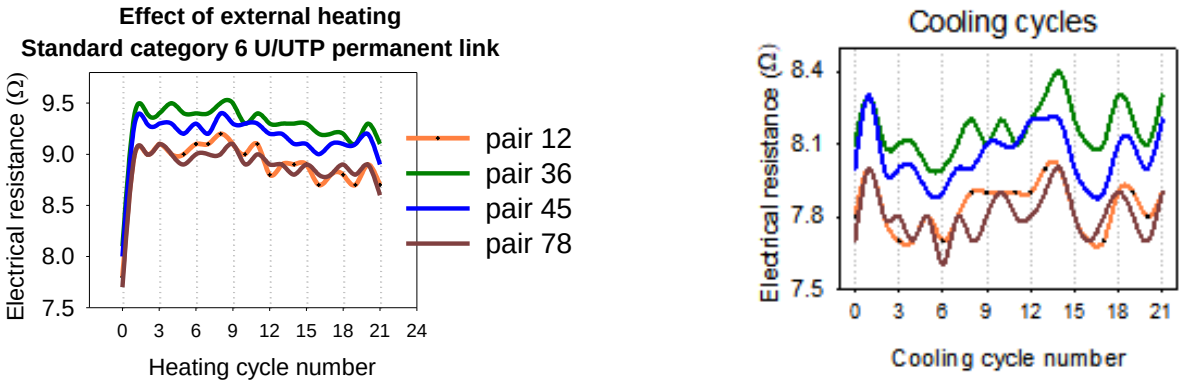

Figure 7.1: Changes in the electrical resistance of a standard Category 6 U/UTP

Figure 7.2 shows that the first heating of the cable caused the electrical lengths of the green and brown pairs to change while that of the blue and orange pairs was unchanged. However, the first cooling of the cable caused the electrical lengths of the orange and green pairs to decrease. After the third cooling of the cable, it was observed that the electrical lengths of all the twisted pairs remained relatively constant with the highest decrease of 0.4 m, measured on the orange twisted pair (pair 1,2) for the thermal cycling conducted within +20^{0}C to 70^{0}C.

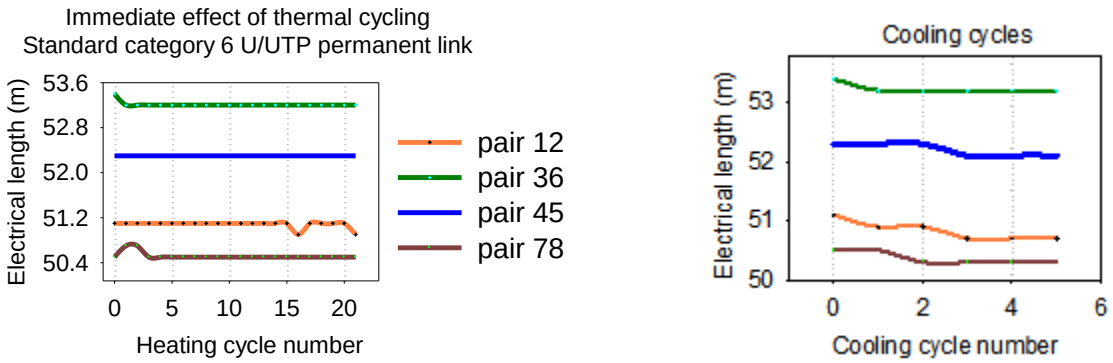

Figure 7.2: Changes in the electrical length of the standard Category 6 U/UTP cable

As shown in table 7.1, the thermal cycling of the cable with a high temperature of up to 120^0C caused the electrical length of each twisted pair to decrease more with the highest decrease of 0.7 m measured at room temperature, on the longest pair (pair 3,6) in the cable.

Table 7.1: Effects of thermal cycling on the electrical properties of standard Cat 6 U/UTP

Long-term effects of thermal cycling on the electrical properties of the fully insulated standard Cat 6 U/UTP cable					
	Effects of thermal cycling within ($+20^0$C to 70^0C)			Effects of thermal cycling within ($+20^0$C to 120^0C)	
	Baseline electrical length at (23^0C)	Final electrical length at (23^0C)	The difference in the electrical length	Final electrical length at 24^0C	The difference in the electrical length
Pair 3,6	53.4 m	53.2 m	0.2 m	52.7 m	0.7 m
Pair 4,5	52.3 m	52.1 m	0.2 m	51.9 m	0.4 m
Pair 1,2	51.1 m	50.7 m	0.4 m	50.5 m	0.6 m
Pair 7,8	50.5 m	50.3 m	0.2 m	50.1 m	0.4 m

The proportional changes in the end-to-end propagation delay of each pair as a result of the changes in the electrical length are presented in figure 7.3.

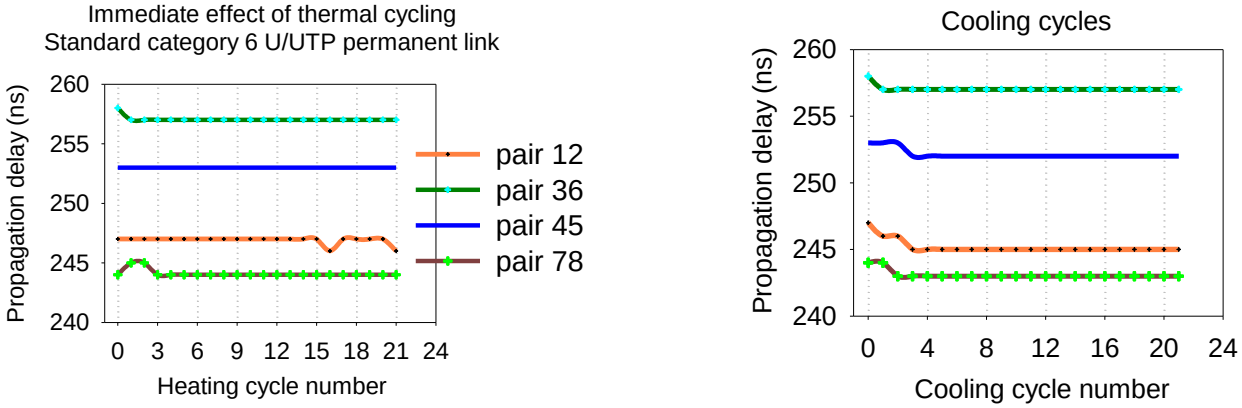

Figure 7.3: Changes in the propagation delay of the standard Cat. 6 U/UTP cable

Furthermore, the induced skew during the first and second thermal cycling of the cable as a result of the changes in the propagation delay is presented in figure 7.4. As shown, it is apparent that delay skew on the differential pairs varied during the first and second thermal cycling.

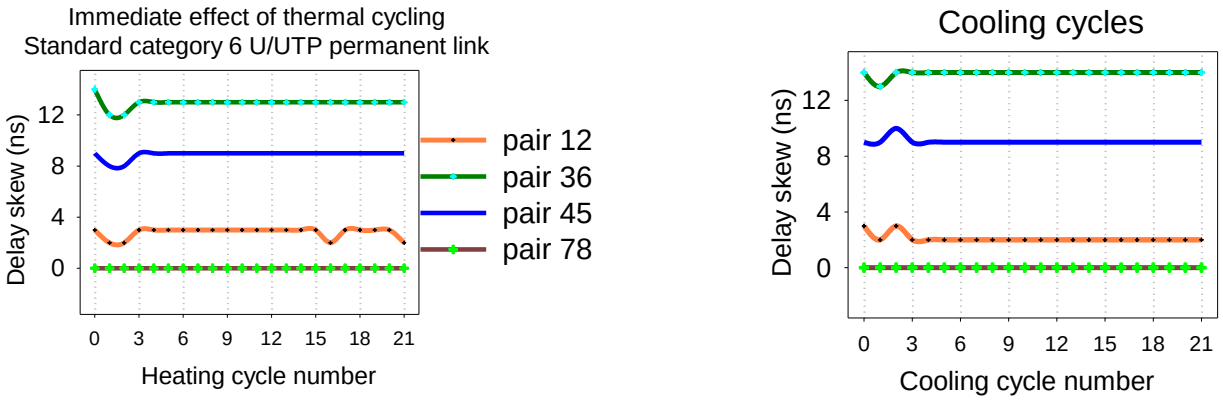

Figure 7.4: Changes in the delay skew of the standard Cat. 6 U/UTP cable

Moreover, because the electrical length of each twisted pair had changed, the VF of the conductor insulation of each twisted pair also changed accordingly (figure 7.5).

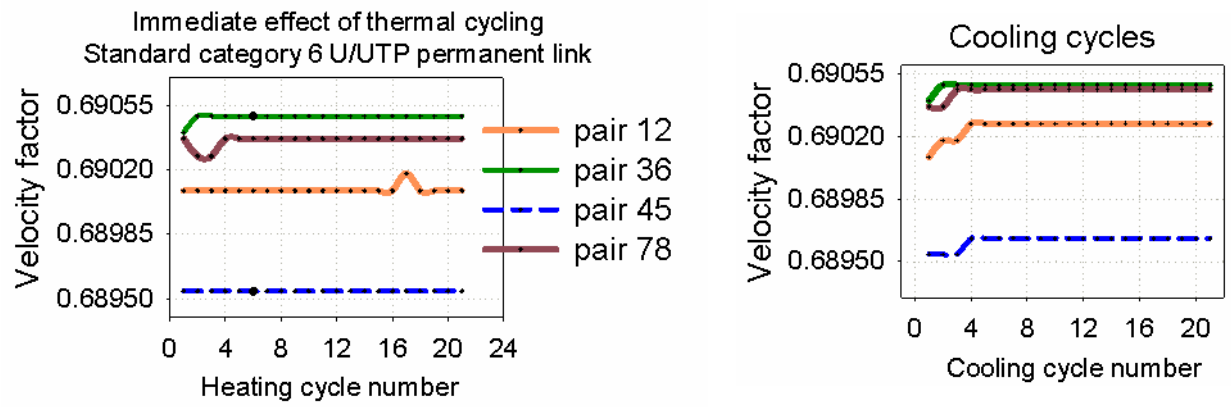

Figure 7.5: Effect of thermal cycling on the VF of Cat 6 U/UTP conductor insulation

Lastly, figure 7.6 depicts the changes observed in figure 7.5. That is, changes in the effective medium of the signal propagation (ε_r) caused the speed (VF) of the propagating signal to change.

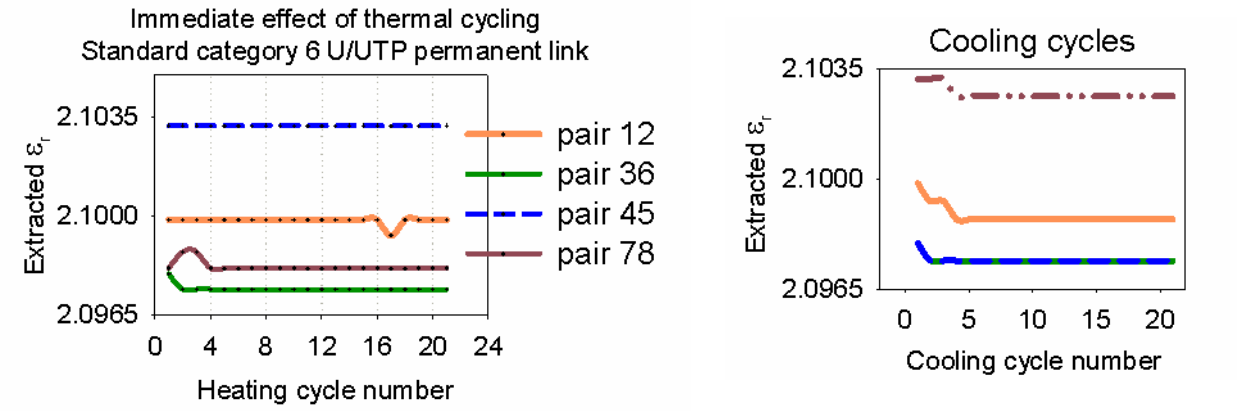

Figure 7.6: Effect of thermal cycling on the $\boldsymbol{\varepsilon_r}$ of Cat 6 U/UTP conductor insulation

7.1.2 Immediate changes in the performance of the fully insulated Cat 6 U/UTP

This section presents the immediate changes in the transmission performance of Category 6 U/UTP PL based on the effects of thermal cycling within $+20^0$C to $+70^0$C. The HDTDR plots and measured impedance variations on each twisted pair of the Category 6 U/UTP cable are presented side by side in figures 7.7 – 7.10.

The section starts with the discussion of the changes in the impedance of the permanent link knowing full well that the characteristic impedance is a function of the line geometry, the material properties of both the copper conductor and its insulator. Also, the velocity of propagation of the signal along the link depends on the values of μ and ε_r. As discussed in the methodology section, efforts were made towards terminating the ends of the cable in the impedance (~100Ω) close to the characteristic impedance of the cable to minimise reflection on the link. Moreover, the baseline performance of the link (see figure 5.5) shows that the baseline measurement met the specification of the test standard limit with an acceptable level of reflection. In other words, the impedance variations presented in figures 7.7 – 7.10 are based on the measured changes in the geometry and material properties of the cable as a result of the heating and cooling of the cable. It should be noted that the immediate changes in the VF and ε_r have already been established in the previous section. Given these, the changes in the ε_r in figure 7.6 suggest that the capacitance has also changed.

Furthermore, an electrical signal travels at a rate controlled by the effective capacitance and inductance per unit of length of the transmission line. Given this, changes in the separation distance

between a pair imply the inductance will change. The permittivity of the medium of propagation of the signal will depend on the field in the dielectric as well as the one in the air around the conductor pair, leading to the effective permittivity of the medium. Thus, the results presented in figures 7.7 to 7.10 establish the main causes of the changes in the impedance profile of each twisted pair in the standard Category 6 U/UTP cable.

Immediate changes in the characteristic impedance of the standard Category 6 U/UTP cable

Figure 7.7 shows the HDTDR plot and the changes in the differential impedance profile of the pair 7,8. The increase in the inductance during the heating of the cable predominates the increased impedance of pair 7,8. The reason for this, as indicated in figure 7.6 is that the ε_r of pair 7,8 increased during heating, which implies that capacitance increased, and inductance decreased. However, because of the thermal expansion of the twisted pair during heating, the capacitance decreased while the inductance increased due to the increased separation distance between the conductor pair. Clearly, the dominant factor for the increased impedance of pair 7,8 during the heating of the cable is due to the changes in the dimension (increased electrical length and separation distance) of the twisted pair. In addition, this explains the reason why the velocity factor (speed) decreased (see figure 7.5), and the propagation delay increased (see figure 7.3) on pair 7,8 during the heating cycles.

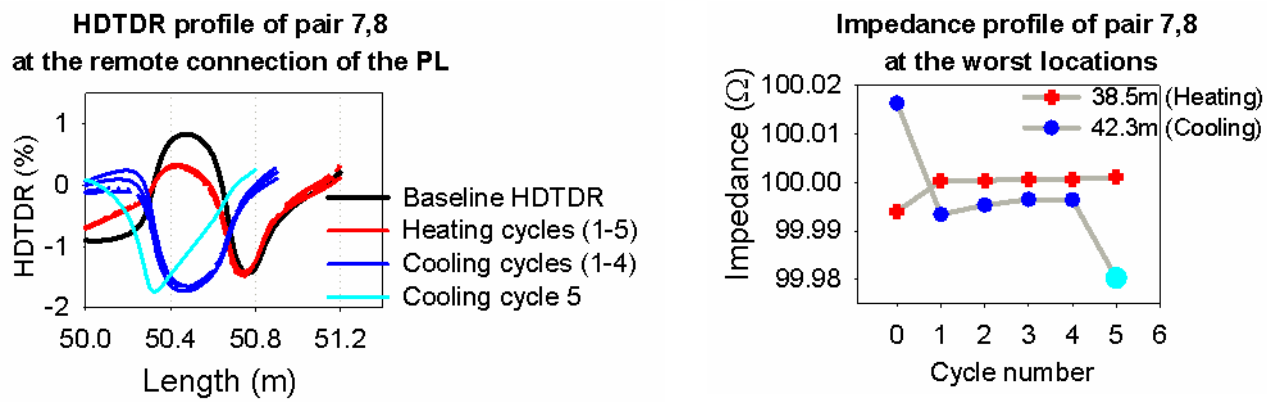

Figure 7.7: HDTDR plot and impedance profile of pair 7,8 (standard Cat 6 U/UTP)

Also, the HDTDR plot (figure 7.7) suggests that the shrinking of the conductor pair during the cooling of the cable caused the separation distance between the conductors of pair 7,8 to decrease. This led to an increase in the capacitance and a decrease in the impedance of the twisted pair. Moreover, figure 7.6 indicates a decrease in the ε_r, which suggests that the capacitance had

decreased, and the impedance increased. In addition, the HDTDR plot shows that the signal on pair 7,8 was not reaching the remote side of the link during the cooling cycles because of the decrease in the dielectric constant. The decrease in impedance of pair 7,8 as a result of the increase in the ε_r and capacitance of the pair can be linked with the shrinking of the copper conductor insulator during cooling of the cable.

Figure 7.8 shows the HDTDR plot and the changes in the differential impedance profile of the pair 1,2. Similar to the behaviour of pair 7-8, the increase in the inductance of pair 1,2 predominates the increase in the impedance of the twisted pair during the heating cycles. Note that the HDTDR plot in figure 7.8 shows that the increase in the impedance of pair 1,2 is due to the thermal expansion of the twisted pair during the heating cycles. Also, it can be observed from the HDTDR plot that the transmitted pulse signal was not reaching the end of the line during cooling cycle 1 and 2. The decrease in the electrical length of the line by 0.2 m also caused the impedance of the twisted pair to decrease. Moreover, a further decrease in the electrical length during cooling cycle 3 to 5 as a result of the delay and thermal pulling of the dielectric also caused the impedance of pair 1,2 to decrease further.

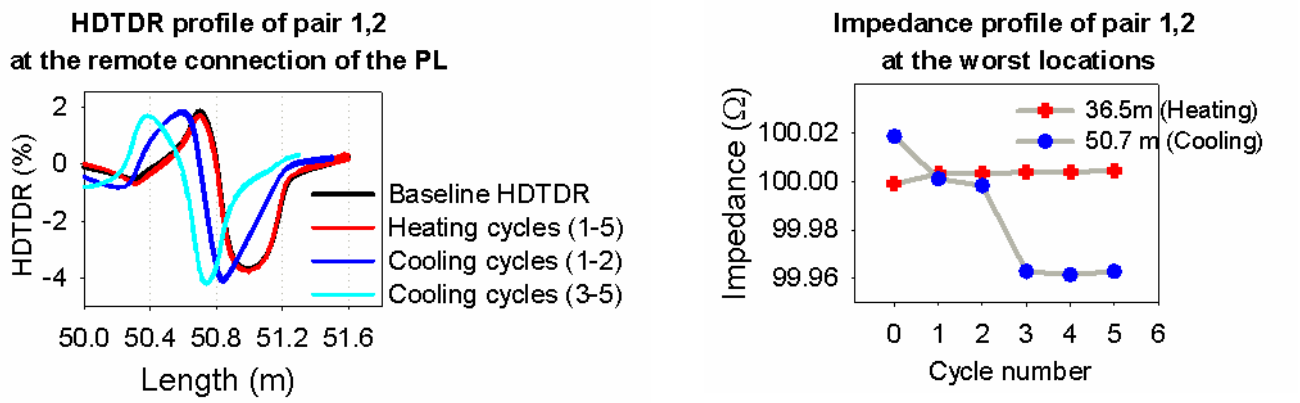

Figure 7.8: HDTDR plot and impedance profile of pair 1,2 (standard Cat 6 U/UTP)

From figure 7.9, it can be observed that the differential impedance of pair 4,5 increased within the first and second cooling cycles due to the decrease in the ε_r of the conductor insulation of the twisted pair. (See figure 7.6). Also, from the HDTDR plot, the electrical length of the pair 4,5 decreased during cooling cycle 3 to 5 because of the time delay of the pulse signal and the thermal pulling of the dielectric. In this case, the decrease in the separation distance between the insulated

conductors of the pair 4,5 caused the capacitance of the twisted pair to increase, leading to the decrease in the impedance of the link during cooling cycle 3 to 5.

Figures 7.5 and 7.6 show that the ε_r and VF of the conductor insulation of the pair 4,5 did not change during the heating cycles. Given this, it is valid to conclude that the decrease in the impedance of pair 4,5 during the heating cycles 1 to 5 is linked to the decrease in the separation distance between the insulated conductors of the pair because of the thermal pushing effect that stretched out the pair during heating.

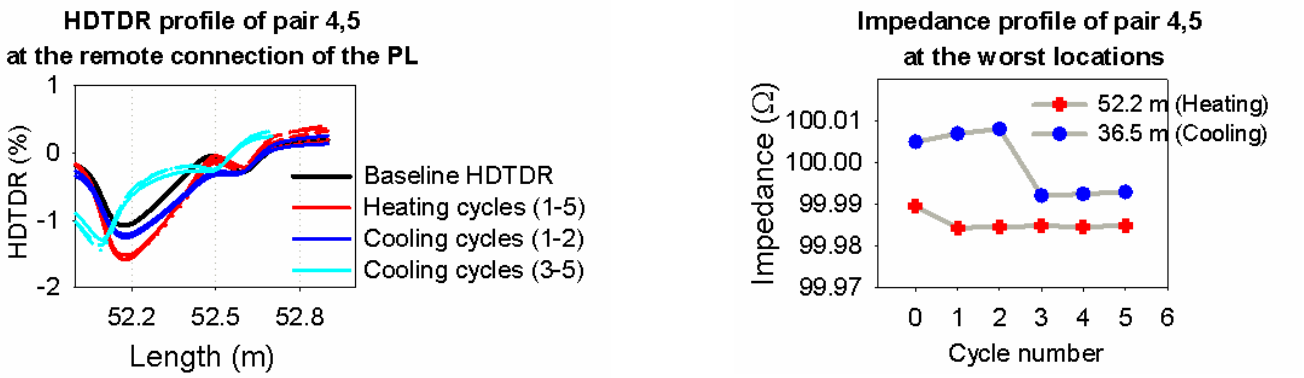

Figure 7.9: HDTDR plot and impedance profile of pair 4,5 (standard Cat 6 U/UTP)

The HDTDR plot and impedance profile of pair 3,6 are shown in figure 7.10. As shown, it was found that the first heating and cooling of the cable caused a permanent decrease in the impedance of the twisted pair. Moreover, figure 7.6 shows that the extracted effective ε_r of the pair conductor insulation decreased during the heating and cooling cycles which imply a decreased capacitance and increased impedance. Clearly, the decrease in the impedance of the longest pair in the cable (pair 3,6) was dominated by the changes in the mechanical dimension rather than the electrical dimension. It is noteworthy that the resulting long-term effect of the thermal push and pull of the dielectric around the conductors of pair 3,6 at a higher temperature of 120^0C was an open connection (See Figure 7.16). The corresponding changes in the crosstalk performance of the cable due to dimensional changes are presented in figure 7.11.

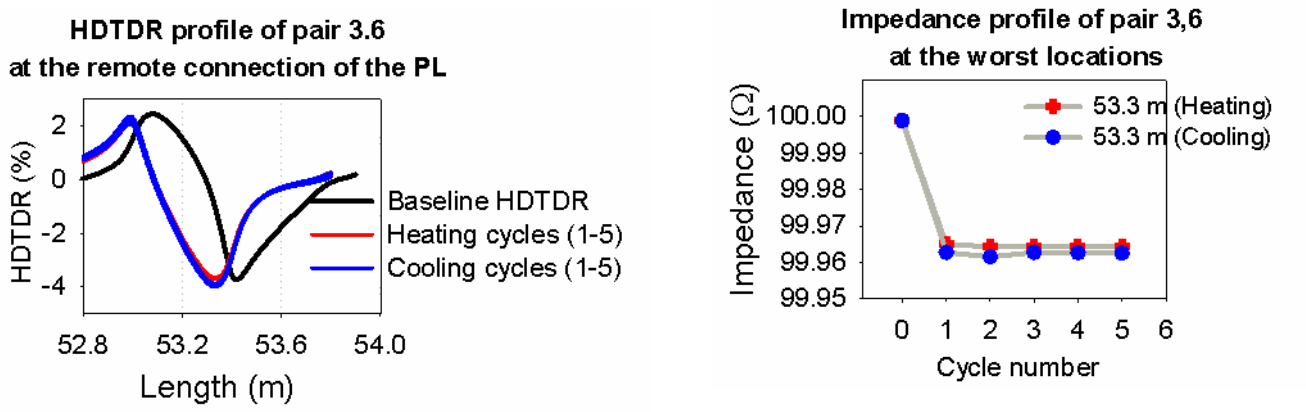

Figure 7.10: HDTDR plot and impedance profile of pair 3,6 (standard Cat 6 U/UTP)

An immediate decrease in the NEXT performance of the standard Category 6 U/UTP PL

Figure 7.11 shows that the crosstalk headroom improved during the first heating of the cable and remained relatively constant after the second heating. However, the crosstalk headroom decreased progressively within the first eight cooling cycles. After that, it increased slightly and remained relatively constant afterwards. The poor crosstalk performance during the cooling cycles can be attributed to the proximity effect, which caused strong, unwanted signal coupling from one twisted pair to the other (capacitive coupling). The thermal expansion of the cable during heating means less noise coupling between the twisted pairs in the Category 6 U/UTP cable.

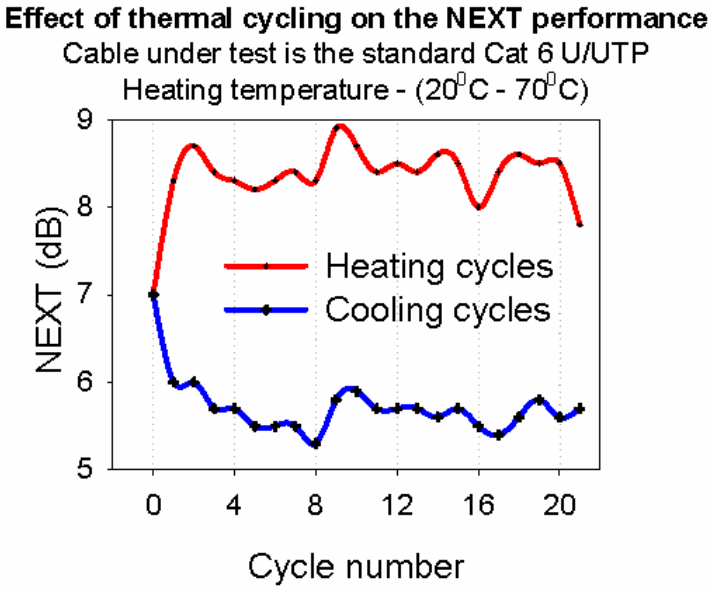

Figure 7.11: Immediate changes in the NEXT headroom of the standard Cat 6 U/UTP

Immediate decrease in the RL performance of the standard Category 6 U/UTP PL

The total reflected energy of the pulse signal passing through pair 1,2 during heating and cooling cycles 1 to 5 is presented in figure 7.12. The results showed that thermal cycling at lower temperatures of +20 ^{0}C to 70 ^{0}C caused an immediate decrease in the RL performance of the PL. The trend of the RL performance of the PL is also similar to that of the NEXT performance as captured in figure 7.11.

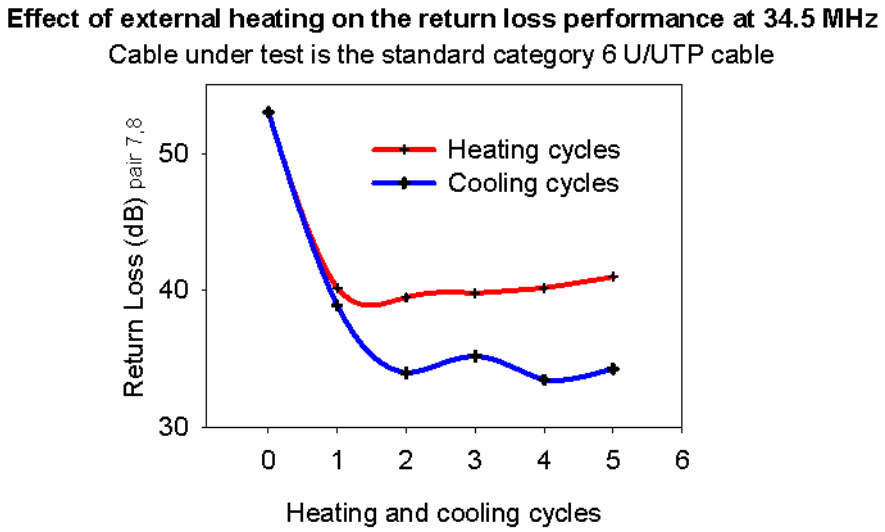

Figure 7.12: Decrease in the RL value of the worst performing pair (7,8) at 34.5 MHz

Also, as indicated on the left-hand side of figure 7.13, the first heating and cooling of the cable caused a 45^0 phase shift in the RL signal and a reduction in the amplitude of the reflected waveforms due to the cooling of the cable. Besides, a 90^0 phase shift from the baseline signal was observed at the frequency (34.5 MHz) at which the worst reflected signal was measured.

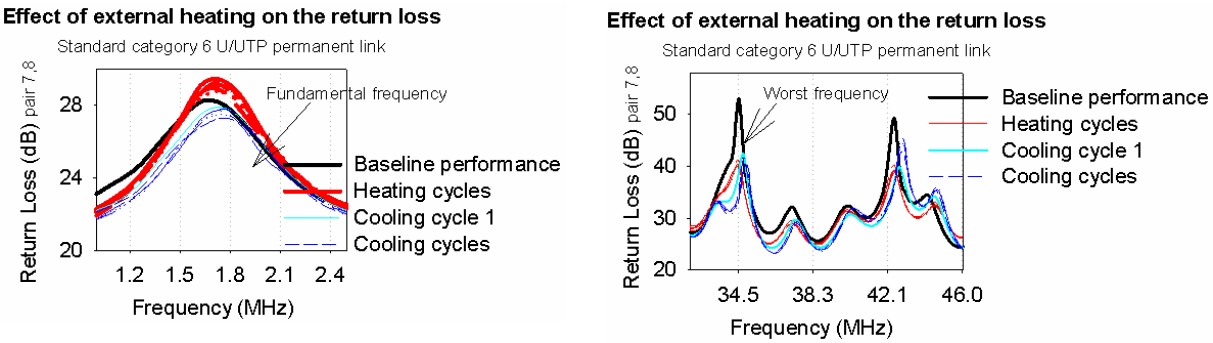

Figure 7.13: Shift in the RL traces of the standard Cat 6 U/UTP cable

Changes in the PSACR-N headroom of the fully insulated standard Cat 6 U/UTP cable

Figure 7.14 shows that the immediate performance of the cable was affected by thermal cycling. Another key observation is the hysteresis in the measurement plots. The improved crosstalk performance of the cable is concomitant with the decrease in the ε_r of the conductor insulation as a result of heat cycling. In addition, after the heat cycling of the cable for few times, the changing of the physical structure of the twisted pairs settles and the effect of capacitive coupling decreases. The decrease in the ε_r because of the effects of temperature fluctuations is discussed in section 9.2.1 and 9.3.1. Generally, the PSACR-N performance of the standard Category 6 U/UTP cable was affected more during heating in comparison to the observed effect during the cooling phase of the cable (within the first 10 thermal cycles).

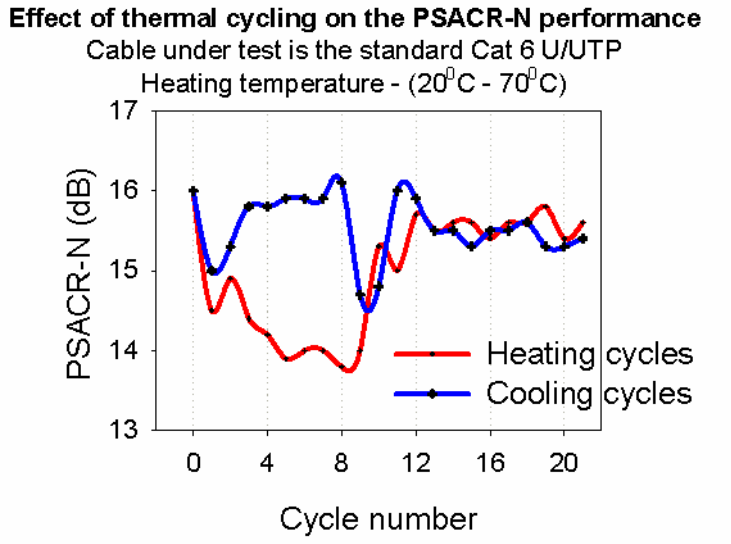

Figure 7.14: Changes in the PSACR-N headroom of the standard Cat 6 U/UTP PL

7.1.3 Long-term effects of thermal variation on the performance of the Cat 6 U/UTP

The previous section (section 7.1.2) presented the results of phase 1 of the studies described in section 5.2. In this section, the results of phase 2 of the studies are presented. It was shown in section 7.1.2 that the first few cycles of heating and cooling brought about some changes to the overall profile of the standard Category 6 U/UTP cable. It is noteworthy that these changes did not result in the failure of the cable. However, the performance of the standard Category 6 U/UTP PL failed within +20^{0}C and 120^{0}C due to the changes caused by the repeated thermal cycling of the cable at elevated temperature. It is also worth mentioning that the catastrophic failure of the PL did not occur

at the peak of 120^{0}C but at ~25^{0}C when the cable temperature was cooling to near the room temperature after 9 hours of localised heating. From figure 7.15, the first red arrow represents the point where the Cable Analyser reported the initial permanent link failure, which was an open connection (see figure 7.16). Also, the open circuit observed at this point caused the loss of the PL and 100% of the pulse reflection (see figure 5.9). Note that the T1, T2d and Ta2 in figure 7.15 represent the positions of the thermocouple sensors placed on the cable jacketing material as described in section 3.1.

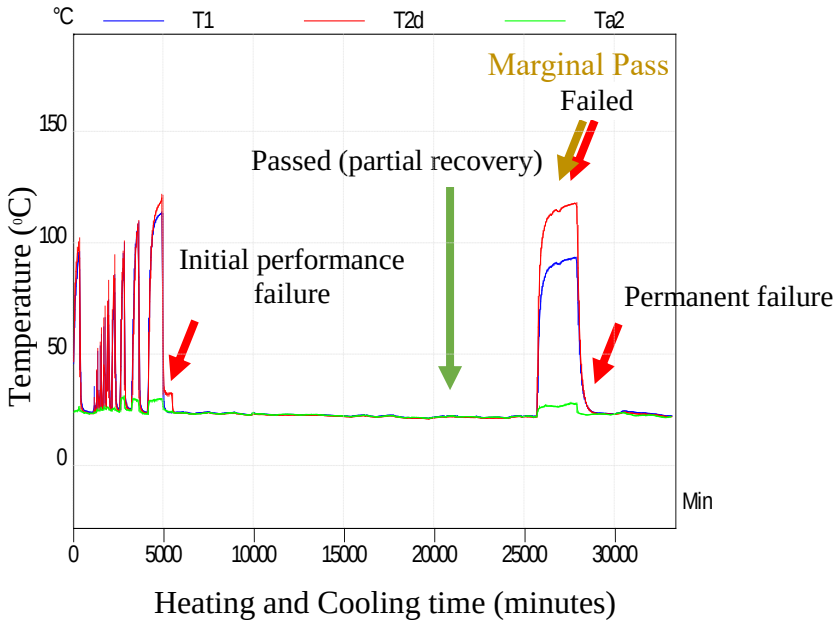

Figure 7.15: Temperature profile for the cyclic performance of the standard Cat 6 U/UTP PL

The failure could as a result of the fracture of the dielectric around one of the conductor pair of 3,6 due to the thermal pulling of the dielectric during the cooling phase. Also, due to the combination of stresses: localised heating, high temperature, mechanical degradation, and loss due to the change in impedance.

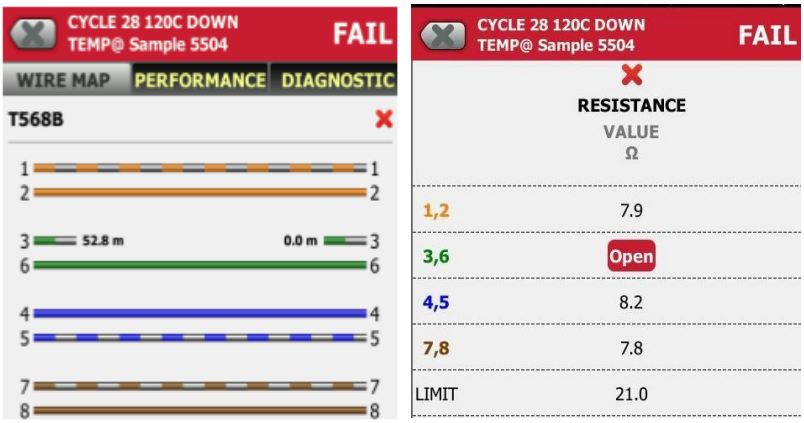

Figure 7.16: Showing the loss of the communication link due to a high resistance connection

Furthermore, it was observed that the cable recovered partially from the stress (the green arrow in figure 7.15) when it was left unpowered for some days. The red and golden arrows in figure 7.15 show that the cable performance passed at 120^0C when it was heated again, whereas the last red arrow shows that the PL failed again at 24^0C.

The DC loop resistance and Intra Pair Resistance Unbalance (IPRU) were measured in-between the heat cycling test, and the results obtained are presented in figures 7.17 and 7.18. The first indicated value (8.1 Ω) in figure 7.17 is the baseline DC loop resistance while the middle figure is the DC loop resistance obtained at room temperature after the initial failure of the PL. The right figure in figure 7.17 shows the RL measured after the initial failure of the PL. As shown previously in figure 7.1, the baseline DC loop resistance increased from 8.1Ω at 21^0C to 9.1Ω due to a temperature increase to ~60^0C. However, due to the effect of multiple insertion and removal of the RJ45 plugs from and into its jacks, and the fatigue of the cable conductors at high temperature, high contact resistance developed at the termination point of pair 3,6, (split pair) which caused the reflection of the transmitted signal (the right figure in figure 7.17). The significance of an increase in the resistance of the link is the loss of the signal strength and a limit on the available power to the connected end devices. More also, high resistance connection reflects signal.

Effect of high contact resistance

	RESISTANCE VALUE Ω
1,2	7.8
3,6	8.1
4,5	8.0
7,8	7.8
LIMIT	21.0

	RESISTANCE VALUE Ω
1,2	7.9
3,6	8.5
4,5	8.2
7,8	7.9
LIMIT	21.0

Baseline resistance (a) High contact resistance (b) Return Loss of the PL (c)

Figure 7.17: Baseline resistance (a), high contact resistance (b) and (c) RL of the PL

The poor Intra Pair Resistance Unbalance between the conductors of pair 3,6 is shown in figure 7.18. As indicated, the unbalance in the resistance of pair 3,6 exceeded the specified limit of 0.05Ω as a result of the high contact resistance. Note that the impact of the high resistance connection in a real PoE channel is a loss of the communication link when data traffic is launched on the channel.

Resistance unbalance between the pins of the Rj45 connector

Cycle12 11621 23.9C+ALL PASS

	RESISTANCE VALUE Ω	RESISTANCE UNBALANCE VALUE Ω	RESISTANCE UNBALANCE LIMIT Ω
1,2	7.9	0.01	0.24
3,6	8.2	0.05	0.25
4,5	8.1	0.01	0.24
7,8	7.8	0.03	0.23
LIMIT	21.0		

CYCLE 28 120C DOWN TEMP@22.9 Sample 33120 FAIL

	RESISTANCE VALUE Ω	RESISTANCE UNBALANCE VALUE Ω	RESISTANCE UNBALANCE LIMIT Ω
1,2	7.9	0.01	0.24
3,6	10.8	2.63	0.32
4,5	8.1	0.02	0.24
7,8	7.8	0.01	0.23
LIMIT	21.0		

Cycle 12 Cycle 28

Figure 7.18: Showing the Intra Pair Resistance Unbalance of pair 3,6 at cycle 12 and 28

Summary of results - Phase 1 of the thermal cycling tests (+20^{0}C to +70^{0}C)

The immediate and long-term effects of thermal variation on the performance of the fully insulated standard Cat 6 U/UTP cable have been reported in this section. It was established that the first few cycles of heating and cooling affected the performance of the standard Cat 6 U/UTP cable. Moreover, the impact of thermal cycling within +20^{0}C to +70^{0}C affected the electrical performance of each pair differently; but the impact was more pronounced during the cooling phase than the heating phase. The effective ε_r of the dielectrics of all the twisted pairs in the cable decreased permanently due to the cooling of the cable. Also, the electrical length of the cable decreased by 0.4 m due to the effect of thermal cycling conducted between +20^{0}C and +70^{0}C. Furthermore, the decrease in the electrical length of the cable is attributed to the decrease in the ε_r, which resulted in an increase in the VF of the conductor insulation and a reduction in the propagation delay. The changes in the propagation delay caused the delay skew to change also. The variations in the characteristic impedance of each pair caused reflections to occur, which was measured as RL. Moreover, a 45^0 phase shift was observed at the fundamental frequency of the RL signal on pair 7,8 while 90^0 phase difference was observed at 34.5 MHz. Immediate changes in the crosstalk performance of the permanent link were also observed. The reduction in the crosstalk loss between the twisted pairs was also observed after the repeated resistive free air heating tests section 6.2.3 (see figure 6.13). Lastly, the PSACR-N performance of the cable was more affected during the heating phase than the cooling; although it was found that the PSACR-N of the cable improved after a few heating and cooling cycles.

Summary of results - Phase 2 of the thermal cycling tests (+20^{0}C to +120^{0}C)

The thermal impact at an extended temperature of about 120^{0}C caused the electrical length of each twisted pair in the Category 6 U/UTP to decrease more with the highest decrease of 0.7 m measured at room temperature. It was also shown that the cable had a partial recovery from the combination of stresses when unpowered for some days. Moreover, after the initial failure of the PL, the cyclic performance of the fully insulated standard Cat 6 cable was observed. Furthermore, the heating of the cable to a higher temperature of 120^{0}C caused the loss of the link at room temperature and a DC contact resistance issue which of course resulted in poor intra-pair resistance unbalance of pair 3,6. The next section reports the effects of thermal variation on a similar Category 6 unshielded twisted pair cable under a different installation condition.

7.2 Effects of thermal variation on the performance of portion insulated Cat 6 CMP

In this section, the effects of intermittent and prolonged thermal cycling on the performance of Category 6 U/UTP CMP cable in which its portion was thermally insulated are presented. The rationale for the study was to establish whether the effect of heating and cooling of the conductor insulation around the insulated portion of the cable cause performance degradation. In examining this, the dielectric rod sample, which was extracted from the Category 6 U/UTP CMP cable under test, was also heated and cooled repeatedly following the same heating regime of its cable in order to compare the cable behaviour to its dielectric behaviour. The response of the cable's dielectric properties to this treatment is presented in section 9.3.

The cable performance failure points; transition points and thermal cycles at which the electrical length of the cable decreased are presented first, to establish the cyclic behaviour in the cable performance and the key points in the performance degradation of the cable. After that, the measured and extracted electrical properties of the PL are reported (section 7.2.1). Lastly, section 7.2.2 presents the observed changes in the transmission parameters of the PL.

Cyclic performance of the portion insulated Category 6 U/UTP CMP cable

Figure 7.19 to 7.24 present the cyclic behaviour in the performance of the portion insulated Category 6 U/UTP CMP cable and the temperature profile for the cyclic behaviour. The maximum heating temperature set for the thermal cycling test was within the PoE operating temperature of 60^0C and that the measured baseline RL performance of the PL was a marginal pass (see figure 5.14).

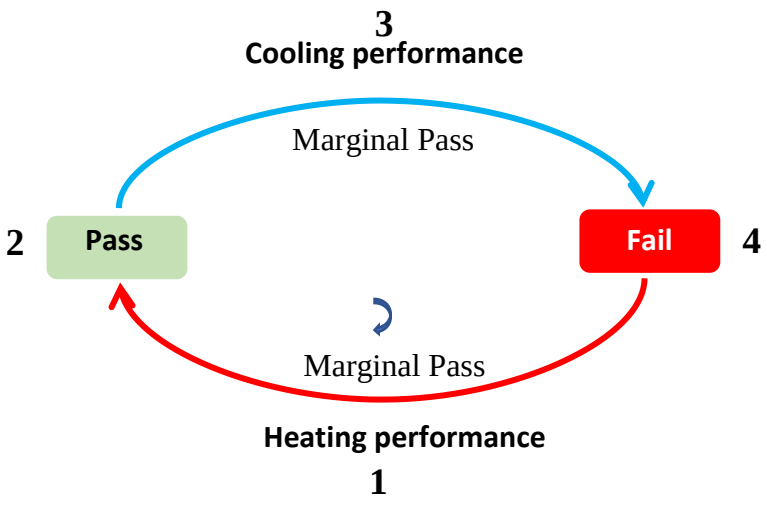

Figure 7.19: Initial cyclic performance of the portion insulated Cat 6 U/UTP CMP cable

Figure 7.19 shows the key points in the RL behaviour of the PL. As indicated (see 1 in figure 7.19), the baseline RL performance of the PL was a marginal pass with a marginal value of 0.8 dB at 22.5^{0}C. However, the RL performance of the PL passed (see 2 in figure 7.19) during the heating of the cable when the temperature of the cable was at 30^{0}C, 40^{0}C and the peak of 60^{0}C. Furthermore, when the cable was cooling to the room temperature (during cooling cycle 1), the RL performance of the PL was a marginal pass again at 40^{0}C and room temperature (see 3 in figure 7.19). Moreover, during the second heating cycle of the cable, the RL performance passed again at the peak of 60^{0}C, and the cyclic behaviour of the RL performance of the PL continued until the cooling cycle 5 when the RL performance failed for the first time at 20^{0}C (see 4 in figure 7.19). After this point, the RL performance continued with a cyclic behaviour of (marginal pass)-pass- (marginal pass)-fail during the initial ten intermittent (daily) cycles and the subsequent four prolonged (weekly) cycles. However, after the 5th prolonged heating cycle (after 15 cycles altogether), the electrical length of pair 4,5 of the Cat 6 U/UTP cable decreased by 0.2 m, and the cyclic performance continued until the RL performance failed permanently at cooling cycle 18. After this point, the cyclic performance of the link changed from (marginal pass)-pass-(marginal pass)-fail to fail - (marginal pass) - (marginal pass)-fail as illustrated in figure 7.20.

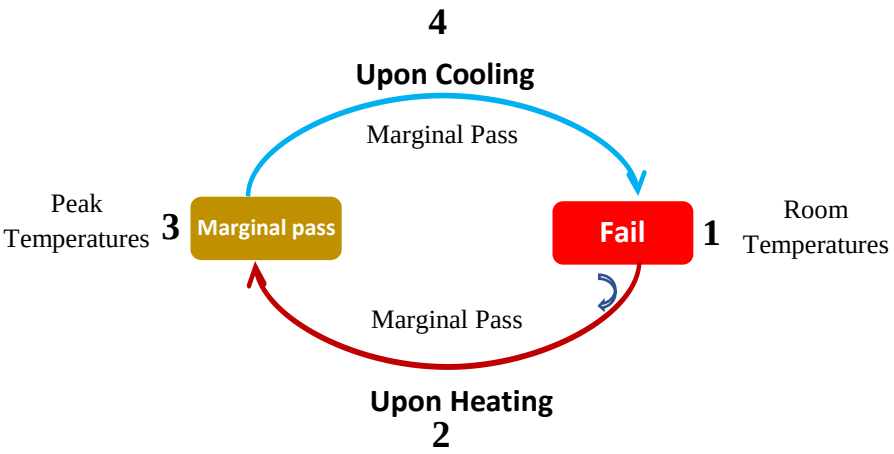

Figure 7.20: Cyclic performance of the portion insulated Cat 6 U/UTP CMP cable

Figure 7.21 shows the temperature profile for the 10 intermittent thermal cycles, whereas figure 7.22 shows the temperature profile for the prolonged thermal cycles (11 weekly and 4 monthly thermal cycles). From figure 7.21, the highest cable temperature during the intermittent heating cycles was 60^{0}C. However, as indicated in figure 7.22, the peak temperature increased at cycle 15 where the electrical length of the PL decreased.

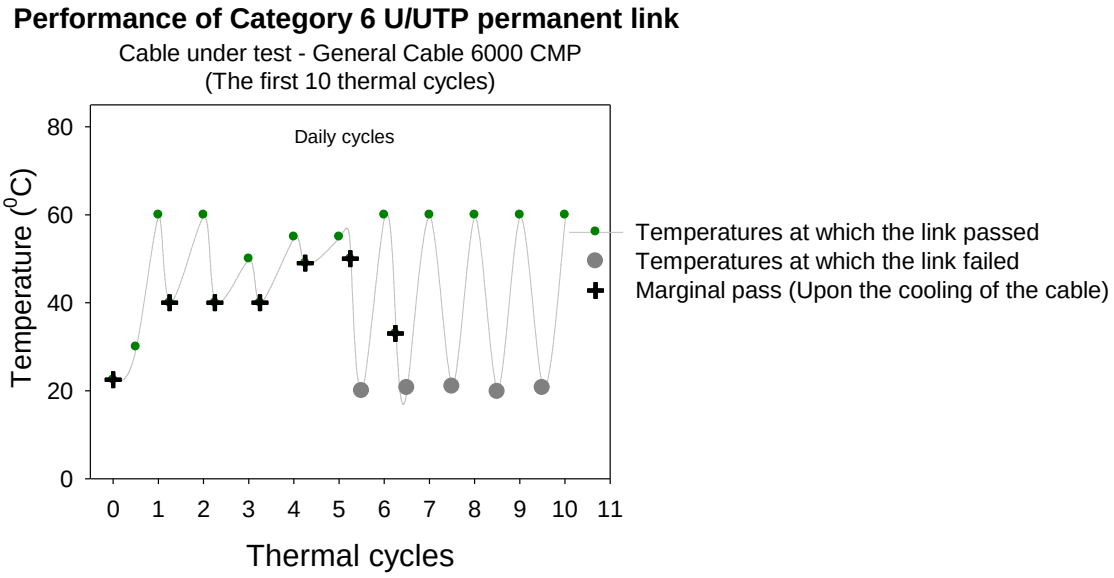

Figure 7.21: Temperature profile for the intermittent thermal cycles

It is evident in figure 7.22 that the RL performance of the permanent link passed at the peak temperatures (until cycle 18) but marginally passed in-between the peak temperatures and room temperature. It was also observed that the RL performance of the link failed at temperatures near the room temperatures (see the grey dot in figure 7.22). The last observation in figure 7.22 is that the temperatures at which the RL performance of the PL passed marginally upon cooling were approaching the failure temperature during the prolonged monthly thermal cycling (see the red arrow in figure 7.22). The drift in the failure and recovery temperatures is also clearly shown in figure 7.23.

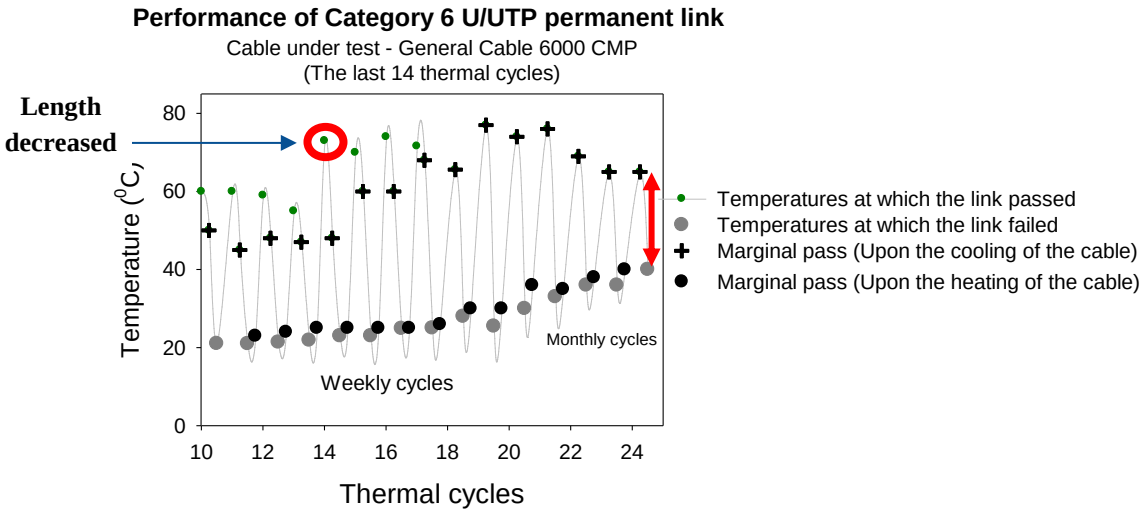

Figure 7.22: Temperature profile for the last 14 thermal cycles (weekly and Monthly cycles)

The significance of the drift in the performance of the link is that the RL performance of the link was also moving from the marginal pass to a complete failure even at the peak temperatures.

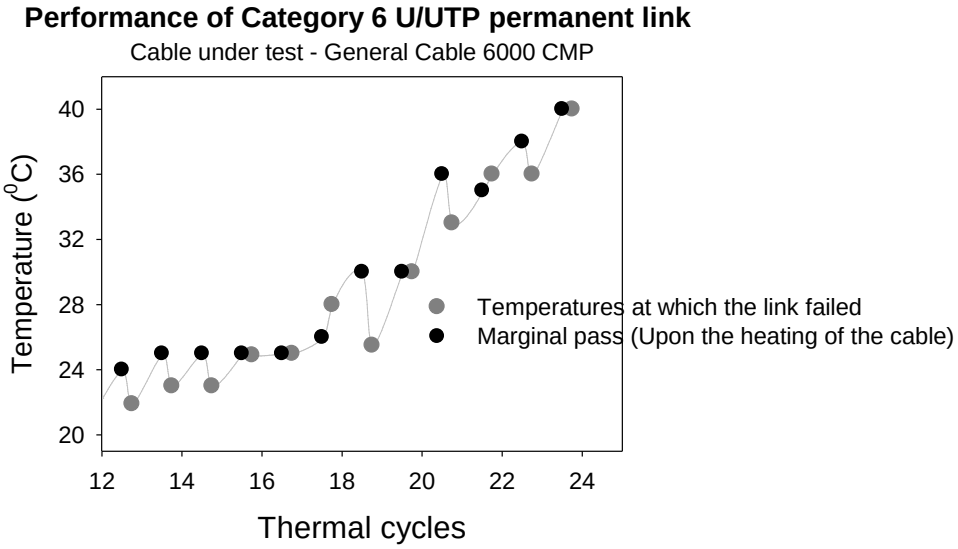

Figure 7.23: Showing the drift in the failure and recovery temperatures

The drift in the RL marginal values and the corresponding failure temperatures in figure 7.24 confirm the degradation in the RL performance of the PL as a result of the thermal variation and prolonged heat cycling.

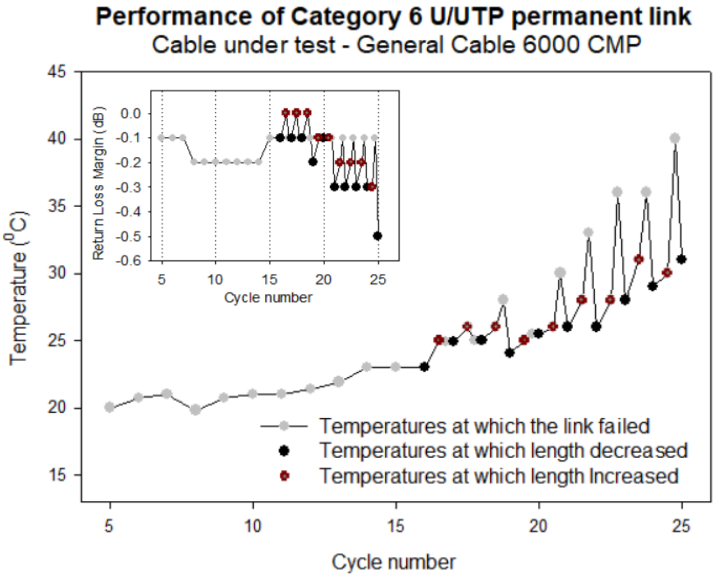

Figure 7.24: Drift in the RL marginal values and the corresponding failure temperatures

7.2.1 Electrical properties of the portion insulated Cat 6 U/UTP CMP cable

Figure 7.25 presents the decrease in the effective ε_r of the conductor insulation of pair 4,5 and its electrical length. The effective ε_r was calculated from the room temperature measurements of the cable's electrical characteristics.

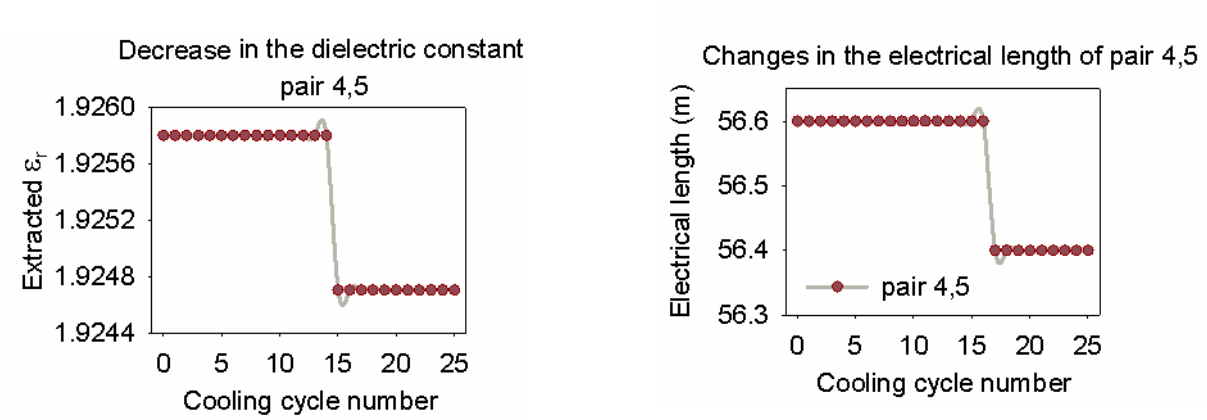

Figure 7.25: $\boldsymbol{\varepsilon_r}$ of the conductor insulation and electrical length of Cat 6 U/UTP CMP cable

From figure 7.25, it can be observed that the electrical length of the pair 4,5 decreased at cycle 15 by 0.2 m, causing a proportional propagation delay of 1 ns (figure 7.26 - Left). Moreover, the decrease in the route length of a propagating signal means the speed will increase. It was also found that the velocity factor of the conductor insulation of pair 4,5 increased (figure 7.26 - Right) due to the decrease in the electrical length of the cable.

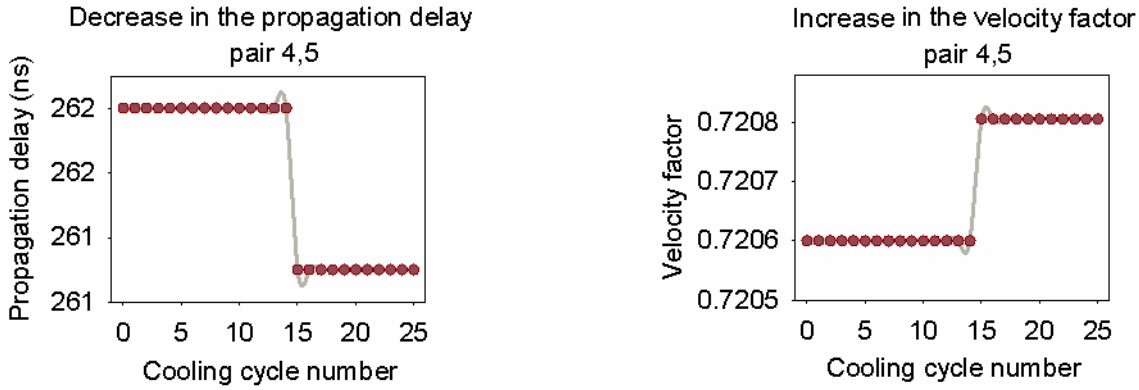

Figure 7.26: Increase in the VF and propagation delay of Cat 6 U/UTP CMP cable

Figure 7.27 presents the delay skew measured on the longest twisted pair (pair 1,2) in the cable. It was observed that delay skew increased on all the twisted pairs in the cable, except the shortest pair (pair 4,5). Delay skew is the difference in propagation delay between the shortest pair and any pair in the same cable.

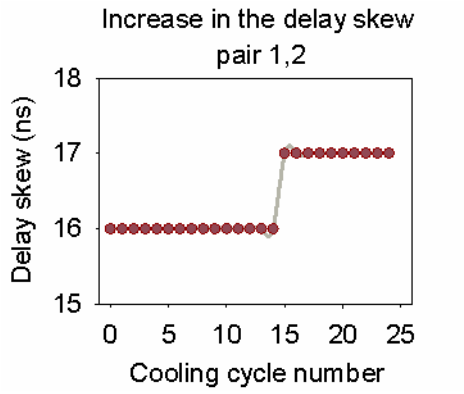

Figure 7.27: Increase in the delay skew of the longest pair in the Cat 6 U/UTP CMP cable

7.2.2 Changes in the transmission performance of the portion insulated Cat 6 CMP cable

Changes in the characteristic impedance of the portion insulated Cat 6 U/UTP CMP cable

Figure 7.28 shows the impedance mismatches at the two ends of the Category 6 U/UTP CMP PL based on the effects of localised heating of the cable. Note that the precision in the impedance measurements is less important for this study in comparison to the trend observed in the impedance of the PL as a result of localised heating of the cable.

The impedance profile on the left-hand side of figure 7.28 is the observed impedance variations at the reference plane of the PL, while the right figure shows the electrical length mismatches towards the end of each twisted pair in the cable. The impedance profile of the heated portion of the cable is presented in figure 7.29.

As shown on the left-hand side of figure 7.28, the differential impedance increased slightly at the reference plane of each twisted pair in the cable except pair 3,6 during the intermittent heating of the portion of the cable. Moreover, an abrupt increase in the differential impedance was measured at cycle 11 as a result of the phase change from the intermittent to prolonged thermal cycling. It is

noteworthy that the observed abrupt change in the impedance during the transition period was also observed in the response of the cable's dielectric, as reported in section 9.3.1 (see figure 9.18). More also, it can be observed that impedance decreased at cycle 15 where the electrical length of the shortest pair in the cable decreased.

Furthermore, from the right-hand side of figure 7.28, the increase in the electrical length of each pair suggests an increase in the propagation delay in the arrival of the pulse signal at the end of the PL. Moreover, it is apparent that the behaviour of the cable exhibits reversible thermal push and pull effects as a result of the point-wise heating of the cable. In addition, looking at the impedance profile of the longest twisted pair (pair 3,6) in the cable, it can be noted that the impact of the thermal push and pull of the conductor insulation was minimal on the geometrical distortion of the twisted pair, which also justifies its distinctive impedance profile at the reference plane.

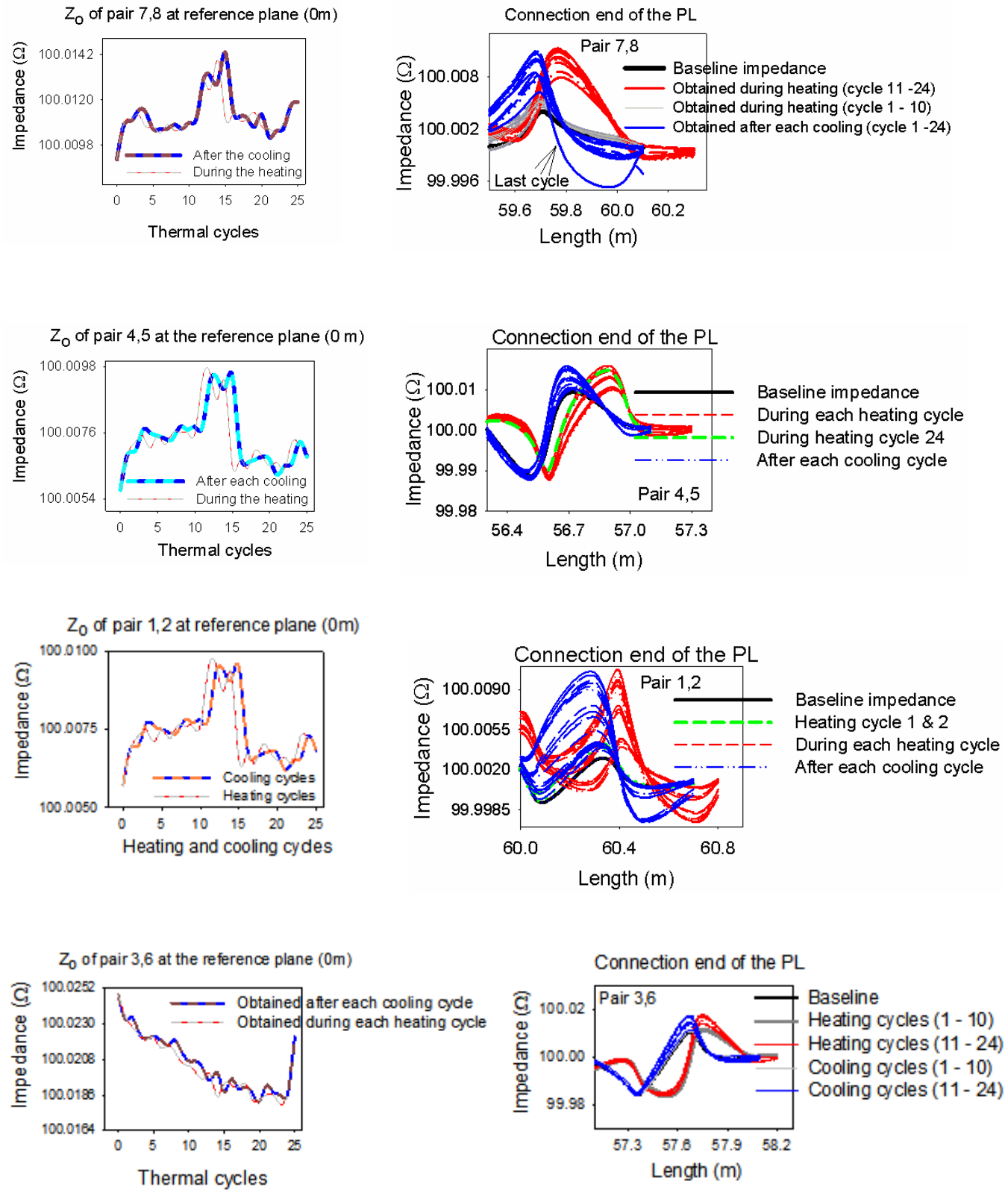

Figure 7.28: Impedance profile of Cat 6 U/UTP CMP cable at the connection ends.

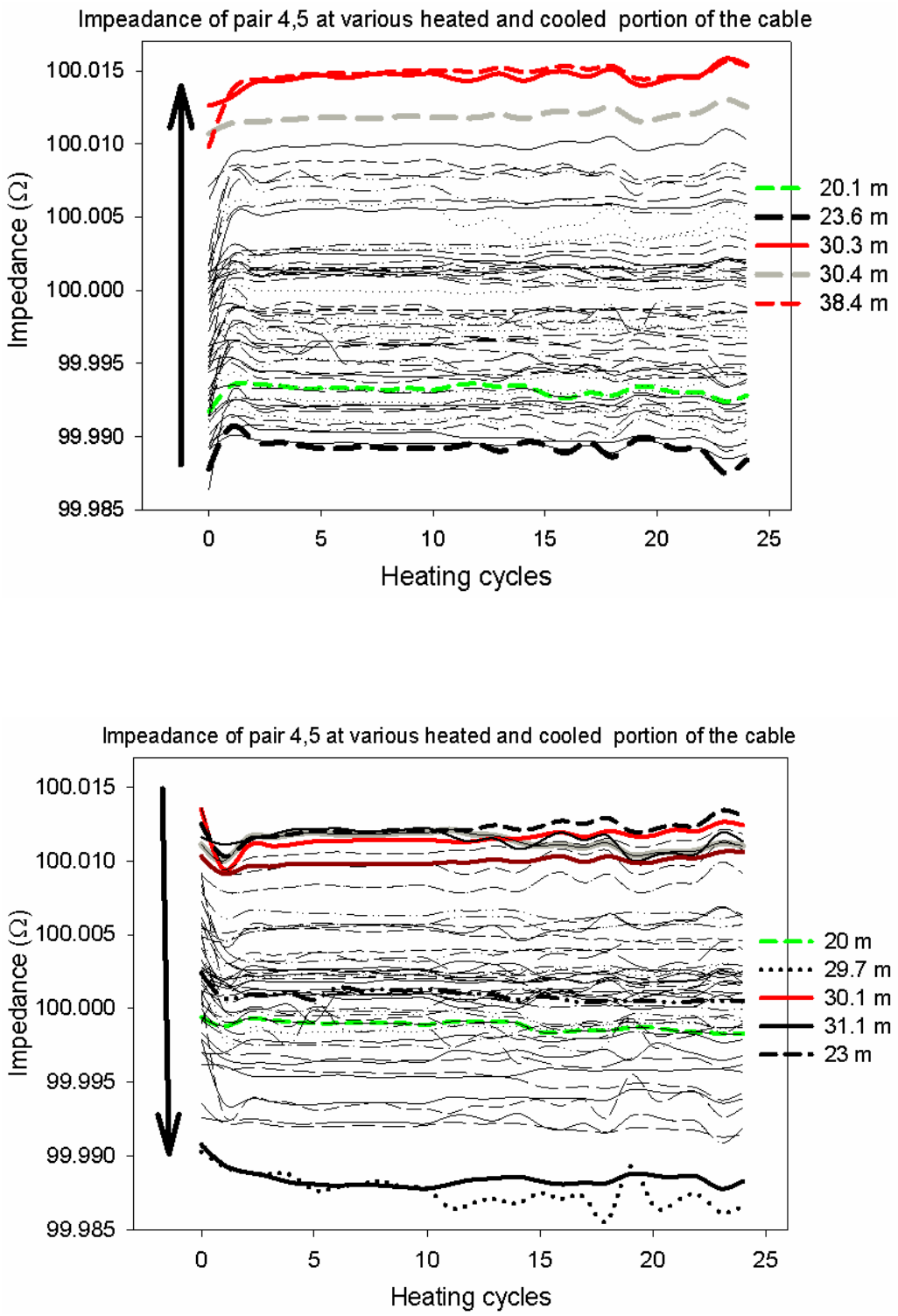

Figure 7.29: Impedance profile of the heated portion of Category 6 U/UTP CMP cable

The impedance profile of the heated portion of Category 6 U/UTP CMP cable, which was obtained during the heating cycles is shown in figure 7.29. As can be seen, the first heating of the cable brought about the overall changes in the impedance profile of the middle portion of pair 4,5. Although after the first heating of the cable, the characteristic impedance of the twisted pair

continued to vary slightly but not significantly during each cycle. Of course, the slight variations in the characteristic impedance are linked to the drift in the unit capacitance and inductance of the twisted pair. Also, the micro-variations in impedance seen along the heated portion of the pair 4,5 were observed to be small for each temperature fluctuation, but they added up due to thermal cycling.

Corresponding to the bandwidth of the cable (250 MHz), it was observed that the impedance along the unheated sides of the cable changed at every $\frac{\lambda}{2}$ (0.4 m) and $\frac{\lambda}{4}$ (0.2 m) but that of the middle portion varied significantly due to thermal cycling, which implies that the impedance of the conductors relative to ground has been altered.

Moreover, as observed in figure 7.28, the measured impedance at the mating of the RJ45 plug and jack was utterly different from the impedance profile of the thermally insulated portion of the CMP cable, which means that the impedance mismatches along the whole length of the PL will lead to the multiple reflections of the signal passing through the cable. That is, the transmitted signal will reflect back to the source at impedance discontinuities and be further re-reflected to contribute to the Insertion Loss Deviation (ILD). Consequently, the mismatches along the transmission path will contribute to the reduction in the quality of the received signal. It is appropriate to mention that the correct operation of the network depends on the constant and matched impedance throughout the cabling systems and connectors. Impedance mismatches along the channel can cause signal reflections that can lead to network faults.

Increase in the insertion loss performance of the portion insulated Cat 6 U/UTP CMP cable

The drift in the Insertion Loss (IL) performance of the portion insulated Category 6 U/UTP PL based on the effects of thermal cycling is presented in figures 7.30 and 7.31. However, the maximum increase in IL, which was calculated by subtracting the measured baseline IL from the IL measured during each cycle is presented in table 7.2.

From figure 7.30 and 7.31, it is shown that the IL performance of the PL increased progressively because of thermal cycling and thermal insulation of the middle portion of the cable.

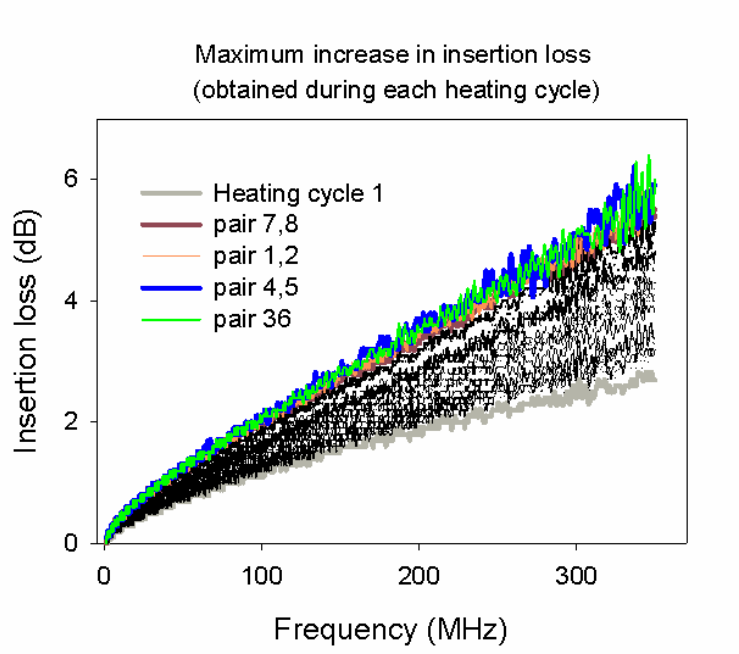

Figure 7.30: Drift in the IL performance of the Cat 6 U/UTP CMP cable during heating

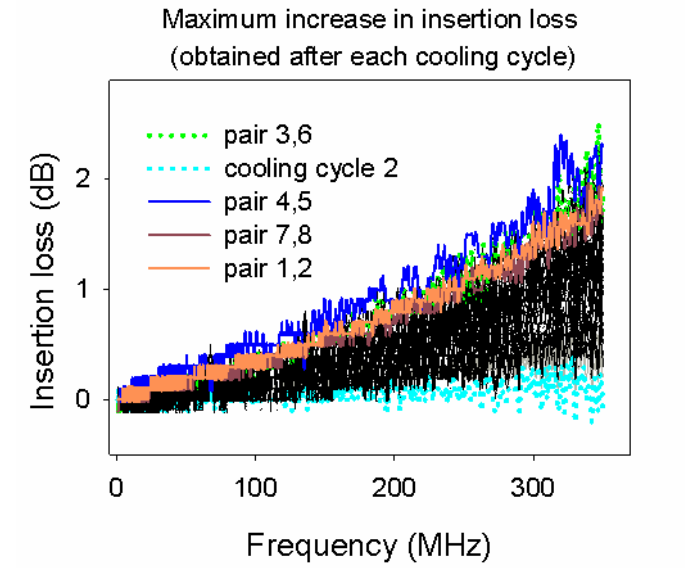

Figure 7.31: Drift in the IL performance of the Cat 6 U/UTP CMP cable during cooling

Although the results in table 7.2 show that the worst IL performance of the Category 6 U/UTP CMP PL was measured during the heating of the cable. A total increase in IL of ~ 8.2 % per degree (6.4 dB at 77.5^{o}C) was calculated due to the heat cycling of the cable and ~ 8.6 % per degree (2.5 dB at 29^{o}C) due to the cooling of the cable.

Table 7.2: Effects of thermal cycling on the IL performance of Category 6 U/UTP CMP cable

Long-term insertion loss performance of Category 6 U/UTP CMP permanent link				
	The maximum increase in insertion loss with the corresponding frequency (dB)		The maximum increase in insertion loss with the corresponding frequency (dB)	
	Heating cycles ~ 8.2 % per degree	Cycle number and Temperature (^{0}C)	**Cooling cycles ~ 8.6 % per degree**	Cycle number and Temperature (^{0}C)
Pair 3,6	**6.4** (346 MHz)	Cycle 20 (77.5^{0}C)	**2.5** (347 MHz)	Cycle 24 (29^{0}C)
Pair 4,5	6.2 (337 MHz)	Cycle 19 (77^{0}C)	2.4 (320 MHz)	Cycle 24 (29^{0}C)
Pair 1,2	5.8 (350 MHz)	Cycle 20 (77.5^{0}C)	1.9 (341 MHz)	Cycle 20 (30^{0}C)
Pair 7,8	5.8 (347 MHz)	Cycle 20 (77.5^{0}C)	1.9 (347 MHz)	Cycle 20 (30^{0}C)

The IL increase can be attributed to the combination of the increase in the *ac* and *dc* resistance of the copper conductors, mismatch loss from the changes in the ε_r of the conductor insulation, and the absorption of energy due to the increased dissipation factor of the conductor insulation. Detailed discussion on the changes in the dielectric properties of the extracted FEP sample from the cable under test is discussed in the dielectric measurement section (Section 9.3.1).

Changes in the return loss performance of the portion insulated Cat 6 U/UTP CMP cable

RL values of pair 4,5 are presented in this section for explanation purpose. Table 7.3 presents the maximum changes in the RL value of pair 4,5 at 68 and 136 MHz, which was calculated by subtracting the measured baseline RL value from the values obtained during each cycle. As can be noted in table 7.3, the RL performance of the PL changed significantly from cycle 1 up to the last thermal cycle.

Table 7.3: Effects of thermal cycling on the RL performance of Category 6 U/UTP CMP cable

Long-term return loss performance of the Category 6 U/UTP CMP permanent link									
	Daily cycles			Weekly cycles			Monthly cycles		
	Cycle number								
	1	**5**	**10**	**15**	**20**	**21**	**23**	**24**	**25**
The maximum decrease in the return loss value (dB) of pair 4,5, obtained after each **cooling** cycle (Maximum temperature 29^0C)									
RL at **68 MHz**	0.3	0.8	1	1	0.7	1	1.1	1.1	1.4
RL at **136 MHz**	1.6	3.7	4.6	**5.3**	4.4	**5.3**	4.9	4.6	4.5
Maximum changes in the return loss value (dB) of pair 4,5, obtained during the **heating** cycles (Maximum temperature 77.5^0C)									
RL at **68 MHz**	-0.6	-0.3	-0.4	-0.8	-0.9	-0.7	-0.3	-0.3	-0.6
RL at **136 MHz**	-3.1	-0.7	-0.5	-0.1	-1	-1	-0.4	-0.5	-3.1

Comparing the RL values of pair 4,5 at 68 MHz and 136 MHz, obtained during the cooling of the cable, it is apparent that the RL values decreased more at 136 MHz in comparison to the decrease in the RL at 68 MHz. In addition, the cooling of the cable caused more reflection of the transmitted pulse signal to occur when compared to the effect of temperature of ~77^0C. Note from table 7.3 that a maximum decrease of 5.3 dB in the RL value was observed during the prolonged weekly heating cycles, at cycle 15 where the electrical length of the pair 4,5 decreased. The cause of the decrease in the RL value at cycle 15 can be associated with the phase-temperature response of the conductor insulation when the electrical length decreased.

Figure 7.32 shows the RL traces of the pair 4,5 from 10 to 18 MHz. Note the resonances and the significant phase shifts in the RL signal from 12.875 MHz and above. The resonances in the RL signal explain why negative RL values (in table 7.3) were obtained during the heating cycles. More also, a distinct resonance in the RL trace obtained during the cooling cycle 2 can be noticed.

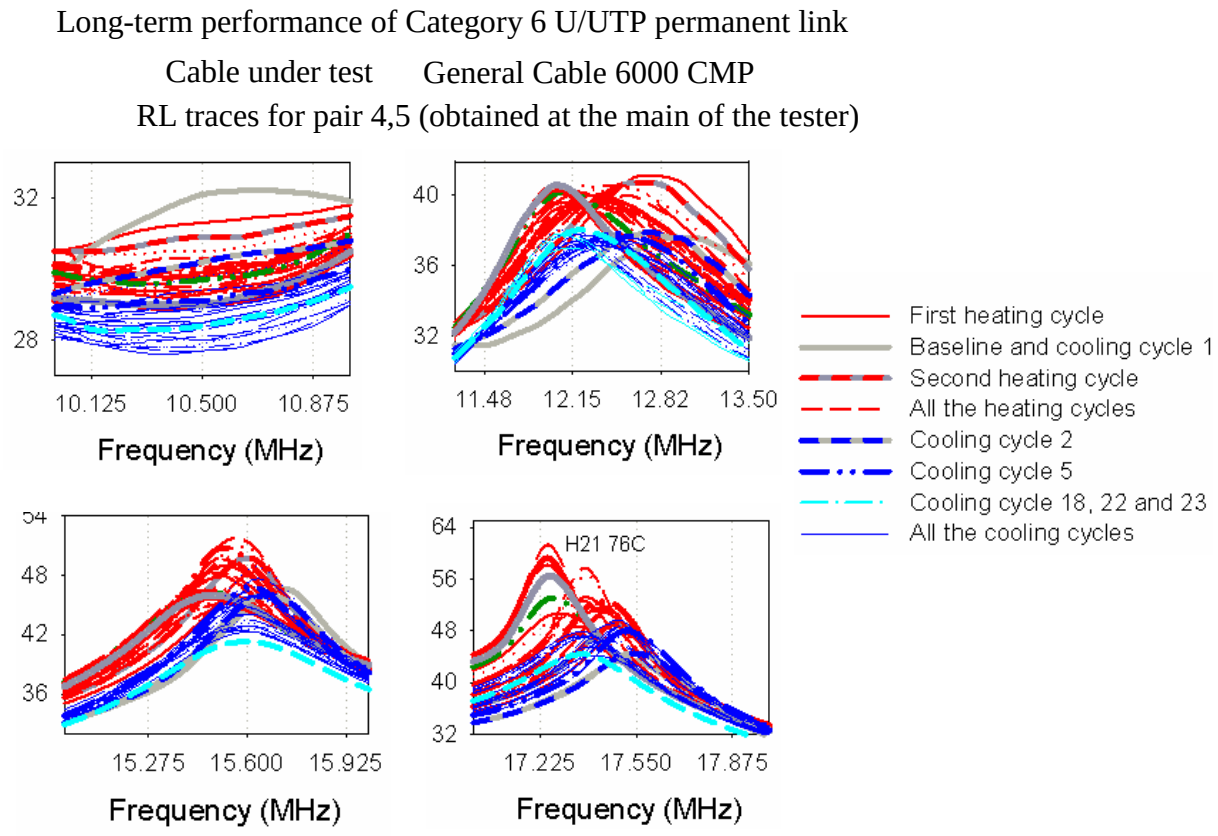

Figure 7.32: Showing the drift in the RL performance of the Category 6 U/UTP CMP cable

Table 7.4 presents the observed phase shifts at 12.875 MHz during the heating and cooling cycles. From the stated results in table 7.4, it can be observed that the phase delay in the RL signal increased during the thermal cycling period. The first heating of the cable shifted the RL signal by 63^0 because of the temperature change to 60^0C while the second heating caused a 90^0 phase delay of the RL signal. In addition, the third heating shifted the RL signal further by 315^0 while the last heating cycle (cycle 24) caused a phase shift of 315^0 of the RL signal towards the lower frequency. It can be observed that the first cooling of the cable did not cause a phase shift of the RL signal. However, the second and sixth cooling cycles caused a delay of 63^0 and 180^0 respectively. Moreover, the last cooling cycle (cycle 24) shifted the RL signal by 270^0. The delay in the RL signal can be attributed to the increase in the inductance and capacitance of the twisted pair ($\beta = \sqrt{LC}$). However, since the internal inductance does not contribute to the phase delay of a returned signal, the predominant factor for the phase difference is likely due to the changes in the capacitance as a result of the change in the ε_r of the conductor insulation. From the discussion in section 7.2.1, the decrease in the ε_r caused the electrical length to decrease by 0.2 m which also caused a proportional reduction in the propagation delay of 1 ns.

Table 7.4: Observed phase shifts in the RL signal on pair 4,5 of the Cat 6 U/UTP CMP cable

Observed phase shifts in the RL signal on pair 4,5 of the Category 6 U/UTP CMP cable			
Cycle number	Phase difference Obtained during the **heating cycle**	Cycle number	Phase difference Obtained after each **cooling cycle**
1	63^0	1	-
2	90^0	2	63^0
3	135^0	6	180^0
24	315^0	24	270^0

It can be noted from table 7.4 that the measured 315° time delay obtained for the entire thermal cycling conducted is almost an entire phase length of 360°. It is to be noted that the delay of one such wavelength can lead to an error on the network. This is because, in 1000BASE-T, the amount of time required to transmit a bit is 1ns, but the actual speed at which the bits are transmitted is subject to the velocity factor of the conductor insulation. Note that one bit is among the numerous bits embedded inside an Ethernet frame. For a frame to be received successfully, the frame check sequence (FCS) is recalculated by the destination node and compared with the FCS number transmitted with the frame. If the two numbers are different, the frame is discarded, and the upper layer protocol such as the Transmission Control Protocol initiates the retransmission and error recovery of the data packets. It is appropriate to mention that the retransmission of data packets will introduce additional network latency.

The observed return loss echoes during the initial RL failure at cycle 5, and at cycle 16 when the electrical length decreased are indicated with the red arrows in figure 7.33. As can be seen on the right-hand side of figure 7.33, the obtained RL traces for the cooling cycle 5 and 16 lagged behind the baseline RL trace at 84.5 MHz by 90^0 because of the timing difference. The cause of the delay will be due to the changes in the dielectric constant of the conductor insulation and capacitive loading.

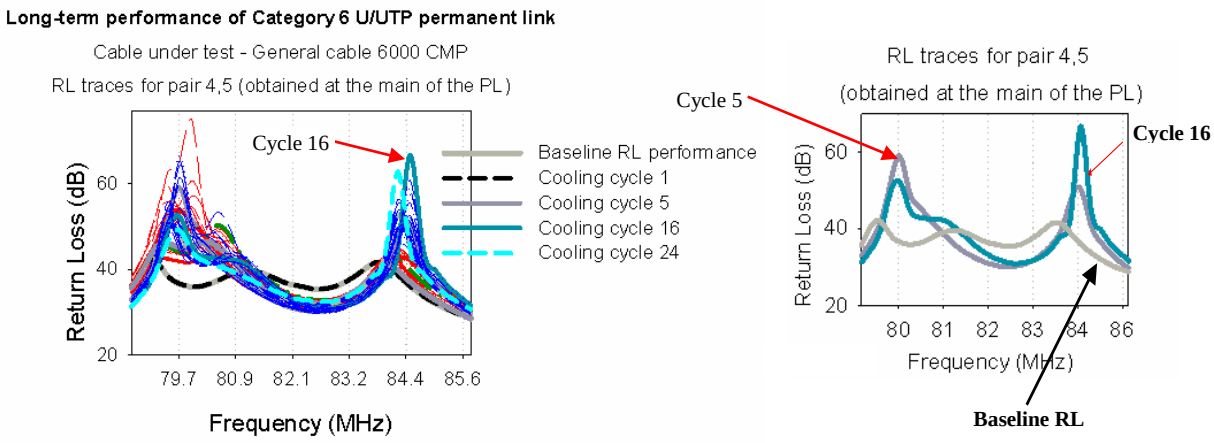

Figure 7.33: Showing the RL echoes in the performance of the Cat 6 U/UTP CMP cable

Changes in the crosstalk performance of the portion insulated Cat 6 U/UTP CMP cable

The NEXT marginal values for the Cat 6 U/UTP CMP PL are presented in figure 7.34. A relatively steep phase change between the baseline NEXT performance and the performance measured at cycle 10 is clearly visible. Moreover, from cycle 10, it appears that the chemical reaction was over. Interestingly, the NEXT performance improved from ~4 dB back to its baseline value of 4.8 dB and remained almost flat with thermal cycling. Moreover, comparing the NEXT performance due to the heating and cooling of the cable, it can be observed that crosstalk performance improved slightly with heating due to the decrease in the ε_r of the conductor insulation with temperature and the increased separation distance between the twisted pairs. Of course, the obtained worst noise coupling between the twisted pairs during the cooling of the cable can be seen in the light of an increased flux linkage, which increased the capacitive coupling between the twisted pairs as they cool down and contract.

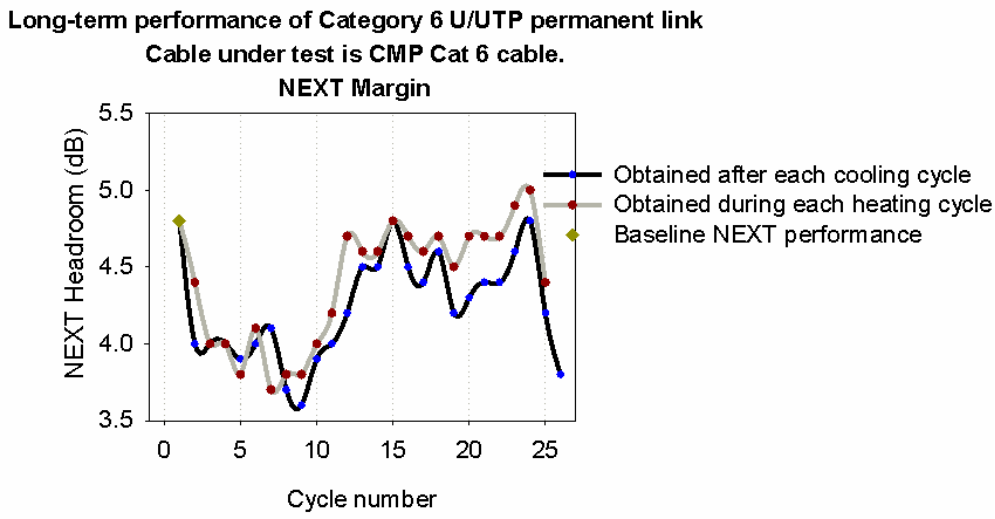

Figure 7.34: NEXT headroom of the portion insulated Cat 6 U/UTP CMP cable

Figure 7.35 to 7.37 are the HDTDX plots for the crosstalk performance between pair 1,2 and 4,5. Figure 7.35 shows the baseline crosstalk performance of the Category 6 U/UTP and the measured crosstalk performance during cooling cycle 15. As can be observed in figure 7.35, the crosstalk, which was not initially present in the RJ45 connector developed at the reference plane (0 m) after the electrical length of pair 4,5 had decreased, this shows that the heating and cooling of the cable influences the structure of the twisted pair.

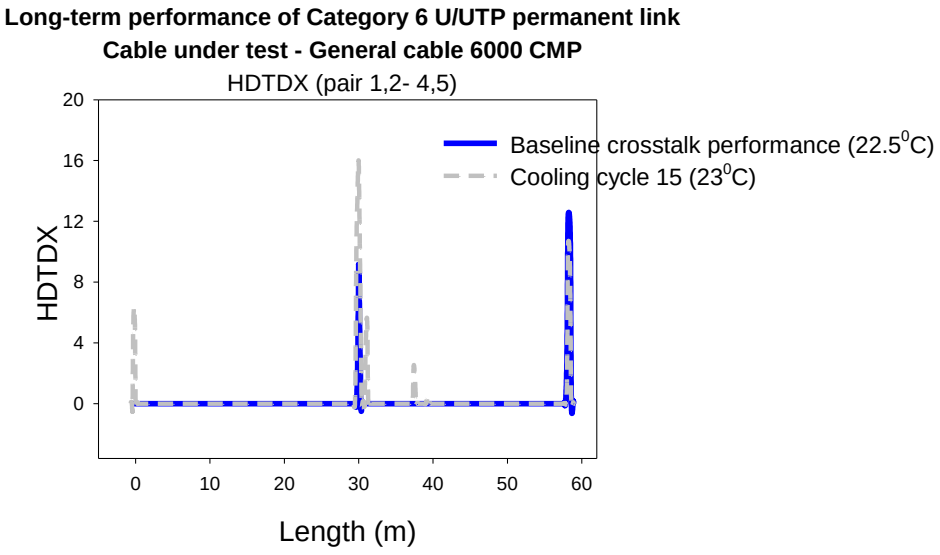

Figure 7.35: Effects of electrical length variations on the noise immunity of Cat 6 CMP cable

From figure 7.36, the crosstalk between pair 1,2 and 4,5 increased rapidly from the point where the electrical length decreased. It should be remembered that the change in the characteristic impedance of pair 4,5 as a result of the change in the electrical length was discussed at the beginning of this section (see figure 7.28). Also, the RL echo generated after the electrical length of the pair 4,5 had decreased was indicated in the RL plot in figure 7.33. From these two observations, it can be argued that the cause of the crosstalk seen at 0 m is attributable to the reflections from the end of the line which manifested as noise signals at 0 m. Of course, this shows that variations in the electrical length have a significant impact on the noise immunity of a cabling system.

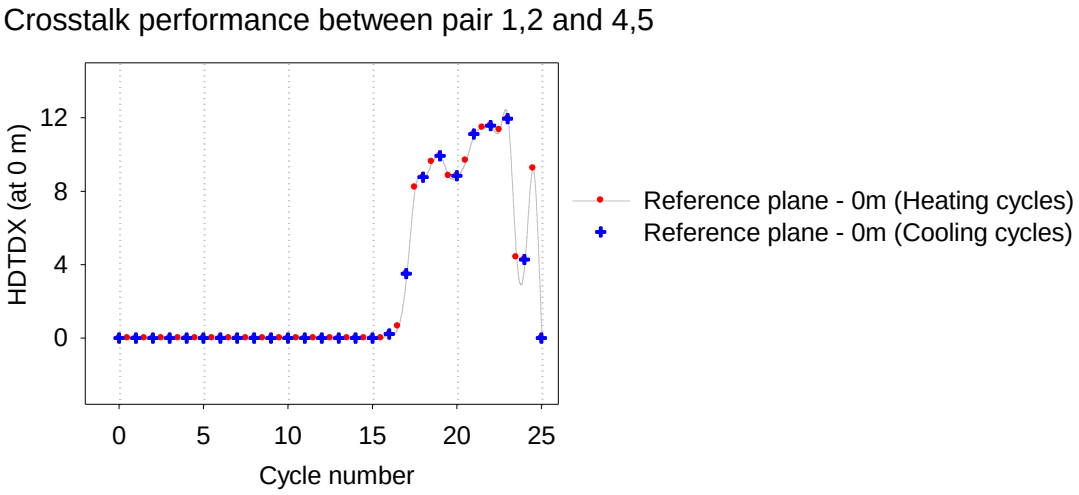

Figure 7.36: Effect of the changes in the electrical length on crosstalk performance

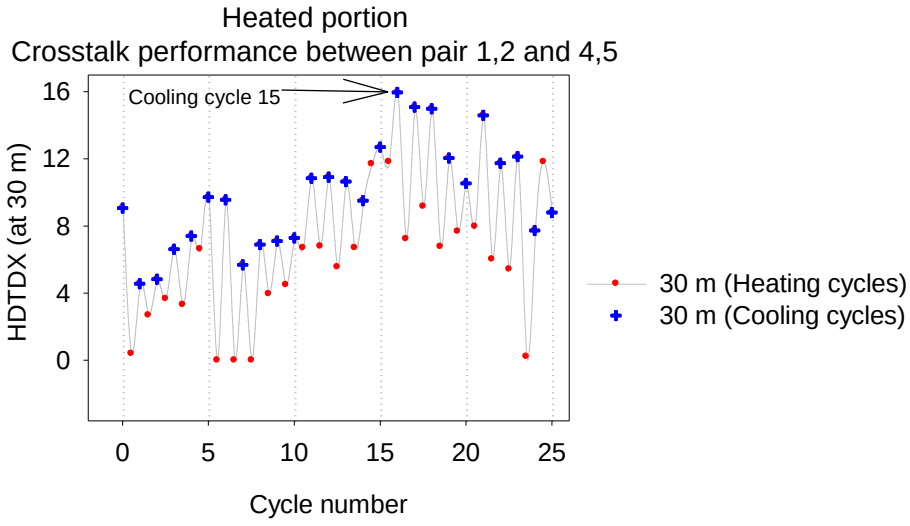

Figure 7.37: Crosstalk performance of the Cat 6 U/UTP CMP cable at the portion insulated

The observed crosstalk performance at the 30 m location of the PL is shown in figure 7.37. As can be seen, the crosstalk between pair 1,2 and 4,5 decreased initially during the first heating of the cable due to the effect of temperature, and then increased progressively with thermal cycling until cycle 15 before decreasing again. The decrease in the crosstalk performance of the cable during the first heating of the cable has been observed in the NEXT performance of the standard Cat6 U/UTP shown in figure 7.11. Moreover, the performance of the two unshielded twisted pair cables (figure 7.11 and 7.37) shows that noise coupling between twisted pairs is more pronounced due to cooling of the cable than heating presumably because of the proximity of the twisted pairs when the cable cools down.

Changes in the TCL performance of the portion insulated Cat 6 U/UTP CMP cable

Figure 7.38 shows the TCL traces obtained for the pair 4,5 from 12 MHz to 18 MHz, while figure 7.39 presents the actual values of the TCL parameter at 16.625 MHz for the 24 thermal cycles conducted. As discussed in chapter 2, the TCL parameter is an important parameter for evaluating the performance of the PLs. Higher values of the TCL indicate better performance of the PL. Given these, it can be seen in figure 7.38 that the performance of the cable drifted. In addition, the drift quantifies the imbalance in the conductors of pair 4,5 with respect to ground.

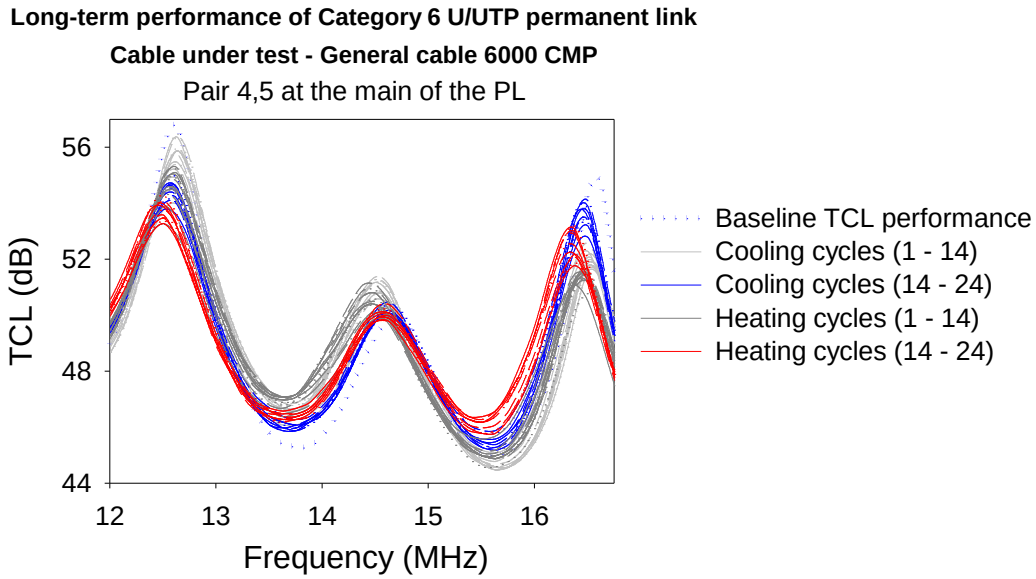

Figure 7.38: Drift in the TCL performance of pair 4,5 of the Cat 6 U/UTP CMP cable

The results in figure 7.39 show that the performance of the Category 6 U/UTP CMP cable was significantly affected during the first thermal cycle. The significance of this is that the impact of an induced noise voltage on the signal passing through the twisted pair will be more pronounced during the first thermal cycling of the cable when the cable is installed in a noisy environment like an industrial and wireless network environment.

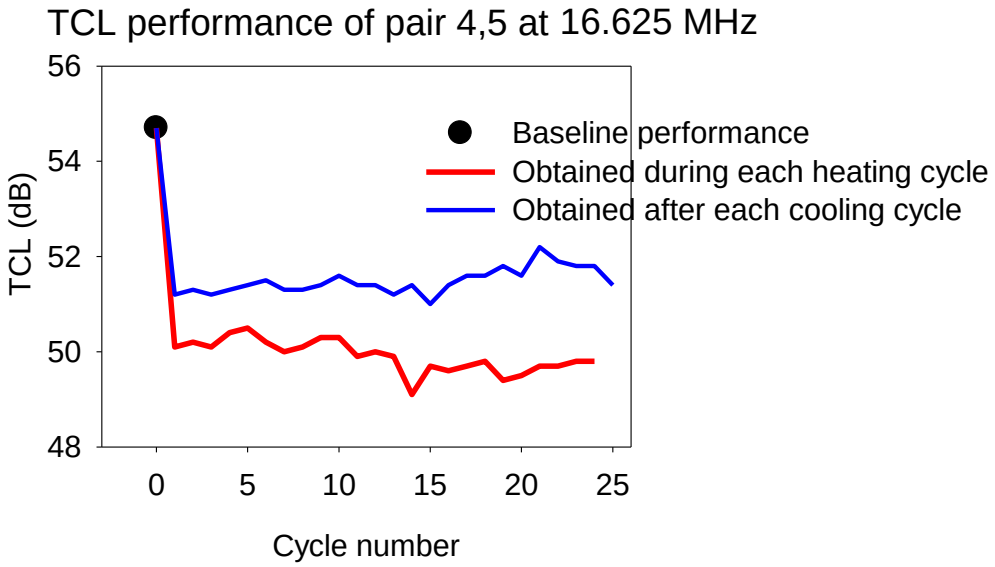

Figure 7.39: TCL values for Pair 1,2 at 16.625 MHz

Furthermore, the equivalent differential mode noise voltages for the TCL values are plotted in figure 7.40. The differential mode noise voltage was calculated based on the assumption of an induced common mode noise of 1 V. As can be seen in figure 7.40, the most substantial noise coupling was at cycle 15 where a voltage spike is indicated. The spike can be attributed to the delay skew observed at this point which converted part of the original differential signal into a common mode signal.

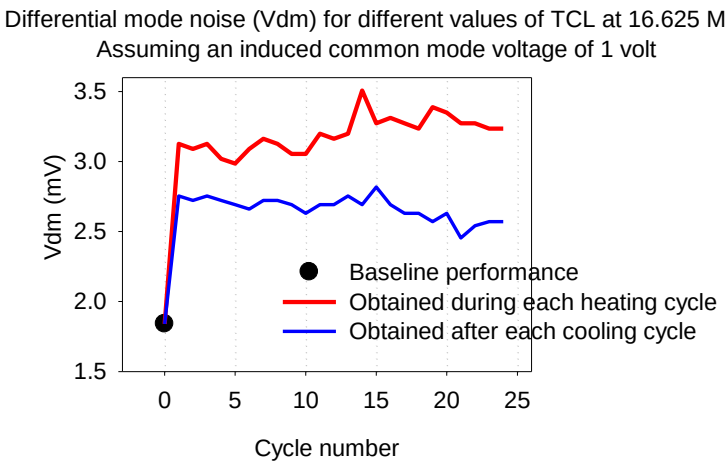

Figure 7.40: Differential mode noise voltage for different values of TCL of pair 4,5

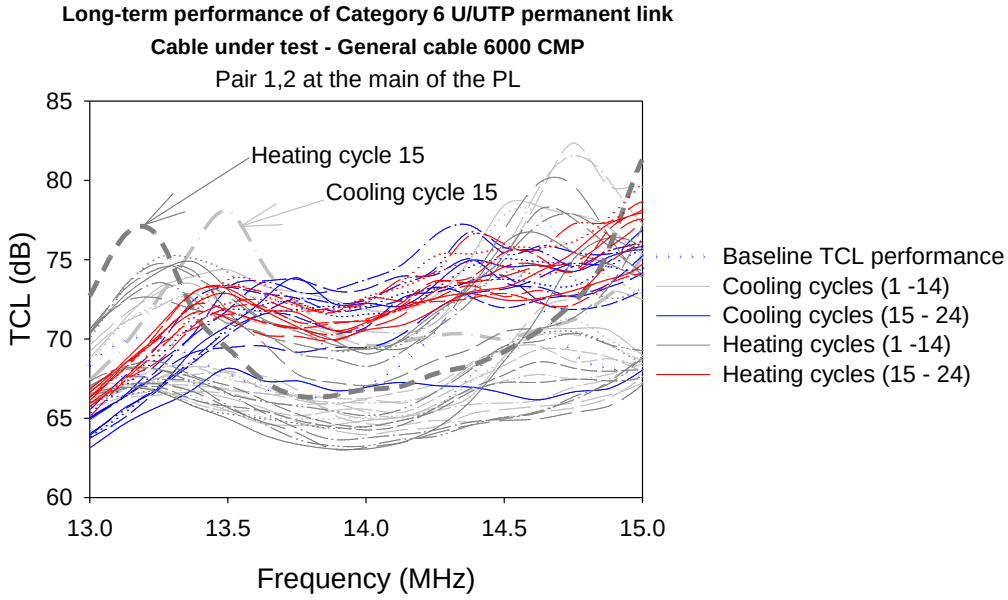

Figure 7.41: Drift in the TCL performance of pair 1,2 of Cat 6 U/UTP CMP cable

Figure 7.41 shows the TCL traces obtained for the longest pair (pair 1,2) in the cable, whereas figure 7.42 presents the values of the TCL performance at 14.5 MHz for the 24 thermal cycles conducted. Twisted pair 1,2 generated spurious resonances, because of the changes in the structure of the cable based on the effects of thermal cycling. Moreover, as indicated in figure 7.41, the resonances at the point (cycle 15) where the electrical length decreased were distinct. Also, it was found that the TCL values (figure 7.42) of pair 1,2 decreased during the first thermal cycle (cycle 1) and at the transition between the intermittent daily cycling and weekly thermal cycling (cycle 11).

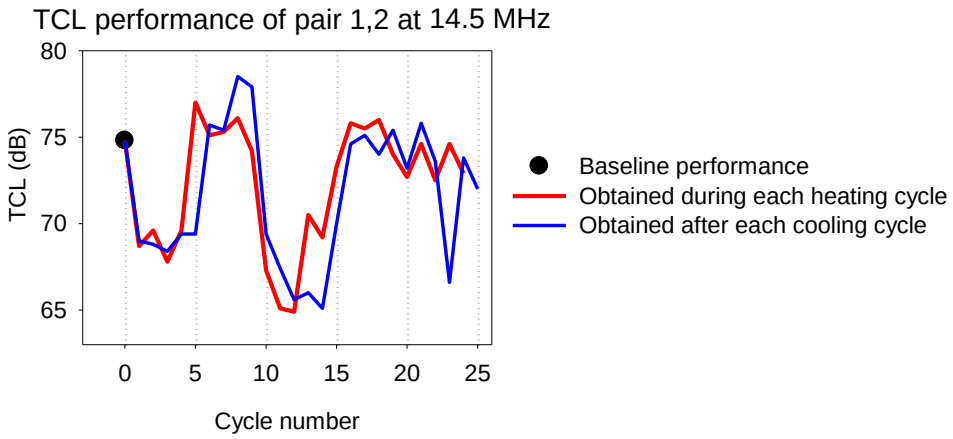

Figure 7.42: TCL values for pair 1,2 of the Cat 6 U/UTP CMP cable at 14.5 MHz

Changes in the ELTCTL performance of the portion insulated Cat 6 U/UTP CMP cable

The TCL and ELTCTL are both used for evaluating the performance of the PLs. The TCL evaluates the mode conversion at the near end, while ELTCTL evaluates the mode conversion at the far end of a channel or PL.

Figure 7.43 is a plot for the ELTCTL performance of all the twisted pairs in the Cat 6 U/UTP CMP cable. As can be observed, the performance of the cable was affected during the first heating and cooling of the cable, but the worst performance was measured during the prolonged thermal cycling after the permanent failure of the link occurred. Also, it is apparent in figure 7.43 that pair 4,5 and 7,8 exhibited similar resonances when compared to pair 3,6 and 1,2. That is, pair 4,5 and 7,8 generated resonances at the critical points: at cycle 5, where the first RL failure occurred, at cycle 11 which is the transition between the daily cycling and the weekly cycling and lastly, at cycle 15 where the electrical length decreased. The reason for the similar behaviour of pair 4,5 and 7,8 is not fully explained but it should be noted that the two twisted pairs have a similar lay length to each other which are quite different from that of pair 3,6 and 1,2. It is also noteworthy that pair 4,5 and 7,8 exhibited similar differential impedance characteristics, as shown in figure 7.28.

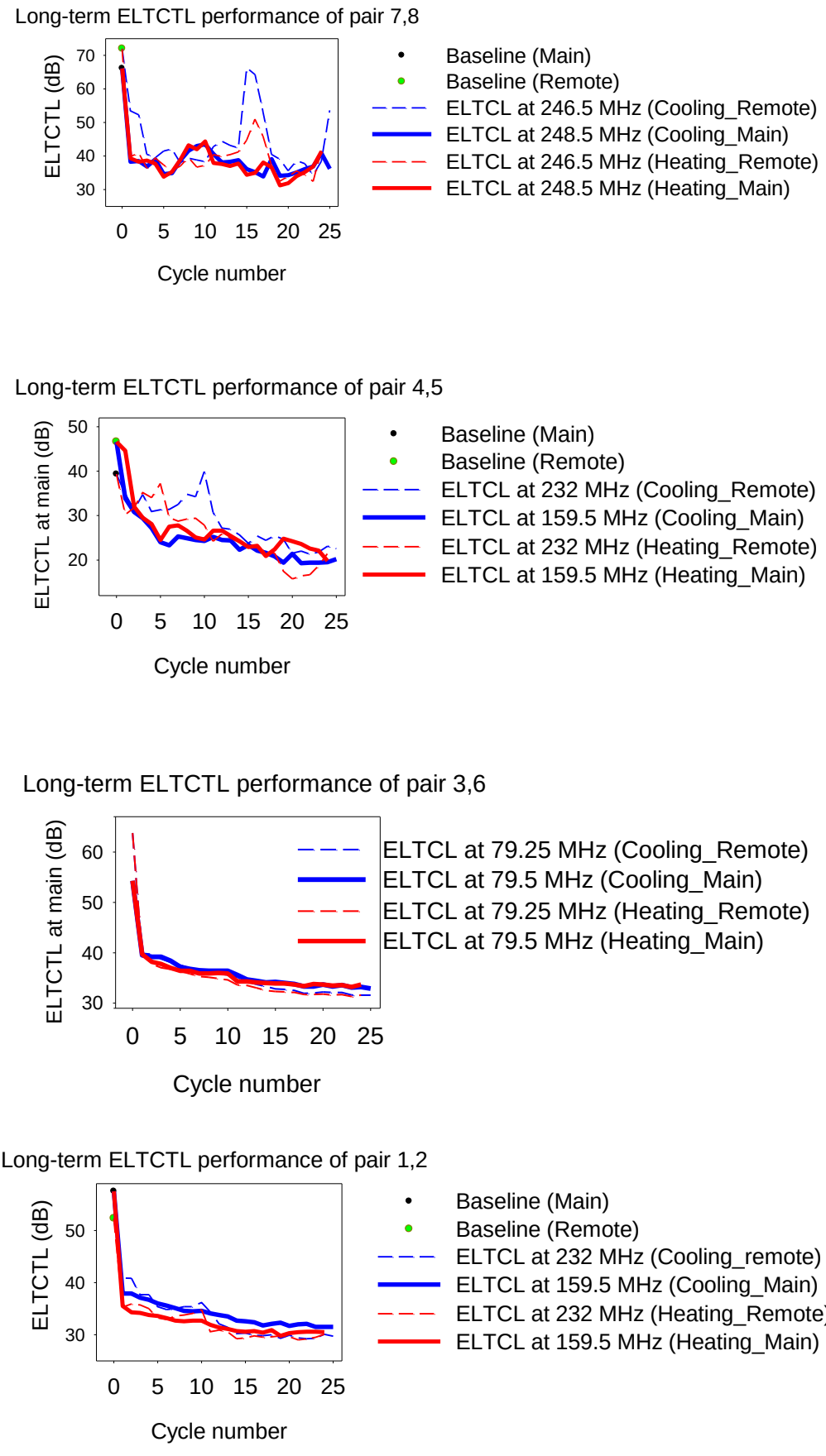

Figure 7.43: ELTCTL performance of all the twisted pairs in the Cat 6 U/UTP CMP cable.

Changes in the CDNEXT performance of the portion insulated Cat 6 U/UTP CMP cable

Figure 7.44 and 7.45 present the traces obtained for the Common Mode Near End Crosstalk (CDNEXT) performance between pair 1,2 and 4,5 at the main and remote of the PL. As can be seen in the figures, the performance of the PL drifted from the first heating of the cable. Also, the CDNEXT performance at the main side of the PL (figure 7.44) shows some distinctive resonances from cycle 13 to cycle 15, where the decrease in the electrical length of the cable was observed.

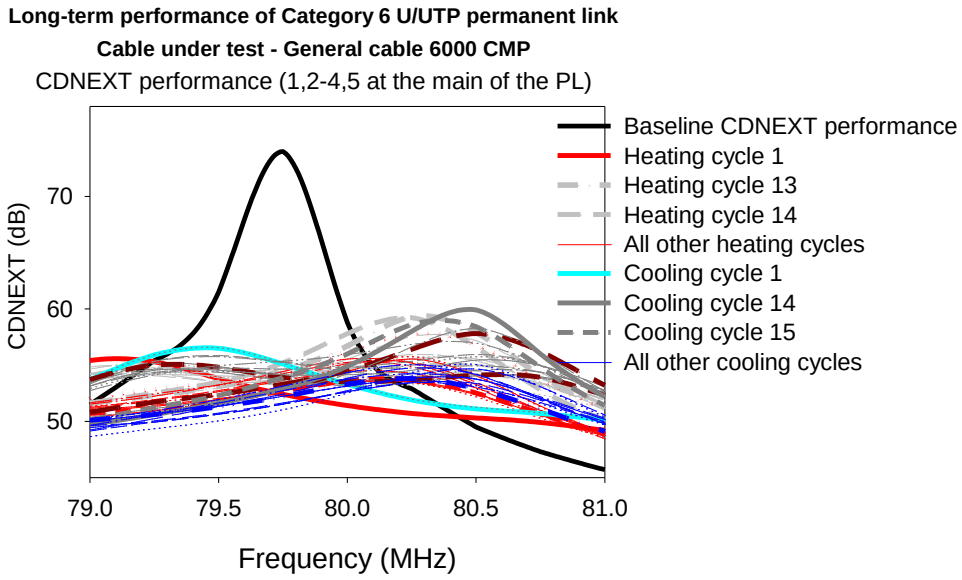

Figure 7.44: CDNEXT performance of Cat 6 U/UTP CMP cable (main of the PL)

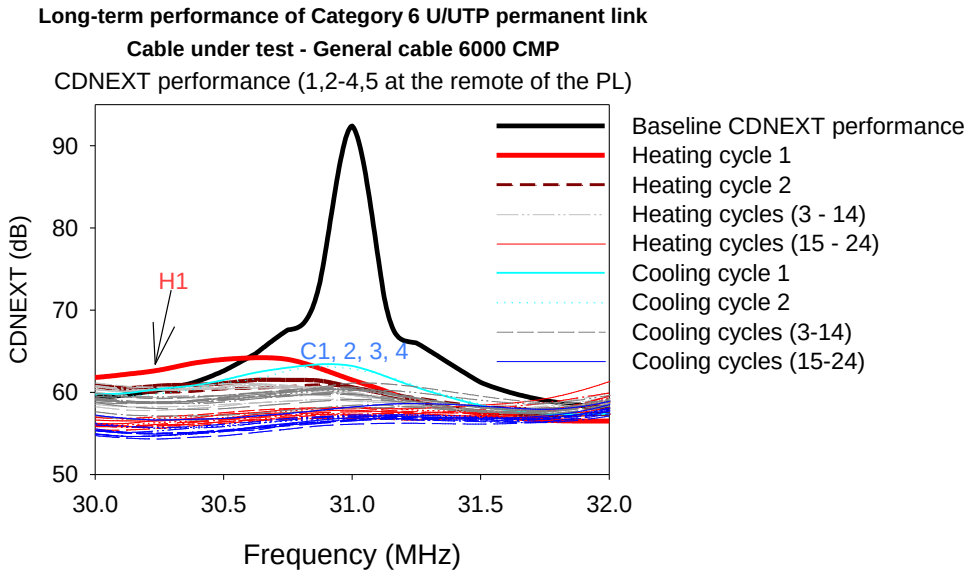

Figure 7.45: CDNEXT performance of Cat 6 U/UTP CMP cable (remote of the PL)

The obtained CDNEXT performance at 31 MHz is shown in figure 7.46. It was observed that the first thermal cycling of the cable caused the CDNEXT performance of the PL to decrease by 30.9 dB while the subsequent heating cycles, up to the last heating cycle caused an extra decrease of 4.2 dB. Note that the reduction in the CDNEXT value corresponds to degradation in the noise immunity of the cabling system. As discussed in the literature review, the main source of mode conversion for balanced twisted pair cabling is the mated point of the 8-pin RJ45 modular plug and jack. Also, common-mode signal readily converts to differential mode signal at the termination point of the cabling system. Given this, the cause of the signal loss through mode conversion can be attributed to the untwisting of the twisted pairs at the termination point during the thermal cycling test. The untwisting of the twisted pairs unequally implies that the noise coupling to the conductors will be unequal because of lack of symmetry. Consequently, part of the original differential stimulus signal injected on a twisted pair will be converted to a common mode signal on another pair.

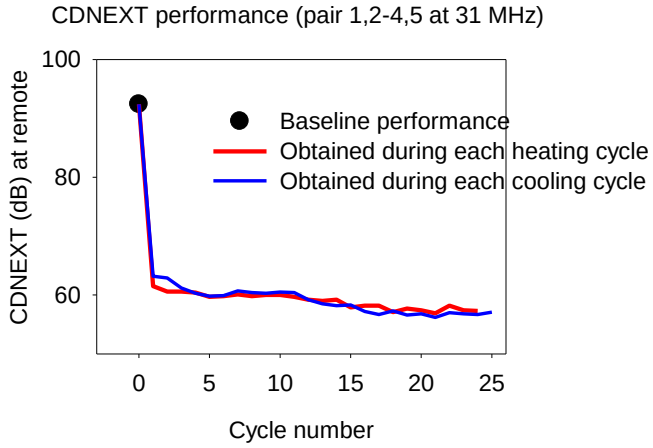

Figure 7.46: CDNEXT performance between pair 1,2 and 4,5 of the Cat 6 U/UTP CMP cable

Changes in the ACR-N performance of the portion insulated Cat 6 U/UTP CMP cable

The ACR-N marginal values for the portion insulated Cat 6 U/UTP CMP PL is presented in figure 7.47. It can be observed that the quality of the cable degraded from the first heating and cooling of the cable. Also, a decrease of 3.1dB in the ACR-N value of the PL was measured during the first thermal cycle. However, the subsequent heating and cooling cycles up to the last thermal cycle caused a further decrease of 0.7 dB to the ACR-N value of the PL.

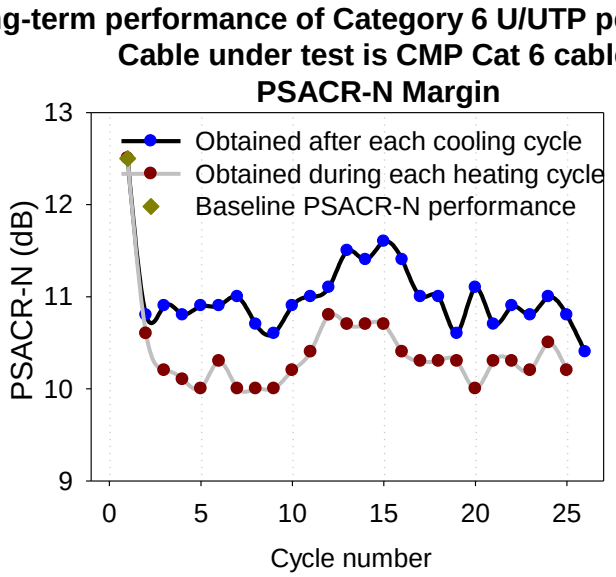

Figure 7.47: ACR-N headroom of the portion insulated Cat 6 U/UTP CMP cable

Summary of results

It was observed that the baseline RL performance of the Cat 6 U/UTP CMP PL was a marginal pass with a marginal value of 0.8 dB at 22.5^0C. However, it was observed in most of the graphs that the first heating and cooling of the cable caused an accentuated decrease in the performance of the cable. Furthermore, after heating and cooling the middle portion of the cable repeatedly for five times, the RL performance of the cable failed for the first time at 20^0C. The initial partial recovery of the cable from the failure was observed at temperatures close to the room temperature. However, results show that the subsequent failure and recovery temperatures accelerated towards higher temperature after the electrical length of the cable had decreased. Moreover, it was observed that the RL marginal values and the cyclic behaviour of its corresponding failure temperatures drifted towards the higher temperature, which portends a degradation in the performance of the PL.

Furthermore, the reduction in the electrical length of the cable was observed to be 0.2 m during the prolonged thermal cycling. The extracted effective ε_r of the conductor insulation also confirmed that the velocity factor of the conductor insulation had decreased. Moreover, the 0.2 m decrease in the electrical length of the cable also caused a proportional decrease of 1 ns in the propagation delay of the cable. In addition, because the propagation delay had decreased, delay skew also increased.

The impedance profile obtained from the HDTDR data of the Category 6 U/UTP CMP PL revealed some electrical length mismatches towards the end of each line and impedance variations

at the reference plane of each of the lines. It was found that the twisted pairs with a similar lay length exhibited similar differential impedance characteristics and ELTCTL performance. Furthermore, the impedance along the unheated sides of the cable reverted at every $\frac{\lambda}{2}$ (0.4 m) and $\frac{\lambda}{4}$ (0.2 m) but the impedance profile of the middle portion of the cable varied significantly, which indicates that the impedance of the conductors relative to ground has been altered due to the thermal cycling of the cable. Moreover, the observed impedance at the mating of the RJ45 plug and jack and that of the thermally insulated portion of the cable show impedance mismatches, which of course caused multiple reflections of the signal on the PL and contributed to the increased insertion loss of the PL. An increase in insertion loss of ~8.6 % per degree was observed while return loss decreased by ~6.8 % per degree for the 24 thermal cycles conducted.

The mismatches in the electrical length of the twisted pair, which caused a delay in the arrival of the pulse signal at the end of the link also caused the phase shifts of the RL signal. Results show that the RL signal drifted during heating from 63^0 to 90^0, from 90^0 to 135^0 and from 135^0 to 315^0 respectively.

NEXT resonance was observed at the point where the electrical length decreased. RL echo was also observed after the electrical length decreased. Crosstalk performance at the heated portion of the cable decreased initially during the first heating of the cable but increased progressively afterwards until cycle 15 before decreasing again. In addition, the crosstalk which was not initially present at the reference plane of the cable, near the RJ45 connector was observed to increase rapidly from the point where the electrical length decreased.

Furthermore, the TCL and ELTCTL of the PL revealed some imbalances in the structure of the twisted pairs. Also, the equivalent differential mode noise voltages for the TCL values of the cable revealed a voltage spike where the electrical length decreased. In addition, the ELTCTL showed a "ghost-like" resonances at the critical points: at cycle 5 where the first RL failure occurred, at cycle 11 which is the transition between the daily cycling and the weekly cycling and at cycle 15 where the electrical length of the cable decreased. Furthermore, the CDNEXT at the main side of the PL showed some distinctive resonances from cycle 13 to cycle 15 where the electrical length of the cable decreased. In addition, it was found that the first heating of the cable caused the CDNEXT value to decrease by 30.9 dB while the subsequent heating cycles up to the last heating cycle caused just a decrease of 4.2 dB in the CDNEXT value of the PL.

The ACR-N, which is an important parameter for evaluating the Signal-to-Noise Ratio (SNR) of a cabling system was significantly affected during the first heating and cooling of the cable. Also, it was observed that the ACR-N value decreased by 3.1 dB during the first heating of the cable while the subsequent heating cycles caused the ACR-N value of the cable to decrease by 0.7 dB.

7.3 Effects of thermal variation on the performance of portion insulated Cat 6A F/UTP

The immediate and long-term effects of repeated non-electrical heating on the performance of the portion insulated Cat 6A F/UTP PL are presented in this section. Section 7.3.1 presents the effects of thermal variation on the electrical properties of the cable, while section 7.3.2 presents the effects of thermal variation on the transmission parameters of the cable.

7.3.1 Effects of thermal variation on the electrical properties of insulated Cat 6A

The extracted ε_r of the conductor insulation of pair 1,2 in the Category 6A F/UTP cable is presented in figure 7.48 whereas the changes in the electrical length of pair 1,2 are presented in figure 7.49. The first and second thermal cycles caused the effective ε_r of the conductor insulation of pair 1,2 to decrease at room temperature (figure 7.48). Furthermore, figure 7.49 shows that the electrical length of pair 1,2 decreased by 0.2 m during the first and second cooling cycles. It can be noted that the effective ε_r and the electrical length of pair 1,2 decreased permanently due to cooling during a phase change (cycle 21) between the intermittent thermal cycling and prolonged thermal cycling. However, while the effective ε_r and electrical length of pair 1,2 decreased permanently due to cooling during the transition period, results show that the ε_r and the electrical length of pair 1,2 increased briefly, back to the baseline values during the heating cycle 39 before decreasing back again. It should be noted that the values of ε_r are extracted from the tester and indicate small changes in the capacitance. However, previously discussed PL performance suggests that the real changes are much higher than this and direct representation of the dielectric constant is needed. This is presented in chapter 9.

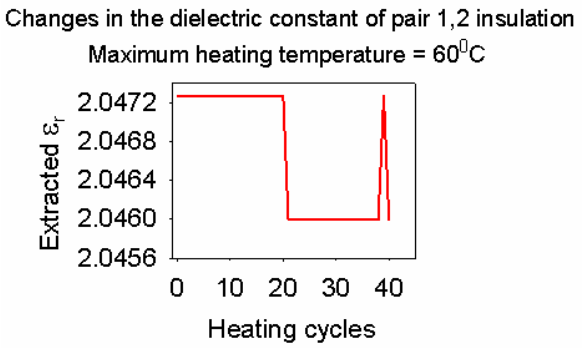

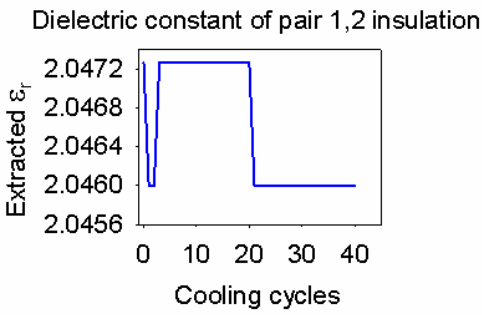

Figure 7.48: Changes in the effective $\boldsymbol{\varepsilon_r}$ of the Category 6A F/UTP conductor insulation

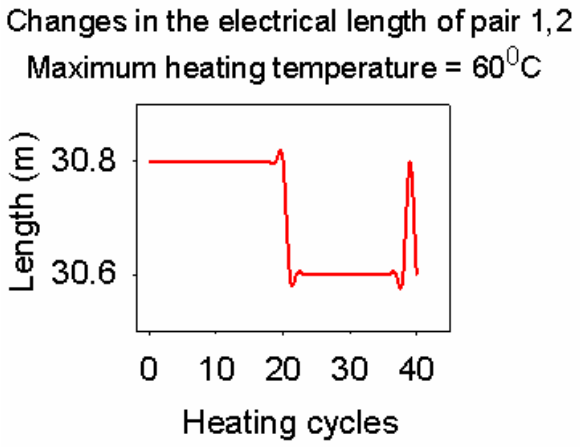

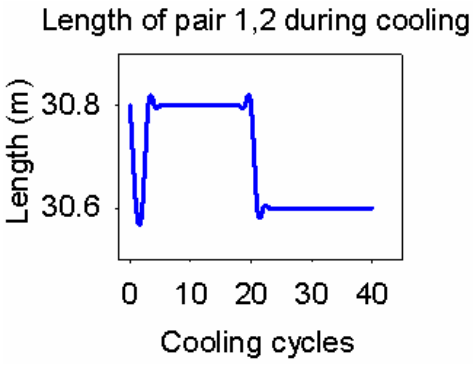

Figure 7.49: Changes in the electrical length of the Category 6A F/UTP cable

Figure 7.50 shows that the speed of the pulse signal on pair 1,2 changed due to the changes in the effective medium of the signal propagation.

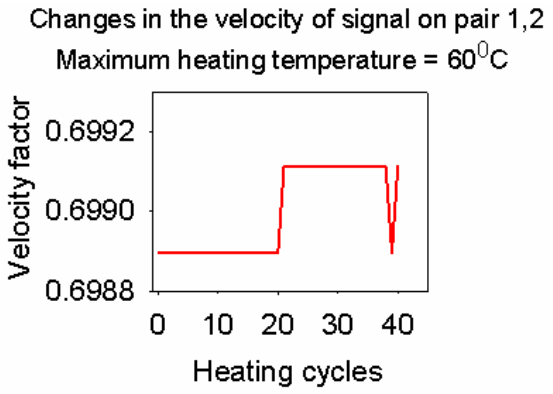

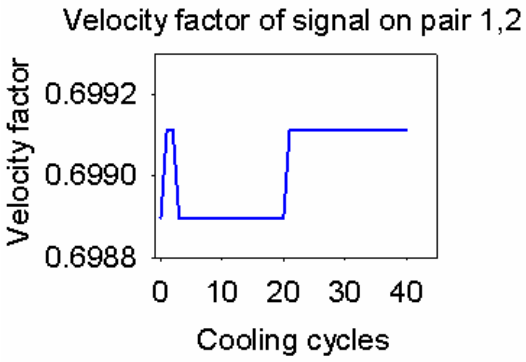

Figure 7.50: Changes in the VF of the Category 6A F/UTP conductor insulation

Also, the time taken for the pulse signal to travel and reflect from the source of the impedance mismatch during each thermal cycle is presented in figure 7.51. The propagation delay decreased by 1 ns at the thermal cycles while the electrical length of the cable decreased by 0.2 m.

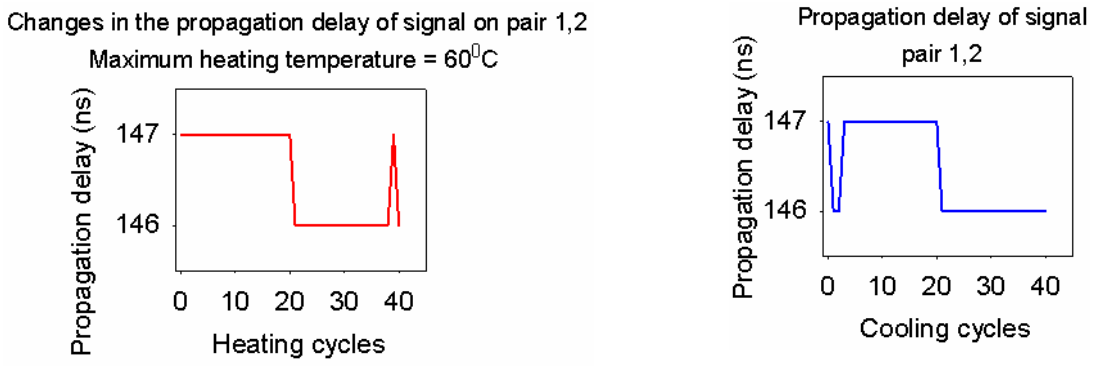

Figure 7.51: Changes in the propagation delay of Category 6A F/UTP cable

Lastly, signal skew was observed on the Category 6A F/UTP cable due to the difference in the propagation delay of the signal on the longest and shortest twisted pair in the cable (figure 7.52).

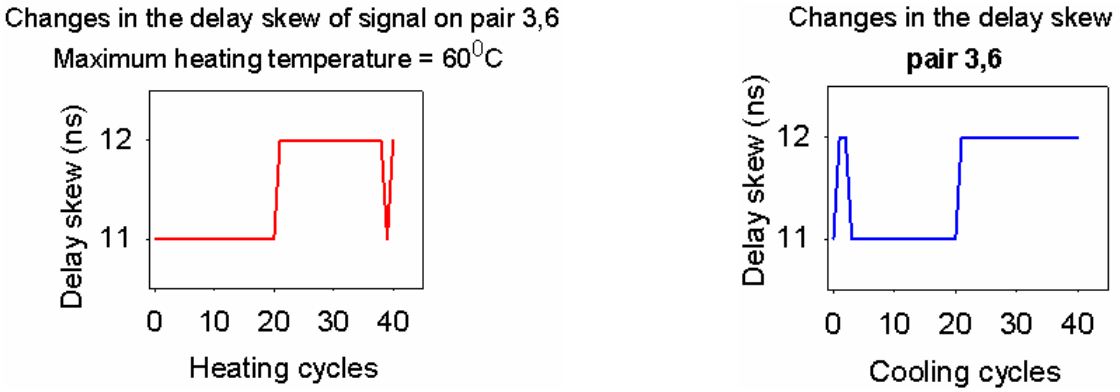

Figure 7.52: Changes in the signal skew on Category 6A F/UTP cable

As mentioned previously, these small (extracted) changes in the ε_r do not necessarily explain the already observed changes in the PL performance. Direct measurement of ε_r is needed to understand the changes in the secondary parameters of the cable, and this is shown in chapter 9.

It is also worth mentioning that the values of the extracted ε_r shown in figure 7.48 are effective ε_r; therefore, because of the existence of air gaps around the twisted pair, the values of the effective ε_r

will be slightly lower than the actual ε_r of the conductor insulation. Moreover, the reduction in the overall diameter of the copper conductor over its insulation due to thermal cycling, (see figure 7.74) implies that the ε_r will increase. Consequently, the per unit capacitance of the twisted pair will increase also and the characteristic impedance (Z_o) of the twisted pair will decrease. The next section presents the effects of thermal variation on the transmission parameters of the portion insulated Category 6A F/UTP cable.

7.3.2 Effects of thermal variation on the transmission performance of Cat 6A F/UTP

Changes in the impedance profile of the longest and shortest pairs in the Category 6A F/UTP cable

Figure 7.53 shows the baseline HDTDR plot of all the twisted pairs in the Category 6A F/UTP cable. Note the impedance discontinuity on the pair 1,2 at ~19.5 m location along the length of the cable, which could be due to a kink, bent or damage from the manufacturing process. Although the amplitude of the impedance discontinuity at 19.5 m exceeded the limit of 0.8 m, the baseline results (see figure 5.15) show that the cable met the specification of both the TIA and ISO test limits and that there was no electrical length reduction before the heating of cable began.

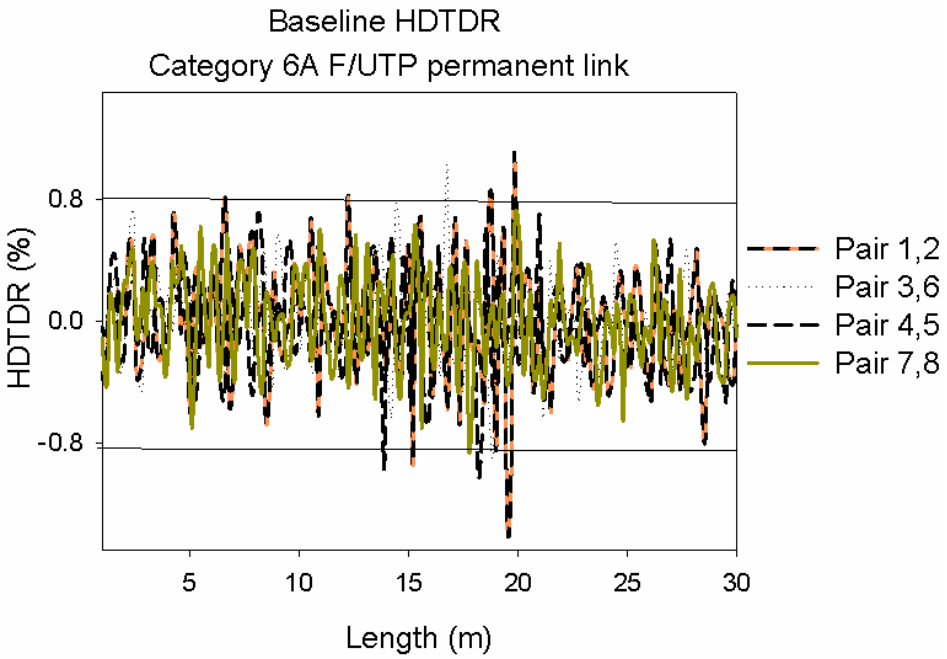

Figure 7.53: Baseline HDTDR plot of all the twisted pairs in the Category 6A F/UTP cable

The HDTDR plots for all the twisted pairs during the transition period (cycle 21) are plotted in figures 7.54 and 7.55. The amplitude of the discontinuity at 19.5 m increased by 0.65% during the heating of the cable and by 0.79% due to the cooling of the cable (Figure 7.54).

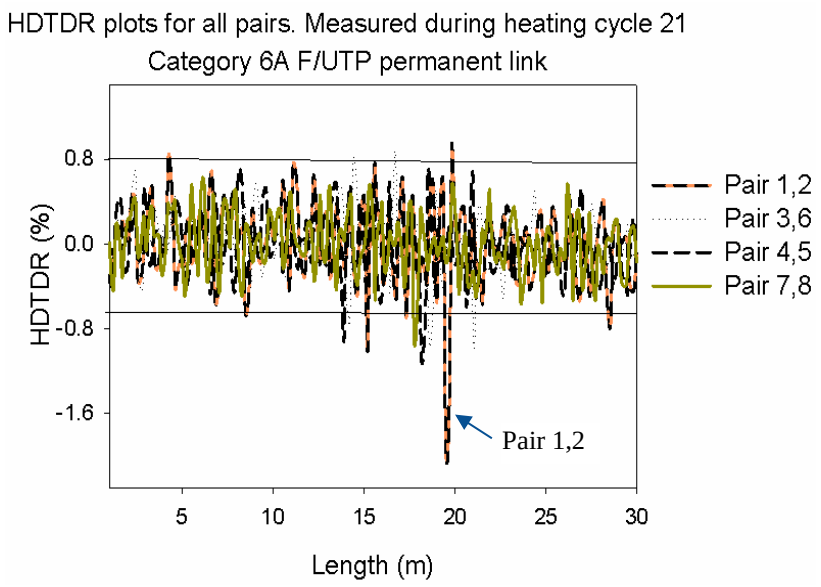

Figure 7.54: HDTDR plot of the portion insulated Cat 6A F/UTP PL (heating cycle 21)

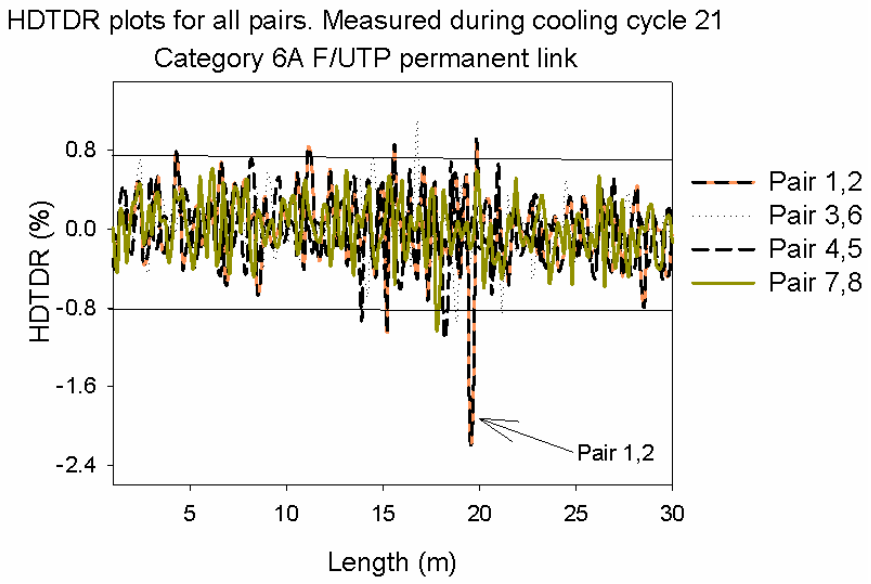

Figure 7.55: HDTDR plot of the portion insulated Cat 6A F/UTP PL (cooling cycle 21)

To verify the impedance discontinuity at 19.5 m location on the PL, the baseline electrical length and the mismatched electrical length of pair 1,2 (see figure 7.49) were calculated as follows: electrical length = physical length*$\sqrt{\varepsilon_r}$. Baseline electrical length = 30.8m * $\sqrt{2.0472}$ = 44.07m and the mismatched electrical length = 30.6 m * $\sqrt{2.0461}$ = 43.77m. Furthermore, since the pulse signal must be transmitted and the reflection from the discontinuity must be received, the physical distance to the source of the mismatch will be half of the calculated value of the electrical lengths. Given this, it can be argued that one of the sources of the impedance mismatch on the cable segment will be around 19 to 22 m as indicated in figure 7.55.

The impedance profile along the length of pair 1,2 (figure 7.56) reveals the three major events on the cable during the thermal cycling tests. The characteristic impedance of pair 1,2 at 11 m and 15.5 m were inductive during the heating cycle 2 and 39 while that of the 19.5 m was capacitive during cycle 21. The extracted primary line constants from the calculated impedance confirm the dominant factors or the impedance mismatches at 11.1 m and 19.5 m of the pair 1,2 (See section 7.5).

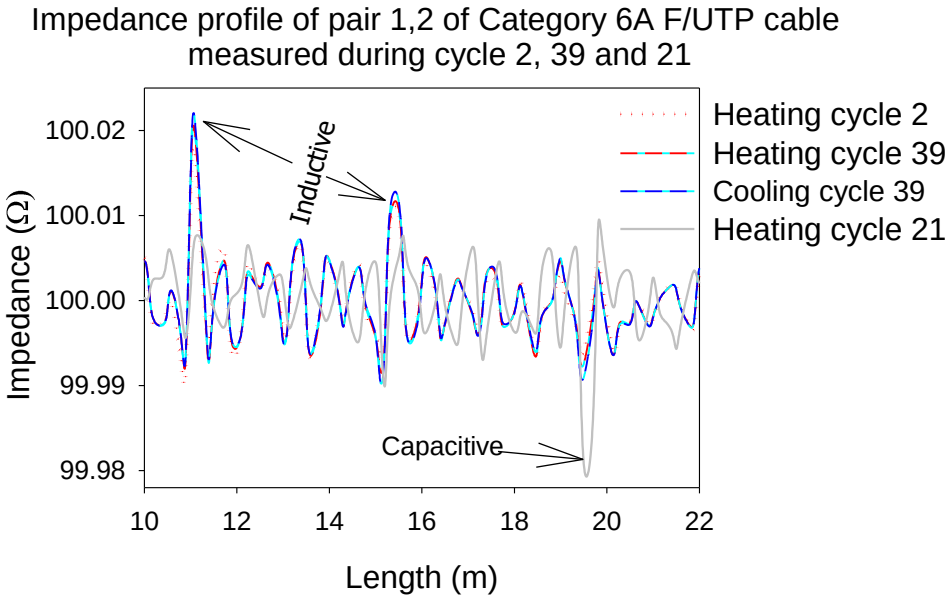

Figure 7.56: Showing the discontinuities on the Cat 6A F/UTP PL due to thermal cycling

As shown in figure 7.57, the Z_o of pair 1,2 at 11.1 m location increased progressively from cycle 1 to cycle 40.

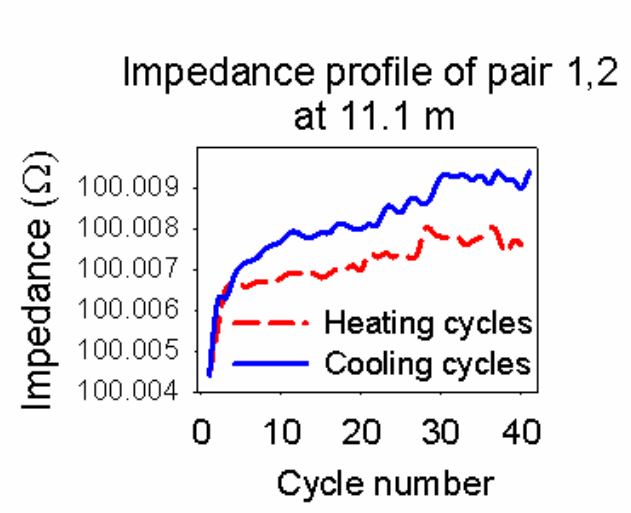

Figure 7.57: Increasing impedance of pair 1,2 at 11.1m location on the Cat 6A PL.

Figure 7.58 shows that the Z_o of pair 1,2 at 19.5 m decreased from its baseline value from cycle 1 to 40 except for the heating cycles 2 and 39 where the balance of the twisted pair was compromised. The generated RL echo and the resonances obtained during cycle 2 and 39 are shown in figure 7.62 and 7.60.

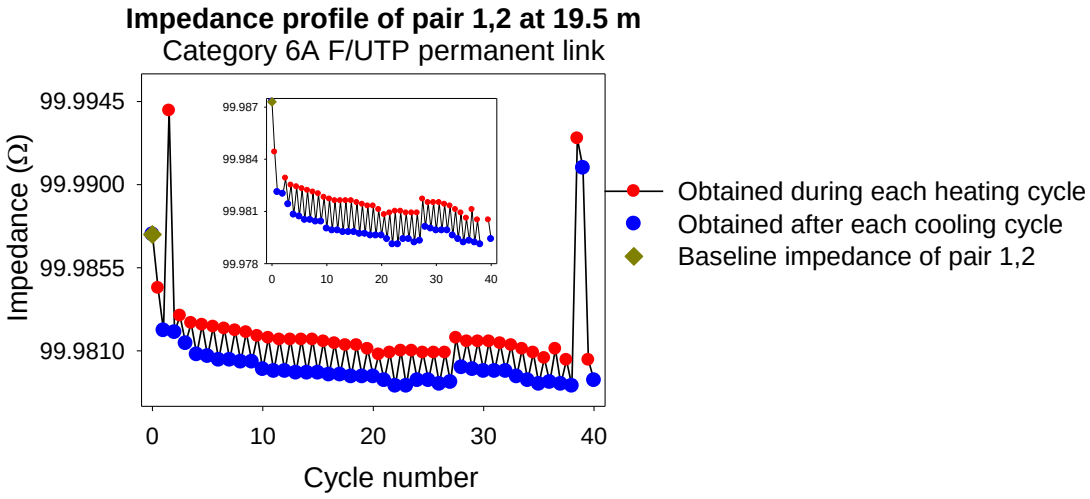

Figure 7.58: Showing the reduction in the impedance of pair 1,2 at 19.5 m.

Figure 7.59 presents the impedance profile of the longest pair (pair 3,6) in the Category 6A F/UTP cable. The profile on the left-hand side of figure 7.59 is the impedance profile of the heated portion of the cable, while the one on the right-hand side, the impedance profile towards the end of the link is presented. As can be seen on the left of figure 7.59, the differential impedance traces obtained during the heating cycle 2 and 39 were distinct when compared to the impedance traces obtained for other thermal cycles. From this observation, it is apparent that the impedance bridging on the PL, due to the localised heating of the cable and the simultaneous thermal expansion of the twisted pair caused the electrical length mismatches, which are evident at the end of the link. From the right of figure 7.59, it can be observed that the pulse signal on the pair 3,6 did not reach the end of the link during each heating cycle. The significance of this is that the transmitted signal will be reflected at the end of the line without delivering electrical power and data signal to the load when the cable attains certain high temperature under this installation condition. Furthermore, the impedance profile of the heated (middle) and unheated portions of the cable shows some impedance mismatches, which contributed to the poor performance of RL measured from the PL (see figure 7.62). It should be noted that the adverse effect of the impedance mismatches at the end of the line, is a voltage standing wave, which will contribute to the losses of the PL.

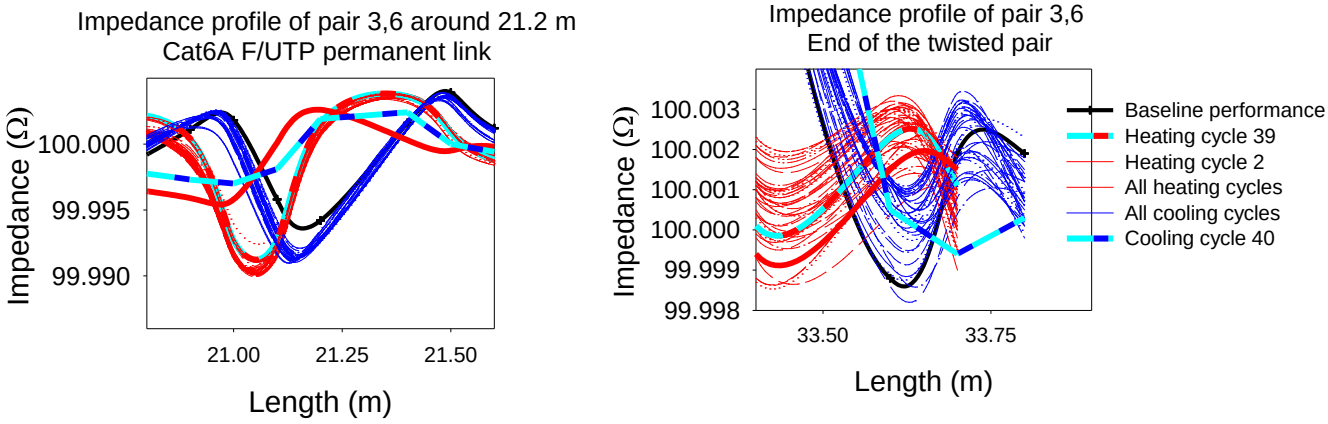

Figure 7.59: Showing the impedance mismatches on pair 3,6 of Category 6A F/UTP PL.

Effects of thermal variation on the balance and crosstalk performance of the portion insulated Cat 6A F/UTP

Figure 7.60 is the ELTCTL plot for the pair 1,2 of the Cat 6A cable, which presents the amount of differential mode voltage signal that is being converted to common mode voltage signal at the far end of the PL. As presented in figure 7.56, the distinct resonances in the differential impedance of pair 1,2 during heating cycle 2 and 39 can also be observed in the ELTCTL of the pair 1,2. Hence, from this correlation, it can be inferred that the noise immunity of the PL has been affected.

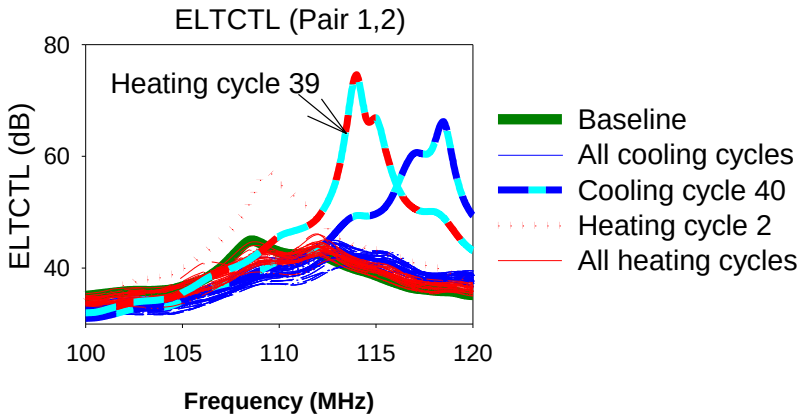

Figure 7.60: ELTCTL performance of the pair 1,2 of Category 6A F/UTP PL.

Figure 7.61 presents the magnitude of the crosstalk measured between the shortest and longest twisted pairs (1,2 - 3,6) at 20.7 m and 20.9 m locations on the PL. The noise coupling between the two twisted pairs increased initially during the first thermal cycle due to the shifting of the twisted pairs and increase in the ε_r of the conductor insulation. However, the crosstalk between the twisted pairs decreased afterwards. The reduction in the crosstalk magnitude after the first thermal cycle may be linked to the reduction in the value of the ε_r of the conductor insulation. Also, due to the fact that changes in the structure of the twisted pairs stabilised after performing a few thermal cycling on the cable. Furthermore, comparing the magnitude of the noise coupling during the heating and cooling of the cable, it is noted that the crosstalk performance improved slightly due to the heating of the cable. Moreover, the observed worst noise coupling between pair 1,2 and 3,6 due to the cooling of the cable was due to an increased flux linkage, which increased the capacitive coupling between the twisted pairs as they cool down and contract. Note that this trend in the crosstalk performance of Category 6A F/UTP cable has been observed in the performance of the standard Category 6 U/UTP (figure 7.11) and Category 6 U/UTP CMP cables (figure 7.37).

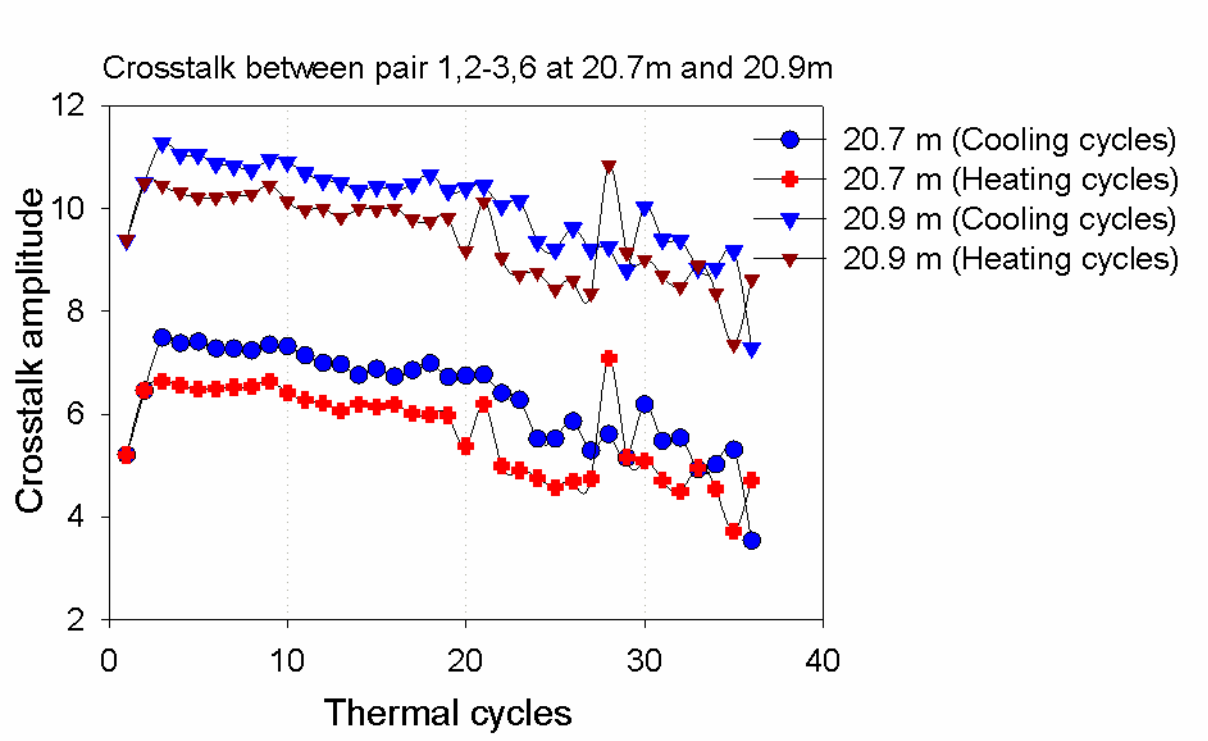

Figure 7.61: Crosstalk performance between pair 1,2 and 3,6 of the Category 6A F/UTP cable.

Effects of thermal variation on the return loss performance of Category 6A F/UTP cable

The obtained RL values for pair 1,2 at 136 MHz (main & remote), using the ISO PL2 Ea test limit are presented in table 7.5 whereas table 7.6 presents the comparison of the RL values using both the ISO PL2 Ea and TIA Cat 6A PL test limits.

From table 7.5, it can be noted that the effects of thermal cycling and installation condition caused the RL value of pair 1,2 to decrease from its baseline value. Although the RL values decreased from the first thermal cycle (cycle 1) up to the last thermal cycle (cycle 40), it can be observed that the most significant change in the RL performance of the Category 6A F/UTP PL was within the first heating and cooling of the cable. Furthermore, comparing the RL performance due to heating and cooling of the cable. Moreover, the RL performance of the PL was more affected due to the cooling of the cable when compared to the effect of heating. Lastly, it was observed that the RL value decreased more at the main of the PL (0.6 dB) in comparison to the decrease in the RL value (0.5 dB) at the remote of the PL.

Table 7.5: Effects of thermal cycling on the RL performance of Category 6A F/UTP

Return Loss (dB) at 136 MHz - ISO PL2 Ea limit						
	Baseline	Cycle 1	Cycle 10	Cycle 20	Cycle 30	Cycle 40
Results obtained from the Main of the DSX-5000 Cable Analyzer.						
Heating	26.9	25.4	24	23.7	23.8	22.2
Cooling	26.9	24.8	23.5	23.3	23.5	21.9
Difference	0	**0.6**	0.5	0.4	0.3	0.6
Results obtained from the Remote of the DSX-5000 Analyzer.						
Heating	25.2	24.2	23.1	23	22.8	22.6
Cooling	25.2	23.7	22.7	22.7	22.4	22.3
Difference	0	**0.5**	0.4	0.3	0.4	0.3

Furthermore, comparing the RL performance of the Category 6A F/UTP PL using the TIA and ISO test standards, it can be observed that there was harmony between the results obtained using the ISO and TIA test limits (table 7.6). That is, the same amount of RL degradation was measured using the two test standards. Moreover, the difference in the baseline RL values was due to the selected wrong cable type for the ISO test limit, which was corrected during the first thermal cycle. That is, Category 6 F/UTP was used for the baseline measurement instead of the Category 6A F/UTP cable type.

Table 7.6: Comparisons of the RL values of pair 1,2 at 136 MHz, (ISO vs TIA test limits)

Comparisons of the return loss measurements using the ISO & TIA test limits							
Results obtained from the remote of the PL, using the DSX-5000 Analyzer Return Loss (dB) at 136 MHz (For pair 1,2)							
ISO11801 Ea limit vs TIA PL2 Ea limit							
		Baseline	Cycle 1	Cycle 10	Cycle 20	Cycle 30	Cycle 40
Heating cycles	ISO test limit	25.2	24.2	23.1	23	22.8	22.6
	TIA test limit	26.2	24.2	23.1	23	22.9	22.7
Cooling cycles	ISO test limit	**25.2**	23.7	22.7	22.7	22.4	22.3
	TIA test limit	**26.2**	23.7	22.7	**22.6**	22.4	22.3

Figure 7.62 shows the RL traces of pair 1,2 of the Category 6A F/UTP cable from 70 to 90 MHz. As can be observed, the spurious resonances at the heating cycle 2 and 39 in the ELTCTL traces are also evident in the RL plot for the pair 1,2. It should be noted that the amplitude of the RL echoes at 74.8 MHz and 81.3 MHz, which indicate severe impedance mismatches on the PL.

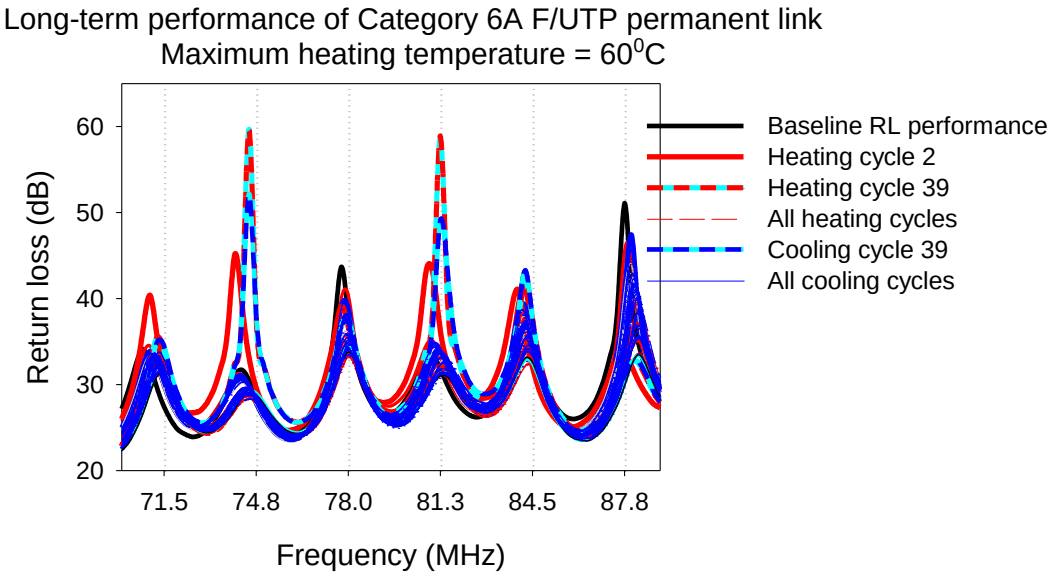

Figure 7.62: Showing the generated RL echoes by the pair 1,2 at 74.8 and 81.3 MHz

Figure 7.63 presents the RL traces measured on pair 1,2 of the Category 6A F/UTP cable from 135 to 140 MHz. The magnitude of the RL signal around 136 MHz, which is an indication of the superposition of the reflected signal on the transmitted pulse signal as the reflected signal travels from the point of the impedance mismatch down to the source. Also, it is apparent that the magnitude of the superimposed signal decreased from its initial value from cycle one up to the last thermal cycle due to the phase shift of the RL signal.

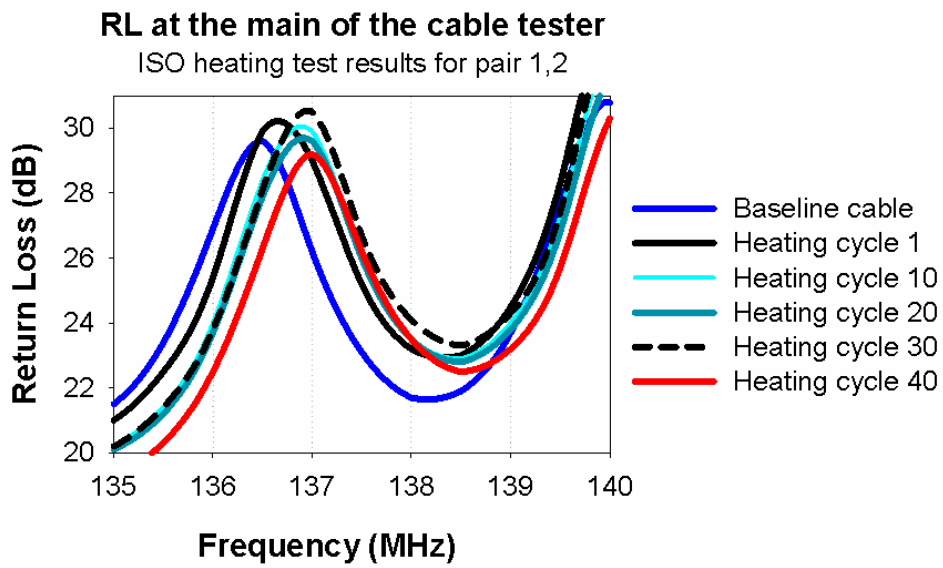

Figure 7.63: Showing the significant phase shifts in the RL signal on pair 1,2 around 136 MHz

Long-term effects of thermal variation on the insertion loss performance of the portion insulated Cat 6A F/UTP

Figure 7.64 is the insertion loss (IL) margin of the Category 6A F/UTP PL, which shows that the IL headroom decreased progressively from the first heating and cooling of the cable up to the last thermal cycle (cycle 40).

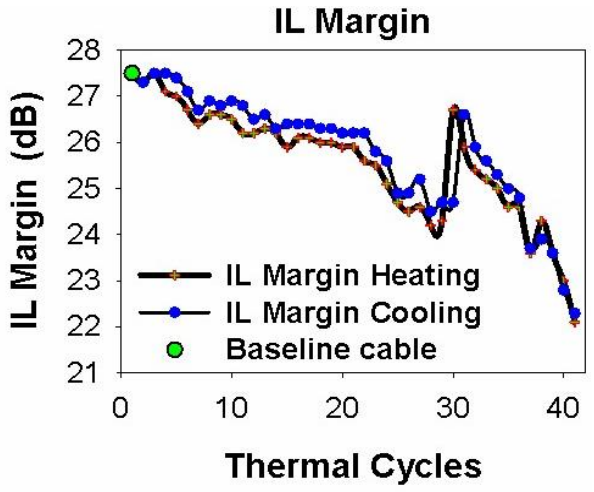

Figure 7.64: Degradation in the insertion loss performance of the Cat 6A F /UTP PL.

Also, figure 7.65 shows that the effects of thermal cycling caused the IL performance of the pair 3,6 to increase progressively from its baseline performance. As can be seen, the highest increase in the IL due to the heating and cooling of the Category 6A F/UTP cable was measured at 500 MHz during cycle 40. With these set of results, it is noted that the dielectric and conductor losses are frequency dependent and that long-term thermal variation on the cable contributes to the loss of the signal strength.

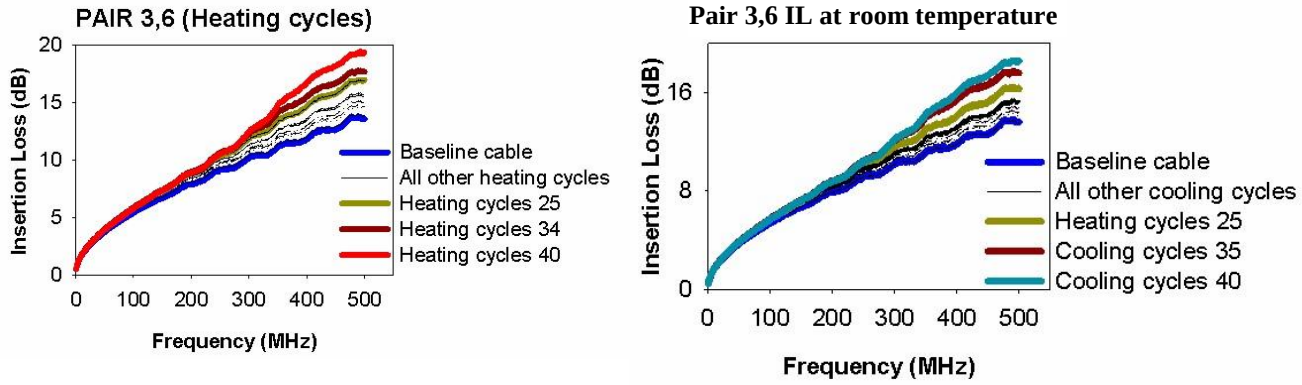

Figure 7.65: Showing the drift in the IL performance of the Category 6A F/UTP PL

Table 7.7: IL performance as a function of the physical length of the twisted pairs

Long-term insertion loss performance of the Category 6A F/UTP PL at 500 MHz Obtained using the ISO PL2 Ea test limit				
Pair number	Length of the twisted pair (m)	**Baseline** Insertion loss (dB)	Insertion loss for **last heating** cycle (dB)	Insertion loss for the **last cooling** cycle
Pair 3,6	**33.8**	13.6	**19.4**	19.1
Pair 4,5	33.1	12.6	18.0	17.3
Pair 7,8	32.1	12.2	17.9	17.1
Pair 1,2	31.3	11.8	17.6	16.9

The IL of pair 3,6 at 500 MHz, which was measured before the heating of the cable began and during the last heating and cooling cycle are presented in table 7.7 while table 7.8 presents the comparison of the IL values using both the ISO PL2 Ea and TIA Cat 6A PL test limits. As stated in table 7.7, it is apparent that the IL of the Category 6A F/UTP PL at 500 MHz is length dependent as ohmic losses depend on the DC loop resistance of the twisted pair. Moreover, as can be noted, pair 3,6 which is the longest pair in the cable had the highest IL value (19.4dB) in comparison to the IL values measured on the other twisted pairs.

Furthermore, the results in table 7.8 show that the IL value of the Cat6A F/UTP PL at 500 MHz drifted from its baseline value due to the effect of thermal cycling. It was observed that the maximum IL increase due to the 40 thermal cycles conducted on the middle portion of the cable was 9.2% per degree. Also, comparing the measured IL performance of the Category 6A F/UTP PL using the TIA and ISO test limits, it can be noted from the table that there is harmony between the amounts of IL degradation obtained using the ISO and TIA test limits. Any observed difference in the IL values was due to the time difference between when the TIA and ISO measurements were conducted.

Table 7.8: Comparison of the IL performance of Cat6A F/UTP PL (ISO vs TIA IL values)

	Insertion loss (dB) at 500 MHz using the ISO PL2 Ea test limit						
	9.2% / °C	Baseline	Cycle 1	Cycle 10	Cycle 20	Cycle 30	Cycle 40
	Results obtained from the DSX-5000 cable Analyzer						
Heating cycles	ISO test limit	13.6	13.8	14.7	15.6	15.8	19.4
	TIA test limit	13.5	13.8	14.7	15.6	15.8	19.0
Cooling cycles	ISO test limit	13.6	13.6	14.4	15	15.3	19.1
	TIA test limit	13.5	13.6	14.4	15	15.2	19.1

Long-term effects of thermal variation on the PSACR-N performance of the portion insulated Cat 6A F/UTP PL

The degradation in the PSACR-N performance of the Category 6A F/UTP PL is presented in figure 7.66. As shown, the PSACR-N performance of the Category 6A F/UTP PL decreased progressively from the first heating and cooling of the cable. Furthermore, as can be noted, the PSACR-N plot shows a similar trend to that of the IL performance presented in figure 7.64. The reason for the similar trend is because the impact of attenuation was more substantial when compared to the impact of the crosstalk on the received signal. Additionally, because of the impedance bridging on the cable, part of the transmitted signal from the far end transmitter would have been reflected to the source, which implies that only part of the transmitted signal will be received at the near end. Also, because attenuation is temperature dependent, it can be observed from figure 7.66 that the PSACR-N performance was more affected due to the heating of the cable than the cooling of the cable.

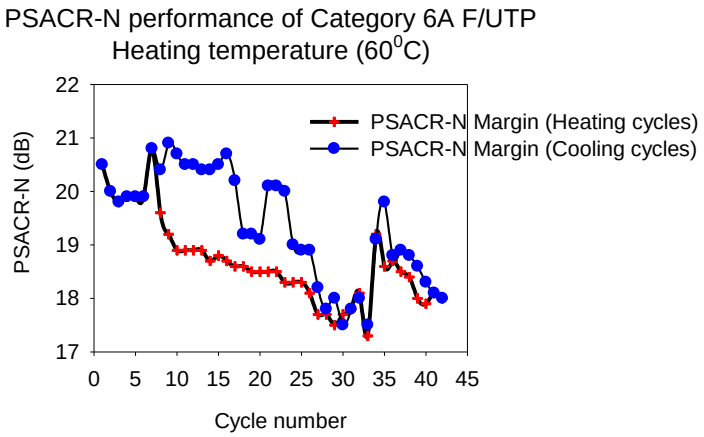

Figure 7.66: Degradation in the PSACR-N performance of the Category 6A F/UTP PL

7.4 Validation of the drifts in the RL and IL performance of Cat 6A using the FSV tool

Having seen the drifts in the RL (table 7.6) and IL (table 7.8) performances of the Category 6A F/UTP PL because of the effects of thermal cycling and long-term thermal variation, this section presents the validation of the drifts using the Feature Selective Validation (FSV) technique. Table 7.9 presents the FSV validation rating scale used for the analysis of the result.

Table 7.9: Validation rating scale with its associated natural language description

FSV Value (Quantitative)	FSV Interpretation (qualitative)
Less than 0.1	Excellent
Between 0.1 and 0.2	Very good
Between 0.2 and 0.4	Good
Between 0.4 and 0.8	Fair
Between 0.8 and 1.6	Poor
Greater than 1.6	Very poor

Baseline RL and IL performances vs degradation in the RL and IL performances of the Category 6A PL

It has been shown in table 7.6 and 7.8 that the obtained RL and IL results using the TIA test limit are in good agreement with that of the ISO test limit. However, to quantify and validate the degradation in the Category 6A F/UTP PL performance, the baseline RL and IL traces were compared with the RL and IL traces measured during cycle 1, 10, 20, 30 and 40 respectively. Table 7.10 and 7.11 present the GDMtot values for each of the comparisons, whereas figures 7.67 to 7.70 are the plots for the GDMtot values.

7.4.1 Comparison of the return loss measurements (ISO vs TIA test standards)

The averaged GDMtot value (0.24) for the comparison made between the baseline RL performance and the RL performance measured during cycle 1 shows that the baseline RL performance of the cable was still in good agreement with the performance of the cable due to the

first heating and cooling of the cable. Similarly, the GDMtot value (0.34) for the comparison made between the baseline and cycle 20 RL performances falls within the good agreement range (see the rating scale in table 7.9). However, the comparison between the baseline RL and that of the last cycle (cycle 1 vs cycle 40) shows that the baseline RL performance of the cable was in poor agreement with the performance of the cable due to the long-term thermal variation on the cable.

Table 7.10: Validation of the return loss degradation (ISO vs TIA test limits)

Comparisons of the **return loss** measurements using the ISO & TIA test limits							
Results obtained from the remote of the DSX-5000 cable Analyser							
Results, using the FSV tool (ISO11801 Ea limit vs TIA PL2 Ea limit)							
GDMtot Values							
		Baseline	**Cycle 1**	**Cycle 10**	**Cycle 20**	**Cycle 30**	**Cycle 40**
Heating cycles	ISO test limit	-	0.24	0.30	0.32	0.31	0.86
	TIA test limit	-	0.17	0.27	0.30	0.33	0.89
Cooling cycles	ISO test limit	-	0.28	0.30	0.32	0.34	0.86
	TIA test limit	-	0.25	0.32	0.34	0.37	0.88

As presented in figure 7.67 and 7.68, the set of the results show the degradation in the RL performance of the Category 6A F/UTP PL due to the long-term effects of thermal variation on the cable and installation condition. More also, it can be noted that the quantification of the RL degradation using the ISO test limit agrees with that of the TIA test limit.

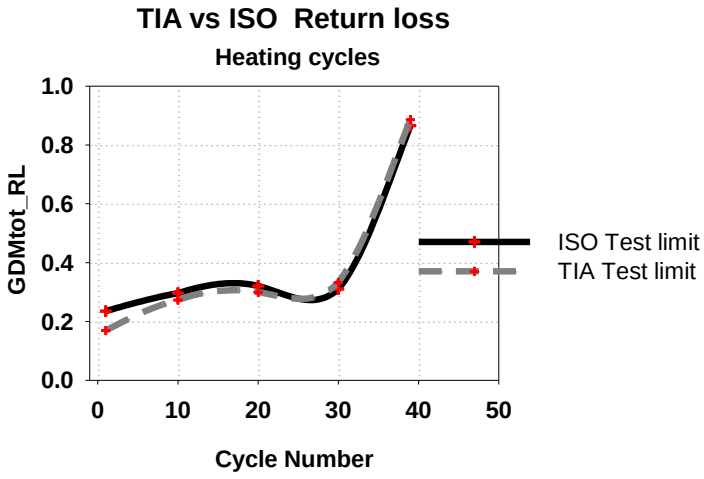

Figure 7.67: Comparisons of the return loss measurements - heating (ISO vs TIA test limits)

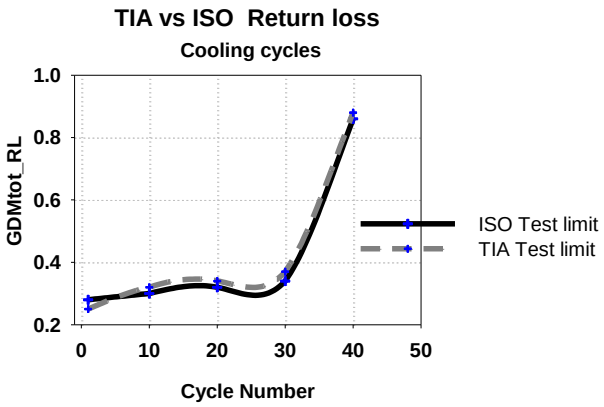

Figure 7.68: Comparisons of the return loss measurements - cooling (ISO vs TIA test limits)

7.4.2 Comparison of the insertion loss measurements (ISO vs TIA test standards)

The averaged GDMtot value (0.11) for the comparison made between the baseline IL performance and the measured IL performance during cycle 1 shows that the baseline IL performance of the cable was in very good agreement with the performance of the cable due to the first heating and cooling of the cable. However, the averaged GDMtot value (0.25) for the comparison made between the baseline and cycle 20 IL performances falls within the good agreement range (see the rating scale in table 7.9), which shows that the amplitude of the transmitted pulse signal has decreased slightly. Furthermore, the comparison made between the baseline IL and that of the last cycle (cycle 1 vs cycle 40 IL traces) shows a further degradation in the quality of the transmitted signal. That is, the baseline IL performance of the PL was in fair agreement with the performance of the cable due to the long-term effects of thermal variation on the cable as well as installation condition such as localised heating.

Table 7.11: Validation of the insertion loss degradation (ISO vs TIA test limit)

	Comparison of **insertion loss** measurements using the ISO & TIA test limits						
	Comparisons of the Insertion Loss results using the FSV tool						
	ISO11801 Ea test limit - Baseline IL vs degradation in IL TIA PL2 Ea test limit - Baseline IL vs degradation in IL						
		GDMtot Values					
	Pair 3,6	**Baseline**	**Cycle 1**	**Cycle 10**	**Cycle 20**	**Cycle 30**	**Cycle 40**
Heating cycles	ISO test limit	-	0.12	0.19	0.28	0.29	0.55
	TIA test limit	-	0.11	0.19	0.27	0.29	0.54
Cooling cycles	ISO test limit	-	0.08	0.13	0.21	0.23	0.53
	TIA test limit	-	0.09	0.14	0.21	0.23	0.53

Figure 7.69 and 7.70 show that the effects of non-electrical heating, long-term thermal variation and installation condition accelerated the degradation of the IL performance of the Category 6A F/UTP PL. It also shows that the amount of the IL performance degradation measured using the TIA test limit is in good agreement with that of the ISO test limit.

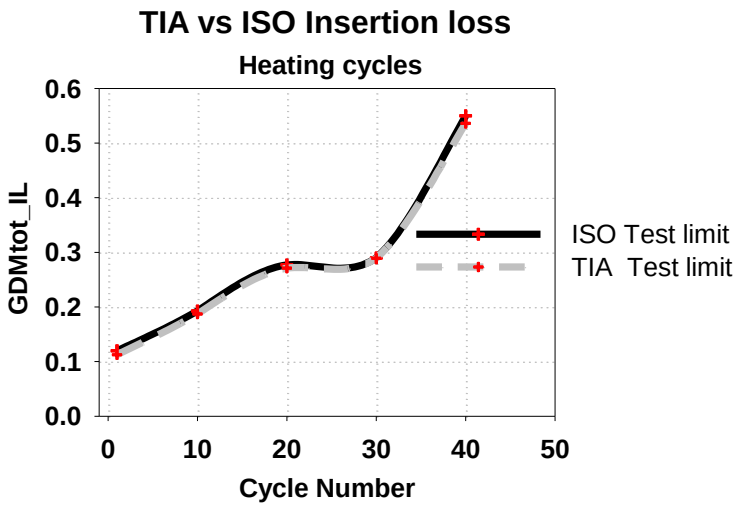

Figure 7.69: Comparisons of the IL measurements - heating (ISO vs TIA test limit)

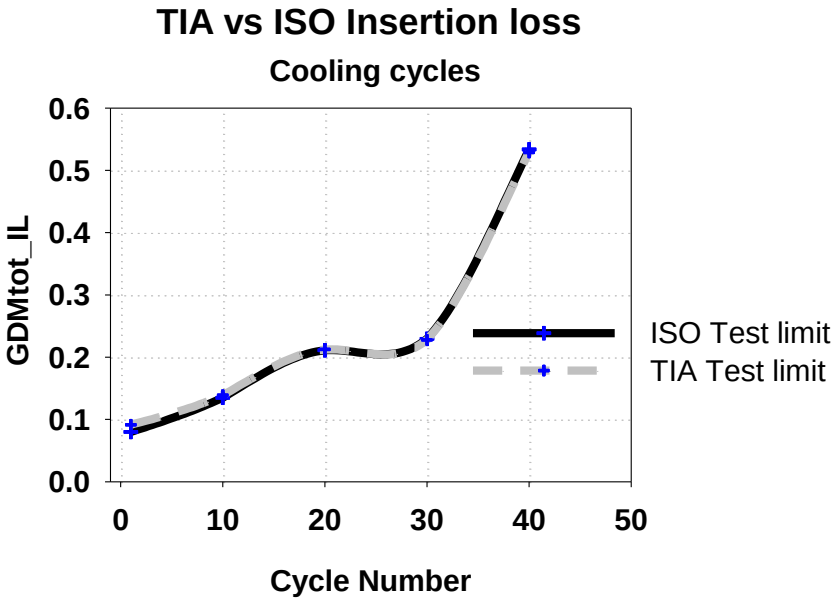

Figure 7.70: Comparisons of the IL measurements – cooling (ISO vs TIA test limit)

7.5 Extraction of the primary line constants of Category 6A F/UTP cable

Figure 7.71 and 7.72 show that the characteristic impedance (Z_o) of pair 1,2 of the Category 6A F/UTP cable increased at 11.1m and decreased at 19.5m locations on the PL. As the changes in the Z_o can be due to the changes in the unit capacitance or inductance, investigating the dominant factor is important. In view of this, using the impedance variations obtained during cycle 39 and 21, the predominant factors for the observed changes in the Z_o at 11.1m and 19.5m locations on the cable were identified from the extracted primary line constants.

Figure 7.71 presents the extracted inductance and capacitance of the pair 1,2 from the Z_o of the line, which was obtained during the heating cycle 39. It was observed that the inductance of pair 1,2 increased from 4.7689E-07 H/m to 4.7696E-07 H/m at 11.1m while the capacitance of that location decreased from 4.7685E-11 F/m to 4.7677E-11 F/m during the heating cycle 39. From this analysis, however, it can be argued that the increase in the inductance was the predominant factor for the increase in the Z_o (see figure 7.57) of the pair 1,2 at 11.1m. The reason for this is that the increase in the centre-to-centre spacing between the conductors of a twisted pair due to thermal expansion (during heating) causes the inductance of the twisted pair to increase. Moreover, the increase in the inductance of a twisted pair implies that the characteristic impedance of that twisted pair will increase.

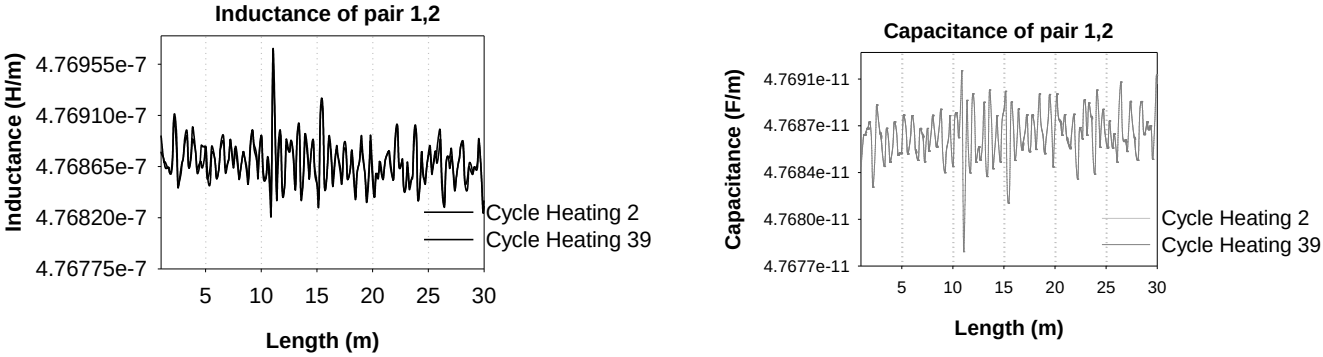

Figure 7.71: Showing the root cause for an increased impedance of pair 1,2 at 11.1 m.

Figure 7.72 presents the extracted inductance and capacitance of the pair 1,2 from the impedance obtained during cycle 21. It was observed that the capacitance increased from 4.76931E-11 F/m to 4.76959E-11 F/m at 19.5m location on the cable while the inductance decreased from 4.76807E-07 H/m to 4.76778E-07 H/m at the same location. Hence, the increase in the unit capacitance can be linked to the observed decrease in the Z_o of pair 1,2 at 19.5m location of the cable segment.

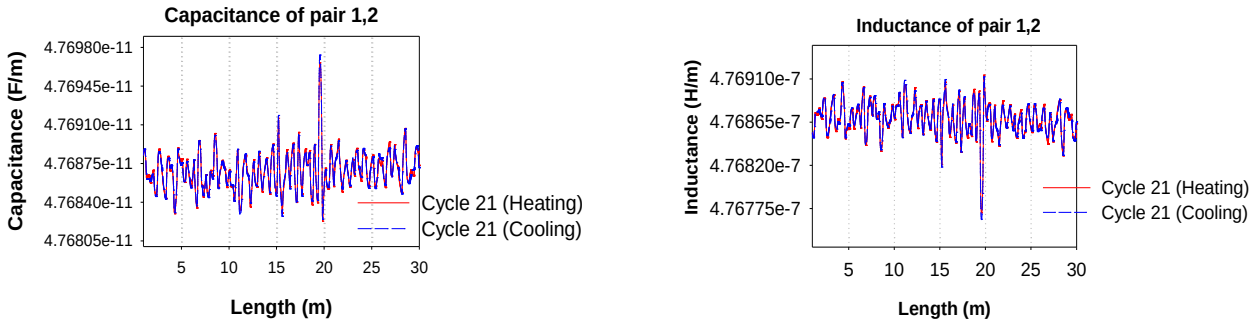

Figure 7.72: Showing the root cause for the decrease in the impedance of pair 1,2 at 19.5 m

Moreover, as discussed in chapter 2, if the effective area of the twisted pair decreases due to the decrease in the overall diameter of the copper conductor over its insulation as a consequence of thermal cycling, the ε_r will increase, the unit capacitance will increase, then impedance will decrease as observed in the impedance profile of pair 1,2 shown in figure 7.58. Also, if the separation distance between the conductors of a twisted pair decreases due to the contraction of the twisted pair as a result of the cooling of the cable, the capacitance will increase, the impedance will decrease. As any of these could cause the Z_o of the twisted pair to decrease, finding the exact cause is necessary. The next section presents the investigation of the changes in the elemental composition and dimensions of the materials of a twisted pair sample.

7.6 Changes in the dimensions and elemental composition of a twisted pair sample

Electrical length mismatches towards the end of the three cables under study (see figures 7.7, 7.28 and 7.60) have been observed due to the insulation of the full length of the cable and localised heating of the cables. Moreover, the decrease of 0.2 m length and the increase of 1ns in the propagation delay of the signal on the cable suggest that the pulse signal was not reaching the end of the link. Given this, since electromagnetic energy propagates through the dielectric, the electrical length mismatches at the end of the link during the heating and cooling of the cable suggest that the conductor insulation suffered a thermal push and pull effect as a result of the strain on the cable. Furthermore, the degradation in the RL and overall performance of the cable based on the effect of non-electrical heating indicates that thermal cycling has effects on the dimensions and materials of the cable. Given these, in the investigation of the changes in the dimensions of a twisted pair sample, Scanning Electron Microscope (SEM) was used to observe the deformation in the physical structure of a short length of a twisted pair sample. The results of these observations are presented in section 7.6.1.

7.6.1 Changes in the dimensions of the Ethernet cable conductor insulation

Figure 7.73 shows the baseline dimensions of a copper and its dielectric obtained from Category 6A F/UTP cable before the twisted pair sample was heated and cooled, whereas figure 7.74 shows the dimensions of the twisted pair after the heating and cooling of the twisted pair sample.

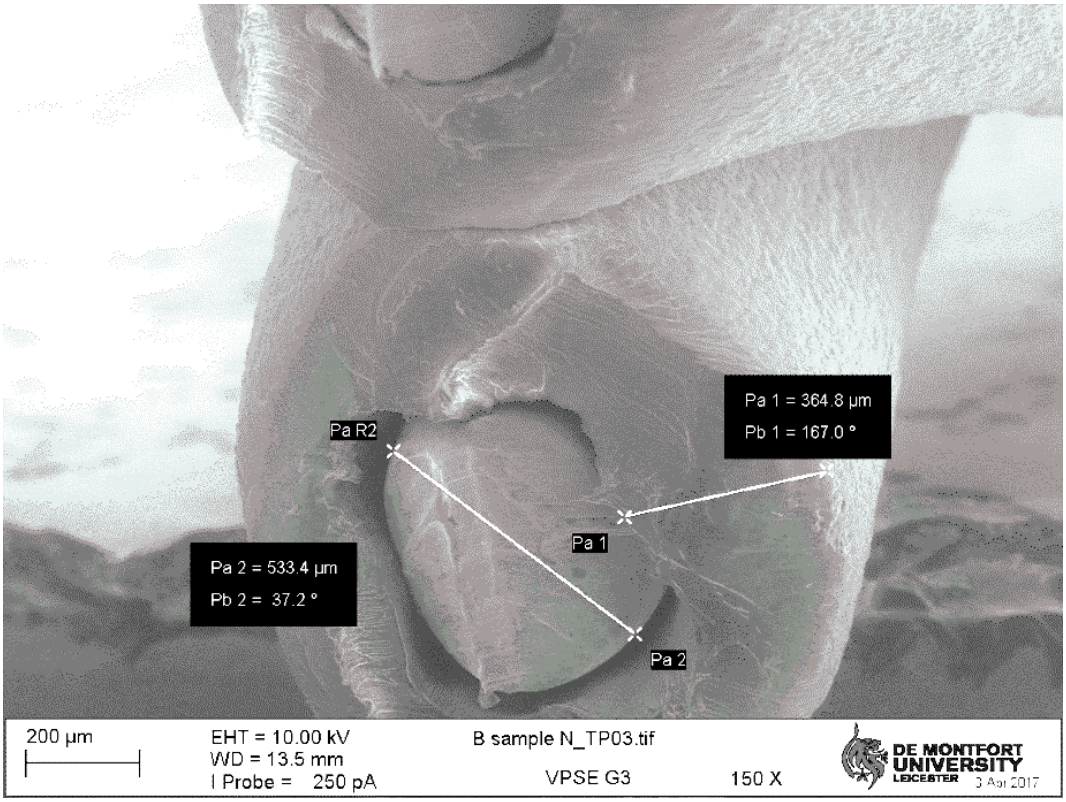

Figure 7.73: Baseline dimensions of a short length of a twisted pair sample.

Comparing the baseline thickness of the conductor insulation in figure 7.73 to that of the heated sample in figure 7.74, it can be observed that the thickness of the conductor insulation decreased by 222.4 μm because of the effects of thermal cycling. It is worth mentioning that the shrinking of the conductor insulation of a twisted pair will lead to a decrease in the effective area of the overlapping conductors, which will, of course, lead to an increase in the ε_r of the conductor insulation. More also, the increase in the ε_r will cause the unit capacitance of the twisted pair to increase. Furthermore, an increase in the unit capacitance will cause the Z_o of the twisted pair to decrease.

From figure 7.74, the adhesion of the twisted pair insulator to its copper conductor can be observed to be affected near the end of the twisted pair sample, of which evidently justifies the

observed thermal push and pull effects seen in the HDTDR plots of the cable performance. The significance of the poor interfacial adhesion of the insulator to its copper conductor is that, in an installation condition in which a portion of the cable passes through thermally insulated areas, the resultant deformation in the conductor insulation as a result of the local heating of the cable will lead to an irreversible damage to the cable and its performance.

Clearly, figures 7.73 and 7.74 indicate an increasing gap between the copper and its dielectric as a result of thermal cycling. However, more precise cable preparation would help quantify the deterioration in the physical structure of the twisted pair.

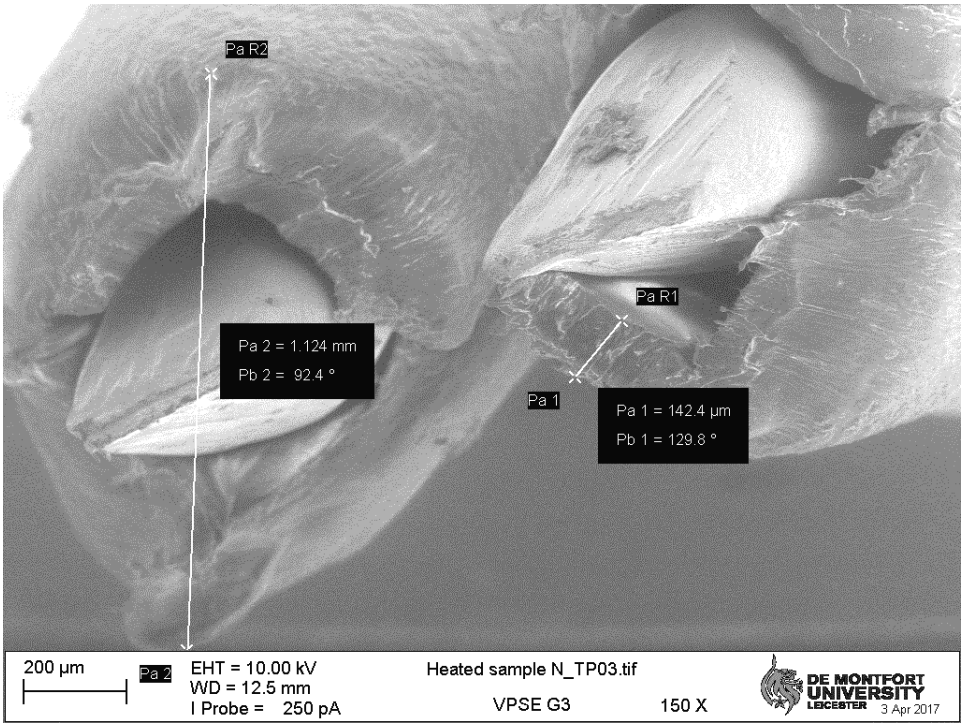

Figure 7.74: Deformation of the conductor insulation

Summary of results

It has been shown in section 7.3.1 that the extracted effective ε_r of the conductor insulation and the electrical length of pair 1,2 of the Category 6A F/UTP decreased permanently due to prolonged thermal cycling. Also, the reduction in the electrical length of the cable caused the propagation delay of the pulse signal on the cable to decrease and the velocity factor of the conductor insulation to increase. Signal skew was observed based on the changes in the propagation delay of the pulse signal on the cable. Moreover, while the electrical properties of pair 1,2 decreased permanently due

to the cooling of the cable, results show that the electrical properties of pair 1,2 increased briefly, back to the baseline values during the heating cycle 39 before decreasing back again.

The observed impedance discontinuity at the 19.5m location of the shortest twisted pair (pair 1,2) in the cable was reported in section 7.3.2. It was observed that the amplitude of the discontinuity increased by 0.65% during the prolonged heating cycle 21 and by 0.79% due to the cooling of the cable after the heating cycle 21. Other discontinuities at 11.5m and 15.5m on pair 1,2 generated RL echoes and spurious resonances during heating cycle 2 and 39 as shown in the ELTCTL and RL traces (figures 7.60 and 7.62). Moreover, the extraction of the primary line constants from the obtained impedance profile of the link revealed that the impedance of pair 1,2 at 19.5 m location decreased due to an increased unit capacitance while the increased differential impedance at 15.5m was due to an increase in the unit inductance of the twisted pair. Furthermore, the obtained differential impedance profile of the longest pair in the cable (pair 3,6) was distinct during cycle 2 and 39 in comparison to the impedance traces obtained during other thermal cycles. It was observed that the impedance bridging on the PL due to the localised heating of the cable caused the thermal push and pull of the dielectric, which further caused the observed electrical length mismatches towards the end of the PL. More also, the impedance profile of the heated and unheated portions of the cable shows some impedance mismatches which contributed to the poor RL performance of the PL in general.

As observed in the crosstalk performance of the standard Category 6 U/UTP and Category 6 U/UTP CMP cables, crosstalk performance between the longest and shortest pair in the Category 6A F/UTP cable was also observed to be better due to the heating of the cable in comparison to the measured crosstalk performance due to the cooling of the cable. More also, it was found that the crosstalk performance of the portion insulated cables was initially worse during the few heating and cooling cycles but improved afterwards.

The effects of the long-term thermal variation and installation condition caused the RL value of pair 1,2 to decrease progressively from its baseline value, whereas the effects of thermal cycling and installation condition caused the IL performance of the Category 6A F/UTP PL to increase progressively. Although the RL values decreased from the first thermal cycle (cycle 1) up to the last thermal cycle (cycle 40), it was observed that the worst RL performance of the Category 6A F/UTP PL was within the first heating and cooling of the cable. Furthermore, comparing the RL performance due to the heating and cooling of the cable, it was found that the RL performance was more affected due to the cooling of the cable than when it was heated. Also, the RL value at the

main of the PL was found to be lower in comparison to the RL value measured at the remote side of the PL. The maximum reduction in the RL value due to the 40 thermal cycles conducted was observed to be 1 % per degree, whereas the maximum IL increase due to the 40 thermal cycles conducted was observed to be 9.2 % per degree.

The quantification and comparison of the baseline RL performance with the long-term RL performance of the Category 6A F/UTP PL using the FSV tool showed a poor agreement, which implies a degradation in the RL performance of the PL. More also, the comparison of the baseline IL performance with the long-term IL performance of the Category 6A F/UTP PL showed a fair agreement, which also implies a deviation from the baseline IL performance of the PL. Lastly, the quantification of the RL and IL degradation using the ISO test limit agreed with that of the TIA test limit.

The PSACR-N performance of the Category 6A F/UTP PL decreased progressively due to the effect of thermal variation and installation condition. It was found that the impact of attenuation was more substantial in comparison to the impact of the crosstalk on the received signal. Also, the PSACR-N performance of the PL was found to be lower during the heating of the cable in comparison to the PSACR-N performance obtained due to the cooling of the cable.

Lastly, the results of the Scanning Electron Microscope (SEM) revealed the deformation in the conductor insulation of a twisted pair sample. It was observed that the conductor insulation decreased by 222.4 μm based on the effects of one thermal cycle. Also, the adhesion of the twisted pair insulator to its copper conductor was observed to be affected near the end of the twisted pair sample, of which justifies the observed thermal push and pull effects seen in the HDTDR plots of the cable performance. On examination of the deformation in the Ethernet cable dielectric, it was observed that dielectric deformation is due to the slippages at the atomic level, which is not the focus of this research. However, the next chapter examines the properties of the Ethernet cabling dielectrics to understand the root causes of Ethernet cable performance degradation.

CHAPTER 8 - RECTANGULAR RESONANT CAVITY DESIGN AND MEASUREMENTS OF ETHERNET CABLE DIELECTRIC

This chapter starts with the theoretical analysis of a 2.4 GHz Rectangular Resonant Cavity (RRC) design (section 8.1) based on the Cavity Perturbation Method (CPM) of the ASTM D2520-13 standard. This is followed by the modeling and actual fabrication of the cavity (section 8.1.2 and 8.1.3). Furthermore, the verification and validation of the accurate sample position inside the simulated and fabricated cavities were carried out in section 8.2. Section 8.3 presents the assessment of the baseline dielectric properties of different Ethernet cable dielectrics. In section 8.4.1, the immediate effects of an increase in temperature to 65^0C and continuous 30-day heating were examined on the dielectric constant (ε_r) of the FEP at 2.4 and 5 GHz. The rationale for the constant heating of the sample without cooling was to differentiate the immediate effects of temperature increase from the long-term effects of temperature increase on the dielectric properties of the FEP sample, which was obtained from the Category 6 U/UTP CMP cable.

The drifts in the transmission parameters of the portion insulated Category 6A F/UTP and Category 6 U/UTP CMP PLs have been observed in response to long-term thermal variations and localised heating. As discussed in chapter 2, if the dielectric constant of the cable dielectrics around the cable portion, passing through insulated area, changes as a result of thermal variation and localised heating, the capacitance of the cable will also vary (figure 7.72), leading to the impedance variation on the cable. After a long time, the impedance variations along the length of the cable (figures 7.7, 7.28 and 7.58) will cause multiple reflections of the signal passing through the cable (7.12, 7.32 and 7.63) and ultimately, contribute to an increase in the Insertion Loss of the system (figures 7.30 and 7.64). In view of these, the aim of the study in section 8.4.2 was to examine the drifts in the dielectric properties of the FEP sample at 2.4 GHz as functions of the intermittent and prolonged thermal cycling to establish correlations between the drifts in the transmission parameters of the Category 6 U/UTP CMP cable and its dielectric properties.

8.1 Design of the 2.4 GHz rectangular resonant cavity

This section presents the design procedure for the construction of Rectangular Resonant Cavities (RRCs). The design process begins with the analytical expression for a Transverse Electric (TE) TE_{101} mode rectangular cavity that is capable of operating within the Industrial, Scientific, and Medical (ISM) frequency band. This is followed by the simulation of the cavities using CST

Microwave Studio. After that, the rectangular cavities were manufactured in the Mechanical workshop of De Montfort University (DMU), tested and verified to be working according to the designed specifications. The RRCs were after that calibrated following standard procedure.

8.1.1 Theoretical analysis of the 2.4 GHz rectangular resonant cavity design

Three Rectangular Resonant Cavities (RRCs) were modeled and simulated (figure 8.2) before they were fabricated (figure 8.4), but the analytical design of a 2.4 GHz RRC is given in this section. Depending on the cavity dimensions and the Electromagnetic boundary conditions, a different number of modes exist inside a cavity. For instance, consider a TE_{lmn} rectangular cavity (figure 8.1), its dimensions, and the integral number of half-waves and their directions of propagation as terminated by the walls of the cavity, the resonant frequency of a given mode is determined according to (8.1).

$$f_{lmn} = \frac{c}{2\sqrt{\mu_r \epsilon_r}} \sqrt{\left(\frac{l}{a}\right)^2 + \left(\frac{m}{b}\right)^2 + \left(\frac{n}{d}\right)^2} \tag{8.1}$$

Where l, m, n are the mode numbers *a*, *b* and *d* are the width, height, and the length of the rectangular cavity, respectively. *c* is the speed of light in free space, μ_0 is the permeability of free space and ε_0 is the permittivity of free space.

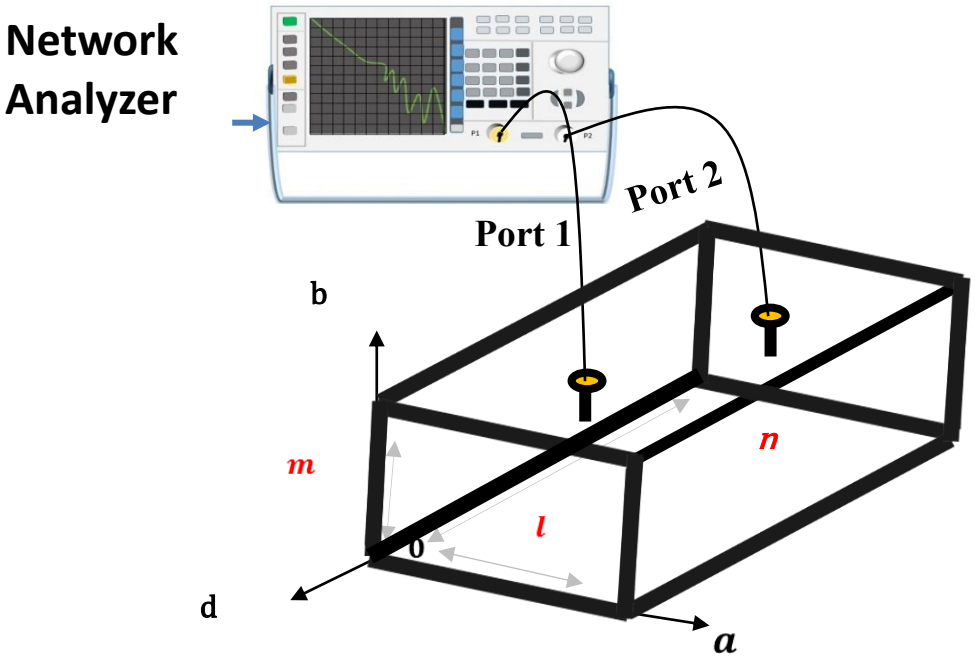

Figure 8.1: Schematic of the RRC connected to a Network Analyzer

Assuming the cavity rejects all other modes in the cavity except the fundamental mode TE_{101} and operates at 2.45 GHz, then the width of the cavity is determined by (8.2).

Width of the cavity (*a*)

$$a = \frac{c}{(2.45)\,10^9\sqrt{2}} \quad \frac{3\,x\,10^8}{(2.45)\,10^9\sqrt{2}} \qquad = 86mm \tag{8.2}$$

For $TE_{101} \rightarrow TE_{lmn}$, l represents the number of half-waves across the cavity. As indicated in the schematic of the cavity in figure 8.1, a is only one-half wavelength across the cavity (x-direction). The cutoff wavelength (λ_c) is given as (8.3):

$$\lambda_c = \frac{2}{\sqrt{\left(\frac{l}{a}\right)^2 + \left(\frac{m}{b}\right)^2}} \qquad \lambda_c = \frac{2}{\sqrt{\left(\frac{1}{86}\right)^2 + (0)}} \quad = 172mm \tag{8.3}$$

Height of the cavity (b)

The height of the cavity is given according to (8.4)

$$\frac{a}{b} = 2 \qquad b = 43mm \tag{8.4}$$

Similarly, for $TE_{101} \rightarrow TE_{lmn}$, m represents the number of half-waves from the top to the bottom of the cavity. In this case, m is zero.

Length of the cavity (d)

It is required that the following assumptions be met for the length of the rectangular cavity.

$$a > b \quad \text{and} \quad b < d \tag{8.5}$$

Therefore, the length of the rectangular cavity (d) was chosen to be 88mm. Where n accounts for the number of waves along the cavity. For $TE_{101} \rightarrow TE_{lmn,}$ n is just one and must be a positive integer. Hence, the resonant frequency of the fundamental (TE_{101}) mode operating in the 2.4 GHz cavity with the above dimensions is determined by (8.6).

$$f_{lmn} = \frac{c}{2\sqrt{\mu_r \epsilon_r}} \sqrt{\left(\frac{l}{a}\right)^2 + \left(\frac{m}{b}\right)^2 + \left(\frac{n}{d}\right)^2} \tag{8.6}$$

$$f_{(GHz)} = 150\sqrt{\left(\frac{1}{86}\right)^2 + (0) + \left(\frac{1}{88}\right)^2} = 2.4\ GHz$$

Since the resonant frequency of a particular mode must be higher than its cutoff frequency, the cutoff frequency (fc) of the first-order mode TE_{10} is determined by (8.6).

$$f_{c10} = \frac{c}{2\sqrt{\mu_r \epsilon_r}} \sqrt{\left(\frac{1}{a}\right)^2 + \left(\frac{1}{b}\right)^2} \tag{8.7}$$

$$f_{c10} = \quad 150\sqrt{\left(\frac{1}{86}\right)^2 + (0)} \quad = 1.7\ GHz$$

8.1.2 Cavity Modelling

The goal of the cavity modeling was to develop a model that would allow the cavity and its antenna dimensions to be optimised before the construction of the actual cavity. Given a resonant frequency, the physical dimensions of the cavity had to be large enough to contain the sample and include the antennas at the frequency of interest. It must also allow sufficient modes to be supported within the structure. As a result, the dimensions of the rectangular cavities were determined mainly by (8.2) to (8.5). Using the various building blocks available in the CST Microwave Studio, three rectangular cavities were modelled, as shown in figure 8.2. Brass material was chosen for the cavity and copper for the energy coupling device. To obtain the desired resonant frequency for each cavity, the length of the two monopole antennas built into the cavity lids for energy coupling into the RRCs

were varied and optimised. The cavities were designed to resonate around 1 GHz, 2.4 GHz and 5 GHz respectively.

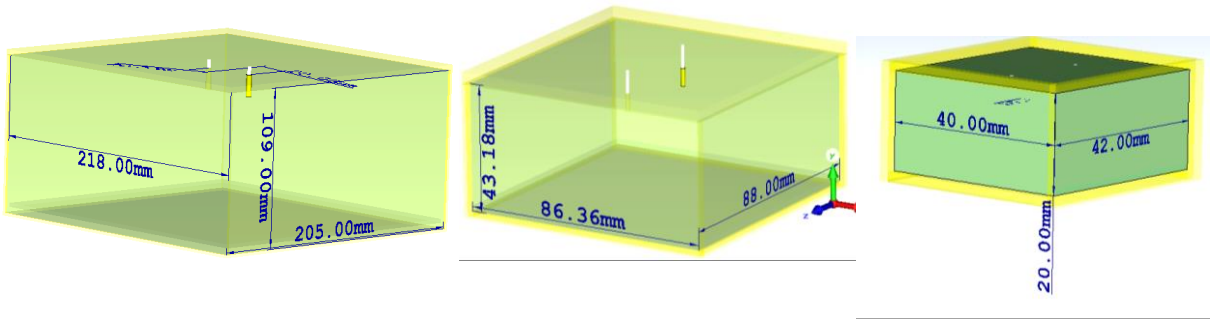

(a) (b) (c)

Figure 8.2: Simulated 1 GHz (a), 2.4 GHz (b) and 5 GHz (c) RRC

8.1.3 Material selection and the construction of the three resonant cavities

The Quality factor (Q-factor) of a resonant cavity defines the sharpness of its resonance curve against frequency. That is, it characterises the resonator's bandwidth relative to its centre frequency. It is a function of the conductivity of the inner surfaces of the cavity. High Q-factor is an indication of a low electrical loss of the cavity. To have a very sharp Q-factor, material such as Perfect Electrical Conductor (PEC) would be ideal for the construction of the cavity. However, in the absence of a PEC, metallic conductors such as copper, silver, aluminium, and brass are used. Copper and silver are expensive; aluminium is difficult to solder; brass material was chosen for the construction of the rectangular cavity. Brass has no soldering problem but has a lower electrical conductivity when compared to the electrical conductivities of aluminium, copper, and silver. The Q-factor of the cavities was enhanced by polishing the inside surfaces with a metal polish to remove any contamination that would be less conductive.

Before the cavity was modeled, thought was given to make the cavity lids as adaptable as possible. That is, to have a cavity lid with an aperture that will allow the sample to be fed through into the cavity (figure 8.3) or a completely covered lid that will allow the samples to be placed inside the cavity (figure 8.4). Moreover, the cavity lid (figure 8.3) that allows for the insertion of the samples has an aperture of a certain diameter depending on the measurement frequency. The diameter of the aperture was chosen to give a cutoff frequency of f_c as determined by (8.8) [147].

$$fc = \frac{c}{r.3.142} \tag{8.8}$$

where

c = Speed of light in a vacuum

r = Radius of the aperture

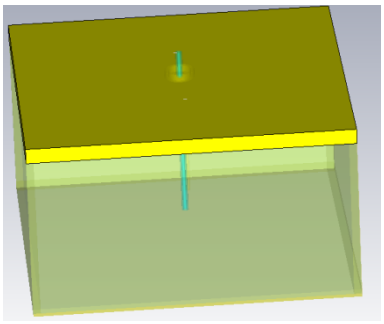

(a) Simulated RRC

(b) Fabricated RRC

Figure 8.3: Introduction of the DUT into the RRCs

(a)

(b)

(c)

Figure 8.4: Fabricated 1 GHz (a), 2.4 GHz (b) and 5 GHz (c) RRC

The volume of each RRC at room temperature was calculated from the cavity, inner width, length, and height, as shown in table 8.1. The measurements at room temperature assume the constant volume of the cavities.

Table 8.1: Volume of the three RRCs at near the room temperature

Room Temperature = 20^0C – 22^0C				
Resonant Frequencies	Width (*mm*)	Length (*mm*)	Height (*mm*)	Volume (mm^3)
1 GHz	205.00	218.00	109.00	487121
2.4 GHz	86.36	88.00	43.18	328154
5 GHz	40.00	42.00	20.00	33600

8.2 Requirements of the ASTM D2520-13 for the implementation of the CPM

The assessment of dielectric properties of different Ethernet cable dielectrics was performed using a method based on the Cavity Perturbation Method. However, for the successful implementation of the CPM, sample volume and placement, which are the two critical factors in achieving good precision of the measurements and accurate results were considered. The following section provides a detailed description of the samples used in this research.

8.2.1 Sample preparation for the material testing

The dielectrics under test (DUT) are the samples of materials extracted from the data grade cables. The dielectric samples were obtained from Category 5e U/UTP, standard Category 6 U/UTP, CMP Category 6 U/UTP, Category 6 F/UTP, Category 6A F/UTP, Category 6A F/FTP and Category 7A S/FTP cables respectively. Before the testing of the dielectrics, the twisted pair wires were separated and prepared for the material testing. Also, before measuring the materials as extruded dielectrics, the copper conductors were removed carefully from the insulated copper conductors. That is, the DUT is approximated to be rod-shaped. The active length of the DUT is the same as the inner height of the RRCs. The Ethernet cable dielectrics tested in this research are shown in figure 8.5.

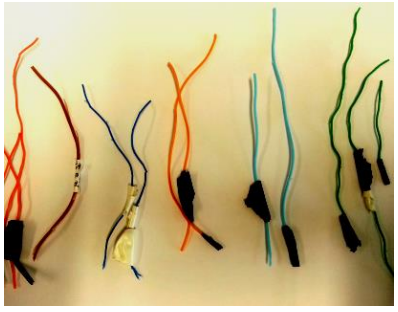

Figure 8.5: Dielectric rod samples obtained from data grade cables

8.2.2 Sample volume at room temperature and elevated room temperature

Different numbers of the dielectric samples were tested to assess the impact of the sample volume on the baseline ε_r of FEP and HDPE at an elevated room temperature of 25^0C and across three frequencies (1GHz, 2.4GHz and 5GHz). The volume of a single dielectric rod or multiple dielectric rods (figure 8.6) at room and the elevated temperature was calculated according to (8.9) and (8.10).

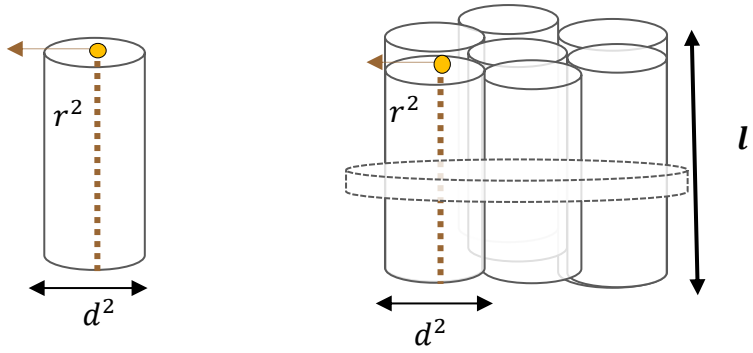

(a) (b)

Figure 8.6: Schematic, illustrating the dimensions of a tube (a) and a bundle of tubes (b)

$$V_{smax} = (V_{somax} * \left(1 + 3 * (\alpha * \Delta T)\right) * N \quad (8.9)$$

$$V_{smin} = \left(V_{somin} * \left(1 + 3 * (\alpha * \Delta T)\right) * N\right) \quad (8.10)$$

Where

V_{somax} = Initial maximum sample volume, considering the variations in the copper diameter and diameter over insulation.

V_{somin} = Initial minimum sample volume, considering the variations in the copper diameter and diameter over insulation.

V_{smax} = Maximum sample volume, considering ΔT

V_{smin} = Minimum sample volume, considering ΔT

ΔT = Difference in temperature between the room and the material temperature

α = Linear temperature expansion coefficient of the material

N = Number of tubes in a bundle

8.2.3 Verification of the accurate sample position inside the RRC

The primary requirement for accurate dielectric property measurements is to place the sample in a region of a uniform E-field inside the cavity. Before the testing of the dielectric samples was conducted, a region for the accurate dielectric property measurements was located inside the cavity, with the aid of a removable template shown in figure 8.7. The removable template was placed inside the cavity to obtain the resonance curves of a single PTFE rod; that was introduced into different locations inside the cavity.

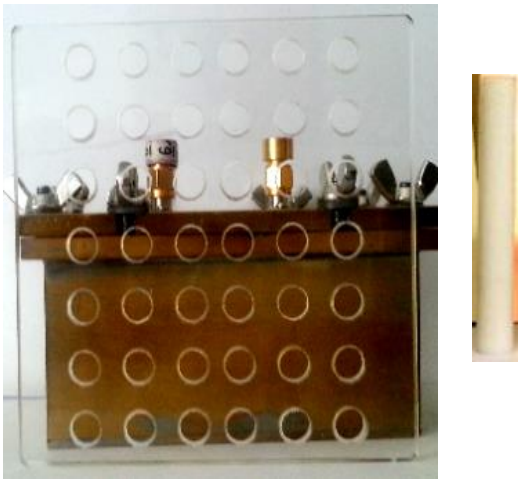

Figure 8.7: PTFE rod with the dielectric placeable template

A set of phase-preserving cables was connected in-between the RRC and the network analyser. Then, the calibration of the system was performed using the standard calibration kits (Rohde and Schwarz®) with short, open and match loads. After that, the resonances of the empty (unloaded) cavity were obtained first by measuring the Scattering parameter (S_{21}) of the unloaded RRC. Then, the resonance curves for the PTFE in all the locations were obtained one after the other, under approximately the same room temperature. The different resonances of the loaded cavity as a function of the PTFE's placement positions are shown in figure 8.8. As indicated, the resonance of the PTFE rod placed in the centre of the cavity appears to be the last; from the resonance of the unloaded cavity. That is, the resonance of the PTFE placed at the centre of the cavity experienced the highest frequency shift.

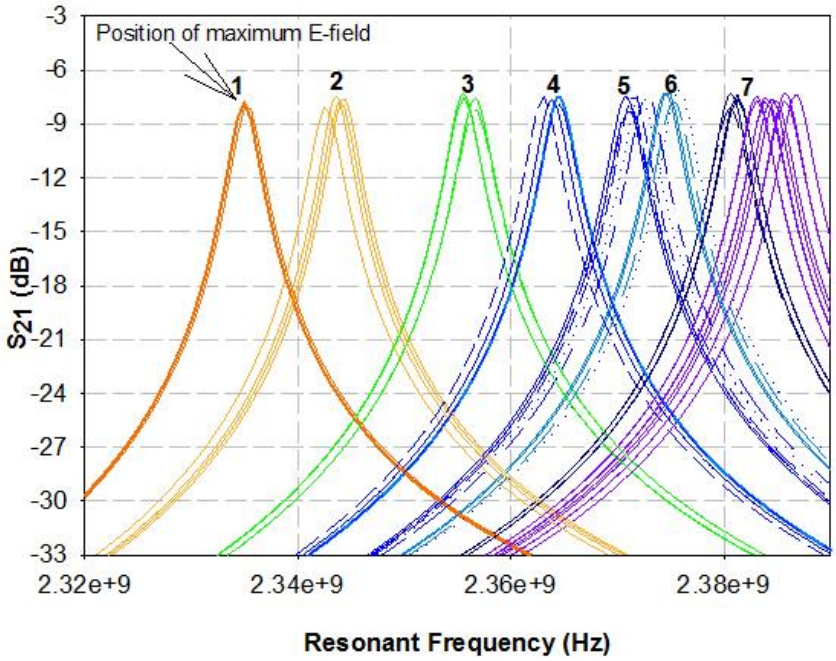

Figure 8.8: Resonances of a single PTFE placed in different positions in the fabricated RRC

Moreover, this accurate position was also verified by simulating each position inside the RRC with a single PTFE rod (Figure 8.9).

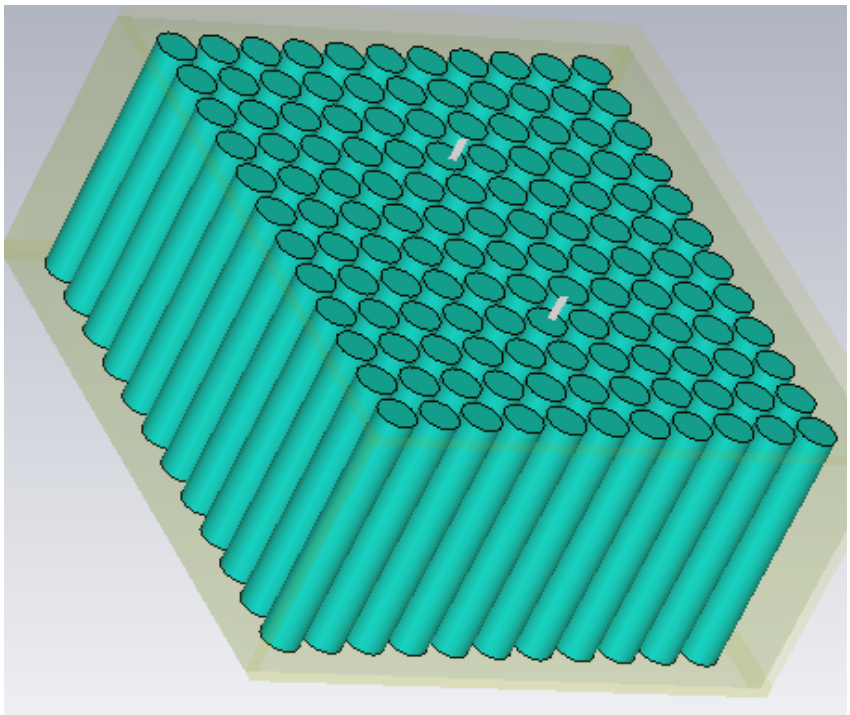

Figure 8.9: PTFE rod placed in different locations inside the simulated RRC

Using (8.11), the dielectric constant of the single PTFE in various locations inside the cavity was calculated. The ε_r obtained by measurements are shown in Figure 8.10, while that of the simulation is shown in Figure 8.11.

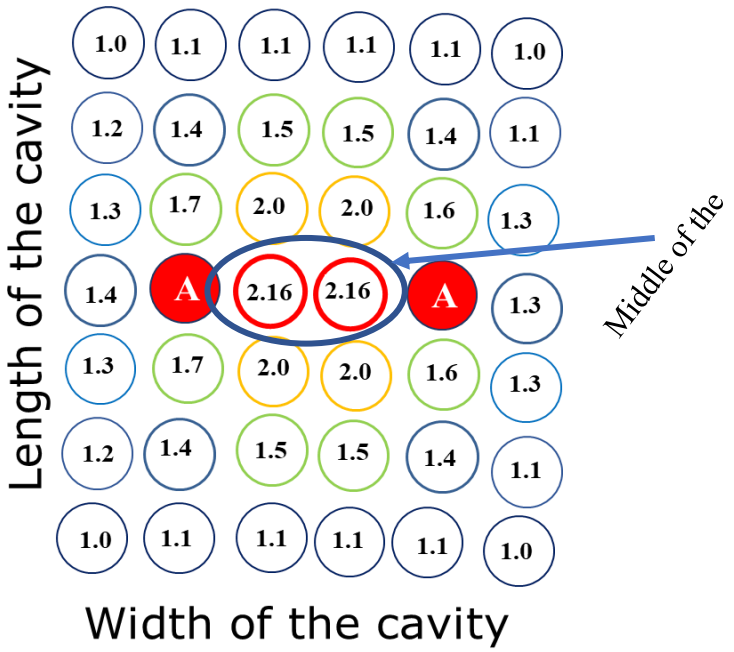

Figure 8.10: $\boldsymbol{\varepsilon_r}$ of the PTFE placed in different positions inside the fabricated cavity

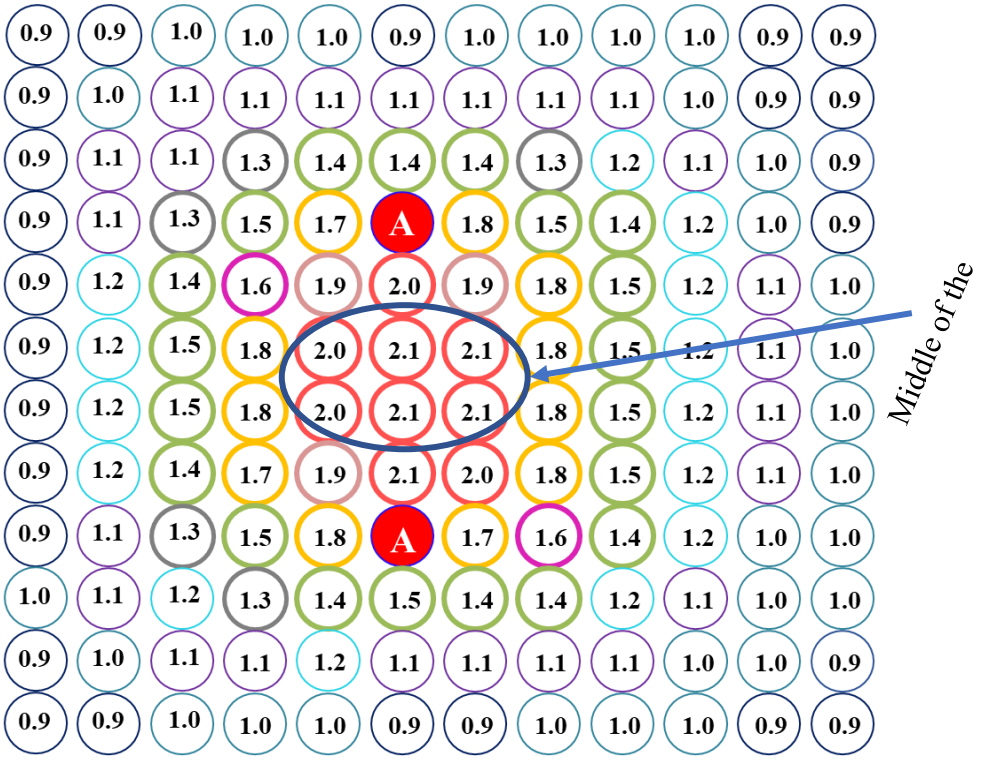

Figure 8.11: $\boldsymbol{\varepsilon_r}$ of the PTFE placed in different positions inside the simulated cavity

As indicated in figure 8.10 and 8.11, the highest and most accurate ε_r obtained for the PTFE rod at room temperature was 2.1 and 2.16. These values are in good agreement with the value (2.1) reported in the published literature [148]. However, the indication of these results is that the dielectric rod sample must be placed in about 90% of the maximum E-field to obtain an accurate value of ε_r.

To visualise the field distributions inside the cavity, the measured and simulated resonances of the PTFE rod as a function of the sample positions were plotted and shown in Figure 8.12. As shown, a very weak tangential component of the E-field was found near the surface of the brass material. However, the position of the maximum field obtained was at the centre of the cavity, in between the two antennas. This location was used for the sample placement throughout the measurements conducted in this study.

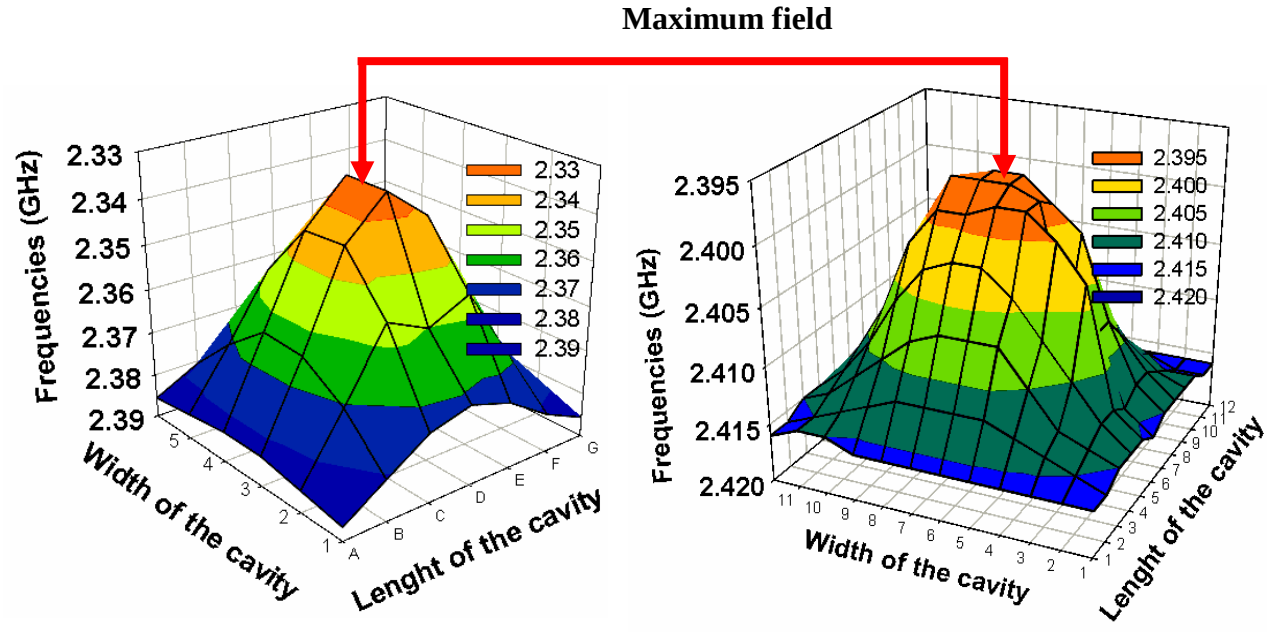

(a) (b)

Figure 8.12: Field distribution inside the fabricated (a) and simulated (b) RRCs

8.3 Assessment of dielectric properties of Ethernet cable dielectrics

8.3.1 Assessment of the baseline dielectric properties of Ethernet cable dielectrics

To assess the baseline, ε_r, of the FEP at 1GHz, 2.4GHz and 5GHz, at about the same room temperature and humidity, three network analysers (Rohde and Schwarz®) were set up in one area. In addition to the network analysers, the measurement setup consisted of a humidity meter and a temperature acquisition system. Two thermocouple sensors were used to monitor and record the room temperature whenever a set of dielectric type (1GHz, 2.4GHz and 5GHz samples) is tested across the three frequencies. However, to obtain the actual temperature of the DUT, three thermocouple sensors were placed around each cavity. One thermocouple sensor was connected to the lid of the cavity, one was connected beside the cavity, and the last one was placed underneath the cavity. Although the cavities have small apertures that allow the samples to be fed through, no thermocouple sensor was introduced into the cavity to measure the material temperature. This was to ensure that the perturbation on the E-field inside the cavities was mainly due to the introduction of the dielectrics. Hence, the average cavity temperature, obtained from the three thermocouple sensors placed around each cavity, is referred to as the material temperature in this study.

Measurements of the resonances of the loaded and unloaded cavities

To measure the scattering parameter (S_{21}) of the DUT, each of the dielectrics was inserted into the RRCs through an aperture one after the other, as shown in figure 8.13. The resonant curves of the samples were then obtained at 1GHz, 2.4GHz and 5GHz from the network analysers.

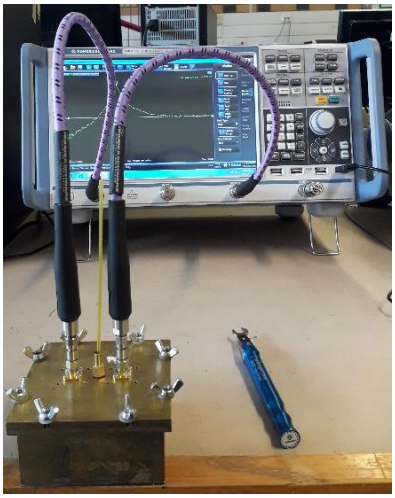

Figure 8.13: Measurement setup with a rectangular resonant cavity

Calculation of the ε_r for a rod sample

After the resonances of the loaded and unloaded cavities have been obtained at room temperature, the baseline, ε_r, for the DUT was calculated according to (8.11) and (8.12). The two equations eliminate two different types of error from the calculatedε_r. (1) It eliminates errors from the measured dimensions of the rod samples. (2) It eliminates systemic error or quantisation error from the shifts in the resonances of the loaded and unloaded cavity.

$$\varepsilon_{rmax} = \left(\frac{V_c}{2V_{smin}}\right) * \left(\frac{(f_c - f_s + \Delta f)}{(f_s - \Delta f)}\right) + 1 \tag{8.11}$$

$$\varepsilon_{rmin} = \left(\frac{V_c}{2V_{smax}}\right) * \left(\frac{(f_c - f_s - \Delta f)}{(f_s + \Delta f)}\right) + 1 \tag{8.12}$$

where

$\varepsilon_{\mathrm{rmax}}$ = Maximum relative permittivity (Dielectric constant)
$\varepsilon_{\mathrm{rmin}}$ = Minimum relative permittivity (Dielectric constant)
V_c = Volume of the cavity
f_c = Resonant frequency of the unloaded cavity
f_s = Resonant frequency of the loaded cavity
Δf = Frequency step size

Calculation of the dielectric loss for a rod sample

The dielectric loss was calculated using (8.13), (8.14) and (8.15) respectively.

$$L_{max} = \left(\frac{V_c}{4V_{smax}}\right) * \left(\frac{1}{Q_s} - \frac{1}{Q_c}\right) \tag{8.13}$$

$$L_{min} = \left(\frac{V_c}{4V_{smin}}\right) * \left(\frac{1}{Q_s} - \frac{1}{Q_c}\right) \quad (8.14)$$

$$\frac{1}{Q} = \frac{(f_{2\alpha} - f_{1\alpha})}{B * f} \quad or \ \frac{B_w}{B*f} \quad (8.15)$$

Where

$Q_c =$ Quality factor of the unloaded cavity

$Q_s =$ Quality factor of the loaded cavity

$Q \ = Q_s \ or \ Q_c$

$f \ =$ Resonant frequency of the loaded or unloaded cavity

$f_{2\alpha}$ = Frequency setting above resonant mode for the loaded or unloaded cavity

$f_{1\alpha}$ = Frequency setting below the resonant mode for the loaded or unloaded cavity

$B_w = (f_{2\alpha} - f_{1\alpha})$ Bandwidth at 6dB or 20dB points down the resonant frequency of the loaded or unloaded cavity

$B =$ Constant (which is either 1 or 3) at 6dB or 20dB points down the resonant frequency of the loaded or unloaded cavity

$L_{max} =$ Maximum dielectric loss of the sample

$L_{min} =$ Minimum dielectric loss of the sample

Calculation of $tan\delta$ for a rod sample

The loss tangent, or dissipation factor, is the ratio of the imaginary part of dielectric permittivity to the real part. The loss tangent was calculated according to (8.16) and (8.17).

$$tan\delta_{max} = \left(\frac{\varepsilon''}{\varepsilon'}\right) = \frac{L_{max}}{\varepsilon_{rmax}} \quad (8.16)$$

$$tan\delta_{min} = \left(\frac{\varepsilon''}{\varepsilon'}\right) = \frac{L_{min}}{\varepsilon_{rmin}} \quad (8.17)$$

Where

$\tan\delta_{max}$ = Maximum dissipation factor of the dielectric rod sample
$\tan\delta_{min}$ = Minimum dissipation factor of the dielectric rod sample

After the measurement of the cavity resonances, the baseline dielectric properties assessments started with the baseline dielectric constant (ε_r) of the CMP Category 6 U/UTP conductor insulation (FEP). This was examined at an elevated room temperature of 25^0C and 1 GHz, 2.4 GHz and 5 GHz (results are in section 9.1). After that, the baseline ε_r of HDPE and FEP at 5 GHz were examined for comparison purpose. This was followed by the assessment of the baseline dielectric properties of different Ethernet cabling dielectrics. As detailed below, the last study in this section examined the potential of using a dielectric measurement method based on CPM in assessing the baseline VF of different Ethernet cable dielectrics. For instance, the VF of the Category 6A F/UTP and Category 6 U/UTP conductor insulation verified.

The verification of the VF of Category 6A F/UTP and Category 6 U/UTP conductor insulation started by examining the baseline ε_r of the dielectric rods extracted from the two cables. After that, the values of the VF were calculated using 8.18.

$$VF = \frac{1}{\sqrt{\varepsilon_r}} \tag{8.18}$$

However, since the electrical distance (length) and the propagation time of the signal passing through the PLs are obtainable from the cable Analyzer, the propagation speed and VF were calculated from the measured data using (8.19) and (8.20).

$$propagation\ speed = \frac{Length}{propagation\ delay} \tag{8.19}$$

$$VF\ or\ NVP = \frac{propagation\ speed}{speed\ of\ light\ in\ a\ vacuum} \tag{8.20}$$

Where

Propagation delay = propagation time for the signal to be transmitted and received
Length = electrical length of the signal on a twisted pair
c = speed of light in a vacuum

The calculated VF from the measured characteristics of the line was verified with the calculated VF obtained from the baseline ε_r of the dielectric rod extracted from Category 6A F/UTP cable first, then, with the VF reported in the datasheet of the cables. The results of this section are detailed in section 9.1.3 and 9.1.4.

8.4 Assessment of ε_r of FEP at 2.4 GHz and 5 GHz with the temperature of ~65^{0}C

The first assessment in this section examines the immediate effects of an increase in temperature to 65^{0}C and a continuous 30-day heating cycle on the ε_r of FEP at 2.4 and 5 GHz. After that, the drifts in the $\boldsymbol{\varepsilon_r}$ and $\mathbf{tan\delta}$ of FEP at 2.4 GHz as functions of intermittent and prolonged thermal cycling were examined. The rationale for the constant heating of the sample without cooling was to differentiate the immediate effects of temperature from the long-term effects of heating on the dielectric properties of the FEP sample across two frequencies. However, since the drifts in the transmission parameters of the CMP Category 6 U/UTP PL have been established in chapter 7 based on the effects of intermittent and prolonged thermal cycling, the extracted dielectric sample of the cable was also examined in a like manner in this section to establish correlations between the drifts in the cable performance and its dielectric properties.

8.4.1 Assessment of ε_r of FEP at 2.4 and 5 GHz based on constant heating of ~65^{0}C

Two fresh FEP samples obtained from a Category 6 U/UTP cable were continuously heated in two separate ovens for 30 days without cooling. However, for the heating of the samples, the temperature setting on the ovens was slightly above 60^{0}C to compensate for the temperature loss due to the small openings on the ovens, but the maximum material temperature was ensured to be below 65^{0}C. The maximum peak temperature of the sample was obtained and recorded every day using thermocouple sensors attached to the resonant cavities. Also, the resonances of the loaded and unloaded cavities were manually obtained separately for the calculation of the Q-factor,

bandwidth and ε_r during the constant heating of the FEP. Figure 8.14 shows the temperature profile for the loaded 2.4 GHz cavity. It can be observed from the temperature profile that the fluctuations in the environmental temperature had an influence on the oven temperature and that the influence was not the same for the 5 GHz material testing because the two sets of tests were not started on the same day.

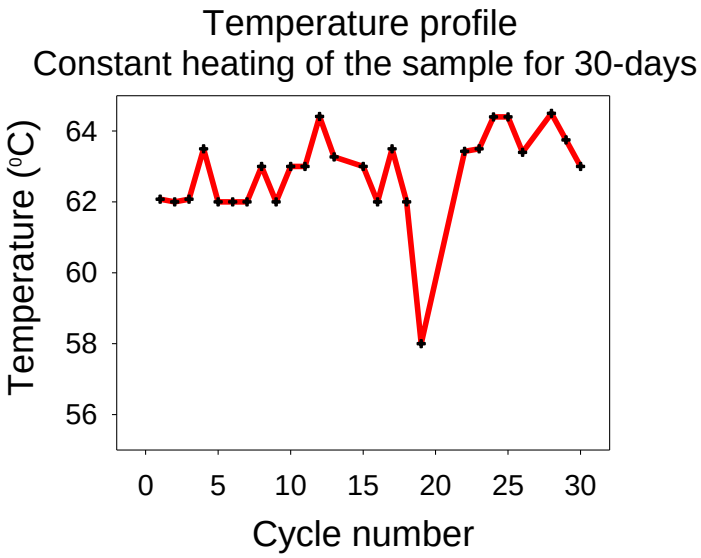

Figure 8.14: Temperature profile for the constant heating of the FEP sample

8.4.2 Assessment of dielectric properties of FEP at 2.4 GHz based on thermal cycling

This section evaluates the dielectric properties of FEP rod sample based on the effects of intermittent and prolonged thermal cycling at 2.4 GHz. Firstly, ten intermittent (daily) thermal cycles were performed, followed by three consecutive prolonged (weekly) thermal cycles. For both daily and weekly thermal cycles, the FEP sample was heated from the room temperature up to a set limit, which is ~65^{0}C. However, when the temperature on the material reaches the maximum set limit, the oven control stays on to maintain the temperature set-point until the oven is manually turned off. For each of the daily thermal cycles, the sample was heated for ~ 500 minutes and cooled naturally for ~1000 minutes. However, for the weekly thermal cycles, the sample which had been heated and cooled repeatedly ten times was further subjected to a heating period of 7000 minutes and natural cooling of ~ 3000 minutes. The temperature profile for one of the daily and weekly thermal cycles is shown in figure 8.15. It should be noted that the material

properties were monitored as the temperature of the material was rising to the peak temperature, and when the temperature on the material was cooling to the room temperature. That is, the measurements of the material properties were in synchronisation with the material temperature by controlling the Vector Network Analyzer and temperature logger using SCPI commands. The results of the study in this section are presented in section 9.3.

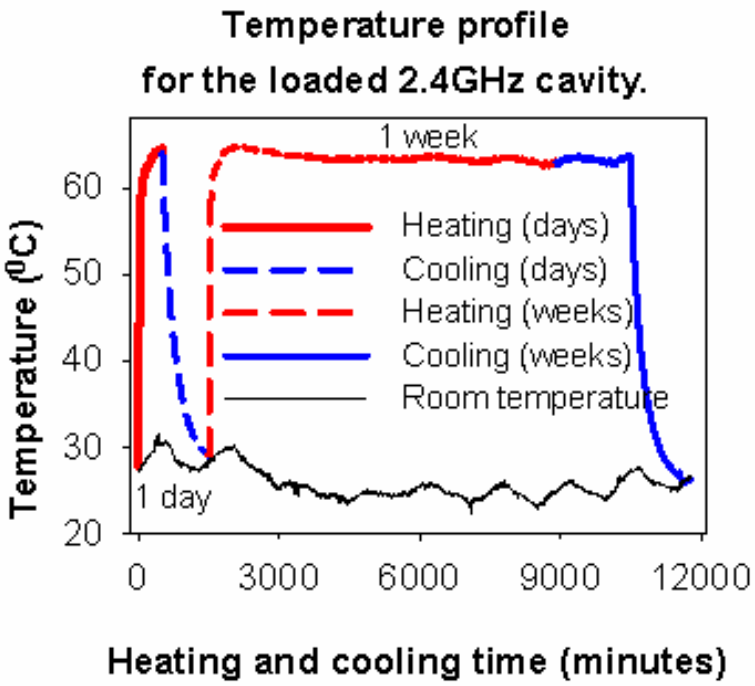

Figure 8.15: Temperature profile for one of the intermittent and prolonged thermal cycles

The volume of the loaded and unloaded cavities used for the calculation of the baseline material properties in section 8.3.1 was different from the volume used for the calculations of dielectric properties with temperature. This is because all materials expand with an increase in temperature. It was assumed that the empty cavities would expand equally in all directions (isometrically) in response to a change in temperature. Therefore, the coefficient of the thermal expansion for a fractional change in the volume of a brass material ($57\,x\,10^{-6}\,K^{-1}$) [149] was taken into consideration. The volume expansion coefficient (α_c) was input into (8.21) for the calculation of the volume of the cavities due to the effect of temperature.

$$V_{cT} = V_c\,(1 + 3\alpha_c(\Delta T)) \tag{8.21}$$

Where

V_{cT} = Volume of the RRCs due to an increased temperature

V_c = Volume of the RRCs at room temperature

α = Volume temperature expansion coefficient of brass

ΔT = Change in temperature

Similarly, the vast majority of dielectrics expand in response to temperature increase. An assumption made in this study is that the dielectrics have a constant diameter along the length. This is because any change in the inner diameter of the DUT will be challenging to determine as the dielectric heats up. Also, the proportional change in diameter of the DUT with temperature in the range of $+20^0$C - 65^0C is minimal. Hence, the linear thermal expansion coefficients (α) of the solid and foamed dielectrics used are $13.5\,x\,10^{-5}\,{}^0C^{-1}$ and $12\,x\,10^{-5}\,{}^0C^{-1}$ respectively [150, 151]. These coefficients were input into (8.9) and (8.10) to calculate the new volume of the DUT at different temperatures.

CHAPTER 9 - DIELECTRIC MEASUREMENT RESULTS

In this chapter, the baseline dielectric constant (ε_r) of the Category 6 U/UTP CMP cable conductor insulation (FEP) at an elevated room temperature of 25^0C and 1 GHz, 2.4 GHz and 5 GHz are presented first. After that, comparisons between the baseline ε_r of the HDPE and FEP at 5 GHz are made. This is followed by the assessment of the baseline dielectric properties of different Ethernet cabling dielectrics. The last results in section 9.1 demonstrate the impact of using an incorrect cable type for the testing of the PL length. It also demonstrates the potential of using a method based on Cavity Perturbation Method (CPM) in validating the Velocity Factor (VF) supplied by the cable manufacturers for Ethernet cable dielectrics. In section 9.2, the immediate effects of temperature (65^0C) and a continuous 30-day heating cycle on the ε_r of FEP at 2.4 and 5 GHz are presented. The last set of results in this chapter (section 9.3) presents the drifts in the $\boldsymbol{\varepsilon_r}$ and $\mathbf{tan}\boldsymbol{\delta}$ of FEP at 2.4 GHz as functions of intermittent and prolonged thermal cycling and drawn correlations between the drifts in the cable performance and its dielectric properties as functions of intermittent and prolonged thermal cycling. Note that the upper frequencies used in the measurements of the dielectric properties are significantly outside the current maximum operational frequency of the current cables. However, the results obtained using the three RRCs help to build a picture of the dielectric behaviour at extended frequencies.

9.1 Results of the assessment of the baseline dielectric properties

9.1.1 Baseline dielectric constant of Ethernet cable dielectrics

The baseline ε_r of FEP at an elevated room temperature of 25^0C and at 1GHz, 2.4 GHz and 5GHz are presented in table 9.1. However, table 9.2 shows the comparisons between the baseline ε_r of the standard Category 6 U/UTP dielectric (HDPE) and that of the CMP Category 6 U/UTP conductor insulation (FEP) at 5 GHz and elevated room temperature.

It was noted that the ε_r of the FEP under test was in good agreement with the published ε_r of FEP (table 9.1), Also, as noticeable in the table, the ε_r of FEP remained consistent across the three frequencies at room temperature. The reason for the consistency in the ε_r is based on the low loss and non-dispersive nature of the FEP sample under study.

Table 9.1: Baseline $\boldsymbol{\varepsilon_r}$ of FEP at 25^0C and at 1GHz, 2.4GHz and 5GHz.

Dielectric constant of FEP at 25^0C (Humidity = 36%)						
Number of tubes	$\boldsymbol{\varepsilon_r}$ (1 GHz)	±	$\boldsymbol{\varepsilon_r}$ (2.4 GHz)	±	$\boldsymbol{\varepsilon_r}$ (5 GHz)	±
1	2.01	0.27	1.96	0.03	2.06	0.04
2	1.98	0.14	2.03	0.03	2.06	0.03
3	2.03	0.10	2.05	0.03	2.03	0.03
4	2.03	0.08	2.04	0.02	2.10	0.03
5	2.05 [99]	0.07	2.04	0.02	2.03	0.02

Also, comparing the ε_r of FEP and HDPE at room temperature and at 5 GHz, it was found that the ε_r of FEP was lower than that of the HDPE. Furthermore, it is shown in table 9.2 that the ε_r of FEP was more stable across the configurations used for the volume of the sample (number of tubes tested).

Table 9.2: Comparison between the $\boldsymbol{\varepsilon_r}$ of FEP and HDPE at 5 GHz

Comparison between the $\boldsymbol{\varepsilon_r}$ of FEP and HDPE at 5 GHz				
Number of tubes	$\boldsymbol{\varepsilon_r}$ of FEP (5 GHz)	±	$\boldsymbol{\varepsilon_r}$ of HDPE (5 GHz)	±
1	2.06	0.04	2.23	0.04
2	2.06	0.03	2.36	0.03
3	2.03	0.03	1.96	0.02
4	2.10	0.03	2.06	0.02
5	2.03	0.02	2.11	0.03

9.1.2 Baseline dielectric properties of the extracted dielectric samples

The summary of the baseline dielectric properties of different Ethernet cable dielectrics is presented in table 9.3. As stated in the table, the calculated values of the VF for all the cables agree with the values of the VF supplied by different manufacturers of Ethernet cable with a difference of 1 – 4%. Also, the $\boldsymbol{\varepsilon_r}$ obtained for the foamed dielectrics was found to be lower when compared to the $\boldsymbol{\varepsilon_r}$ obtained for the solid dielectric materials. Lastly, the $\boldsymbol{\varepsilon_r}$ obtained for the foamed dielectrics was found to be between 1.64 and 1.70 at room temperature and at 2.4 GHz, which suggests that the VF for the two foamed dielectrics will be in the range of 77% - 80% of the speed of light in a vacuum.

Table 9.3: Baseline dielectric properties of the extracted dielectric rods at 2.4 GHz

					Calculated	Manufacturer	VF
Cable Types	**Room Temperature**	**ε'**	**ε"**	**tanδ**	**VF**	**VF**	**Difference (%)**
	^{o}C						
Category 7A S/FTP Foamed material	23.3	1.64	0.000584	0.000357	0.78	0.82	4
Category 6A F/UTP. Solid	25.8	2.12	0.001046	0.000492	0.69	0.70	1
Category 6A F/FTP Foamed **Polyethylene**	26.0	1.70	0.000649	0.000382	0.77	0.76	1
Category 5e U/UTP Polyethylene	25.0	1.93	0.000861	0.000446	0.72	0.72	0
Category 6 U/UTP	27.8	2.06	0.000982	0.000477	0.70	0.69	1
Category 6 F/UTP	27.8	1.93	0.000864	0.000447	0.72	0.72	0

9.1.3 Validation of the extracted baseline ε_r and VF of Cat 6A F/UTP dielectric

Table 9.4 presents the baseline dielectric properties of the extracted Category 6A F/UTP conductor insulation. Also, in table 9.5, the VF reported by the cable manufacturer for the Category 6A F/UTP cable under study is compared with the VF calculated from the ε_r obtained with the CPM first and then, with the calculated VF from the measured electrical characteristics of the PL.

Table 9.4: Baseline dielectric properties of the Category 6A F/UTP conductor insulation

Baseline dielectric properties of a dielectric rod extracted from Category 6A F/UTP cable		
Results obtained from a method based on Cavity Perturbation Method (CPM)		
Frequency = 2.4GHz Temperature = 22.8^{0}C Humidity = 52%		
Dielectric Constant	Dielectric Loss	Loss Tangent
ε_r	ε''	Tan δ $\left(\frac{\varepsilon''}{\varepsilon'}\right)$
2.0438	0.00064	0.00031

Table 9.5: Comparisons of the VF of Cat 6A cable (manufacturer's data vs measured data)

Comparisons between the VF reported by the cable manufacturer, the VF calculated from the ε_r using CPM and the one extracted from the measured electrical properties of the line.				
	Manufacturer's data TIA Cat 6A perm link (+All)	Manufacturer's data ISO11801 PL2 Class Ea (+All)	CPM	Extracted from the line properties
ε_r	2.0407	2.0407	2.0438	2.098
VF	70 %	**70 %**	**69.95 %**	69.04 %

From table 9.5, the baseline VF supplied by the cable manufacturer is in good agreement with the calculated VF from the ε_r obtained using the CPM. The 0.05% difference in the values of the VF could be due to the fact that the extracted dielectric rod was tested at a frequency (2.4 GHz) which is significantly higher than the maximum operating frequency of the cable. Also, given the tolerance in the measurement results in table 9.5, it can be argued that the two values of the ε_r agree.

Furthermore, a difference of 0.96% in the values of the VF was recorded when the VF supplied by the cable manufacturer is compared with VF extracted from the measured electrical properties of the cable itself. The reason for this difference is because VF is also a function of the line geometry (Capacitance and Inductance). That is, it depends on the variation in the twist rate of the twisted pairs. If the heating and cooling of the cable change the twisting of the cable, part of the propagating wave will be in the air; hence, the effective ε_r will be lower.

9.1.4 Validation of the extracted baseline ε_r and VF of Cat 6 U/UTP CMP dielectric

From table 9.6, the baseline VF extracted from the measured electrical properties of the Category 6 U/UTP CMP PL agrees with the VF (NVP) supplied by the cable manufacturer when the correct cable type (CMP Category 6 U/UTP) was selected from the cable analyser memory. As stated in the table, VF of 72.1% was obtained when the correct cable type was selected with both the TIA and ISO/IEC test limits. With the correct cable type selection, it was found that the calculated VF from the ε_r obtained using a method based on CPM and that which was obtained from the line characteristics were in agreement with the VF supplied by the cable manufacturer but with the deviations of 1 and 0.04%. However, using the standard Category 6 U/UTP instead of the actual cable type (Category 6 U/UTP CMP) in testing the PL, VF of 69 % was obtained from the cable analyser. The 69 % gave a deviation of 2.1 and 3.1 % from the values of the VF calculated from

the ε_r obtained using a method based on CPM and that which was obtained from the measured line characteristics.

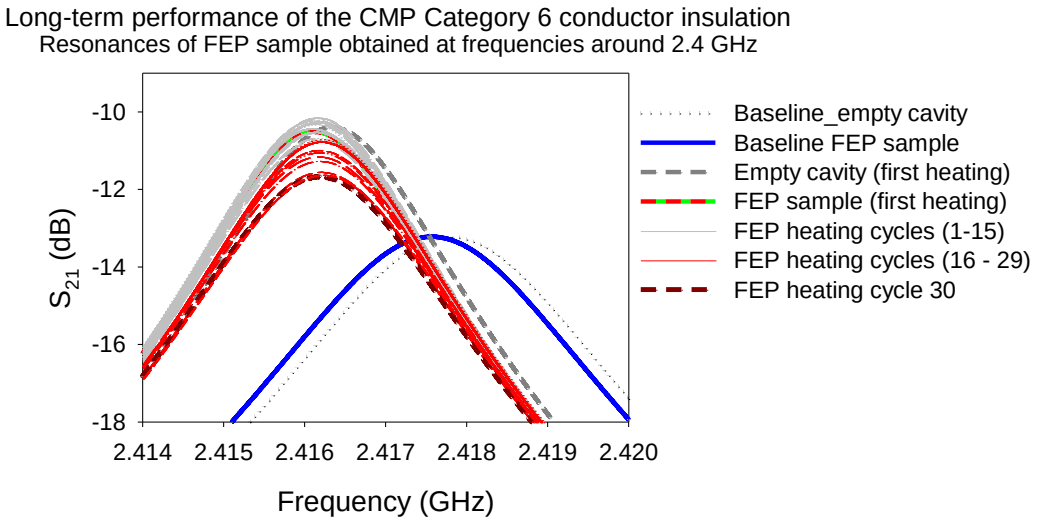

Figure 9.1: Resonances of the FEP at frequencies around 2.4 GHz

Table 9.6: Comparison of VF of Cat 6 insulation (manufacturer's data vs measured data)

Comparison between the VF reported by the cable manufacturer, the VF calculated from the ε_r using CPM and the one calculated from the measured electrical properties of the line.					
	Manufacturer's data TIA Cat 6 perm link (+All)	Manufacturer's data ISO11801 PL Class E (+All)	Manufacturer's data ISO11801 PL Class E (+All) **Standard Cat 6 U/UTP**	CPM	Extracted from the line properties
ε_r	1.924	1.924	**2.1**	1.98	1.926
VF	72.1 %	72.1 %	**69 %**	71.1 %	72.06 %

9.2 Immediate effects of temperature and prolonged heating on the ε_r of FEP

The immediate effects of temperature and continuous heating without cooling on the ε_r of FEP at 2.4 and 5 GHz are presented in this section.

9.2.1 Immediate effects of temperature on the performance of FEP at 2.4 GHz

The immediate effects of an increase in temperature and continuous heating on the ε_r of FEP at 2.4 GHz and the temperature around 65^0C are presented in this section. Figure 9.1 shows the resonances of the loaded and unloaded 2.4 GHz cavities that were obtained during the 30-day constant heating, whereas figure 9.2 shows the maximum peaks in the S_{21}-magnitude data.

As depicted in figure 9.1, it is apparent that the introduction of the FEP sample into the cavity caused the resonant frequency shifts of the loaded cavity to below the resonance of the unloaded cavity, as expected. Moreover, figure 9.2 shows an immediate frequency shift of 1.43 MHz in the resonance of the loaded cavity to below the resonance of the unloaded cavity during the first-day heating of the sample. After the first heating, the resonance of the loaded cavity shifted slightly up by 1.234 MHz. Furthermore, it was observed that the third day heating of the sample caused the highest frequency shift of 1.507 MHz and after the third-day heating, the resonant frequency shift was ~1.4 MHz, and that continued to change slightly, up to the last day heating of the material.

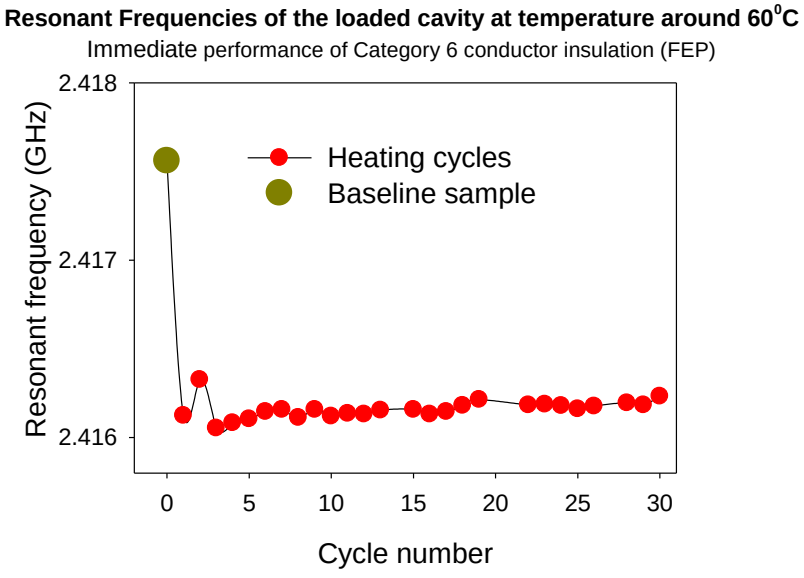

Figure 9.2: Peak frequencies in the resonance shifts of the loaded cavity around 2.4 GHz

An immediate increase in the magnitude of the S_{21} was measured during the first-day heating of the sample (figure 9.3). As can be observed, the magnitude of the S_{21} continued to increase up to the 7^{th}-day heating before decreasing. The immediate increase in the magnitude of the S_{21} implies

that the loaded cavity was less damped initially because of the low loss nature of the FEP sample and this is evident in the Quality factor of the loaded cavity (figure 9.4).

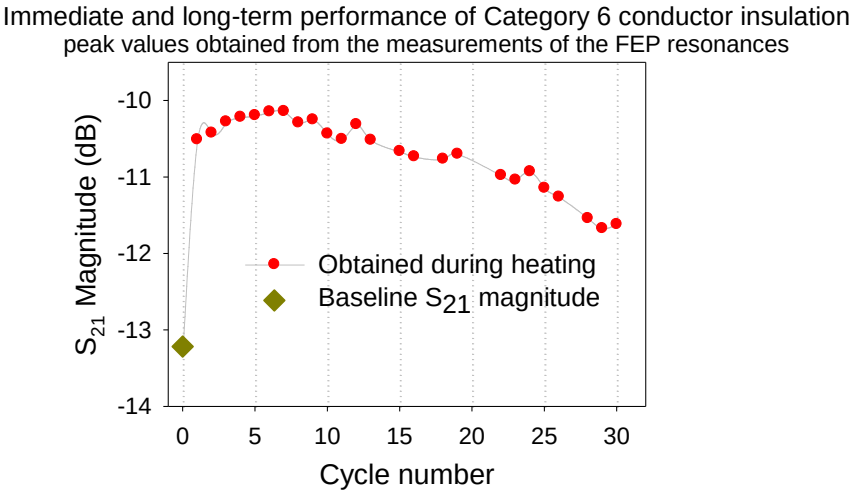

Figure 9.3: Maximum peaks in the S_{21}-magnitude data around 2.4 GHz

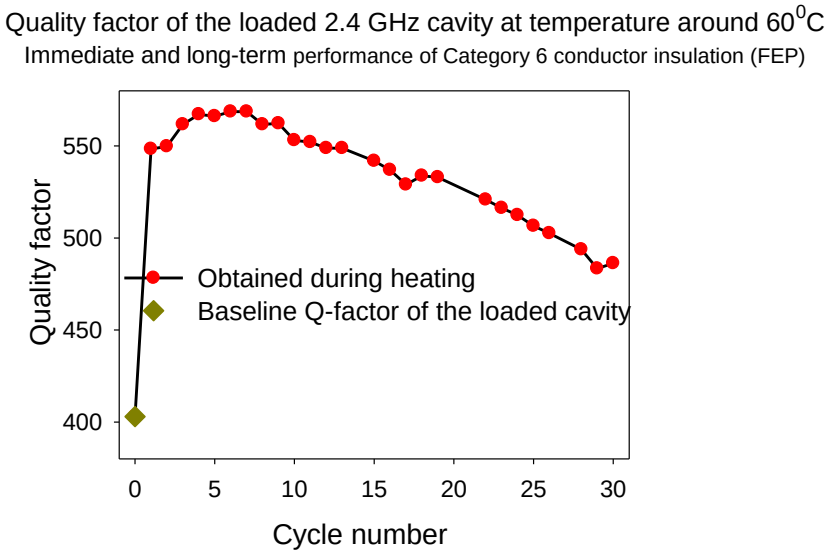

Figure 9.4: The Quality factor of the loaded cavity at frequencies around 2.4 GHz

Moreover, as the FEP sample becomes lossy after the 7th day heating, the magnitude of the S_{21} and the Quality factor of the loaded cavity began to decrease progressively (increase in insertion

loss) up to the last heating of the sample. As can be expected, a decrease in the loaded Q-factor implies that the bandwidth of the loaded cavity will increase (figure 9.5).

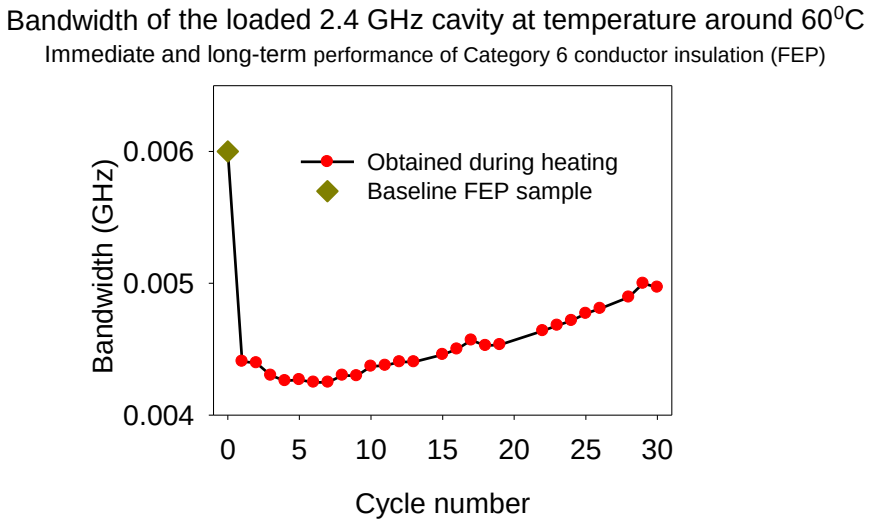

Figure 9.5: Bandwidth of the loaded cavity at frequencies around 2.4 GHz

The ε_r of FEP at 2.4 GHz based on the 30-day constant heating is presented in figure 9.6. It can be observed that the ε_r of FEP decreased during the first- and second-day heating of the sample. Moreover, as previously observed in figure 9.2, the third day heating of the sample caused the highest resonant frequency shift, and that is also evident in figure 9.6. That is, the third day heating of the sample caused the observed highest ε_r. Moreover, after the third day of heating, a progressive decrease in the values of the ε_r could be seen, as in figure 9.6.

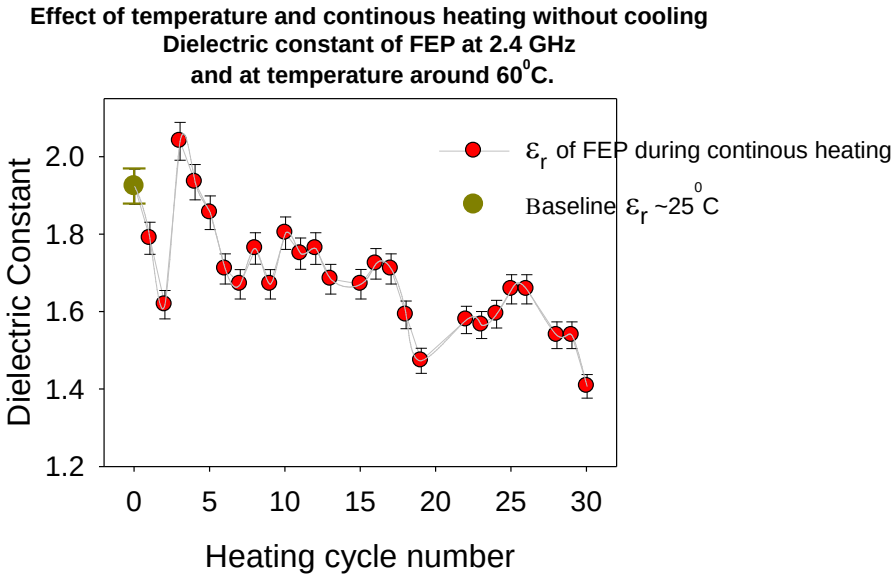

Figure 9.6: Effect of temperature and prolonged constant heating on the $\boldsymbol{\varepsilon_r}$ of FEP at 2.4 GHz

9.2.2 Immediate effects of temperature on the performance of FEP at 5 GHz

Figure 9.7 presents the maximum peaks in the resonance frequency shifts of the loaded cavity around 5 GHz, while figure 9.8 presents the S21 magnitude peaks. Similar to the behaviour of the sample at 2.4 GHz (figure 9.2), an immediate resonant frequency shift of 3.6 MHz was measured during the first-day heating of the sample. However, the second and third heating of the sample caused the highest frequency shift of 4.425 MHz to below the resonance of the unloaded cavity. After the third day heating, it was observed that the resonant frequency shift was relatively constant at 4.425 MHz up to the last day measurement.

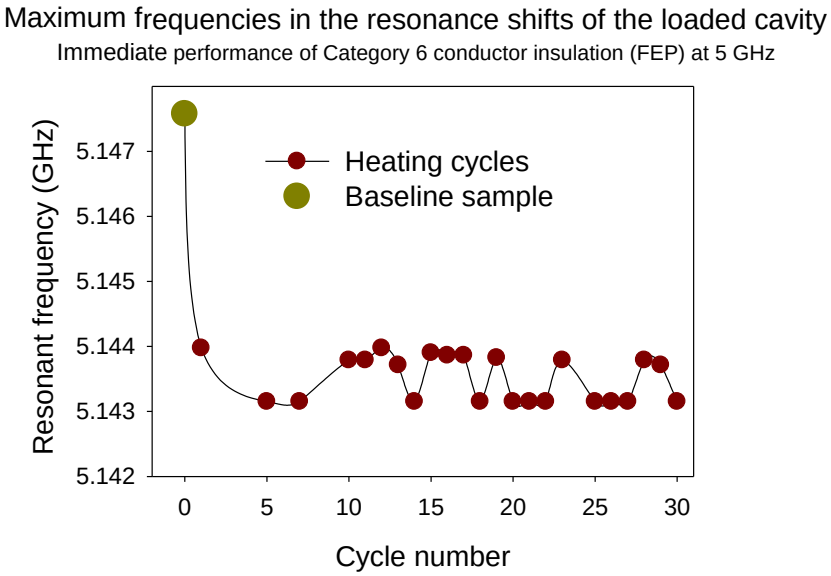

Figure 9.7: Peak frequencies in the resonance shifts of the loaded cavity around 5 GHz

An immediate reduction (increase in insertion loss) in the magnitude of the S_{21} was observed during the first day heating of the sample (figure 9.8). After the first day heating, insertion loss increased further and that brought about the changes to the overall profile of the sample for the 30-day heating of the sample. That is, after the first few days of the heating of the sample without cooling, the performance of the FEP sample remained relatively constant.

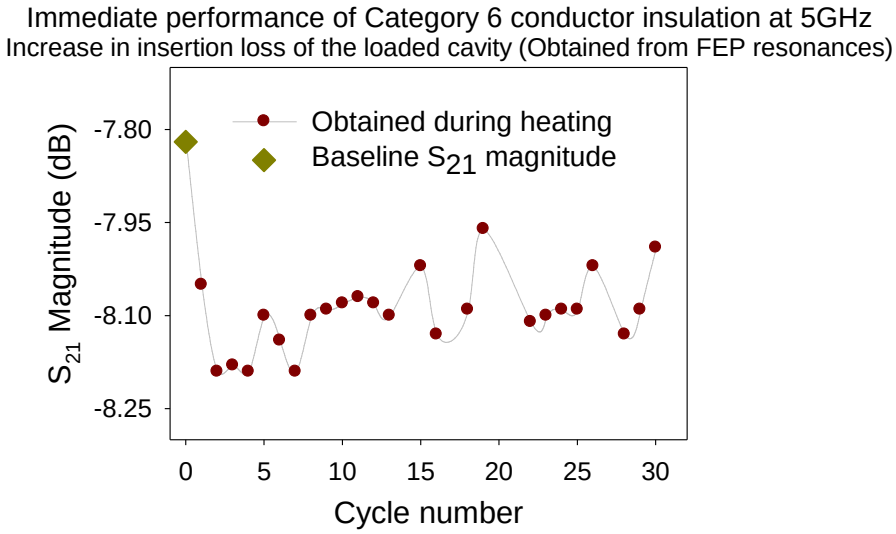

Figure 9.8: Maximum peaks in the S_{21}-magnitude data around 5GHz

It can be observed in figure 9.9 that the Q-factor of the loaded cavity decreased immediately due to the first heating of the sample and decreased permanently afterwards.

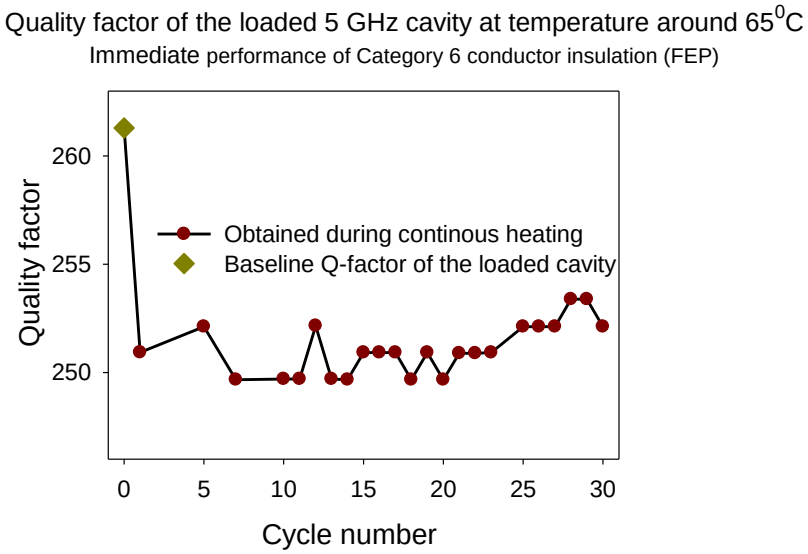

Figure 9.9: The Quality factor of the loaded cavity at frequencies around 5 GHz

Moreover, low Q-factor indicates high electrical loss of the cavity and that of the FEP sample. Also, a decrease in the loaded Q-factor implies an increase in the bandwidth of the loaded cavity (figure 9.10).

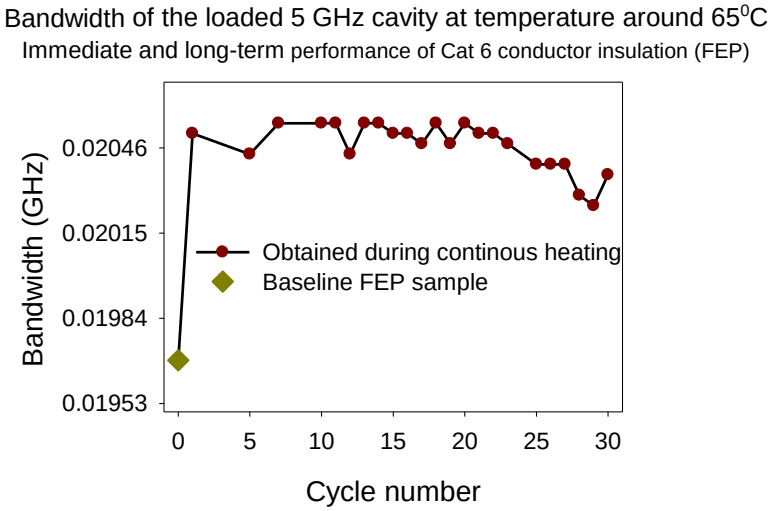

Figure 9.10: Bandwidth of the loaded cavity at frequencies around 5 GHz

The calculated ε_r of FEP at 5 GHz based on the 30-day constant heating are plotted in figure 9.11. As shown, the effect of temperature initially caused the ε_r of FEP to decrease during the first day heating of the sample. Moreover, after the first-day heating, ε_r increased during the second and third-day heating and then decreased and increased permanently.

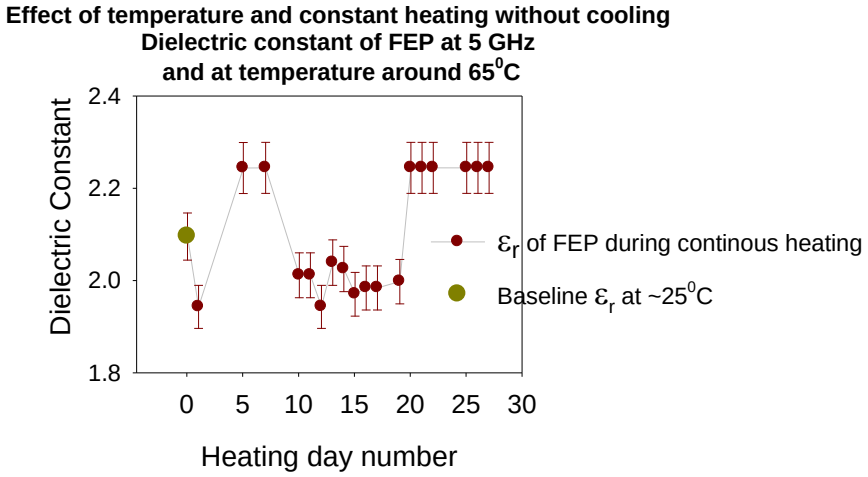

Figure 9.11: Effect of temperature and prolonged constant heating on the $\boldsymbol{\varepsilon_r}$ of FEP at 5 GHz

9.3 Effects of thermal cycling and prolonged heating on the dielectric properties of FEP

The effects of thermal cycling and prolonged heating on the dielectric properties of FEP sample at 2.4 GHz are presented in this section. As discussed in chapter 5, the rationale for the study in this section is to:

(i) observe the effects of intermittent and prolonged thermal cycling on the behaviour of a dielectric rod (FEP sample) extracted from Category 6 U/UTP CMP cable and

(ii) correlate the observed behaviour of the cable itself to the behaviour of its dielectric.

Figure 9.12 and 9.13 present the resonances and bandwidths of the loaded and unloaded cavity at 2.4 GHz during the intermittent heating and cooling (initial ten thermal cycles) of the FEP sample. As presented in figure 9.12, it is apparent that the resonances of the FEP sample shifted more to the lower frequencies due to the cooling of the sample when compared to resonances measured during heating. Furthermore, as observed in figure 9.2, the distinct resonance of the

FEP sample during the third heating of the sample is also evident in figure 9.12. More also, as can be seen, the fifth heating of the FEP sample caused the resonance of the sample to shift above all other resonance curves. It is worth noting that this behaviour of the FEP sample during the fifth heating of the cable is related to the spurious resonance observed in the RL performance of its cable (figure 7.33), where the first performance failure of the cable occurred. Although not shown in figure 9.12, another observation in the resonances of the loaded cavity was a spurious resonance that was measured during the transition between the intermittent heating and prolonged heating of the sample.

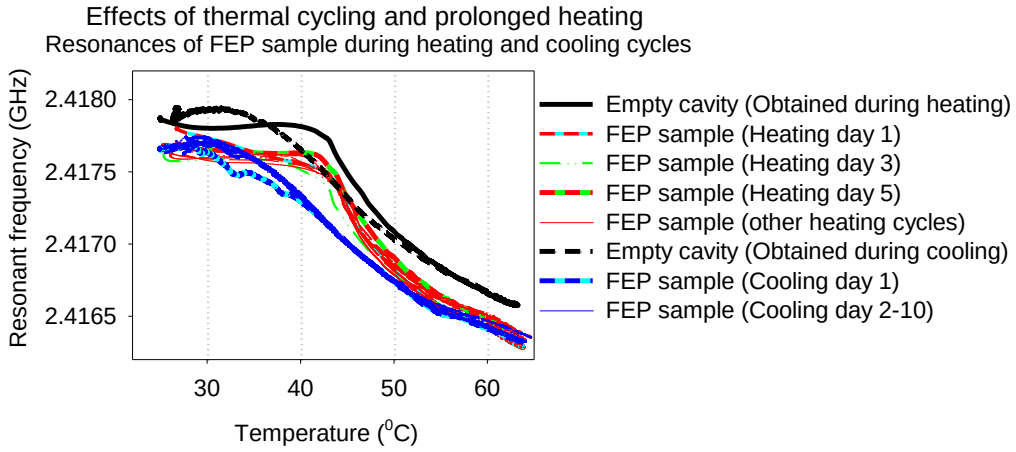

Figure 9.12: Resonances of loaded and unloaded cavities at frequencies around 2.4 GHz

Figure 9.13 shows that the bandwidth of the loaded cavity increased more during heating than during cooling, which implies that the Q-factor of the loaded cavity decreased more during the heating phase than during the cooling phase. The reason for the worst Q-factor during heating is because the Q-factor is related to the loss factor in the cavity and insertion loss is more temperature dependent.

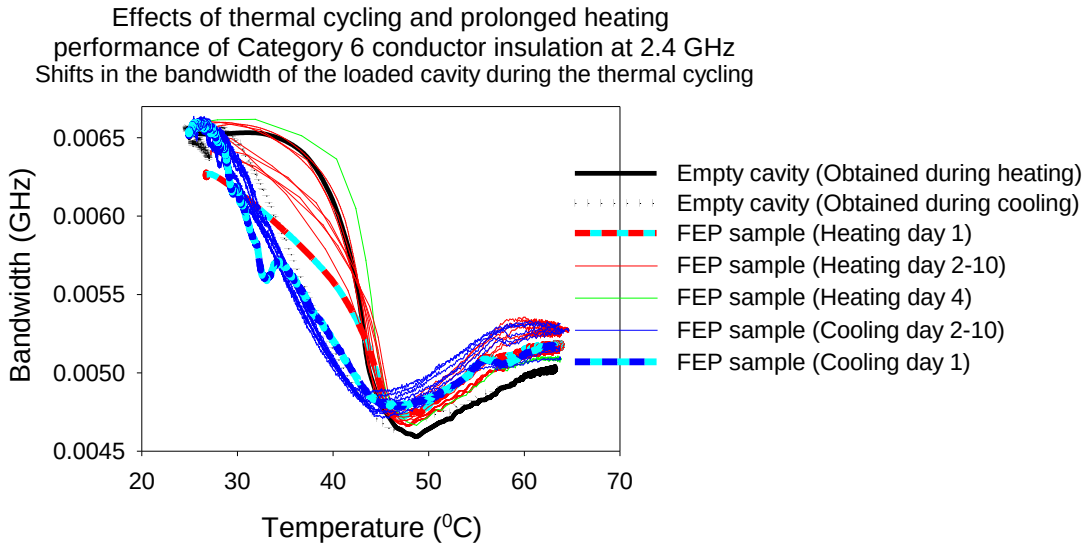

Figure 9.13: Drifts in the bandwidth of the loaded cavity at frequencies around 2.4 GHz

Figure 9.14 and 9.15 show the effect of prolonged thermal cycling on the bandwidth of the loaded cavity. As can be observed in both figures, the bandwidth of the loaded cavity increased more due to the prolonged thermal cycling of the sample when compared to the measured bandwidth due to the intermittent heating of the sample. The significance of this is that dielectric loss will be more accentuated due to heating than cooling. Evidently, it is sufficient to correlate the worst insertion loss performance (figure 7.30 and 7.31) of the CMP cable having the FEP under study, during the prolonged thermal cycling to the observed larger bandwidth of the loaded cavity shown in figures 9.14 and 9.15.

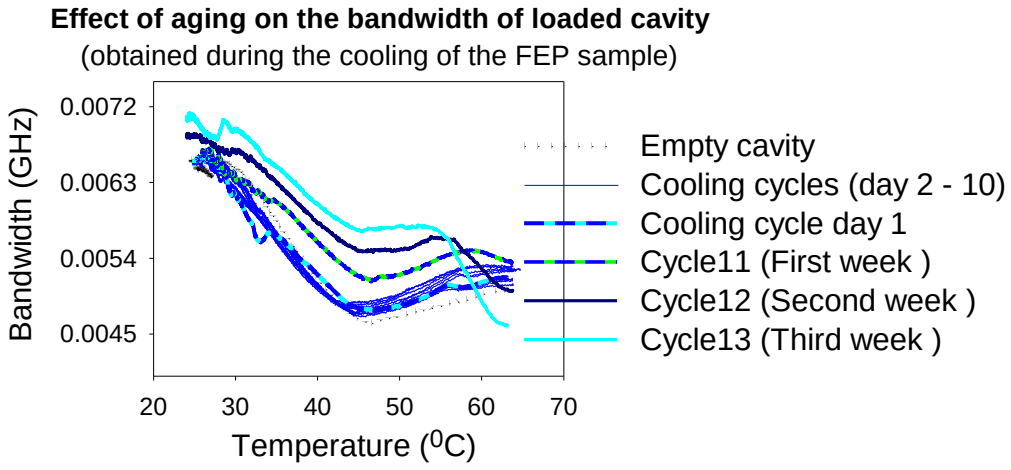

Figure 9.14: Effect of prolonged thermal cycling on the bandwidth of loaded cavity (cooling)

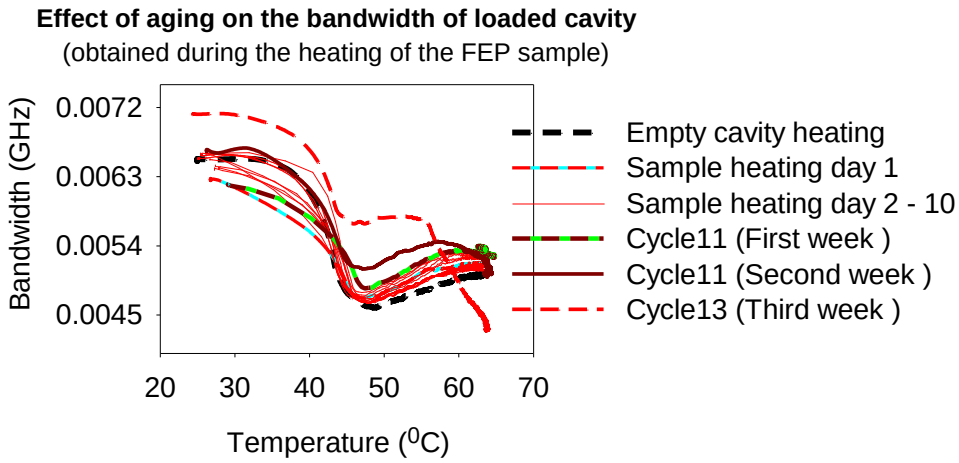

Figure 9.15: Effect of prolonged thermal cycling on the bandwidth of loaded cavity (heating)

The drift in the bandwidth of the loaded cavity at the transition points and the corresponding transition temperature for the drift are presented in figures 9.16 and 9.17. As can be noted, the drift in the bandwidth of the loaded cavity is more noticeable due to the prolonged thermal cycling following the intermittent thermal cycling (figure 9.16). The significance of these results is that the quality factor of the FEP sample will be more affected a consequence of prolonged thermal cycling than the effects of intermittent thermal cycling. Of course, the net effect of this observation is that the sample would not be able to hold its charges due to the effect of prolonged thermal cycling and as a result, it will begin to lose energy as heat under the influence of a rapidly changing Electric field. Consequently, the effect of the drift in the bandwidth of the loaded cavity is the drift in the transition temperature of the loaded cavity, which is evident in figure 9.17.

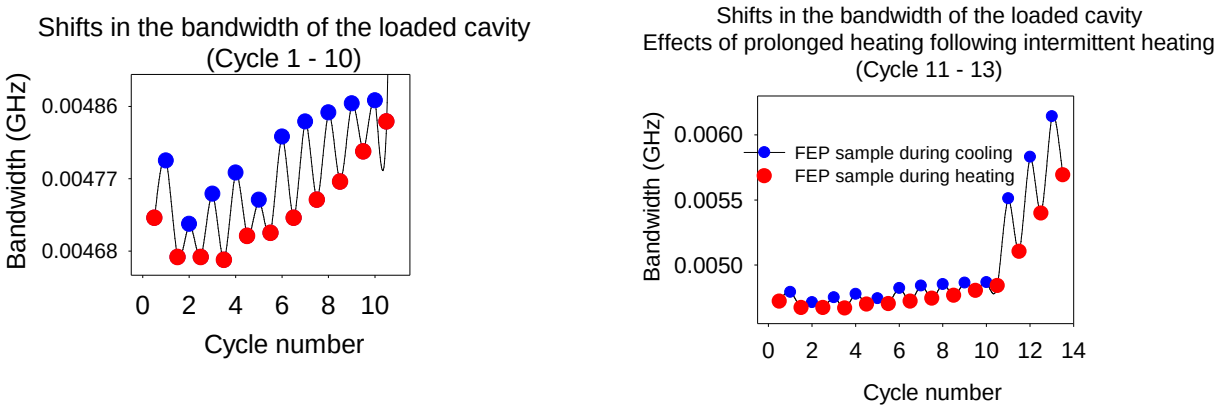

Figure 9.16: Showing the drift in the bandwidth of the loaded cavity

Furthermore, as observed in the performance of the cable, the temperature at which the RL performance of the cable failed and passed drifted during the intermittent heating, and the drifting accelerated during the prolonged heating (see figure 7.23). Similarly, the transition temperatures for the drift in the bandwidth of the loaded cavity also followed the same pattern. It is evident in figure 9.17 that the amplitude of the transition temperatures from cycle 11 became larger as a result of the prolonged thermal cycling.

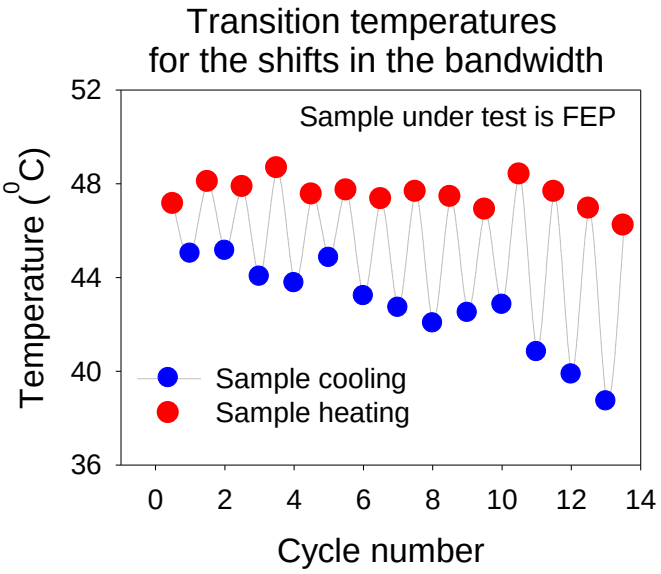

Figure 9.17: Transition temperature for the drifts in the bandwidth of the loaded cavity

9.3.1 Effects of thermal cycling on the dielectric properties of FEP at 2.4 GHz

The effects of intermittent and prolonged thermal cycling on the dielectric properties of FEP sample are presented in this section. Figures 9.18 and 9.19 present the calculated ε_r and tanδ for the initial ten intermittent (daily) cycles and subsequent three prolonged (weekly) thermal cycles. As shown in figure 9.18, the effect of temperature of 60^0C (upon heating and cooling) caused the ε_r of FEP to decrease during the intermittent thermal cycling. Furthermore, it was observed that the ε_r of the FEP decreased further due to the prolonged thermal cycling. It is apparent that the ε_r of the FEP increased due to the cooling of the sample. Moreover, while the ε_r of the FEP decreased sharply at 60^0C during the transition between the intermittent and prolonged thermal cycling, it was found that the ε_r of the FEP increased sharply due to cooling during the transition period. Generally, the rise in temperature caused the ε_r of the FEP understudy to decrease but cooling caused it to

increase at 2.4GHz. Consequently, an increase in the ε_r of the FEP sample under test means the unit capacitance of its twisted pair will increase, then impedance will decrease (see figure 7.28) and return loss performance of the cable will be affected (see table 7.3).

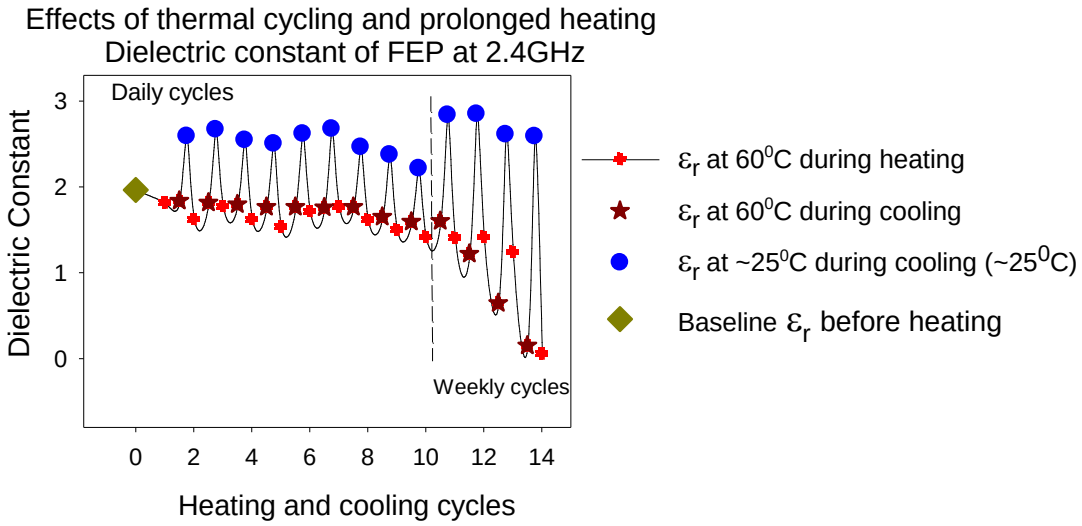

Figure 9.18: Effects of thermal cycling and prolonged heating on the $\boldsymbol{\varepsilon_r}$ of FEP at 2.4 GHz

Furthermore, it has been observed that the thickness of the conductor insulation decreased by 222.4 μm because of the effects of thermal cycling (figure 7.74). The shrinking of the conductor insulation of a twisted pair as a result of thermal cycling indicates a decrease in the effective area of the overlapping conductors, which will, of course, led to an increase in the ε_r of the conductor insulation. In addition, an increase in the ε_r will cause the unit capacitance of the twisted pair to increase and the Z_o of the twisted pair to decrease. Moreover, the decrease in the characteristic impedance of a propagating signal implies more current will be drawn for the same amount of power transmitted. The more the power drawn, the more temperature rise; which will cause the resistance of the cable to increase. More also, an increase in the resistance of the cable will cause an increase in the conductor losses, which of course will contribute to the attenuation of the transmitted signal. From this result (figure 9.18) however, it can be suggested that an increase in the ε_r of the FEP sample due to cooling was part of the contribution to the increase in the IL performance of the Category 6 U/UTP CMP PL.

Figure 9.19 presents the loss tangent (tanδ) of the FEP sample at 2.4GHz. As can be observed, the tanδ of the FEP understudy increased in response to, intermittent heating and cooling as well as prolonged thermal cycling of the sample. The observed increase in the $tan\delta$ of the FEP during

heating and cooling of the sample implies absorption of electromagnetic energy by the material and the heating of the material at 5GHz. Evidently shown, in figure 9.19, the increasing loss tangent of the FEP sample extracted from the Category 6 U/UTP CMP cable suggests the cause of the increasing IL of the PL during the heating and the cooling (Figures 7.30 and 7.31) of the cable. Similar to the observation in figure 9.18, a sharp increase in the tanδ of the sample is also apparent during the transition period (cycle 11).

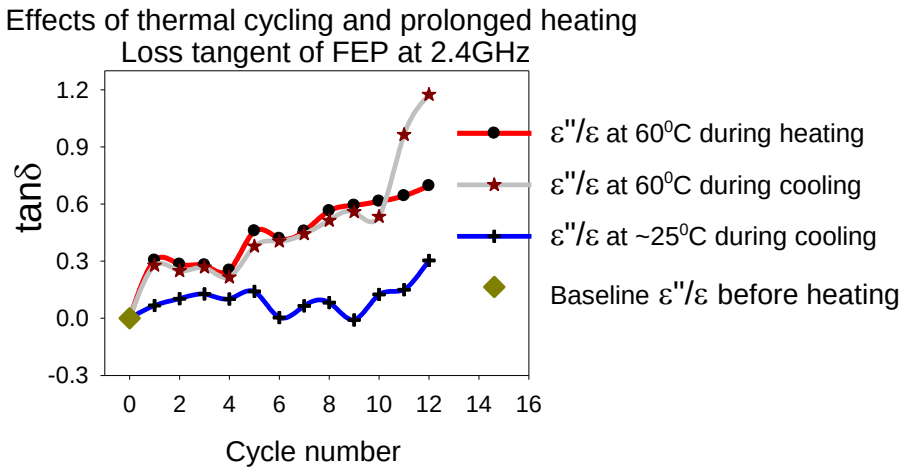

Figure 9.19: Effects of intermittent and prolonged thermal cycling on the $tan\delta$ of FEP

Chapter summary

This chapter has demonstrated the potential of using a method based on the Cavity Perturbation Method in the validation of the extracted Velocity Factor of different PLs based on measured electrical characteristics of the PLs (Section 9.1). The study investigated the baseline dielectric constant (ε_r) of the Category 6 U/UTP CMP cable conductor insulation (FEP) at an elevated room temperature of 25^{0}C and at 1 GHz, 2.4 GHz and 5 GHz. It was noted that the measured ε_r of the FEP under test was in good agreement with the published ε_r of FEP. Also, the ε_r of the FEP remained consistent across the three frequencies at room temperature based on its low loss and non-dispersive nature. To establish the unique properties of the FEP, its baseline ε_r was compared to that of the HDPE at 5 GHz. It was found that the ε_r of FEP was lower than that of the HDPE. Furthermore, to establish the accuracy of the dielectric properties measurement methods, the baseline ε_r of different Ethernet cabling dielectrics was investigated. The obtained $\boldsymbol{\varepsilon_r}$ for the foamed dielectrics was found to be lower when compared to that of the solid dielectric materials.

More also, the calculated baseline VF from the obtained dielectric constant of different Ethernet cabling dielectrics was compared with the VF supplied by different manufacturers. It was observed that the VF for all the cables agreed with the values of the VF supplied by the manufacturers of the different Ethernet cables with the differences of 1 – 4%. The last results in section 9.1 demonstrate the impact of using an incorrect cable type for the testing of the PL length. When the correct Category 6 U/UTP cable type was selected for the testing of the PL length, it was found that the calculated VF from the ε_r obtained using a method based on CPM and the VF which was obtained from the PL characteristics were different by just 1 and 0.04 % from the VF supplied by the cable manufacturer. However, using a different Category 6 U/UTP cable type instead of the actual Category 6 U/UTP CMP cable type for the testing of the PL length, differences of 2.1 and 3.1 % in the values of the VF were obtained. In other words, the results demonstrate the potential of using a method based on CPM in validating the VF supplied by the manufacturers of Ethernet cables.

Furthermore, the observed changes in the material properties also provide insight into the cable behaviour as was similarly reported in chapter 6 and 7. For instance, it has been established in chapter 7 that the first heating of the cable changes the performance of the cable drastically. In investigating the immediate effects of temperature increase and continuous heating on the performance of the cable, the extracted dielectric rod sample from the Category 6 U/UTP CMP cable was heated continuously without cooling. It was found that an increase in temperature to ~65^0C caused an immediate frequency shift in the resonance of the loaded 2.4 and 5 GHz cavity. In addition, it was found that the third day heating of the sample caused the highest frequency shift of 1.507 MHz in the resonance of the loaded 2.4 GHz cavity and 4.425 MHz in the resonance of the loaded 5 GHz cavity to below the resonance of the unloaded cavity. After the third day heating, it was observed that the resonant frequency shift was relatively constant. Based on the observed highest resonant frequency shift on the third day heating of the sample, it was also observed that the ε_r of the FEP increased permanently within the first 3-days of the heating of the sample both at 2.4GHz and 5GHz. Furthermore, due to the low loss and non-dispersive nature of the FEP sample, the electrical loss, Q-factor and bandwidth of the loaded cavity improved initially at 2.4 GHz due to the immediate effect of temperature increase but were affected after a few days of heating of the sample. However, while the internal loss, Q-factor and bandwidth of the loaded cavity improved initially at 2.4 GHz with an increase in temperature, it was observed that the performance of the FEP sample was affected at 5 GHz from the first day of heating of the sample.

The dielectric rod (FEP sample) extracted from the Category 6 U/UTP CMP cable was subject to intermittent and prolonged thermal cycling in order to investigate the root cause of the observed drifts in the return loss and insertion loss performances of the cable itself based on the effects of intermittent and prolonged thermal cycling. It was found that the resonances of the FEP sample shifted more to the lower frequencies due to the cooling of the sample than when it was heated. Furthermore, the fifth heating of the FEP sample caused the resonance of the sample to shift above all other resonance curves. It is worth noting that this behaviour of the FEP sample during the fifth heating of the cable is related to the spurious resonance observed in the RL performance of its cable (figure 7.33), where the first performance failure of the cable occurred. An echo of RL measured during the transition between the intermittent and prolonged thermal cycling of the cable can also be correlated to the spurious resonance, which was observed in the resonance of the FEP sample during the transition period.

The ε_r of the extracted FEP rod sample from Category 6 U/UTP CMP cable increased due to the effect of cooling and prolonged thermal cycling, which also suggests the root cause of the observed poor RL performance measured was due to cooling. Furthermore, as observed in the performance of the cable, the temperature at which the RL performance of the cable failed and passed drifted during the intermittent heating, and the drifting accelerated during the prolonged heating (figures 7.23 and 7.24). Similarly, the transition temperatures for the drift in the bandwidth of the loaded cavity also followed the same pattern (figure 9.17). That is, the amplitude of the temperatures at which the RL performance of the PL was passing marginally upon heating and cooling was approaching the temperature at which the RL performance was failing (figure 7.22) during the prolonged thermal cycling. Similarly, the amplitude of the transition temperatures for the drift in the bandwidth of the loaded cavity also increases during the prolonged thermal cycling (Figure 9.17).

The effect of temperature of 60^0C (upon heating and cooling) caused the ε_r of FEP to decrease during the intermittent thermal cycling but decreased further due to the long-term effect of thermal variation. Also, the ε_r of FEP increased due to the cooling of the sample and increased further due to the long-term effect of thermal variation. It was observed that the thickness of the conductor insulation decreased by 222.4 μm because of the thermal cycling (figure 7.74). The shrinking of the conductor insulation of a twisted pair as a result of thermal cycling indicates a decrease in the effective area of the overlapping conductors, which will, of course, lead to an increase in the ε_r of the conductor insulation. As presented in figure 9.18, the increase in the ε_r of the FEP sample due

to the cooling of its cable was part of the contribution to the increase in the RL and IL performance of the Category 6 U/UTP CMP PL.

Furthermore, it was found that the bandwidth of the loaded cavity increased more due to the effect of prolonged thermal cycling of the sample when compared to the measured bandwidth due to the intermittent heating of the sample. The significance of this is that dielectric loss will be more accentuated by the effect of prolonged thermal cycling. The increased $\tan\delta$ of the FEP because of the thermal cycling, suggests that IL performance degradation of the Ethernet cables will increase both due to heating and cooling when the Ethernet cables are subjected to thermal cycling. Although on a long-term, IL performance will drift due to the cooling and thermal cycling, there will be more IL performance degradation as temperature rises than at low temperature. It is, therefore, safe to infer that the long-term effect of thermal variation on the cable conductor insulation has a direct effect on the long-term performance of the cable.

CHAPTER 10 – CONCLUSIONS, RECOMMENDATION AND FURTHER WORK

Summary and conclusion of the research study, recommendations and suggestions for future work are presented in this chapter. Section 10.1 detailed the summary and conclusions. Section 10.2 outlines some recommendations on how to intelligently manage PoE infrastructure. Lastly, section 10.3 suggests some further studies on the long-term performance of Balanced Twisted Pair Cabling.

10.1 Summary and Conclusions

The steady growth in the development and deployment of IP enabled devices requiring to be remotely powered and networked will continue to drive the demand for improved Power over Ethernet Technology worldwide. Coping with the diversity and growing intensity of the demand for more power standardisation will require an adequate appraisal of the challenges being faced with the existing technology, to provide informed designed considerations improvement. Moreover, the peculiarity of the deployment environments, the inherent nature of power and data transmission in the cables, the range of options in material selection both for the cable conductors and the insulator as well as the twisting and cable bundle size demand critical appraisal in order to slow degradation and improve the operational performance. To this end, this research study was conducted to simulate some of the possible scenarios that could trigger thermal variation (thermal cycling) in cable bundles in service.

In the first sets of experiments, temperature rise in shielded and unshielded Ethernet cable bundle consisting of 37 cables was assessed under two different installation environments (ventilated - "Free air" and unventilated- insulated spaces) using three different approaches; which are thermocouple approach, resistivity approach and mathematical modelling. The experiment was conducted at three DC Power levels (PoE+ at 34.2 watts, UPoE at 60 watts and HDBase-T at 100 watts). Furthermore, cable bundle heating was evaluated with various cable construction such as the material of the crossweb, conductor material, the quality of the conductor insulation and cable screening mode. In addition, temperature rise on 24 (24 cables in a bundle) and 37 (37 cables in a bundle) cable bundles of Category 6A F/UTP was assessed in two installation environments using six current levels: 0.3A, 0.45A, 0.6A, 0.75A, 0.9A, and 1A respectively (values of current below and above the specified 0.6 A of the IEEE 802.3at). Furthermore, temperature distribution across 37 cable bundle (36 around 1) was validated using the thermocouple approach and compared with the prediction made using the

mathematical model. As a close of the cable bundle heating experiments, the temperature rise in Ethernet cable bundles using the three temperature measurement approaches on a 37 CB was compared. That is, the thermocouple approach was used to validate the mathematical model and the resistivity approach. Note that in most cases, the worst-case scenario of cable bundle heating was chosen because, in some typical hidden insulated pathway systems, the cable bundle will generally be larger than a 37 CB and installed inside a conduit before being placed under the floor or ground or inside wall and so on. Also, as climatic conditions and installation environments vary all over the world, knowing the results of the worst-case scenario, the effects of a higher power in restricted heat dissipation environments can be considered or avoided.

Summary of the results of the cable bundle heating assessment

Results from these sets of experiments showed that the maximum temperature rise above ambient temperature occurred in the centre of each cable bundle. Also, the CBs heated in the free air environment generated less temperature rise than the CBs under insulated heating. It was observed that the resistance of the CBs increased due to heat, and the magnitude of the increase was directly proportional to the temperature rise in all the CBs. In addition, high power (100W) deployment over the bundled insulated unshielded Ethernet cables caused an extremely high temperature rise in the cable bundle. Category 5e cable (which has the smallest conductor diameter) produced the highest temperature rise during the free air heating test and failed along with other unshielded Ethernet cables due to the extreme heat build-up within the cable bundle. However, shielded cables such as Category 6 FTP, Category 6A F/UTP, Category 6A F/FTP and Category 7A S/FTP did not reach a point of failure when tested in the free air, and insulated environments at all power levels even though there was a temperature rise. Category 7A S/FTP cable with a large overall diameter and the lowest conductor resistance along with a large amount of screening generated the lowest temperature rise at 100Watts. Temperature rise in the shielded cable bundles met the standard limit of 60 ^{0}C at IEEE 802.3at power level and did not fail, even in the worst-case scenario of cable bundle heating.

From the results in these sets of the experiment, it can be concluded that cable constructions (material and size) and installation environments play pivotal roles in the dissipation of the heat generated in cables used in PoE applications. Cables with larger conductor size and screened construction, such as an individual screening of the conductor pairs and overall screening, will likely generate lower temperatures. Furthermore, conductor material and the quality of the

conductor insulation (cables whose conductor insulation made from Fluoropolymers did not fail), as well as installation conditions, will determine the amount of heat generated and dissipated by a CB. Larger cable bundles tend to prevent free dissipation of heat, leading to heat ageing of the conductor insulating materials. Thus, factors such as overall screening, individual pair screening and conductor diameter influence the heat generation and dissipation properties of bundled Ethernet cables.

Since it has been established that regardless of the amount of power transmitted through the CB, heating occurs within the cables and their surroundings due to the passage of the electrical current. Also, that installation condition and long-term thermal variation may affect the transmission performance of the cable. The second set of experiments was conducted to investigate the hypothesis.

Summary of the results of the resistive heating conducted on Category 6A F/UTP PL

The first experiment in this set simulated the long-term effect of repeated electrical heating on the performance of Category 6A F/UTP PL. Repeated resistive heating affected both the electrical properties and transmission parameters of the Ethernet cables. Moreover, repeated resistive heating in the ventilated environment caused a minimal degradation to the performance of the PL whereas repeated resistive heating under insulation environment at high temperature caused severe degradation to the Category 6A F/UTP performance. Although it was observed that the heating of the cable improved the crosstalk performance slightly when the cable was heated and cooled repeatedly in the ventilated environment, the failure of Category 6A F/UTP PL was dominated by the RL, IL and crosstalk performance at 35 MHz when the cable was insulated and tightly bundled.

Non -resistive heating tests results

Summary of the results on the fully insulated Standard Category 6 U/UTP PL

The experiments on the immediate and long-term effects of thermal variation on the performance of the fully insulated Standard Cat 6 U/UTP PL, established that the first few cycles of heating and cooling affected the performance of the Standard Cat 6 U/UTP cable and the impact of

thermal cycling within $+20^0$C to $+70^0$C affected the electrical performance of each pair differently. The impact was more pronounced during the cooling phase than the heating phase. The effective ε_r of the dielectrics of all the twisted pairs in the cable decreased permanently due to the cooling of the cable. Also, the electrical length of the cable decreased in response to thermal cycling between $+20^0$C and $+70^0$C. Furthermore, the decrease in electrical length of the cable resulted in an increase in the velocity factor of the conductor insulation while propagation delay decreased. The changes in the propagation delay caused changes in the delayed skew. The variations in the characteristic impedance of each pair caused reflections to occur, which was measured as RL. Moreover, a 45^0 phase shift was observed at the fundamental frequency of the RL signal on pair 7,8 while a 90^0 phase difference was observed at 34.5 MHz. As observed in the crosstalk performance measured during the repeated resistive heating test, an immediate change in the crosstalk performance of the fully insulated Standard Category 6 U/UTP cable was also observed. Lastly, the PSACR-N performance of the cable was more affected during the heating phase than the cooling phase; although it was found that the PSACR-N of the cable improved after a few heating and cooling cycles due to some chemical reactions in the dielectric material (hysteresis). In the second phase of the full cable bundle heating tests that investigated the effects of thermal cycling between $+20^0$C and $+120^0$C, the thermal impact at an extended temperature of about 120^0C caused the electrical length of each twisted pair in the Category 6 U/UTP cable to decrease more with the highest decrease measured at room temperature. It was observed that the cable had a partial recovery from the combination of stresses when left unpowered for some days. Moreover, after the initial failure of the PL, the cyclic performance of the fully insulated Standard Cat 6 cable was observed. The heating of the cable to a higher temperature of 120^0C caused the loss of the link at room temperature and a DC contact resistance issue which of course resulted in poor intra-pair resistance unbalance between the split pair, pair 3,6.

Summary of the results for the portion insulated Category 6 U/UTP CMP PL

For the experiment conducted on the portion insulated Category 6 CMP cable, the result showed that the baseline RL performance of the Cat 6 U/UTP CMP PL was a marginal pass with a marginal value of 0.8 dB at 22.5^0C. However, the first heating and cooling of the cable caused an accentuated decrease in the performance of the cable. Furthermore, after heating and cooling the middle portion of the cable repeatedly for five times, the RL performance of the cable failed

for the first time at 20^0C. The initial partial recovery of the cable from the failure was observed at temperatures close to the room temperature, while subsequent failure and recovery temperatures accelerated towards higher temperature after the electrical length of the cable had decreased. The RL marginal values and the cyclic behaviour of its corresponding failure temperatures drifted towards the higher temperature, which portends degradation in the performance of the PL. Furthermore, the reduction in the electrical length of the cable was observed during prolonged thermal cycling. The extracted effective ε_r of the conductor insulation also confirmed that the electrical length of the cable had decreased. The decrease in the length of the cable caused a proportional decrease in the propagation delay of the cable. In addition, because the propagation delay had decreased, the velocity factor of the conductor insulation of the cable also increased. Moreover, the timing difference also caused the signal skew on all the twisted pairs except the shortest pair in the cable. Electrical length mismatches towards the end of each line and impedance variations at the reference plane of each of the lines were observed. Moreover, the observed impedance at the mating of the RJ45 plug and jack and that of the thermally insulated portion of the cable show impedance mismatches along the whole length of the PL, which of course caused multiple reflections on the PL and contributed to the increased insertion loss of the PL. An increase in insertion loss of ~8% per degree was observed while return loss decreased by ~6.8% per degree for the 24 thermal cycles conducted within the specified operating temperature of PoE. The mismatches in the electrical length of the twisted pair which caused a delay in the arrival of the pulse signal at the end of the link also caused the phase shifts from cycle to cycle. NEXT resonance was observed at the point where the electrical length decreased. RL echo was also observed after the electrical length decreased. Crosstalk attenuation at the heated portion of the cable decreased initially during the first heating of the cable but increased progressively afterwards until cycle 15 before decreasing again. In addition, the crosstalk which was not initially present at the reference plane of the cable, (mating at the RJ45 connector) was observed to increase rapidly from the point where the electrical length decreased. Furthermore, the TCL and ELTCTL of the PL revealed some mode conversion as a result of the imbalances in the structure of the twisted pairs during the thermal cycling tests. Also, the equivalent differential mode noise voltages for the TCL values of the cable revealed a voltage spike where the electrical length decreased. In addition, the ELTCTL showed a "ghost-like" resonances at the critical points: at cycle 5 where the first RL failure occurred, at cycle 11 which is the transition between the daily thermal cycling and weekly thermal cycling and finally, at cycle 15 where the electrical length of the cable decreased. The CDNEXT at the main side of the PL showed some distinctive resonances from cycle 13 to cycle 15 where the electrical length

of the cable decreased, and delay skew was observed. It was found that the first heating of the cable caused the CDNEXT value of the PL to decrease by 30.9 dB while subsequent heating cycles up to the last heating cycle caused just a decrease of 4.2 dB. The ACR-N, which is an important parameter for evaluating the Signal-to-Noise Ratio (SNR) of a cabling system was significantly affected during the first heating and cooling of the cable. Lastly, it was observed that the ACR-N value decreased by 3.1 dB during the first heating of the cable while the subsequent heating cycles caused a decrease of 0.7 dB.

Summary of the results for the portion insulated Category 6A F/UTP PL

For the experiment investigating the long-term effects of thermal variation on the performance of portion insulated Category 6A F/UTP, the electrical length of the shortest pair of the Category 6A F/UTP, pair 1,2 decreased permanently due to prolonged thermal cycling. Also, the reduction in the electrical length of the cable caused the propagation delay of the cable to decrease and the velocity factor of the conductor insulation to increase. Signal skew was observed based on the changes in the propagation delay of the cable. Impedance discontinuity at the 19.5 m location on the shortest twisted pair (pair 1,2) in the cable was observed. The amplitude of the discontinuity increased by 0.65 % at the transition point to the prolonged heating (cycle 21) and by 0.79 % due to the cooling of the cable after the heating cycle 21. Other discontinuities at 11.5m and 15.5m on pair 1,2 generated RL echoes and spurious resonances during heating cycle 2 and 39. Moreover, the extraction of the primary line constants from the obtained impedance profile of the link revealed that the impedance of pair 1,2 at 19.5 m location decreased due to an increased unit capacitance while the increased impedance at 15.5 m was due to an increase in the unit inductance of the twisted pair. The obtained impedance profile of the longest pair in the cable (pair 3,6) was observed to be distinct during cycle 2 and 39. Furthermore, it was observed that the impedance bridging on the PL due to the localised heating of the cable caused the thermal push and pull of the dielectric, which further caused the observed electrical length mismatches towards the end of the PL. More also, the impedance profile of the heated and unheated portions of the cable shows some impedance mismatches which contributed to the poor RL performance of the PL in general.

As observed in the crosstalk performance of the standard Category 6 U/UTP and Category 6 U/UTP CMP cables, crosstalk performance between the longest and shortest pair in the Category 6A F/UTP cable was also observed to be better due to the heating of the cable in comparison to the measured crosstalk performance due to the cooling of the cable. More also, it was found that the crosstalk

performance of the portion insulated cables was initially worse during the first few heating and cooling cycles, but improved afterwards due to some chemical reaction in the conductor insulation. Long-term thermal variation and installation condition caused the RL value of pair 1,2 to decrease progressively from its baseline value, whereas the effects of thermal cycling and installation condition caused the IL performance of the Category 6A F/UTP PL to increase progressively. Although the RL values decreased from the first thermal cycle (cycle 1) up to the last thermal cycle (cycle 40), it was observed that the worst RL performance of the Category 6A F/UTP PL was within the first heating and cooling of the cable. Furthermore, comparing the RL performance due to the heating and cooling of the cable, it was found that the RL performance was more affected due to the cooling of the cable than heating. Also, the RL value at the main of the PL was found to be lower in comparison to the RL value measured at the remote side of the PL. The maximum reduction in the RL value due to the 40 thermal cycles conducted was observed to be 1 % per degree, whereas the maximum IL increase due to the 40 thermal cycles conducted was observed to be 9.2 % per degree. The PSACR-N performance of the Category 6A F/UTP PL decreased progressively due to the effect of thermal variation and installation condition, but in general, the PSACR-N performance of the PL was found to be lower during the heating of the cable in comparison to the values obtained due to the cooling of the cable. The Feature Selective Validation tool was used to validate the long-term performance degradation of the Category 6A F/UTP PL. The comparison of the baseline performance with the long-term performance of the Category 6A F/UTP PL showed a fair agreement, which implies a deviation from the baseline performance of the PL. More also, the quantification of the RL and IL degradation using the ISO standard agreed with the quantification of the degradation made using the TIA standard. The last study conducted on the portion insulated Category 6A F/UTP PL was using the Scanning Electron Microscope (SEM) to investigate the deformation in the conductor insulation of a twisted pair sample. The SEM results revealed the deformation in the conductor insulation of the twisted pair sample. Furthermore, the adhesion of the twisted pair conductor insulator to its copper conductor was observed to be affected near the end of the twisted pair sample, of which justifies the observed thermal push and pull effects seen in the HDTDR plots of the cable performance.

Investigation of the Ethernet cable dielectric properties

The last study conducted in this research examined the properties of Ethernet cabling dielectrics to understand some of the root causes of the observed Ethernet cable performance degradation. In this regard, Rectangular Resonant Cavities were designed and fabricated based on the Cavity Perturbation Method (CPM). The verification and validation of the accurate sample position inside the simulated and fabricated cavities were carried out. After that, the cavities were used to assess the baseline dielectric properties of different Ethernet cable dielectrics. Moreover, the immediate effects of an increase in temperature to 65^{0}C and continuous 30-day heating at this temperature were examined on the ε_r of the extracted FEP at 2.4 and 5 GHz. The last study in the dielectric measurement section examined the drifts in the dielectric properties of the extracted FEP sample at 2.4 GHz as functions of intermittent and prolonged thermal cycling to establish correlations between the drifts in the transmission parameters of the Category 6 U/UTP CMP cable and its dielectric properties.

The study demonstrated the potential of using a method based on the Cavity Perturbation Method in the validation of the extracted Velocity Factor of different Ethernet cables based on measured electrical characteristics of the PLs. The designed cavities were able to measure the ε_r of the FEP and the value obtained was found to be in good agreement with the published ε_r of FEP. Also, the baseline ε_r of the extracted FEP was found to remain consistent across three frequencies (1GHz, 2.4 GHz and 5 GHz) at room temperature based on its low loss and non-dispersive nature. The increase in temperature to ~65^{0}C caused an immediate frequency shift in the resonance of the loaded 2.4 and 5 GHz cavity, while sustained heating at this temperature caused a further frequency shift in the resonance of the loaded cavities. The ε_r of the extracted FEP rod sample from Category 6 U/UTP CMP cable increased as a consequence of prolonged thermal cycling, particularly during the cooling phase, which suggests the root cause of the poor RL performance observed during the cooling phase. Moreover, thermal cycling between 60^{0}C and room temperature caused the ε_r of FEP to fluctuate depending on the phase i.e. cooling or heating. Furthermore, the bandwidth of the loaded cavity increased in response to the prolonged thermal cycling of the sample as compared to the measured bandwidth during the intermittent heating of the sample. This means that dielectric loss will be more accentuated by prolonged thermal cycling. The increased tanδ of the FEP during thermal cycling also indicate that Insertion Loss (IL) performance degradation of the Ethernet cables will increase during the heating and cooling process in Ethernet cables. Although on a long-term, IL performance will drift due to the cooling of the cable and thermal cycling. Also, there will be more IL performance degradation during temperature rise. Thus, it could be inferred that the long-

term effect of thermal variation on the cable conductor insulation has a direct effect on the long-term performance of Balanced Twisted Pair Cables. Also, from the observed CDNEXT performance of the Category 6 U/UTP CMP PL, it is apparent that the connection end of the PL plays a significant role in the performance of the PL within the first thermal cycling of the cable. Obviously, these statements raise an important question: how can PoE infrastructure be intelligently managed?

10.2 Recommendations

Remote powering is a fact of networked life. Ageing and degradation are to be expected during remote powering operations, but it can be minimised by avoiding extreme temperatures. To reduce the effects of cable bundle temperature, several factors contributing to the heat generation could be controlled during the manufacturing process. For instance, twisted pair cables with better construction (good polymers and larger conductor diameter and screening) will enhance the heat dissipation. Similarly, larger conductor size (e.g. AWG 22) has low resistance, therefore, will generate less heat. The material of the conductor is also important. As much as possible, Copper Clad Aluminium (CCA) cables should be avoided for remote powering applications, as aluminium has higher resistance in comparison to copper. Furthermore, the results from the resistive heating in lower cable bundle sizes; showed that power capabilities of structured cabling could be enhanced with a reduction in the cable bundle sizes. In practical terms, this implies the separation of large cable bundles into smaller bundles and avoiding tight bundles to allow free dissipation of the heat generated within the cable bundle in service. The research equally demonstrated that both the immediate and long-term, thermal variations affect the performance of Balanced Twisted Pair cables. While changes to the performance of the lower category of cables within the 'usual' range of temperatures can modify the performance profile, these are generally within specification except for the inferior/dodgy cables. However, should the temperature exceed 60^0C, the performance of the cable under tight cable bundling and full cable bundle insulation conditions will be off the standard limit. Also, while different types of Ethernet cables can be deployed for remote powering operations, it is essential to install efficient high bandwidth shielded cables for the upcoming connectivity. Ethernet cables should be robust enough to withstand temperature fluctuations and fulfil at least their designed working life. This means that Balanced Twisted Pair cable should be designed with Fluoropolymers and rated to transmit high DC power ($100\,Watts$) and high frequency ($\geq$10 GB/s) data. This can be achieved by ensuring good material composition and polymer processing. Given that heat rise as a function of the conductor insulation, a material

composition such as fluoropolymers will enhance heat dissipation in the cable. In particular, the composition of the insulating material for single-pair Ethernet cables to be deployed in heavy industrial environments should be ruggedized, as it is possible for the industrial robots to run over the cables during operation.

As bandwidth demands increase and more powered devices are added to the network, it is appropriate to 'futureproof' the cabling infrastructure for both higher-speed applications and more power demand, to avoid the replacement of the installed cables. This may involve the deployment of the higher categories of cables with enhanced dielectric materials. Furthermore, this study has demonstrated that the electrical length of twisted pair copper cable decreased during the phase change, between intermittent and prolonged thermal cycling. Also, as one the major sources of noise and mode conversion is a change in the electrical length of the cable, robustness needs to be put into the chemical composition of Ethernet cable dielectrics to withstand the variation in the weather and operating conditions. More also, an important property needed for the insulated copper conductor is high interfacial adhesion to metal surfaces. Thus, this should be given special consideration in cabling design to avoid dielectric fracture at the termination points. Also, as phase stability is required for the correct operation of any system, cable manufacturers should provide phase stability data for the balanced twisted pair cables in the datasheets. More also, crosstalk between the longest and shortest pair in the cable seems to be the highest crosstalk observed during the thermal cycling test. Thus, deviation from the ideal conductor twisting and unequal lengths of the twisted pair may not eliminate crosstalk between pairs caused by the portion insulation condition and thermal variations that change the alignment of the twisted pair. Hence, it is important to resolve the electrical length mismatches that were observed. As much as possible, the length of each pair in the cable can be made equal while the dielectric constant of the conductor insulation is made to be as close as possible to that of air. In addition, the untwisting of the pair in the termination area to a large extent or pigtailing should be avoided as these contribute to the poor crosstalk performance.

The use of the higher categories of cabling does not foreclose the complimentary use of the superb lower cabling categories as they still support applications under IEEE802.3af and IEEE 802.3at. When higher power cable is to be deployed, it is recommended that the length of the cable link should be short/reduced, since this has some advantages such as, a reduction in the resistance which ensure less power dissipation and higher signal strength. Moreover, given that installation environments play pivotal roles in the dissipation of the heat generated, it is recommended that simulations also need to include data cable pathway temperature simulation, which includes potential self-heating effects and those areas with greater risk of excess heat. For instance, cable

bundles for remote powering end equipment passing through a non-air-conditioned building roof space may experience temperature exceeding 100 degrees Centigrade. This has an implication on the integration of cabling within building design. As data services in 'smart' buildings become more fundamental to the operation and management of the building, health monitoring and management of the data infrastructure becomes vital to ensuring that other services and operations of the building do not become impaired. Also, it is typical that new buildings will be modeled for airflow, insulation, and temperature (for the comfort of those who use the building). Hence, support structures and pathways should be designed to provide greater airflow. If the cables must pass through insulated walls or fire stopping areas, for instance, heatsink should be provided around the insulated portion of the cable that is thermally insulated. Also, as high ambient temperature limits the current carrying capacity of the cables by limiting the amount of self-heating that can be tolerated before the temperature rating of the conductor insulation is reached, cables should be kept ventilated by loosely grouping cables to avoid tight bundles.

Furthermore, given that the average length of an electric vehicle is 2 m and the length of the single pair cable installed in an automotive environment could be up to 1000 m, it is likely that the cable will be bent around the car. In this case, return loss performance will be a critical parameter to consider when looping the cable around the car.

Given that an immediate and permanent change in the performance of the cables under test and their dielectrics have been observed in this research work, it is suggested that the newly designed cables should be pre-aged prior to installation and then rechecked that they still meet specifications. Also, it may be appropriate to retest the links after the installation. If possible, the certification test should be conducted after performing three thermal cycling on the newly installed cable by considering the maximum temperature rating of the cable conductor insulation. Finally, the field testers should be configured or programmed to be able to detect any nominal length correctly and report the exact changes in the Nominal Velocity of Propagation (NVP) value as a result of any changes to the dielectric constant of the conductor insulation of the installed cables.

10.3 Further work

Future work will investigate the impact of thermal variation and localised heating on cross mode conversion in single pair Ethernet cabling using four-port Vector Network Analyser. In particular, the per unit length transmission line parameters of the cable will be extracted to draw some conclusions on the ageing of the cabling system. Also, given that the attenuation constant is a function of both dielectric and conductor loss, future work will examine and analytically relate the contributions of the changes in the dielectric behaviour and increased conductor resistance to the degradation in the insertion loss performance of the PoE PL. Furthermore, having determined the changes in the Return Loss performance of the cables understudy, future work will examine the impact of jitter on data-signal speeds to verify the quality of the transmitted data based on the effects of thermal variation and localised heating. Lastly, future work will develop or use an Arrhenius model to predict the thermal life expectancy of a single pair Ethernet cable as used in industrial and automotive applications.

CHAPTER 11 - LIST OF PUBLICATIONS AND REFERENCES

11.1 List of publications

[1] F. S. Akinnuoye, H. Sasse, V, Kang and A. Duffy, "Heating effects on channel performance for PoE applications," in *Proc. of the 62nd International Wire & Cable Symposium (IWCS).*, Charlotte, NC. 2013, pp. 508–515.

[2] P. Cave, F. S. Akinnuoye, A. Duffy, "The impact of remote powering (PoE) on balanced twisted pair cables," in *Proc. of the 63rd International Wire & Cable Symposium (IWCS).*, Providence, RI. November 2014.

[3] F. S. Akinnuoye, P. Cave, and H. Sasse, A. Duffy, "Accelerated degradation of balanced twisted pair performance due to the use of remote powering," in *Proc. of the 64th International Wire & Cable Symposium (IWCS).*, Atlanta, Georgia. November 2015, pp. 71–78.

[4] F. S. Akinnuoye, P. Cave, and H. Sasse, A. Duffy, "Enhancing the power and data capabilities of structured cabling," in *Proc. CabWire World Conf.*, Dusseldorf. Germany. 2015, pp. 152–162.

[5] F. S. Akinnuoye, H. Sasse, P. Cave, A. Duffy, "Design and assessment of cavity perturbation method for dielectric constant measurement," in *Proc. of the 65th International Wire & Cable Symposium (IWCS).*, Providence, RI. October 2016, pp140–149.

[6] F. S. Akinnuoye, H. Sasse, P. Cave, S. Prescott, A. Duffy, "Long-term effect of thermal variation on the performance of ethernet cabling dielectrics," in *Proc. of the 66th International Wire & Cable Symposium (IWCS).*, Orlando, FL. October 2017, pp. 123–132.

[7] F. S. Akinnuoye, S. Prescott, A. Duffy, "Progress in dielectric constant measurement," in *Proc. of the 67th International Wire & Cable Symposium (IWCS).*, Providence, RI. October 2018.

[8] G. Zhang, H. Sasse, F. S. Akinnuoye, A. Duffy, "Measurement uncertainty and repeatability: testing for significance," in *Proc. International Wire & Cable Symposium (IWCS.)*, Charlotte NC, October 2019.

[9] F. S. Akinnuoye, H. Sasse, A. Duffy, "The impact of thermal variation and localised heating on the performance of balanced twisted pair cabling," in *Proc. UL and IWCS.*, Shanghai. China. March 2020.

11.2 References

[0] CEC. (2016). LED lighting controls, internet of things [Online]. Available: http://www.solidstatelightingdesign.com/cec-offer-innovative-lightings-poe-system/ [Accessed 27 September 2019].

[1] C. C. Reinwand. (2007, Jan). "Municipal broadband-the evolution of next generation wireless network." *IEEE Radio and Wireless Symposium*, pp. 273 - 276.

[2] A. S. Tanenbaum and D. J. Wetherall, "The Medium Access Control Sublayer," in *Computer Networks*, 5th ed. USA: Pearson Education Inc., 2011, ch.4, sec.4.3.7, pp. 296.

[3] M. Shahwaiz afaqui, E. Garcia-Villegas, and E. Lopez-Aguilera. (2017). "IEEE 802.11ax: challenges and requirements for future high-efficiency wi-fi." *IEEE Wireless Communications, vol. 2,* pp. 130 - 137.

[4] Y. Ghasempour, C. da Silva, C. Cordeiro and E. Knightly. (2017). "IEEE 802.11ay: Next-Generation 60 GHz Communication for 100 Gb/s Wi-Fi." *IEEE Communications Magazine,* vol. 55, pp. 186 - 192.

[5] *IEEE standard for information technology - Telecommunications and information exchange between systems – Local and metropolitan area networks- Specific requirements, Part 3, amendment 3: Data terminal Equipment (DTE) power via the media-dependent interface (MDI) Enhancements,* IEEE Standard 802.3af, 2003.

[6] *IEEE standard for information technology - Telecommunications and information exchange between systems – Local and metropolitan area networks- Specific requirements, Part 3, amendment 3: Data terminal Equipment (DTE) power via the media-dependent interface (MDI) Enhancements,* IEEE Standard 802.3at, 2009.

[7] *IEEE Standard for Ethernet Physical Layer and Management Parameters for Power over Ethernet over 4 pairs,* IEEE Standard for Ethernet Amendment 2: Physical Layer and Management Parameters for Power over Ethernet over 4 Pairs, 2018.

[8] C. Diminico. (2018). Single pair ethernet: data and power for the wired world [Online]. Available: https://www.cablinginstall.com/home/article/16468582/single-pair-ethernet-data-and-power-for-the-wired-world

[9] D. Johns, P. Deroy. (2013, March). Simulating crosstalk and EMI in cables. *Microwave Journal*. [Online]. Available: https://pdfs.semanticscholar.org/667f/1cf7b0e7389de6cb983477b7177b7741c0ee.pdf

[10] Aerohive Networks. (2015). The network impact of 802.11ac, understanding network design considerations for high-speed wi-fi in a mobile-first network. [Online]. Available: https://matweb.tradepub.com/free/w_aaaa3100/prgm.cgi

[11] F. Akinnuoye, P. Cave, H. Sasse and A. Duffy. "Accelerated degradation of balanced twisted pair performance due to the use of remote powering (PoE +)," in *Proc. IWCS*, Atlanta, Georgia. November 2015, pp. 71–78.

[12] F. S. Akinnuoye, H. Sasse, P. Cave, A. Duffy, "Design and assessment of cavity perturbation method for dielectric constant measurement," in *Proc. of the 65th International Wire & Cable Symposium (IWCS).,* Providence, RI. October 2016, pp140–149.

[13] F. S. Akinnuoye, S. Prescott, A. Duffy, "Progress in dielectric constant measurement," in *Proc. of the 67th International Wire & Cable Symposium (IWCS).,* Providence, RI. October 2018.

[14] G. Zimmerman, B. Moffitt, T. Brillhart. (2016). N BASE-T Performance and Cabling Guidelines. [Online]. Available: https://www.nbaset.org/wp-content/uploads/2016/08/NBT_CablingWhitePaper_082916.pdf

[15] C. M. Glew, C. A. Glew, R. Speer., "Limited combustible foamable fluoropolymers for LAN cabling enabling high operating temperatures for Power over Ethernet" in *Proc. IWCS.,* Providence RI, October 2018.

[16] A. Tsetse, E. Bonniord, P. Appiah-Kubi and S. Tweneboah-Kodua. (2018). "Performance study of the impact of security on 802.11ac networks." In *Information Technology - New Generations. Advances in Intelligent Systems and Computing,* vol. 738, pp 11-17.

[17] E. Garza, K. Cornelison "CW and EFT noise coupling to category cables and the effect on 1GB/s ethernet traffic," in *Proc. of the 67th International Cable Connectivity Symposium (IWCS),* Providence RI, 2018.

[18] P. Kish. EMC performance for 10 GBASE-T over category 6a cabling. [Online] Available: https://studylib.net/doc/18704755/emc-performance-for-10gbase-t-over-category-6a-cabling.

[19] V. Maguire. (2016). Zone cabling and coverage area planning. [Online] Available: https://www.cablinginstall.com/articles/print/volume-24/issue-5/features/design/zone-cabling-and-coverage-area-planning.

[20] *Information Technology–Telecommunications cabling Requirements for remote powering of terminal equipment, TCT/7_16_0032, Germany (DIN),* ISO/IEC JTC 1/SC 25, 2016.

[21] *Information technology – cabling installation – part 99-1: remote powering,* CENELEC CLC/TR 50174-99-1, April 2015.

[22] *Guidelines for supporting power delivery over balanced twisted-pair cabling,* TIA TSB-184A D7.1, Revision A, March 2017.

[23] T*elecommunications cabling guidelines for wireless access points plenary meeting,* TIA TSB-162-A, November 2013.

[24] Panduit. (2008). Next-generation high-speed transport systems for smart data center and enterprise networking. [Online]. Available: https://studylib.net/doc/18490489/panduit-s-next-generation-high-speed-transport-systems-fo

[25] F. Akinnuoye, H. Sasse, J. Walling, A. Duffy, "Assessment of bundle heating due to power transmission over Ethernet cabling," in *Proc. IWCS.,* Charlotte, NC. November 2011.

[26] J. Glover, R. Hopper, A. Duffy, C. Oxley, “Infrared thermography for power over ethernet (PoE) reference measurements,” in *Proc. IWCS,* 2012.

[27] P. Cave, F. S. Akinnuoye, A. Duffy, “The impact of remote powering (PoE) on balanced twisted pair cables,” in *Proc. of the 63rd International Wire & Cable Symposium (IWCS).,* Providence, RI. November 2014.

[28] T. Lanoe, C. McNutt, A. Sekhavat, “Four pair power over ethernet (4PPoE) deployment: standards, performance & challenges,” in *Proc. of the 66th IWCS.,* Orlando FL, 2017.

[29] W. Hopkins, “evolving methods of evaluating cable heating” in *Proc. of the 66th IWCS.,* Orlando, FL. October 2017.

[30] F. Akinnuoye, H. Sasse, J. Walling, A. Duffy, “Heating effects on channel performance for Power over Ethernet Applications,” in *Proc., IWCS,* Charlotte, NC. 2013, pp. 508–515.

[31] F. S. Akinnuoye, P. Cave, and H. Sasse, A. Duffy, “Enhancing the power and data capabilities of structured cabling,” in *Proc. CabWire World Conf.*, Dusseldorf. Germany. 2015, pp. 152–162.

[32] UL LLC (The plastics industry trade association), “Fact finding report on power over local area network type cables (4-pair data / communications cables),” September 2015. [Revised: September 25, 2015]

[33] C.Y.O. Lin, J.P. Curilla, “Temperature-related changes in dielectric constant and dissipation factor of insulations increase attenuation in data cables used in building plenums,” in *Proc. of the 16th Conference on Local Computer Networks*. Minneapolis, MN, 1991, pp.74-7.

[34] F. Akinnuoye, H. Sasse, P. Cave, S. Prescott and A. Duffy, “Long-term effect of thermal variation on the performance of ethernet cabling dielectrics.,” in *Proc. of the 66th IWCS.,* Orlando, Florida. USA, 2017.

[35] H. Chin, P. Lee, C. Hsu, and C. Ho. (2016). "Investigation of differential twisted-pairs implemented on silicon ipd and high-performance multilayer organic platforms." *IEEE 66th Electronic Components and Technology Conference*, pp. 2378 – 2383.

[36] G. Zhihong, D. Kang, "Copper cables for mobile base stations in the 5g decade," in *UL and IWCS China Cable & Connectivity Symposium.,* Shanghai, China, 2018.

[37] T. Williams, “Interface and filtering,” in *EMC for Product Designers*,” 5th ed. Elsevier Ltd, 2017, ch. 14, sec. 14.1.8.1, pp. 402.

[38] J. Poltz. "Impact of cable length on NEXT.," in *Proc. of the 67th IWCS*, Providence RI. USA, October 2018.

[39] *United states environmental protection agency, “wire and cable insulation and jacketing: life¬ cycle assessments for selected applications,* EPA 744¬S¬08¬001,” June 2008.

[40] Excel Networking. (2016). Excel cable datasheets [Online] Available: https://www.use-ip.co.uk/datasheets/5475/excel_cat6_external_305m_cable_black_100100.pdf

[41] I*nformation technology - generic cabling for customer premises - part 6: distributed building services,* ISO/IEC 11801-6, 2017.

[42] Nexans. (2014). General Installation guide [Online] Available: https://www.nexans.co.uk/eservice/UK-en_GB/fileLibrary/Download_540209803/UK/files/General+Installation+guide+2014_V2_1.0+DWI_LR.pdf

[43] V. Maguire. (2007). De-Mystifying Cabling Specifications– From 5e to 7A. [Online] Available: https://www.bitpipe.com/detail/RES/1187127774_909.html

[44] *Multicore and symmetrical pair/quad cables for digital communications – part 1-4: assessment of conductor heating in bundled cables due to the deployment of remote powering,* IEC 61156-1-4, 2010.

[45] *Information technology–telecommunications cabling requirements for remote powering of terminal equipment,* TCT/7_16_0032, ISO/IEC JTC 1/SC 25, 2016.

[46] P. Kish. (2010). Mode conversion parameters [Online] Available: https://www.biotcanada.ca/features/mode-conversion-parameters/

[47] F. P. McCluskey, T. Podlesak, R. Grzybowski, "High Temperature Electronics," CRC Press 1st ed. December 13, 1996.

[48] *Commercial building telecommunication cabling standard. part 2: balanced twisted-pair cabling components,* ANSI/TIA/EIA-568-B.2, MAY 2001.

[49] Excel Networking. (2013). NVP, what is it for? [Online] Available: https://www.petalit.cz/soubor/excel-whitepaper-nvp/

[50] J. Poltz, "Attenuation of screened twisted pairs.," in *Proc. The 66th IWCS International Cable Connectivity Symposium*, Orlando, Florida. USA, 2017.

[51] M. N. Sadiku, "Element of Electromagnetics," International 5th Ed. Oxford, New York. 2011, PP. 525.

[52] R. D. Kenny and D. N. Koon, "Characteristic impedance test methods at LAN frequencies: UTP-STP case." in *Proc. IWCS* . USA, 1991.

[53] T. Magesacher, W. Henkel, G. Tauböck, T. Nordström. (2002). Cable measurements supporting xDSL technologies. *e & i Electrotechnics and information technology*. *119(2),* pp 37–43 [Online] Available: https://link.springer.com/article/10.1007/BF03161579

[54] T. Williams, "Interface and filtering," in *EMC for Product Designers*," 5th ed. Elsevier Ltd, 2017, ch. 14, sec. 14.1.9, pp. 406.

[55] I. Michael, "Detecting, localizing and ranking copper connectors," U. S. Patent 9846188, Sept. 18, 2014.

[56] A. S. Tanenbaum and D. J. Wetherall, "The Medium Access Control Sublayer," in *Computer Networks*, 5th ed. USA: Pearson Education Inc., 2011, ch.4, sec.4.3.7, pp. 120.

[57] M. N. Sadiku, "Element of Electromagnetics," *International 5th Ed*. Oxford, New York. 2011, PP. 566.

[58] T. Williams, “Interface and filtering,” in *EMC for Product Designers*,” 5th ed. Elsevier Ltd, 2017, ch. 14, sec. 14.1.9, pp. 277.

[59] T. Williams, “Digital and Analogue circuit design,” in *EMC for Product Designers*,” 5th ed. Elsevier Ltd, 2017, ch. 13, sec. 13.1.3.4, pp. 342.

[60] D. J. Kennefick. “FEP as a dielectric material for multi-gigabit, single pair ethernet cable for automotive," in *Proc. of the 67th IWCS, Rhode Island*, Providence RI. USA, October 2018.

[61] V. Komarov, S. Wang and J. Tang. (2005). Permittivity and Measurement. *Encyclopaedia of RF and Microwave Engineering*. [online]. Available: https://public.wsu.edu/~sjwang/dp-rf-mw.pdf.

[62] B. Gao, G. Wu, L. Zhou, K. Cao, and Y. Luo, " Research on aging characteristics of twisted pair based on dielectric loss under high frequency pulse voltage." in *Proc. of the 9th International Conference on Properties and Applications of Dielectric Materials*. Harbin, China, July 19-23, 2009.

[63] W. L. Gore & Associates, Inc., Understanding Cable Stress and Failure in High Flex Applications [Online]. Available: https://www.gore.com/resources/tech-note-understanding-cable-stress-and-failure-high-flex-applications. [Accessed 28 July 2019].

[64] J. C. Fothergill, S. J. Dodd, L. A. Dissado, T. Liu and U. H. Nilsson. (2011, October) "The measurement of very low conductivity and dielectric loss in XLPE cables: a possible method to detect degradation due to thermal aging." in *IEEE Transactions on Dielectrics and Electrical Insulation,18(5),* pp. 1544-1553.

[65] T. Williams, “Interface and filtering,” in *EMC for Product Designers*,” 5*th* ed. Elsevier Ltd, 2017, ch. 14, sec. 14.1.8.1, pp. 400.

[66] P. Kish. How cabling parameters affect your network’s performance. [Online] Available: https://www.cablinginstall.com/connectivity/article/16464990/how-cabling-parameters-affect-your-networks-performance.

[67] H. W. Ott, “Intrinsic Noise Sources,” in *Electromagnetic Compatibility Engineering*,” Rev ed. John Wiley & Sons, Inc., 2009, ch. 8, sec. 8.1, pp. 328.

[68] H. Ling, S. Liu, Z. Zheng, F. Yan. Low-k. (June 2018). Dielectric- A Potential Solution for Crosstalk Induced Signal Integrity issues in SWCNT Interconnects Methods. [Online] Available:https://pdfs.semanticscholar.org/1dd3/68cfad98c420528f669589fdf4fc28db6bf0.pdf?_ga=2.55511147.1540915156.1574762499-2000591571.1574762499

[69] P. Kish. (2002). Category 6 Cabling Questions and Answers. [Online] Available: http://docplayer.net/14347729-Category-6-cabling-questions-and-answers.html

[70] T. Williams, “Interference coupling mechanisms,” in *EMC for Product Designers*,” 5th ed. Elsevier Ltd, 2017, ch. 11, sec. 11.1.5.

[71] Francois and P. Namy, “Finite element analysis of cables heating due to PoE/PoE+,” in *Proc. COMSOL Conf.,* Paris, France, 2010.

[72] H. P. Tripathy, D. Bej , P.Pattanaik, D.K. Mishra, S. K. Kamilla , and R. K. Tripathy. (2018, June). “Measurement of Zone Temperature Profile of a Resistive Heating Furnace Through RVM Model.” *IEEE Sensors Journal*, vol. 18, pp 4429–4435.

[73] M. Duff, & J. Towey. (2010). Two ways to measure temperature using thermocouples feature simplicity, accuracy, and flexibility. [Online] Available: https://www.analog.com/en/analog-dialogue/articles/measuring-temp-using-thermocouples.html#:~:targetText=The%20reference%20junction%20temperature%20is,reflect%20the%20reference%20junction%20temperature.

[74] G. Prentice. (2015). A Practical Guide to Improving Temperature Measurement Accuracy https://www.miinet.com/images/pdf/whitepapers/A_Practical_Guide_to_Improving_Temperature_Measurement_Accuracy_White_Paper_Moore_Industries.pdf. [Online] Available:

[75] Haefely Hipotronics. Basic TDR Fault Locating Techniques. [Online] Available:http://www.maceyselectrical.com.au/haefely-hipotronics-1_Basic_TDR_Techniques_WP.pdf

[76] DSX-5000 CableAnalyzer, FLUKE networks, [Online]. Available: https://www.flukenetworks.com/datacom-cabling/Versiv/dsx-cableanalyzer-series [Accessed 13 June 2019].

[77] Fluke Networks. (2008). How to Test to TIA/EIA-568-B.2-10 [Online]. Available: https://fluketestery.cz/pdf/TIA-EIA-568-B-10.pdf [Accessed 13 June 2019].

[78] Quabbin Wire & Cable Co., Inc. What is Return Loss? Why is it important?” [Online]. Available https://www.quabbin.com/tech-briefs/what-return-loss-why-it-important [Accessed 13 June 2019].

[79] M. N. Sadiku, “Element of Electromagnetics,” International 5th Ed. Oxford, New York. 2011, PP. 492.

[80] S. Vaden, “Advanced Balunless Measurement,” IWCS Educational short courses (CU 205), 2015.

[81] VDV Works LLC. (2002-2011). Uncle Ted's Guide to Communications Cabling (voice/data/video), [Online]. Available: http://www.vdvworks.com/ [Accessed 13 June 2019].

[82] Fluke Corporation. (2015). Versiv cabling certification product family user’s manual, rev.3,. [Online]. Available: https://www.manualslib.com/manual/1303534/Fluke-Versiv.html?page=67#manual. [Accessed 13 June 2019].

[83] M. M. Al-Asadi, “High frequency performance of structured wire cabling in communication systems,” Ph.D. dissertation, Faculty of Tech., De Montfort University., UK, 2000.

[84] J. Poltz and J. Beckett, “Propagation limits of twisted pair cables.,” in *Proc. The 51st IWCS International Cable Connectivity Symposium*, USA, 2002.

[85] J. Poltz and M. Josefsson, “sensitivity analysis of shielded cables,” in *Proc. The 61st IWCS International Cable Connectivity Symposium,* Charlotte, NC. November 2013

[86] J. Poltz. "Attenuation of screened twisted pairs.," in *Proc. The 66th IWCS International Cable Connectivity Symposium,* Orlando, Florida. USA, 2017.

[87] O. E Ogundapo, “High Frequency Ethernet Cabling Analysis and Optimization,” Ph.D. dissertation, De Montfort Univ., Leicester, 2016.

[88] R. D. Kenny and D.N Koon, “Characteristic impedance test methods,” in *Proc. The 40th IWCS International Cable Connectivity Symposium,* USA, 1991

[89] D. Guezgouz, Y. Raingeaud and J. Lebunetel, “SPICE model for the PLC propagation channel in the high frequency range,” Rio de Janeiro, 2010, pp. 1-6.

[90] A. M. Martin, “Quantitative Data Validation Automated Visual Evaluations,” Ph.D. dissertation, De Montfort Univ., Leicester, Sep. 1999.

[91] O. E Ogundapo, C. Nche, A. Duffy and G. Zhang. (2018). “Application of the feature selective validation method and kolmogorov-smirnov test to evaluate handling effects on crosstalk of ethernet cables”. *American Journal of Electrical and Electronic Engineering,* vol. 6, pp 32-37.

[92] A.Duffy, A. Martin, Antonina, A.Orlandi and C.Ritota. (2005, August). “The Feature Selective Validation (FSV) Method,” in *Proc. of the International Symposium on Electromagnetic Compatibility, vol.1,* pp.272-277.

[93] *IEEE Standard for Validation of Computational Electromagnetics, Computer Modeling and Simulations,* IEEE 1597.1, 2008.

[94] *IEEE Recommended Practice for Validation of Computational Electromagnetics Computer Modeling and Simulations,* IEEE 1597.2, 2010 .

[95] K.D.Vernon-Parry. (2000, July–August). “Scanning electron microscopy: an introduction.” *Elsevier Advanced Technology*, vol. 13, pp. 40–44.

[96] J. F. Mansfield, A. Adamson and K. Coffman. (2000). “Development of a system to provide full, real-time remote control of a scanning electron microscope across the second-generation internet: the teaching sem. microscopy and microanalysis,” *the official journal of Microscopy Society of America, Microbeam Analysis Society, Microscopical Society of Canada, vol. 6*, pp. 31–41.

[97] B. Juna, S. Kimb, S. K. Kwakb, Y. Kwona. (2018, March). “Effect of acidic aqueous solution on chemical and physical properties of polyamide NF membranes.” *Applied Surface Science*. pp. 387–398.

[98] J.T. Wanga. et al. (2018, June). “Improving creep properties of 7075 aluminium alloy by laser shock peening.” *Surface and Coatings Technology. Elsevier,* vol 349, pp. 725–735.

[99] BICSI, “Metallic Media,” in *Principles of Transmission*, 13th ed. [Online] Available:https://www.bicsi.org/docs/default-source/publications/tdmm-13th-chapter-1.pdf?sfvrsn=c87d32a6_2

[100] S. Wasserman, C. Kmiec, “Selection and Use of Materials in Wire and Cable,” IWCS Educational short courses (MA101), 2015.

[101] D.C.Wright, “Failure of plastics due to Thermo-oxidation reaction, Volume 11. 2001 UK

[102] I. Martinez. (1995-2019). Thermal effects on materials [Online] Available: http://webserver.dmt.upm.es/~isidoro/ot1/Thermal%20effects%20on%20materials Last accessed 15/05/2019.

[103] Schneider Electric. (2003–2011). Oily Residue Found in Electrical Distribution and Control Equipment [Online] Available: https://www.schneider-electric.us/en/download/document/0110DB0301/ Last accessed 15/05/2019.

[104] K. Pielichowski and J. Njuguna, “Thermal degradation of polymeric materials”, Volume 11. UK, Rapra Technology Limited. 2005, pp. 66.

[105] M. A. Moreira, L. C. André, & Z. L. Cardeal. (2014, Jan). “Analysis of phthalate migration to food simulants in plastic containers during microwave operations.” *International journal of environmental research and public health*.” vol. 11, pp 507–526.

[106] S. Kisin. (2007, June). “Adhesion changes at metal-polymer interfaces: Study of the copper–(acrylonitrile–butadiene–styrene) system.” *Thin solid films,* vol. 515, pp 6853– 6859.

[107] J.R. Lloyd, M.W. Lane and E.G Liniger IBM TI. “Relationship between interfacial adhesion and electromigration in cu metallization.” *IEEE International Integrated Reliability Workshop Final Report*, Lake Tahoe, CA, 2002, pp. 32-35.

[108] Jeong, Minsu & Kim, Jeong-Kyu & Kang, Hee-Oh & Hwang, Wook-Jung & Park, Young-Bae. (2014). “Effects of wet chemical treatment and thermal cycle conditions on the interfacial adhesion energy of Cu/SiN x thin film interfaces.” *Journal of the Microelectronics and Packaging Society*. Vol. 21, pp 45-50.

[109] *Engineering Tripos Part IIA: Module Manufacturing Engineering Tripos Part IIA*: Module 3P1, 2012-13.

[110] J. Poltz. "Attenuation of screened twisted pairs.," in *Proc. The 66th IWCS International Cable Connectivity Symposium,* Orlando, Florida. USA, 2017.

[111] J. C. Fothergill, S. J. Dodd, L. A. Dissado. (2011, October). “The measurement of very low conductivity and dielectric loss in XLPE cables: a possible method to detectdegradation due to thermal aging.” *IEEE Transactions on Dielectrics and Electrical Insulation,* Vol. 18, pp: 1544 – 1553.

[112] S. K. Dhawan. (1992, Oct.). "Understanding effect of Teflon room temperature phase transition on coax cable delay in order to improve the measurement of TE signals of deuterated polarized targets," in *IEEE Transactions on Nuclear Science,* vol. 39, pp. 1331-1335.

[113] K. Czuba and D. Sikora, "Phase drift versus temperature measurements of coaxial cables," 18th *International conference on microwaves, radar and wireless communications*, Vilnius, 2010, pp. 1-3.

[114] E. Rivier and M. Vergé-Lapisardi. (March, 1979). "Lumped parameters of a reentering cylindrical cavity." *IEEE Trans. Microwave Theory & Tech.*, vol. 19, pp. 309-314.

[115] Y. Kanai, T. Tsukamoto, M. Miyakawa and T. Kashiwa. (2000, July). "Resonant frequency analysis of reentrant resonant cavity by using FEM and FD-TD method." *IEEE Trans. Microwave Theory & Tech.*, vol.36, pp. 1750-1753.

[116] F. Thompson, A. D. Haigh, B. M. Dillon and A. A. P. Gibson. (May 2003). "Analysis and design of a reentrant microwave cavity for the characterization of single wheat grain kernels." *IEE Proc.Sci.Meas. Technol.*, vol.15, pp. 113-117.

[117] G. Brodie, M. V. Jacob and P. Farrell, "Techniques for measuring dielectric properties," in *Microwave and Radio-Frequency Technologies in Agriculture*. An Introduction for Agriculturalists and Engineers, Berlin: De Gruyter Open Ltd, 2015, Ch. 6, sec. 2, pp. 52-77.

[118] *American Standard Test Methods for Complex Permittivity (Dielectric Constant) of Solid Electrical Insulating Materials at Microwave Frequencies and Temperatures to 1650 °C*, ASTM D2520, 2001.

[119] D. Prastiyanto, "Dielectric Measurements and Modelling on Curing of Polymer Composites" Ph.D. Dissertation, Karlsruhe Institute of Technology (KIT). Germany, 2015.

[120] Z. Peng, J.Y., M. Andriese, (2014). "Maximum Sample Volume for Permittivity Measurements by Cavity Perturbation Technique. *IEEE Transactions on Instrumentation and Measurement."* vol. *63*, 450–455

[121] H.E. Bussey, L.A. Steinert. (1958, Jan). "Exact solution for a gyromagnetic sample and measurements on a ferrite." *IRE Trans. Microwave Theory Tech.* vol. 6, pp72-76.

[122] T. Nishikawa, K. Wakino, H. Tanaka, Y. Ishikawa. (1988, June). "Precise measurement method for complex permittivity of microwave dielectric substrate." *Conference on Precision Electromagnetic Measurements*." pp. 155-156.

[123] J. Baker-Jarvis, M. D. Janezic, B. Riddle, C. L. Holloway, N.G. Paulter, "Dielectric and Conductor-Loss Characterization and Measurements on Electronic Packaging Materials." NIST Technical Note 1520, July 2001.

[124] M. D. Janezic, J. A. Jargon. (1999, Feb). "Complex permittivity determination from propagation constant measurement." *IEEE microwave and guided wave letters*, vol. 9, pp 76 – 78.

[125] M. D. Janezic, U. Arz, S. Begley and P. Bartley, "Improved permittivity measurement of dielectric substrates by use of the TE111 mode of a split-cylinder cavity," in *73rd ARFTG Microwave Measurement Conference*, Boston, MA, pp. 1-3.

[126] F. L. Penaranda-Foix, J. M. Catala-Civera, A. J. Canos-Marin and B. Garcia-Banos. (2009, June). "Circuital analysis of a coaxial re-entrant cavity for performing dielectric

measurement.” *IEEE MTT-S International Microwave Symposium Digest*, Boston, MA, pp. 1309-1312.

[127] D. Marqués-Villarroya, F. Pcñaranda-Foix, A. J. Canós, B. García-Baños and J. M. Catalá-Civera. (2018, June). “Determination of the complex permittivity of high loss liquids with a novel reentrant cavity.” *IEEE/MTT-S International Microwave Symposium - IMS*, Philadelphia, PA, pp. 1381-1384.

[128] E. Rivier and M. Vergé-Lapisardi. (March, 1971). “Lumped parameters of a reentering cylindrical cavity.” *IEEE Trans.Microwave Theory & Tech.*, vol. 19, pp. 309-314.

[129] K. Uenakada. (1973, Jan). “Equivalent circuit of reentrant cavity.” *IEEE Trans. Microwave Theory & Tech.*, vol. 21, pp. 48-51.

[130] J. Baker-Jarvis and B. F. Riddle, “Dielectric Measurements Using a Reentrant Cavity: Mode-Matching Analysis,” NISTTechnical Note 1384, 1996.

[131] Y. Kanai, T. Tsukamoto, M. Miyakawa and T. Kashiwa. (2000, July). “Resonant frequency analysis of reentrant resonant cavity by using FEM and FD-TD method,” *IEEE Trans. Microwave Theory & Tech.*, vol. 36, pp. 1750-1753.

[132] F. Thompson, A. D. Haigh, B. M. Dillon and A. A. P. Gibson. (2003, May). “Analysis and design of a re-entrant microwave cavity for the characterisation of single wheat grain kernels,” *IEE Proc.Sci.Meas. Technol.*, vol. 150, pp. 113-117.

[133] F. L. Penaranda-Foix. “Application of the Generalized Circuital Analysis to Solve Electromagnetic Diffraction Problems”, PhD thesis, Technical University of Valencia, Spain, 2001.

[134] A. A. Barannik, N. T. Cherpak, I. A. Protsenko and S. A. Vitusevich. (2019, May). "Millimeter-Wave WGM Resonator-Based Characterization of Continuous and Noncontinuous Ultrathin Cu Films," in *IEEE Microwave and Wireless Components Letters*, vol. 29, pp. 363-365

[135] O. Kwon, “Noninvasive and portable diagnoses for brain and heart disorder: angle-distinguishable infrared spectroscopy based upon a three dimensional resonant toroid version of whispering gallery modes”. *IEEE Photonics Conference (IPC)*, Reston, VA, 2018, pp. 1-2.

[136] R. G. Geyer and J. Krupka. (April, 1995). “Microwave dielectric properties of anisotropic materials at cryogenic temperatures," in *IEEE Transactions on Instrumentation and Measurement*, vol. 44, pp. 329-331

[137] S. M. S. Hasan, M. Sundaram, Y. Kang and M. K. Howlader, “Measurement of Dielectric Properties of Materials using Transmission/Reflection Method with Material filled Transmission Line”. *IEEE Instrumentation and Measurement Technology Conference Proceedings*, Ottawa, Ont., May, 2005, pp. 72-77.

[138] J. Baker-Jarvis, E. Vanzura, and W. Kissick. (Aug. 1990). “Improved technique for determining complex permittivity with the transmission/reflection method.” *IEEE Trans. Microwave Theory Tech.*, vol 38, pp. 1096–1103.

[139] A. Rashidian, L. Shafai, D. Klymyshyn and C. Shafai. (2017, August) “A Fast and Efficient Free-Space Dielectric Measurement Technique at mm-Wave Frequencies,” *IEEE Antennas and Wireless Propagation Letters,* vol.16, pp. 2630-2633.

[140] S. Bringhurst, M. F. Iskander. (1993). “New metalized ceramic coaxial probe for high temperature broadband dielectric properties of low permittivity materials.” *Microwaves Theory and Application in Materials Processing* II; pp. 503-510.

[141] J. Baker-Jarvis, M. D. Janezic, P. D. Domich and R. G. Geyer. (1994, Oct). “Analysis of an open-ended coaxial probe with lift-off for non-destructive testing,” *IEEE Transactions on Instrumentation and Measurement,* vol 43, pp. 711-718.

[142] F. M. Ghannouchi and R. G. Bosisio. (1989, April). “Measurement of microwave permittivity using a six-port reflectometer with an open-ended coaxial line,” *IEEE Transactions on Instrumentation and Measurement,* vol. 38, pp. 505-508.

[143] Y. Ye, T. Liu, X. Zeng, J. He, C. Akyel. “Rectangular cavity design for permittivity measurement at ISM 5.8GHz radio band,” In *2007 International Conference on Microwave and Millimeter Wave Technology*, Builin, China, 2007, pp. 1– 4.

[144] J. Krupka. "Measurements of the complex permittivity from microwave to millimeter wave frequencies," *12th International Conference on Electromagnetic Wave Interaction with Water and Moist Substances (ISEMA),* Lublin, 2018, pp. 1-9.

[145] *Multi-element metallic cables used in analogue and digital communication and control Part 3-1: Sectional specification for unscreened cables characterised up to 100 MHz — Horizontal and building backbone cables*, BS EN 50288-3-1, 2013.

[146] MATLAB and Statistics Toolbox Release 2017b, The MathWorks, Inc., Natick, Massachusetts, United States.

[147] HEICO Company. (2016, Jan 25). How apertures affect EMI shielding [Online] Available: https://leadertechinc.com/blog/how-apertures-affect-emi-shielding/ Last accessed 07/11/2019.

[148] J. Krupka, (2016). “Measurements of the complex permittivity of low loss polymers at frequency range from 5 GHz to 50 GHz,” *IEEE Microwave and Wireless Components Letters*, vol. 26, pp 464–466.

[149] The Engineering ToolBox. Solids - volume temperature expansion coefficients [Online]Available:http://www.engineeringtoolbox.com/volum-expansion-coefficients-solids-d_1894.html Last accessed 05/11/2019.

[150] FEP Handbook. [Online]Available: http://www.rjchase.com/fep_handbook.pdf. Last accessed 05/11/2019.

[151] INEOS Olefins & Polymers. Typical Engineering Properties of High-Density Polyethylene, [Online] Available: https://www.ineos.com/globalassets/ineos-group/businesses/ineos-olefins-and-polymers-usa/products/technical-information--patents/ineos-typical-engineering-properties-of-hdpe.pdf. Last accessed 05/11/2019.

Appendices

Appendix A

Maximum temperature rise for all the CBs (Free air heating test results)										
Cable Types	**Cable diameter (mm)**	**Conductor diameter (AWG)**	**Power (Watts)**	**Temperature (^{0}C) profile for all the CBs. Free air heating results**						
				T1	**T2a**	T3	T2b	T2c	T2d	
Cat5e U/UTP	5.2	24	34.2	14.21	**14.39**	13.79	13.4	11.8	10.02	Solid Polyethylene
			60	25.09	**25.52**	24.57	24.02	21.33	18.08	
			100	40.38	**41.02**	39.62	38.63	34.29	28.73	
Cat6 CCA	-	-	34.2	16.23	**16.20**	15.86	15.23	12.86	9.99	-
			60	28.60	**28.48**	27.99	27.09	23.07	16.81	
			100	45.50	**46.01**	44.81	44.16	36.92	26.93	
Reduced diameter or HD Cat6 U/UTP	-	-	34.2	14.73	**14.78**	14.31	13.7	12.48	14.73	-
			60	25.65	**26.24**	25.78	24.66	21.49	25.65	
			100	41.12	**42.09**	41.38	39.77	34.83	41.12	
Cat6 U/UTP	6.2	23	34.2	14.02	**15.89**	14.45	15.3	14.17	11.5	-
			60	22.9	**26.2**	23.77	25.35	23.39	18.22	
			100	35.16	**40.67**	36.82	39.38	36.36	27.1	
Cat6 F/UTP	7.2	23	34.2	11.18	**11.29**	10.27	11.02	8.99	8.72	-
			60	18.45	**18.73**	17.11	18.53	15.40	14.81	
			100	28.87	**29.48**	27.13	29.46	24.26	23.03	
Cat6A F/FTP	6.9	23	34.2	**11.21**	11.02	10.71	10.35	9.68	11.21	Foamed Polyethylene
			60	**19.20**	18.87	18.51	17.94	16.97	19.20	
			100	**30.52**	30.21	29.62	28.94	27.56	30.52	
Cat7A S/FTP	7.8	23	34.2	9.86	**9.98**	9.64	9.76	8.39	8.03	Foam Skin HDPE material
			60	17.35	**17.71**	17.25	17.6	15.08	14.06	
			100	27.57	**28.28**	27.42	28.31	24.24	22.69	

Appendix B

Maximum temperature rise for all the CBs (Insulation heating test results)									
Cable Types	**Cable diameter**	**Conductor diameter**	**Power (Watts)**	**Temperature (^{0}C) profile for all the CBs. Free air heating results**					
				T1	**T2a**	T3	T2b	T2c	T2d	
Cat5e U/UTP	5.2	24	34.2	52.04	**51.06**	50.89	49.84	47.94	45.93	Solid Polyethylene
			60	88.26	**86.6**	86.19	84.8	81.84	78.93	
			100	117.61	**114.10**	115.51	108.02	104.14	100.92	
Cat6 CCA	-	-	34.2	39.91	**40.73**	39.9	40.08	37.54	34.08	-
			60	68.84	**70.6**	70.4	69.58	59.41	59.95	
			100	111.62	**115.19**	114.75	114.29	109.5	100.95	
Reduced diameter or HD Cat6 U/UTP	-	-	34.2	43.24	**43.79**	42.83	42.65	40.76	39.4	-
			60	80.99	**82.82**	80.95	81.17	77.93	75.44	
			100	112.16	**114.55**	112.44	113.66	108.15	109.04	
Cat6 U/UTP	6.2	23	34.2	45.42	**46.01**	44.15	45.39	44.29	41.39	-
			60	76.34	**77.55**	73.91	76.92	75.26	70.85	
			80	104.66	**106.8**	101.58	106.14	104.25	99.11	
			100	112.62	**114.34**	110.11	113.35	111.37	107.96	
Cat6 F/UTP	7.2	23	34.2	42.10	**42.77**	40.41	42.66	38.87	40.16	-
			60	69.24	**70.16**	66.77	70.23	64.34	66.15	
			80	90.22	**91.30**	87.23	91.44	84.61	86.57	
			90	97.40	**98.67**	94.24	98.75	91.61	94.21	
			100	106.39	**107.98**	103.16	108	100.67	126.7	
			107	111.53	**113.25**	108.32	113.15	106.89	109.26	
Cat6A F/FTP	6.9	23	34.2	36.74	**39.67**	38.87	39.03	37.72	36.74	Foamed Polyethylene
			60	68.06	**70.8**	69.31	70.12	69.02	68.06	
			100	101.59	**103.85**	103.77	103.12	100.82	101.59	
Cat7A S/FTP	7.8	23	34.2	39.14	**40.25**	38.95	39.83	38.43	37.70	Foam Skin HDPE material
			60	63.68	**65.65**	63.94	65.33	63.44	62.00	
			100	96.04	**98.67**	96.43	98.49	96.41	94.29	
			120	106.36	**108.42**	106.25	108.23	106.1	103.98	